

SLAC-R-541
CONF-8005102
June 1999

Proceedings of the
Beam-Beam Interaction
Seminar

Held at

Stanford Linear Accelerator Center,
Stanford, California,

May 22-23, 1980

(Supersedes SLAC-PUB-2624 dated October, 1980)

Prepared for the Department of Energy
Contract DE-AC03-76SF00515

Printed in the United States of America. Available from the National Technical Information Service,
U.S. Department of Commerce, 5285 Port Royal Road, Springfield, Virginia 222161

TABLE OF CONTENTS

Preface	v
Acknowledgements	vi
A Simulation Study of the Beam-Beam Interaction at SPEAR / <i>J. Tennyson</i>	1
The Beam-Beam Luminosity Limitation in Electron-Positron Colliding Rings / <i>S. Peggs & R. Talman</i>	21
Beam-Beam Effect and Luminosity in SPEAR / <i>H. Wiedemann</i>	33
Recent Experimental Results on the Beam-Beam Effects in Storage Rings and an Attempt of their Interpretation / <i>S. Kheifets</i>	40
An Empirical Model for Controlling Beam-Beam Effects in ISABELLE / <i>G. Parzens</i>	70
Beam-Beam Studies with DCI / <i>J. LeDuff</i>	80
Beam-Beam Phenomenology / <i>L. C. Teng</i>	99
Plasma Instability in Electron and Positron Colliding Beams in Storage Rings / <i>H. S. Uhm & C. S. Liu</i>	114
A Beam-Beam Simulation for the Single-Pass Linear Collider / <i>R. Sah</i>	144
Disruption Limits for Linear Colliders / <i>R. Hollebeek</i>	165
Analysis of the Beam-Beam Interaction Using Transfer Maps / <i>A. J. Dragt & O. G. Jakubowicz</i>	205
Measures of Nonintegrability in Two-Dimensional Mappings / <i>J. M. Greene</i>	235
The Role of Resonances, "Stochasticity" and Arnol'd Diffusion in Models of the Beam-Beam Interaction / <i>T. C. Bountis</i>	248
A Preliminary Numerical Study of the Beam-Beam Interaction in Two Dimensions / <i>C. R. Eminhizer</i>	273
Nonlinear Hill's Equations and the Beam-Beam Interaction / <i>P. Vuillermot</i>	312
Enhancement of Diffusion by a Nonlinear Force / <i>D. Neuffer & A. Ruggerio</i>	332
An Investigation of the "Flip-Flop" Beam-Beam Effect in SPEAR / <i>M. H. R. Donald & J. M. Paterson</i>	344

PREFACE

The beam-beam interaction has been and continues to be a performance limiting effect in colliding beam systems. Electron-positron collisions are typically more than a factor of five lower in luminosity than expectations from beam design and with present understanding, extrapolations to future systems are not satisfactory. Prediction and optimized design are even more uncertain for proton-proton and proton-antiproton future systems with the ISR at CERN being the sole precedent. The very health of the high energy physics program in the next decades depends to a significant extent on our ability to unravel the mechanisms of this phenomenon and to control them.

To this end, a symposium was held in March 1979 on nonlinear dynamics, concentrating on the beam-beam interaction. The symposium took place at Brookhaven National Laboratory and the proceedings were issued as part of the conference proceedings of the American Institute of Physics (Number 57). It was felt at that time that the 1979 symposium would be the first of a set of meetings which would be needed. This view has not changed and a second symposium is being considered for sometime late in 1980 or in 1981.

However, since last year, there have been a variety of studies, including a plasma model of e^+e^- collisions, models emphasizing the effects of "noise" and a model involving a diffusion-damping equilibrium. Various nonlinear analyses of the beam-beam systems have also been performed. And finally an entirely new form of beam-beam configuration has been proposed and studied - the very strong single pass collider.

In view of this extensive and broad effort, there was organized an informal seminar to bring many of these ideas into an open forum. This seminar was held at SLAC on May 22 and 23, 1980. Contributors, totaling seventeen, came from universities and national laboratories across the United States. These proceedings represent a record of the seminar. The written versions of the papers presented were submitted by the authors and are included here without editing. It is hoped that this compilation will be of value to both beginning and established physicists in this very interesting field of accelerator research.

M. Month

ACKNOWLEDGEMENTS

Thanks are due to many members of the high energy physics community, especially to Pief Panofsky for his continued encouragement and support and to Jan Adamson for her efforts on the many difficult administrative matters.

A SIMULATION STUDY OF THE
BEAM-BEAM INTERACTION AT
SPEAR

Jeffrey Tennyson

Dept. of Electrical Engineering
and Computer Sciences
University of California
Berkeley CA 94720

ABSTRACT

A two dimensional simulation study of the beam-beam interaction at SPEAR indicates that quantum fluctuations affecting the horizontal betatron oscillation play a critical role in the vertical beam blowup.

I. INTRODUCTION

The luminosity at SPEAR and other electron-positron colliding beam machines is limited by an instability in the betatron oscillation which causes beam expansion and particle loss when the beam densities exceed a certain critical level. This instability is excited via some presently unexplained mechanism by the beam-beam interaction, i.e., the electromagnetic force felt by a particle as it passes through a bunch of the opposing beam. The interaction results in an almost instantaneous

change in the transverse velocity of the particle (see Fig. 1), and a corresponding displacement in the transverse phase space (see Fig. 2). This displacement is quite large in comparison to that produced by the accumulated quantum fluctuations over the period between intersections. A single beam-beam kick at typical operating densities (tune shift $\xi = .02$) produces a displacement that is approximately twenty times as large as the corresponding fluctuation displacement at 2 GeV. If these kicks were uncorrelated, they would result in a diffusion that would produce beam blowup at tune shifts as low as $\xi = .001$. The fact that blowup does not occur at such low densities is explained by nonlinear stability theory which predicts a very high degree of correlation at tune shifts up to about $\xi = .16$ (for a one dimensional model see ref. [1]). In fact, it is far more difficult in this case to explain the small amount of correlation breakdown at the beam-beam limit than it is to explain the correlations themselves.

In seeking to identify the source of the correlation breakdown, it is helpful to note that the potential mechanisms can be divided into two general categories.

In the first category are those mechanisms which involve "intrinsic" stochasticity. (See ref. [2] for details.) The beam-beam interaction provides a nonlinear coupling between the otherwise fairly independent betatron oscillations and the longitudinal motion. If it is strong enough, this coupling can destroy the individual energy invariants of the non-radiating oscillators. Energy is then exchanged between them in a deterministic, but statistically "random" way. The leakage of longitudinal energy into the transverse motion may then result in beam blowup

or particle loss. A specific example of this type of breakdown, the overlap of synchro-betatron resonances, has been studied in detail by Izrailev (ref. [1]) who has shown that under the proper conditions, synchrotron modulation of the beam-beam force can cause significant decorrelation at tune shifts as low as $\xi = .04$.

The second general source of correlation breakdown is externally generated noise. A truly random noise, due for example to quantum fluctuations, can conceivably decorrelate the beam-beam force via phase mixing and amplitude diffusion. Although these processes are not completely understood at the present time, preliminary results from the simulation study described below indicate that quantum fluctuations can also produce beam blowup at $\xi = .04$.

Although this study in no way invalidates the conclusions of Izrailev concerning the role of resonance overlap in the beam-beam limit, it does present an alternative explanation based on noise generated decorrelations. If it does, in fact, turn out that quantum fluctuations play a major role in the beam-beam limit at SPEAR, past attempts to extrapolate beam-beam effects from electron colliders to proton colliders will have to be seriously reconsidered. Section II of this report describes the simulation model in detail. Section III summarizes the preliminary results and Section IV offers some tentative conclusions.

II. THE SIMULATION

The computer simulation uses a simple two dimensional weak-strong beam model. A set of difference equations transports the particles of the weak beam through and between encounters with bunches of the strong

beam. The effects represented in both the vertical and horizontal motions are (1) linear rotation between intersections (2) radiation damping (3) quantum fluctuations and (4) the beam-beam interaction. The individual difference equations are shown in detail below and the Fortran coded main loop is reproduced in Fig. 3.

Linear Rotation.

$$x_1 = x_0 \cos(\omega_x) + \dot{x}_0 \sin(\omega_x) \quad (1)$$

$$\dot{x}_1 = -x_0 \sin(\omega_x) + \dot{x}_0 \cos(\omega_x) \quad (2)$$

$$y_1 = y_0 \cos(\omega_y) + \dot{y}_0 \sin(\omega_y) \quad (3)$$

$$\dot{y}_1 = -y_0 \sin(\omega_y) + \dot{y}_0 \cos(\omega_y) \quad (4)$$

Radiation Damping.

$$\dot{x}_2 = \dot{x}_1 - \dot{x}_1 CD_x \quad (5)$$

$$\dot{y}_2 = \dot{y}_1 - \dot{y}_1 CD_y \quad (6)$$

Quantum Fluctuations.

$$x_3 = x_1 + K\sqrt{D_x} \cos(2\pi R_x) \quad (7)$$

$$\dot{x}_3 = \dot{x}_2 + K\sqrt{D_x} \sin(2\pi R_x) \quad (8)$$

$$y_3 = y_1 + K\sqrt{D_y} \cos(2\pi R_y) \quad (9)$$

$$\dot{y}_3 = \dot{y}_2 + K\sqrt{D_y} \sin(2\pi R_y) \quad (10)$$

Beam-Beam Interaction.

$$\dot{x}_4 = \dot{x}_3 - \xi_x 4\pi x_3 \frac{1}{(1 + x_3^2/5.11)^2} \quad (11)$$

$$\dot{y}_4 = \dot{y}_3 - \xi_y 4\pi y_3 [\exp(-x_3^2/2)] \frac{1}{(1 + y_3^2/2)^{\frac{1}{2}}} \quad (12)$$

where

ω_x , ω_y horizontal and vertical betatron frequencies.

C twice the inverse of the damping time.

K the average integrated phase displacement due to quantum fluctuations between intersections.

R_x , R_y two random numbers between 0 and 1; reset with each iteration of the mapping.

D_x , D_y artificial diffusion attenuation: allows for a variation of the damping time and fluctuation level of each oscillator in such a way that the nonintersecting beam size remains constant.

ξ_x , ξ_y the linear tune shifts.

The variables x, \dot{x}, y, \dot{y} are dimensionless; x and y are normalized to the RMS widths of the strong beam σ_x and σ_y , while \dot{x} and \dot{y} are normalized to σ_x/β_x^* and σ_y/β_y^* (β_x^* and β_y^* are the beta functions at the intersection points). The factors C and K are related by the requirement that the nonintersecting weak beam size be $y_{rms} = x_{rms} = 1$. Thus,

$$K = \sqrt{2C} . \quad (13)$$

The above mapping is extremely general. It is applicable to any electron-positron storage ring with flat beams. The only constant specific to a particular machine is the proportionality constant between C and E^3

$$C = \frac{8.85 \times 10^{-5}}{RN} E^3 \quad (14)$$

where R is the effective radiation radius of the machine in meters, N is the number of bunches and E is the energy in GeV.

In Eq. (12) the vertical beam-beam interaction is modulated by the horizontal motion, but the corresponding dependence in the horizontal interaction has been omitted. The basis for this approximation is intuitively apparent from Fig. 1. The large aspect ratio of the beam, 30/1, accentuates the x dependence in the vertical kick and suppresses the y dependence in the horizontal kick. Since the horizontal energy and energy fluctuations are both about 100 times as large as their vertical counterparts, a small exchange of energy between the vertical and horizontal motion will effect the former far more than the latter. Although the coupling between the x and y motion does not conserve energy, the non-radiative mapping is measure preserving. This is very important because the kicks from the beam-beam interaction would otherwise result in a false dissipation or accretion of energy. From this point of view, the coupling of vertical motion to the horizontal appears as a simple time dependence. Strictly speaking, therefore, the above equations represent two one dimensional systems with time dependence, the time dependence of vertical motion being derived in part from the horizontal motion.

The two denominators in Eqs. (11) and (12) provide the non-linearity and depend on the shape of the strong beam. They were chosen to approximate the on-axis electric fields of a simple model beam. For the horizontal force, the model beam was defined by the charge distribution

$$\begin{aligned} \rho(x,y) &= \rho_0 e^{-x^2/2} & |y| \leq .03 \\ &= 0 & |y| > .03 \end{aligned}$$

The potential along the x-axis was calculated numerically and fitted with a Lorentzian. The resulting forces are compared in Fig. 4a. The Lorentzian gives a force that is approximately 50% less than the "true" force at $x = 5\sigma_x$. But since the horizontal beam rarely shows a blowup greater than $2\sigma_x$, this inaccuracy is thought to be acceptable.

For the vertical force, the charge distribution was given by a slab model,

$$\rho(y) = \rho_0 e^{-y^2/2} \quad (\text{for all } x)$$

The potential was numerically calculated for this distribution and fitted with a hyperbola. The corresponding forces are compared in Fig. 4b. Since the ratio of horizontal width to vertical width is large, ~ 30 in SPEAR and PETRA, this approximation is thought to be good for $y < 10\sigma_y$. The use of a simple Gaussian in Eq. (12) to represent the x dependence is thought to be the least satisfactory element in this approximation. Generally speaking, the model underestimates the beam-beam force at large x and overestimates at large y.

Whether a highly accurate expression for the beam-beam force is really necessary in this simulation will not be known until the beam-beam effect itself is understood. The approximations made above have been designed to streamline the mapping as much as possible, and at the same time to include all of the major ingredients usually associated with correlation breakdown.

III. SIMULATION RESULTS

The weak beam is composed of 64 particles whose initial conditions represent a normalized height and width equal to one. Each particle is run through the mapping n times, where n is equivalent to three damping times. After each of ten equally spaced intervals, the rms dimensions of the beam are calculated and recorded. The last three values are expected to represent the steady state beam size and are averaged to give the final dimensions for that run. The results of a preliminary study of this mapping are described here in five parts.

A. Nonlinearity

The effective tunes ν_x and ν_y are plotted against amplitude in Fig. 5. In Fig. 5a, the horizontal tune ν_x decreases as the horizontal amplitude A_x increases (ν_x is independent of the vertical amplitude A_y). The vertical tune ν_y , which is dependent on both A_x and A_y , is shown in Fig. 5b as a function of A_y when $A_x = 0$. Each curve represents a different linear tune shift ξ_y . In Fig. 5c ν_y is again plotted against A_y , but this time ξ_y is fixed at $\xi_y = .06$ and the different curves represent different values of A_x . These plots were made empirically by analyzing surface of section plots of the conservative x and y motions.

B. Tune Diagram

Using Fig. 5, it is possible to estimate the distribution of weak beam particles in frequency space. This distribution is shown in Fig. 6 for $\xi_Y = .04$, $\xi_X = .02$, $Q_Y = 5.18$ and $Q_X = 5.24$ (Q_Y and Q_X are the number of betatron oscillations in one revolution for the non-intersecting beams). Because of the large aspect ratio, most of the particles in the beam are confined to a fairly narrow band in ν_X . The background lines indicate the locations of the most important parametric and coupling resonances in this frequency locale.

C. Beam Size Dependence on Energy and the Tune Shift

In Fig. 7, the beam height is plotted against tune shift ($\xi = \xi_X = \xi_Y$) for six different energies. (Energy enters the mapping via Eqs. (13) and (14).) At large energies, $E \sim 4$ GeV, blowup begins at about $\xi = .06$ and increases gradually with ξ . As the energy drops, blowup occurs earlier, and rises more rapidly with ξ . Because the damping time is proportional to E^{-3} , energies below 1 GeV have not been run due to the large amount of computer time required. The 1.1 GeV curve shown here required 3.20×10^8 iterations of the mapping described in Sec. II.

Since these beam heights are normalized to the strong beam, the actual beam heights differ from these by a factor specific to each energy curve. It should also be pointed out that the rms values shown take into account all particles including a few which are at very large amplitudes. These particular particles seem to form a non-Gaussian "tail" which extends far beyond the main body of the beam. Their inclusion into the rms value tends to inflate the beam and lower the reproducibility of

each run. In most of the plots shown here, each run was computed at least twice and the results were averaged.

The beam widths have not been plotted because none of these runs have demonstrated significant horizontal blowup.

D. Beam Size Dependence on Radiation Effects

When the vertical fluctuations (Eqs. (9) and (10)) are removed from the mapping, the behavior exhibited in Fig. 7 remains essentially unchanged.

On the other hand, when the horizontal fluctuations are removed instead ($D_x = 0$), the blowup completely disappears. This surprising result is shown in Fig. 8. The vertical tune shift ξ_y is held fixed at $\xi_y = .06$ with the energy at 2.2 GeV. The four curves represent four different horizontal tune shifts $\xi_x = 0, .04, .06, .08$. The factor D_x , which is an attenuation factor for the horizontal diffusion due to quantum fluctuations, is varied from zero to one. $D_x = 1$ corresponds to the diffusion rate in the actual machine, while $D_x = 0$ eliminates all radiation effects in x (both fluctuations and damping). The variation of D_x does not effect the non-intersecting ($\xi_x = 0$) beam size, only the rate of which a particle diffuses from one amplitude to another.

All blowup effects disappear if either D_x or ξ_x are equal to zero. For a fixed non-zero value of ξ_x , take for example $\xi_x = .06$, there is almost no blowup below $D_x = .2$. Between $D_x = .2$ and $D_x = .4$, σ_y increases steadily and at values of D_x higher than .4, σ_y remains approximately constant. It appears as if the mechanism for beam blowup has a threshold at $D_x = .2$ and saturates at $D_x = .4$. Moreover, this seems to be true for each of the different ξ_x values.

How these results depend on v_x , v_y , E , and ξ_y is not known at this time.

The dependence of σ_y on ξ_x for $D_x > .4$ cannot be described as easily as the dependence on D_x . There are fewer data points and the $\xi_x = .06$ curve seems out of place with unusually large fluctuations. These fluctuations indicate that the σ_y values associated with this curve are probably inflated by a few particles at very large amplitudes. It is possible that the same type of threshold and saturation phenomena seen for the D_x dependence exist as well in the ξ_x dependence. A detailed study of the ξ_x dependence is hindered somewhat by the fact that changes in ξ_x effect the frequency space distribution of the beam (Fig. 6). Although partial compensation can be achieved by varying Q_x to keep the zero amplitude tune fixed (as was done in Fig. 8), it may be impossible with this model to separate effects associated with the horizontal nonlinearity from those associated with horizontal nonlinear resonances.

The results shown in Fig. 8 are not understood at present. That small fluctuations in the horizontal motion can have a substantially greater effect on the vertical stability than much larger fluctuations in the vertical motion itself, is difficult to understand. Simple phase mixing arguments have so far proved inadequate.

E. Stochasticity Border

In the absence of radiation effects ($E = 0$) the beam blowup is determined by the resonance overlap condition (ref. [2]). Since this model does not include synchrotron effects, resonance overlap occurs at fairly high tune shifts. The rms beam size for the non-radiative mapping is shown in Fig. 9 as a function of tune shift. The horizontal motion goes

unstable at $\xi_x > .2$. The vertical motion, with a stable but substantial horizontal tune shift $\xi_x = .2$, does not become unstable until $\xi_y = .3$. Both values are almost an order of magnitude above those exhibiting beam blowup in the radiative case. It is therefore quite unlikely that resonance overlap plays a significant role in the blowup phenomena seen in this simulation.

IV. CONCLUSION

A two dimensional simulation that includes both the horizontal oscillation and radiation effects (but not synchrotron modulation), is capable of reproducing many of the experimentally observed characteristics of the beam-beam interaction. The simulation shows a vertical blowup which occurs somewhere between $\xi = .02$ and $\xi = .06$, where $\xi = \xi_x = \xi_y$. The blowup depends on energy, appearing sooner and growing faster with ξ when the energy is low. The expanded beam usually shows a substantial tail consisting of only a few particles extending well beyond the main body of the beam.

The effect does not depend on fluctuations in the vertical oscillation but disappears if either the horizontal fluctuations or the horizontal tune shift go to zero. Apparently the horizontal fluctuations and tune shift can "turn on" the blowup if they both exceed certain threshold values, but the mechanism seems to saturate immediately and above-threshold fluctuation levels have little influence on beam size. Finally, resonance overlap occurs for this model at $\xi = .2$ to $.3$. It is thought to play a negligible role in the blowup phenomena observed here.

ACKNOWLEDGMENTS

I would like to thank F. Izrailev, B. Chirikov, H. Weidemann and A. J. Lichtenberg for their many helpful suggestions. This work was supported by ONR Contract N000 14-79-C-0674 and NSF Grant ECS 7826 376 A01.

REFERENCES

- [1] F. M. Izrailev, "Nearly Linear Mappings and Their Applications", submitted to Physica D for publication in 1980.
- [2] B. V. Chirikov, "A Universal Instability of Many Dimensional Oscillator Systems", Physics Reports 52, 5 (1979).

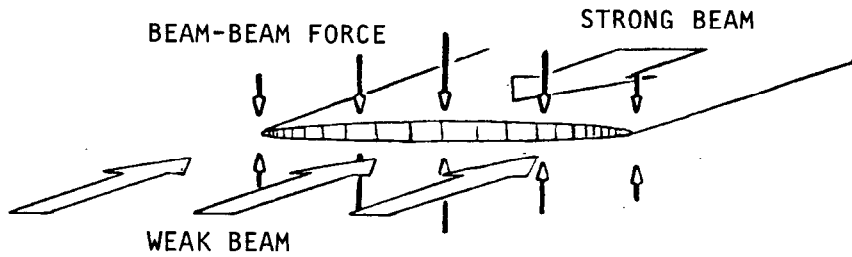


FIG. 1 BEAM-BEAM INTERACTION

In the weak-strong beam approximation, the strong beam is treated as a continuous charge-current distribution, while the weak beam is represented by discrete non-interacting particles. For flat e^+e^- beams, the vertical beam-beam force depends on the horizontal position of the individual particles and tends to compress the weak beam.

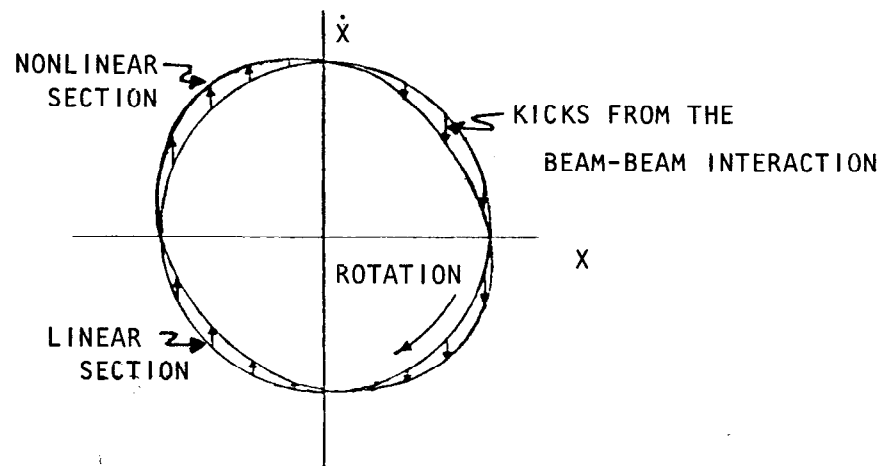


FIG. 2 PHASE SPACE ORBITS

The circular phase space orbits characterizing linear motion are distorted by the beam-beam interaction. The kicks, which always advance the phase, turn the circular sections of the invariant tori into ellipses which rotate at the betatron frequency.

FIG. 3 PARTIAL PROGRAM LISTING

FR1 and FR2 are the unperturbed tunes (usually 5.18 and 5.24),
 TS1 and TS2 are the linear tune shifts (usually between .01 and .1),
 E0 is the energy in GeV, nb the number of bunches, and ranf() a
 random number between zero and one.

```

c      set random number seed
      q=ranset(seed)

c      radial frequencies of betatron and synchrotron oscillation
      wr=twopi*fr2/nb
      ww=twopi*fr1/nb

c      linear rotation elements
      csr=cos(wr)
      snr=sin(wr)
      csv=cos(ww)
      snv=sin(ww)

c      damping time (twice the inverse of)
      c2=6.94e-06*eo**3*d2/nb
      c1=c2*d1/d2

c      quantum fluctuation jump
      ak2=sqrt(2.*c2)
      ak1=sqrt(2.*c1)

c      beam-beam interaction strength
      bs1=ts1*twopi*2.
      bs2=ts2*twopi*2.

c      set initial conditions
      do 110 i=1,8
      do 110 j=1,8
      l=(i-1)*8+j
      p(1,1)=i*.125
      p(1,2)=j*.125
      v(1,1)=0
110 v(1,2)=0

c      main loop starts here
      nn=n/10
      do 400 ic=1,10
      do 355 jc=1,nn
      i=(ic-1)*nn+jc
      do 350 j=1,64

c      this loop is vectorized
c      radial mapping
      hid(j)=p(j,2)
      p(j,2)=p(j,2)*csr+v(j,2)*snr
      v(j,2)=-hid(j)*snr+v(j,2)*csr

      hid(j)=ranf()*twopi
      p(j,2)=p(j,2)+ak2*cos(hid(j))
      v(j,2)=v(j,2)+ak2*sin(hid(j))
      *-v(j,2)*c2

c      radial beam-beam intersection
      v(j,2)=v(j,2)-bs2*p(j,2)/
      *(1.+(p(j,2)/2.26)**2)**2

c      vertical mapping
      hid(j)=p(j,1)
      p(j,1)=p(j,1)*csv+v(j,1)*snv
      v(j,1)=-hid(j)*snv+v(j,1)*csv

      hid(j)=ranf()*twopi
      p(j,1)=p(j,1)+ak1*cos(hid(j))
      v(j,1)=v(j,1)+ak1*sin(hid(j))
      *-v(j,1)*c1

c      vertical beam-beam interaction
      v(j,1)=v(j,1)-bs1*p(j,1)*
      *exp(-(p(j,2)**2)/2.)/
      *sqrt(1.+5*p(j,1)**2)

350 continue
355 continue

```

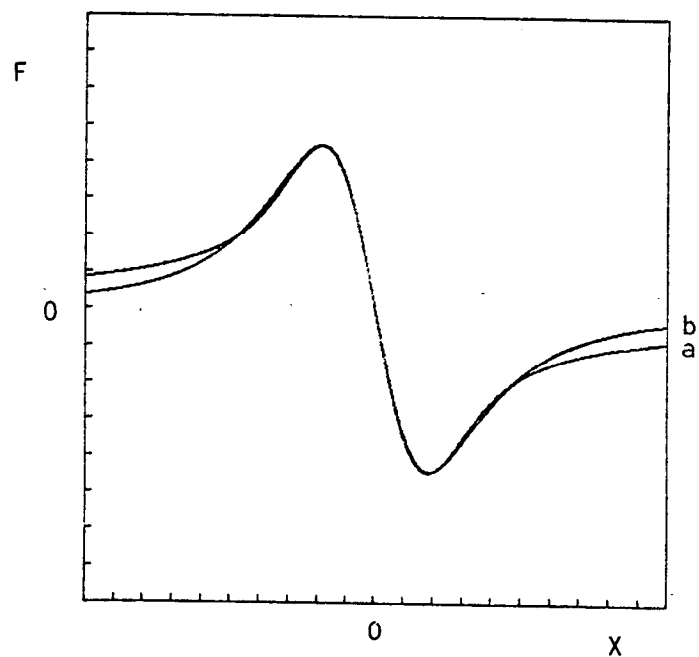


FIG. 4a HORIZONTAL BEAM-BEAM FORCE

- a) numerical result
- b) model result

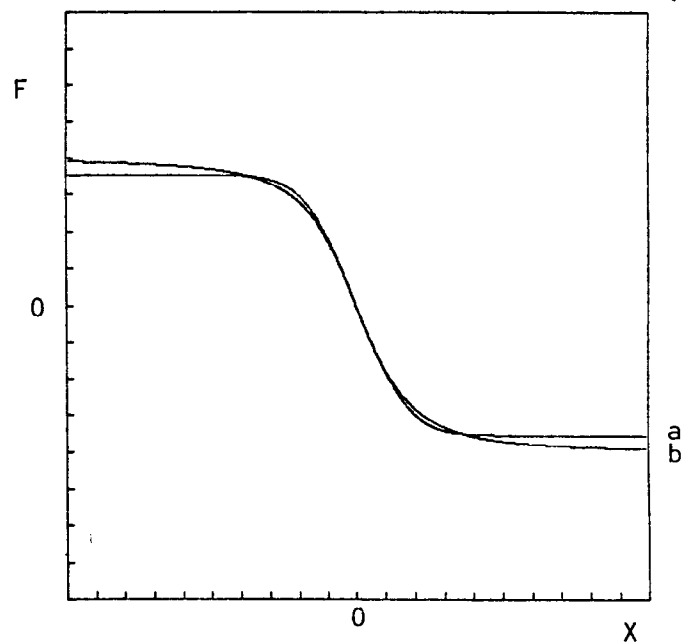


FIG. 4b VERTICAL BEAM-BEAM FORCE

- a) numerical result
- b) model result

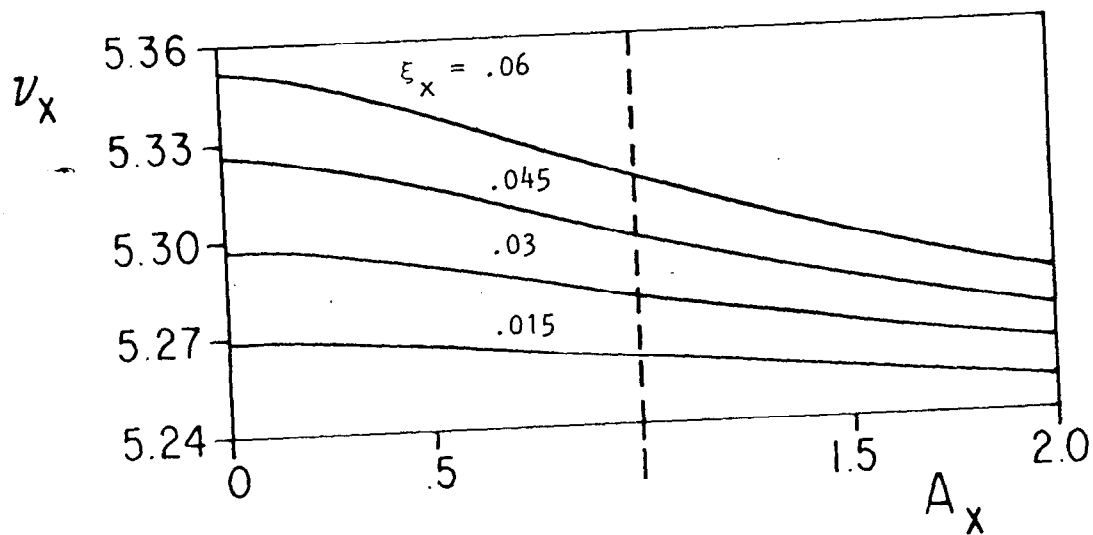


FIG. 5a HORIZONTAL TUNE VS. HORIZONTAL AMPLITUDE

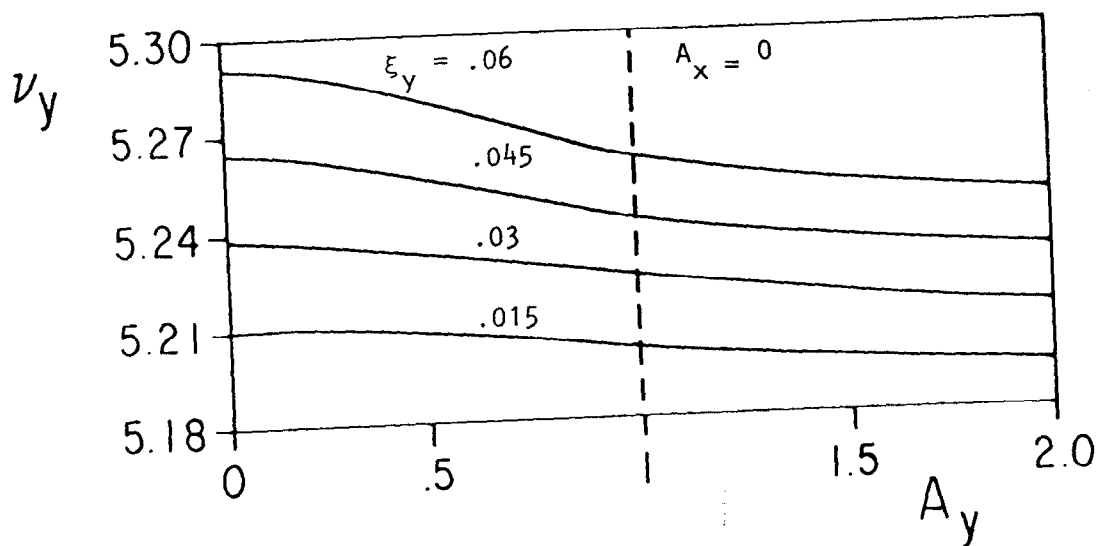


FIG. 5b VERTICAL TUNE VS. VERTICAL AMPLITUDE

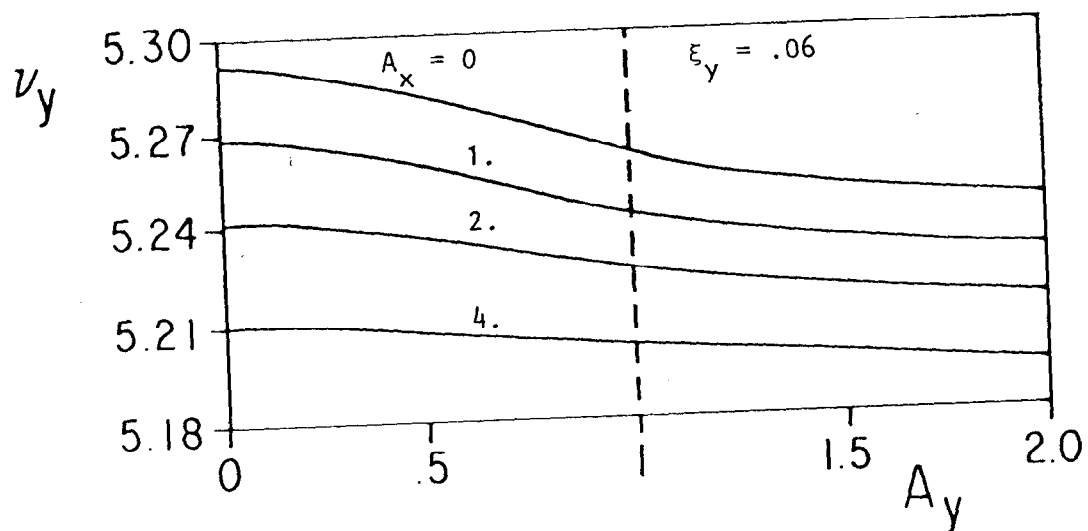


FIG. 5c VERTICAL TUNE VS. VERTICAL AMPLITUDE

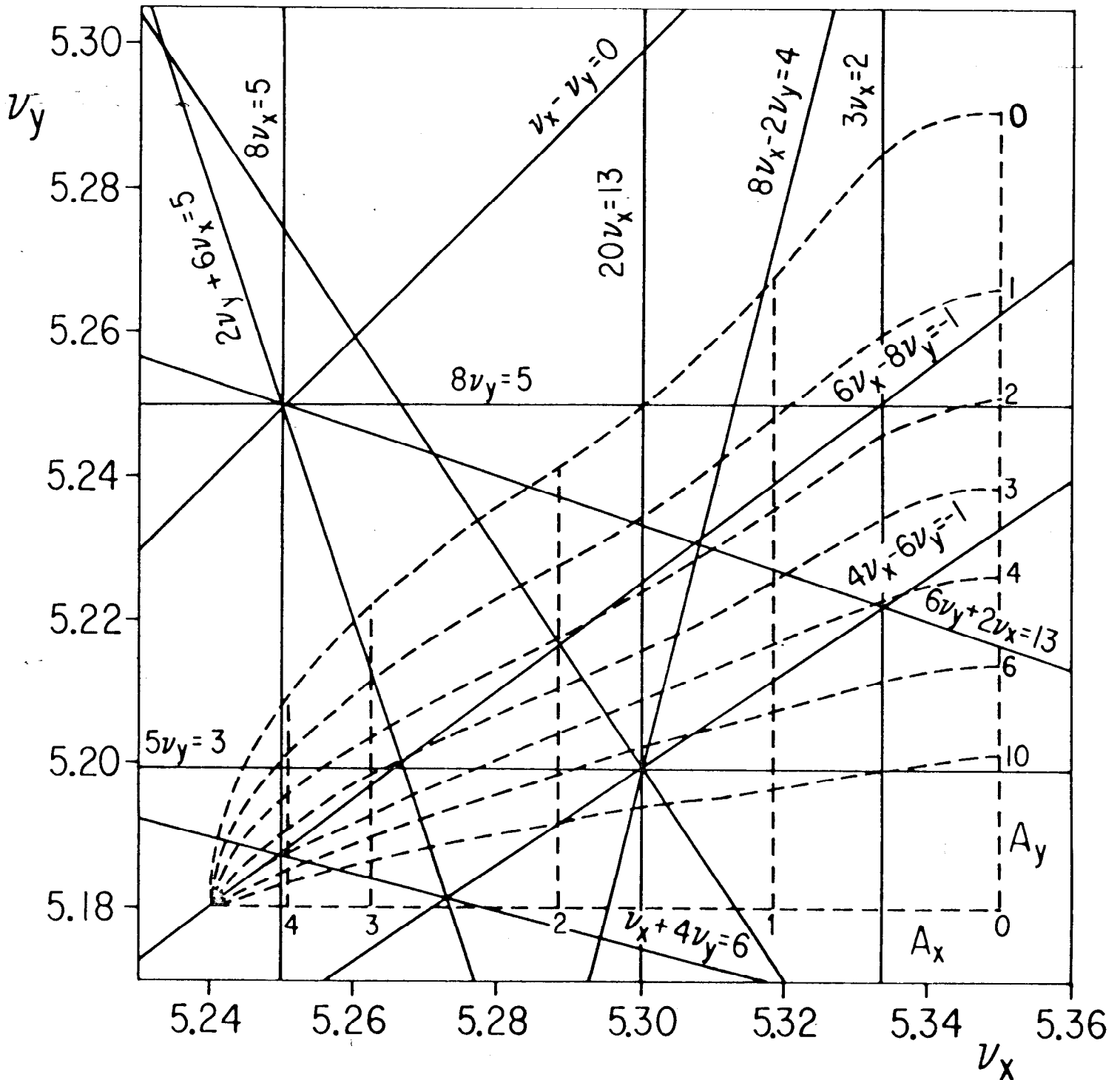


FIG. 6 TUNE DIAGRAM

The amplitude contours (dashed lines) for the weak beam are shown in frequency space. The non-intersecting tunes are $Q_x = 5.24$ and $Q_y = 5.18$, and the tune shifts are $\xi_x = \xi_y = .06$. This plot represents the simulation model and not necessarily the real beam.

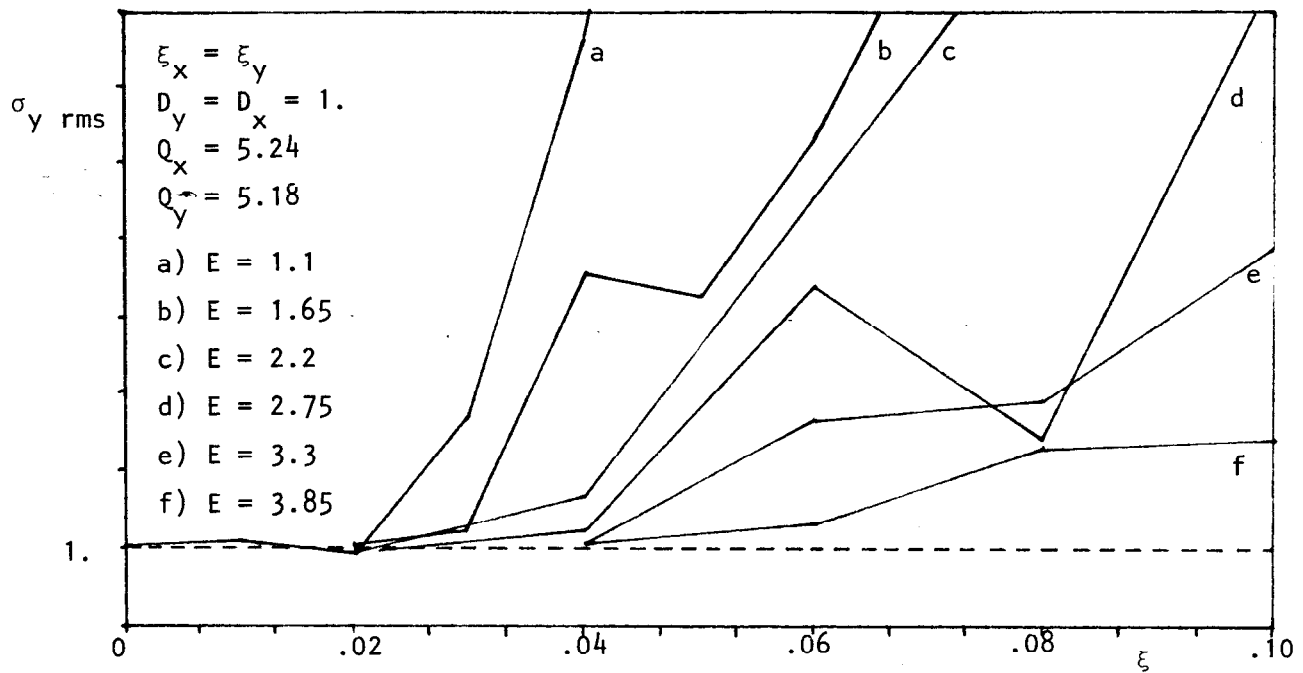


FIG. 7 BEAM HEIGHT DEPENDENCE ON ENERGY AND TUNE SHIFT

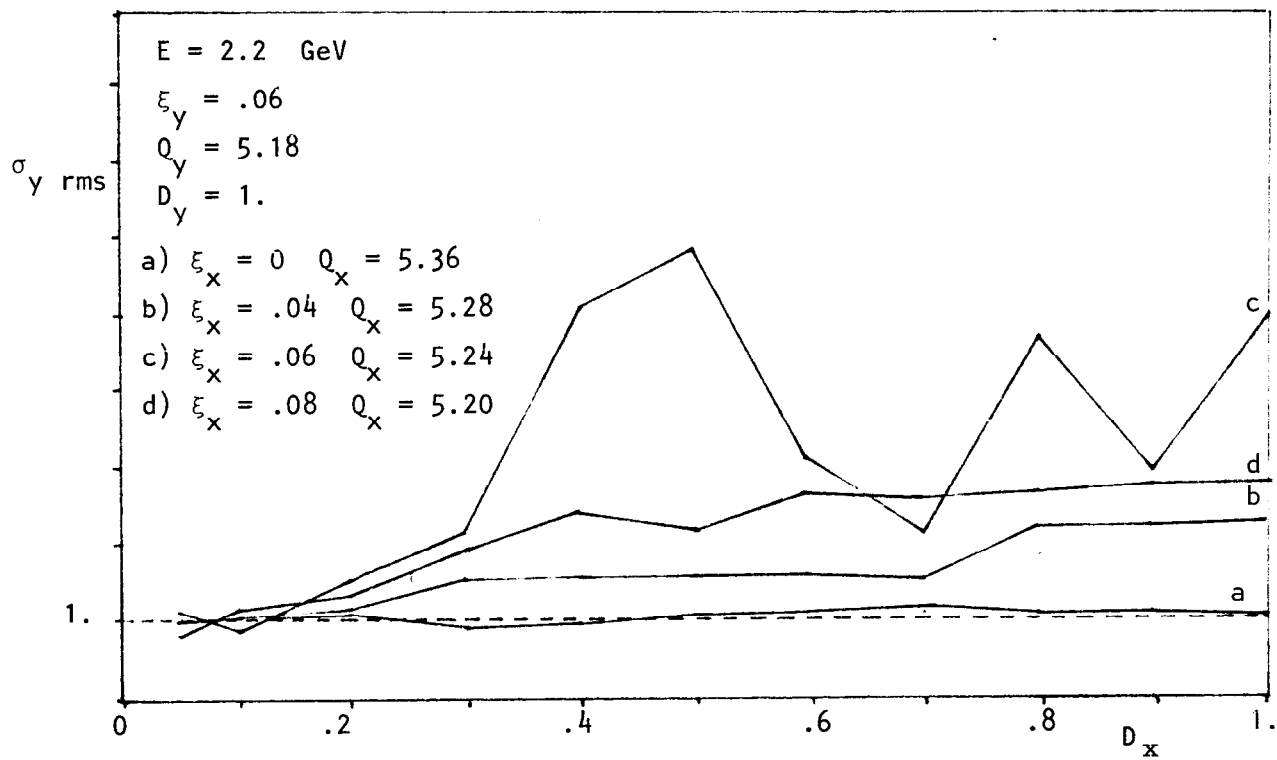


FIG. 8 BEAM HEIGHT DEPENDENCE ON HORIZONTAL FLUCTUATIONS AND TUNE SHIFT.

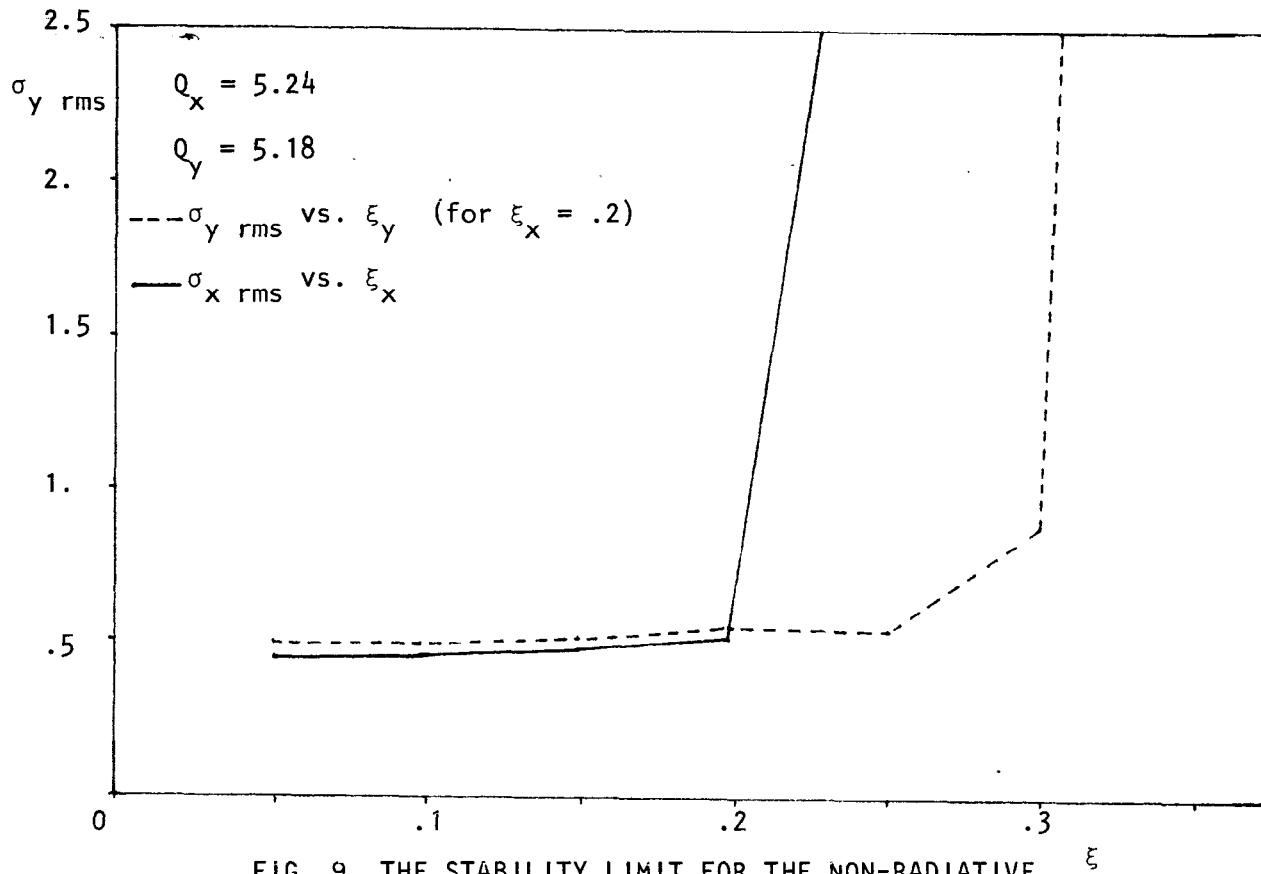


FIG. 9 THE STABILITY LIMIT FOR THE NON-RADIATIVE MODEL.

The beam-beam luminosity limitation in electron-positron colliding rings

Stephen Peggs and Richard Talman

Newman Laboratory of Nuclear Studies, Cornell University, Ithaca,
New York 14853

To account for observed luminosity limitations in electron-positron colliding rings we identify the leading effects, solve the non-linear single particle equation exactly, obtain the strong beam-strong beam equilibrium by numerical simulation, calculate the luminosity, and identify regions of bad beam lifetime.

PACS numbers: 29.20.Dh, 02.60.+y

The luminosity L of e^+e^- colliding rings has been disappointingly low. For sufficiently large beam current I , the luminosity fails to increase proportional to I^2 , as it would if the beam shapes remained constant. Also, beyond a current I_{\max} , the beam lifetimes become unacceptably short. These effects are due to the "beam-beam" interaction; that is, the electrostatic and magnetostatic forces on the particles in one

beam as they pass through the other. In this paper we identify the features of the motion leading to the observed behavior and we describe the solution of the equations governing the situation. The results conform with observations. We also give machine parameters expected to yield good and bad luminosity.

This beam-beam interaction has attracted rather broad interest.¹ A reason for this is that it suggests the possibility of experimental investigation of the onset of stochastic behavior in classical mechanics. Questions first raised in celestial mechanics² can, it is hoped, be studied in accelerators. But the presence of strong fluctuations and damping in electron rings (the only case considered here) reduces the characteristic number of revolutions to, say, 10^4 instead of, say, 10^{10} relevant for protons. As a result, recent rigorous mathematical studies of stability³ do not enter our discussion.

Our theoretical investigations have proceeded at three levels:

- a) Analytic solution of the single particle equation of motion.
- b) Tracking single particles in phase space.
- c) Numerical simulation of the entire strong beam-strong beam situation, including self-consistent relaxation to equilibrium in both transverse directions.

At level (a) it is possible to identify the important resonances controlling the situation and to estimate beam currents at which they become important. For more quantitative comparison with observation it is necessary to proceed to level (c). Simulations are capable of producing a wealth of detailed prediction, but to provide confidence in these results it is almost obligatory to develop parallel intuitive understanding at levels (a) and (b).

The single particle equation of motion of a particle in the presence of the other beam is a non-linear equation potentially exhibiting arbitrarily many resonances. We give an exact analytical solution of this equation accounting for all resonances. (It is hoped that this method can usefully be applied to other non-linear oscillatory systems.) y_m , the vertical "betatron" coordinate on the m 'th passage satisfies⁴

$$y_{m+1} - 2y_m \cos \omega_{y0} + y_{m-1} = f(x_m, y_m) . \quad (1)$$

At level (a) we assume the horizontal coordinate x_m is given inexorably by

$$x_m = a_x \cos(m\omega_{x0} + \phi) . \quad (2)$$

$\omega_{y0}/2\pi$ is called the vertical tune ν_{y0} and similarly for x . $f(x_m, y_m)$ gives the vertical angular deflection on the m 'th crossing. Equation (1) is equivalent to a more familiar first order difference equation, or mapping, relating 2 phase space coordinates on successive turns. For Gaussian beam profiles, x and y are measured in units of σ_x and σ_y , the respective standard deviations. Throughout we assume $\sigma_y \ll \sigma_x$ as the beams are usually ribbon-shaped in actual machines. f is given approximately by⁵

$$f(x_m, y_m) = -4\pi\xi_V \sin \omega_{y0} \frac{y_m}{1 + 1.6y_m^2} e^{-\frac{x_m^2}{2}} . \quad (3)$$

Here ξ_V is the customary vertical "linear tune shift" parameter specifying the strength of the beam-beam interaction. For small values of y_m , a leading term in (3) proportional to y_m can be grouped with the second term in (1) leading to a tune shift ξ_V . For sufficiently large values of ξ_V no real tune exists, corresponding to exponential growth that would occur except for non-linearity of f (such as a term proportional to y_m^3 which causes the tune to depend on amplitude). But controlled vertical beam growth normally

occurs at much lower values of ξ_y .

Parametric amplification of vertical oscillations can occur through terms in (3) such as $y_m a_x^2 \cos^2(m\omega_{x0})$, due to horizontal betatron (or synchrotron) oscillations. That is, the vertical oscillations are parametrically pumped by horizontal oscillations in much the way a garden swing can be pumped by the systematic shortening and lengthening of the pendulum length, and hence the natural frequency.⁶ We claim that this term and other similar terms are responsible for the increase in vertical beam size seen at e^+e^- storage rings in operation.

We now describe an iterative procedure for solving (1). Assume a double Fourier series expansion

$$y_m = a_y \cos(m\omega_y) + \sum_{r,s=1}^{\infty} a_{rs} \frac{\sin(rm\omega_y)}{\cos(rm\omega_y)} \frac{\sin(sm\omega_{x0})}{\cos(sm\omega_{x0})} + \dots \quad (4)$$

where the sum is extended over all combinations of sin and cos. The analysis truncates this series to a finite number of terms. It is not obvious that such an expansion should exist. Damping would usually, but not always, rule it out as it remains finite at large m . Empirically, for relevant values of ξ_y , we have always succeeded in finding such an expansion. The difference of ω_y from ω_{y0} is due to the perturbation.

When (4) is substituted into (3) a similar expansion can be made since f is periodic in $m\omega_y$ and $m\omega_{x0}$. The coefficients can be found by finite (fast) Fourier transform (FFT). The eigenfunctions of the linear difference operator on the left side of (1) are linear sinusoids. Expanding the Fourier transforms of y_m and f into sums of linear sinusoids (all possible sum and difference frequencies appear) enables the iterative production of new a_{rs} 's from old. A

stability threshold ξ_{\max} is reasonably well defined as that value at which the number of harmonics necessary for convergence proliferates. Allowing more harmonics, say 32 instead of 16, or more iterations usually makes little difference to the threshold. Normally one or two harmonics are especially large owing to the "resonance denominators" appearing in the iterative scheme.

For values of ξ_v roughly equal to ξ_{\max} and higher, phase space plots of the motion become very contorted and orbits of sufficient amplitude no longer spiral into the origin when damping is turned on. They damp instead to stable limit cycles reminiscent of those of Ref. 6.

Quantitative comparison with observations at the Cornell facility CESR and other storage rings is possible when other features are incorporated into the model. We have developed a strong-strong numerical simulation in which many particles ($\gtrsim 100$) in each of the two beams are tracked for many turns ($\gtrsim 3000$) in 6-dimensional phase space around a storage ring with two crossing points. The forms of the horizontal and vertical force fields are obtained in the flat beam profile limit, consistent with parametric driving of vertical oscillations by horizontal displacements and not vice versa. Energy oscillations are included since in CESR there is energy dispersion ($\eta^* \neq 0$) at present. The effects which determine the single beam size, namely horizontal quantum excitation, vertical coupling and radiation damping, are included with a betatron damping lifetime T of, typically, 1000 turns.

Self-consistent equilibrium distributions of each bunch and its associated force fields are allowed to develop for $\gtrsim 3T$. For a period of $0.3T$ one bunch is held rigid while the other relaxes. The development is recorded in, typically, 300 (turns) \times 100 (particles) \times 2 (crossing points) instances. From this history smooth distributions of the horizontal and vertical fields

of the relaxed bunch are calculated. Then the roles of rigid and relaxing bunches are reversed. It is possible for a particle to be "lost" if it strikes a mask (typically set at $\pm 10 \sigma_x$ and $\pm 10 \sigma_y$), and the lifetime is declared bad if it is less than (typically) 10 seconds. Otherwise the luminosity is calculated from the equilibrium bunch distributions which are usually identical, within statistics, at small ξ_V values but which may be quite different at high values, consistent with observations in existing storage rings.⁷

With the calculations which have been described we have surveyed the tune plane and typical results are shown in Fig. 1. For $\xi_V = 0.08$, contours of constant relative luminosity are shown. As used here, ξ_V is the "unrenormalized" tune shift parameter which would be observed if the beams maintained their single beam profiles. The measured or "renormalized" tune shift parameter would be less by perhaps a factor of two owing to the increase in beam height. In Fig. 1 some special assumptions have been made for easy comparison with the parametric oscillator model: $\eta^* = 0$, and ξ_H is temporarily neglected.⁸ The straight lines define the resonances associated with instability thresholds of Eq. (1). It can be seen that the valleys of bad lifetime indicated by shading are strikingly parallel with these lines. They are centered at slightly lower ν_y as would be expected since the linear tune shift moves the tune up. Also the regions of high and low ξ_{\max} correspond to the regions of high and low luminosity respectively. A few of the lines in Fig. 1 are reasonably strong resonances for Eq. (1) which do not conform well with the luminosity contours shown. Valleys of bad lifetime tend to show up along them at higher values of ξ_V .

In Fig. 2 a comparison between theory and experiment is shown. There is good agreement on the dependence of L on I and approximate agreement on the

value I_{\max} beyond which the lifetime is bad. In this plot the parameters have been adjusted to fit the data in the low I region where $L \propto I^2$. This is largely a matter of convenience as the expected simple relation between measured beam profiles and I and L is approximately satisfied at small I . The only other arbitrariness in Fig. 2 relates to the location of I_{\max} for which the lifetime is 10 seconds (much less than is acceptable in practice) with masks at $\pm 10\sigma$ (much smaller than is achievable in practice). Actual apertures, especially vertical, are not well known. When the vertical mask was raised to $\pm 12\sigma$ and the lifetime to 100 seconds, I_{\max} was found to be almost unchanged.

Another corroboration of the theory can be obtained, semi-quantitatively, by comparison with experience of the Stanford facility SPEAR at the four lattice points labelled A, B, C and D in Fig. 1. They found⁷ that the maximum luminosity increased steadily by a factor of about 5 in proceeding from A to D, but they could not cross the line

$$v_x = 2v_y$$

with two beams in spite of the fact that the presence of this line was undetectable with single beams. These observations are quite consistent with Fig. 1.

Finally, it is of interest and, one hopes, of practical importance to find optimal running parameters according to the theory. It is plausible, and tends to be borne out by the simulation, that $\eta^* = 0$ is optimal. Also from Fig. 1 the region around $v_{x0} = 0.4$, $v_{y0} \lesssim 0.1$ appears to be the most promising, but we have not expended enough computer time to prove this. On the other hand, many unambiguously bad regions have been identified and should be avoided in practice.

Acknowledgements

This work was supported in part by the National Science Foundation.

References

1. M. Month and J. C. Herrera, Nonlinear Dynamics and the Beam-Beam Interaction. AIP Conference Proceedings (New York, 1979), p. 57.
H. S. Uhm and C. S. Lin, Phys. Rev. Lett. 43, 914 (1979). They attacked the same problem but the picture presented in our paper is totally different and more detailed.
2. H. Poincare, Les Methodes Nouvelles de la Mecanique Celeste III (Gautiers-Villars, Paris, 1892). G. D. Birkhoff, Dynamical Systems, Amer. Math. Soc., 1927 (revised ed., 1966).
3. J. Moser, Ref. 1. Numerous other references are given here.
4. R. H. G. Helleman, Ref. 1. R. Talman, Cornell Internal Report, Jan. 1976 (unpublished).
5. An exact analytical expression for f can be obtained from M. Bassetti and G. A. Erskine, CERN-ISR-TH/80-06 (unpublished), in terms of the complex error function. Numerically, expression (3) agrees with the exact expression, to an accuracy of about 10% of the maximum value, for typical profiles.
6. K. Magnus, Vibrations (Blackie and Sons, Ltd., Glasgow, 1965). N. N. Bogoliubov and Y. A. Mitropolsky, Asymptotic Methods in the Theory of Non-Linear Oscillators (Gordon and Breach, New York, 1961).
7. H. Weidemann, Ref. 1.
8. The results are rather insensitive to the presence of noise in the horizontal motion provided the profile is kept unchanged.

Figure Captions

- Fig. 1. Contours of constant relative luminosity for $\xi_V = 0.08$, $\xi_H = 0.0$, $\eta^* = 0$. Bad lifetime regions are indicated by crosses. They also indicate the grid on which calculations were done. Contours are at 0.2, 0.4, 0.6, 0.8, 1.0, and 1.2. Lines identify instability thresholds of Eq. (1). Points labelled A, B, C and D identify lattice points for an investigation described in the text.
- Fig. 2. Dependence of luminosity on current. Comparison between experiment and theory at CESR. Limits imposed by bad beam lifetime are shown.

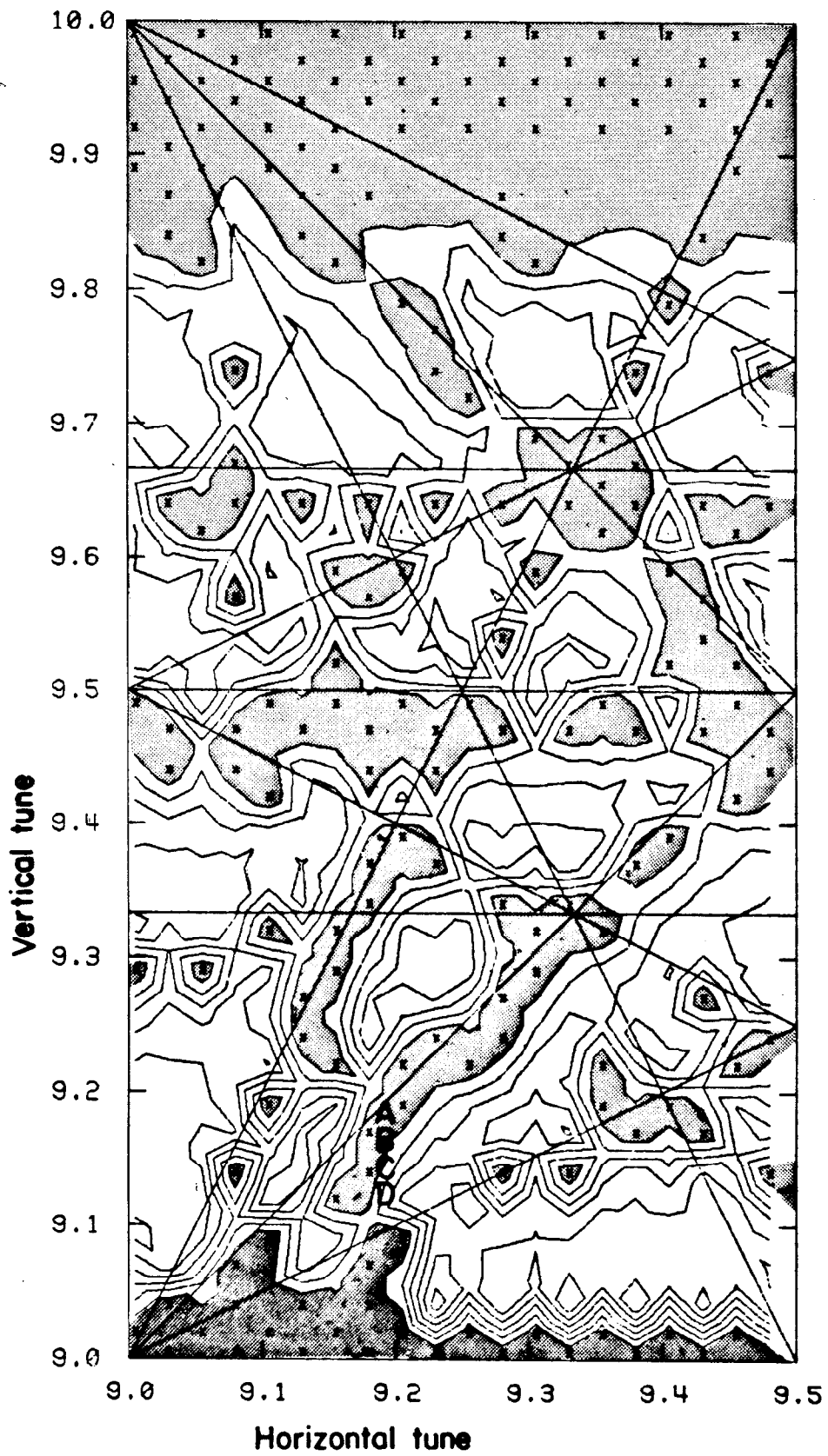


Fig. 1

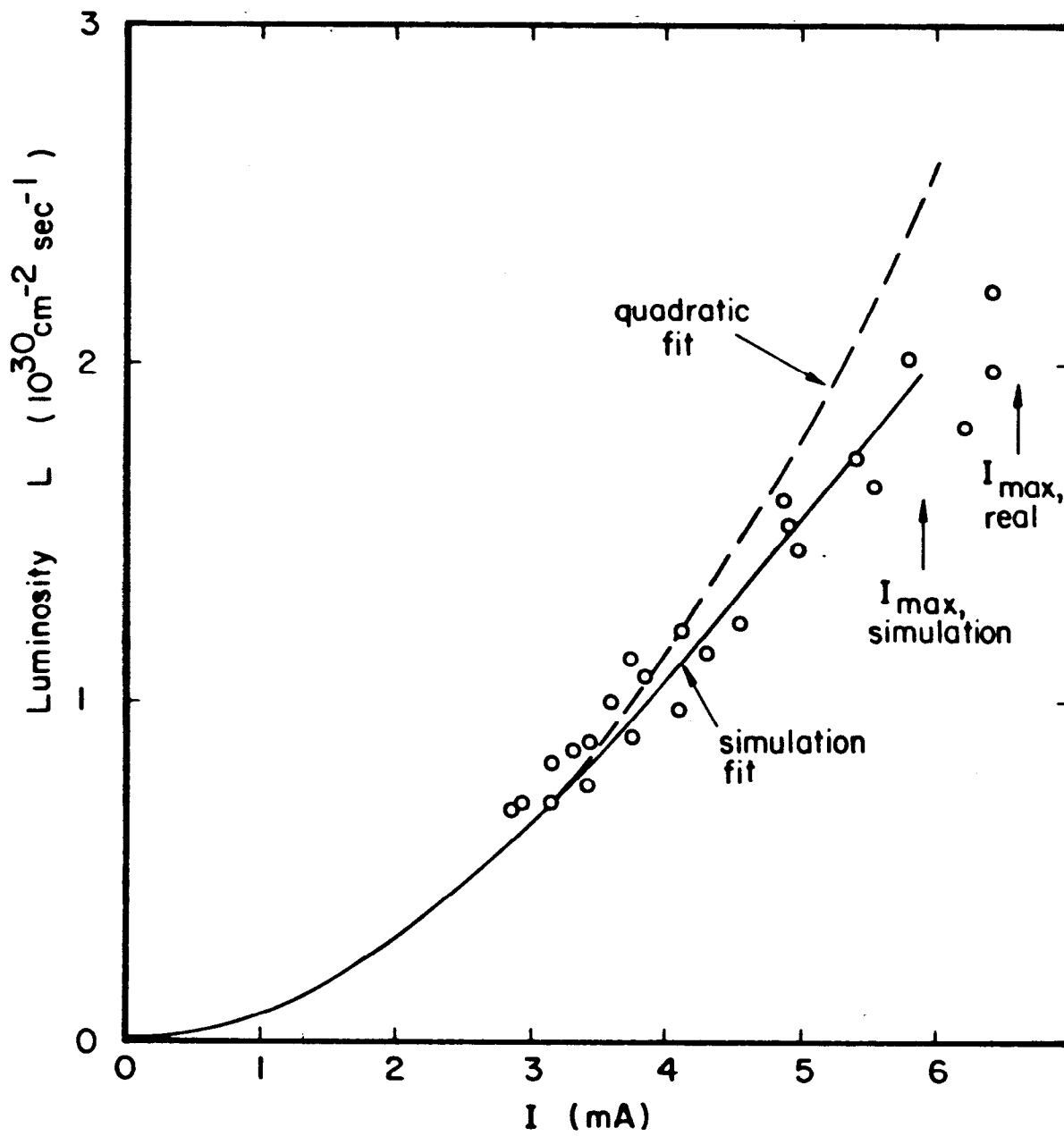


Fig. 2

BEAM-BEAM EFFECT AND LUMINOSITY IN SPEAR *)

H. Wiedemann

Stanford Linear Accelerator Center, Stanford University, P. O. BOX 4349
Stanford, California 94305 USA.

1. INTRODUCTION

Many measurements on the beam-beam limit in SPEAR have been performed over the past eight years since colliding beam operation began. The goal for these measurements was to find the proper parameterization of the beam-beam effect. Earlier measurements^{1,2)} in SPEAR, however, were limited in their validity by two circumstances. First, until 1978 we had no control over the so-called flip-flop phenomenon.³⁾ We did not even know about this effect because it seemed natural that due to the beam-beam interaction one of the beams — the "weaker" one — got vertically blown up when high current beams were brought into collision. In 1978 we found, however, that we could choose which beam gets blown up or, what is more important, we could manage to make the particle distribution in both beams the same. This can be done by adjusting the relative phase of the two rf systems located symmetrically on either side of the interaction points. As yet we do not understand this effect, but control of the flip-flop effect resulted in an increase in luminosity by a factor 1.5 to 2 (Fig. 1). All measurements in this report were done with both beams equally blown up. The second shortcoming of the earlier measurements was the limited energy variation possible in SPEAR. This led to erroneous energy scalings of the beam-beam incoherent tune shift parameter²⁾ ξ . In 1979 the magnet power supplies were modified such that operation at energies as low as 400 MeV was possible. We have made colliding beam measurements at energies as low as 600 MeV and together with earlier measurements we can now present the scaling of some relevant storage ring parameters from 600 MeV up to almost 4 GeV. All measurements have been done with a natural beam emittance of $\epsilon_x(\text{rad m}) = 5.0 \times 10^{-8} E^2$ (GeV^2), the wiggler magnets off, and with the following beam dynamic parameters at the interaction point

$$\begin{aligned} \nu_x &\approx 5.28 & \nu_y &= 5.17 \\ \beta_x^* &= 120 \text{ cm} & \beta_y^* &= 10 \text{ cm} \\ \eta_x^* &= 0 \end{aligned}$$

The damping time for transverse betatron oscillations is given by $\tau_{x,y}(\text{sec}) = 0.226/E^3$ (GeV^3). In all measurements the beam currents were equal to better than 10% and there is only one bunch per beam in SPEAR.

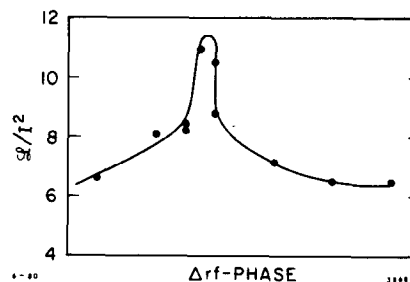


Fig. 1. Effect of the beam beam flip-flop on the specific luminosity.

* Work supported by the Department of Energy under contract DE-AC03-76SF00515.

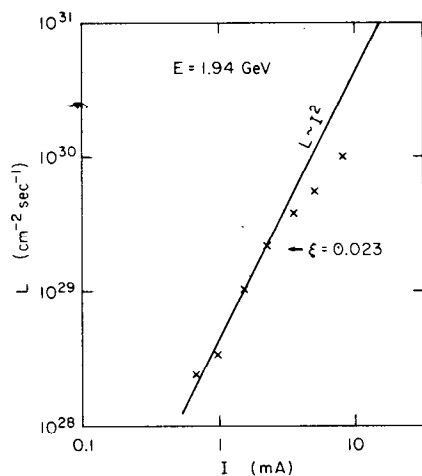


Fig. 2. Typical variation of luminosity with beam current.

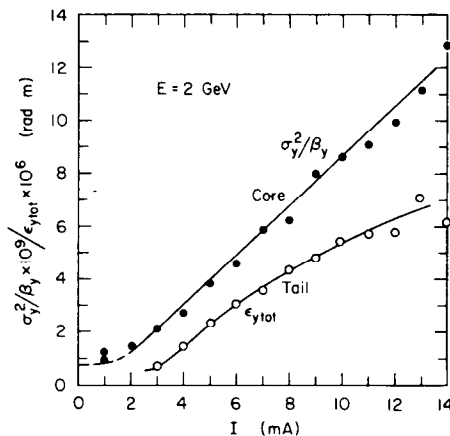


Fig. 3. Beam height as a function of colliding beam current.

2. OBSERVATIONS ON THE BEAM-BEAM EFFECT

When two beams at not too low an intensity are brought into collision usually one beam is blown up much more than the other one. By adjusting the flip-flop effect we can make both beams equal and achieve maximum luminosity. A typical luminosity curve versus beam current I is shown in Fig. 2. At very low currents there is no beam blowup and the luminosity scales as expected, like I^2 . As the current is increased we reach a threshold above which the vertical beam size increases due to the beam-beam effect. The horizontal beam size is not affected within the errors of observation. In Fig. 3, the increase of the vertical beam emittance is shown as a function of the colliding current. One curve represents the vertical emittance of the core of the beam as calculated from the luminosity. The other curve shows the vertical emittance of the total beam (tails) as determined by lifetime measurements with scrapers. The core emittance increases linear with beam current while the emittance of the tail increases somewhat differently. The limit is reached as soon as the tail emittance reaches the acceptance of the storage

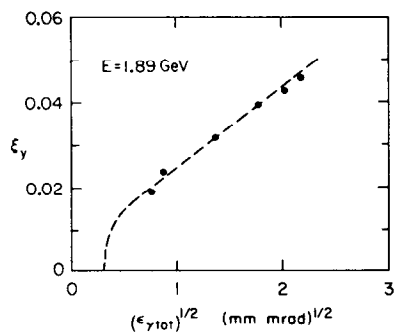


Fig. 4. Maximum tune shift parameter as a function of the ring acceptance.

ring. We have reduced the acceptance of the storage ring by scrapers and measured the maximum beam-beam tune shift as a function of the aperture in SPEAR (Fig. 4). It is clear from these measurements that the beam-beam effect generates a vertical blow up which is stopped by some effect — probably damping. The absolute limit on the beam-beam effect, and, therefore, the maximum luminosity, then is reached when the vertical beam size reaches the aperture limit. Later in this note we will have to come back to this point. In Fig. 5, data at or near maximum luminosity as

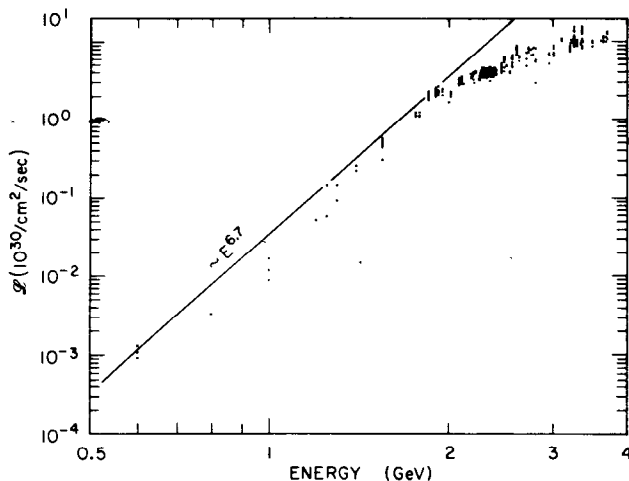


Fig. 5. Maximum luminosity in SPEAR.

linear tune shift parameter ξ_y in Fig. 7. This tune shift parameter ξ_y was calculated from the luminosity by

$$\xi_y = (2r_e mc^2 e) \beta_y^* \frac{\mathcal{L}/I}{E(1 + \sigma_y^*/\sigma_x^*)} \quad (1)$$

This equation is derived by combining the definition of the luminosity $\mathcal{L} = (4\pi e^2 f)^{-1} \cdot I^2 / (\sigma_x^* \sigma_y^*)$ and the linear tune shift parameter

$$\xi_y = (r_e mc^2 / 2\pi e f) I \beta_y^* / E / \sigma_x^* \sigma_y^* / (1 + \sigma_y^* / \sigma_x^*) \quad (2)$$

Here $r_e = 2.84 \times 10^{-15}$ m, $mc^2 = 0.511$ MeV, e the electron charge, f the revolution frequency and σ_x^*, σ_y^* the beam width and height at the interaction point. The effective beam height σ_y^* is calculated from the luminosity assuming the theoretical beam width σ_y^* which is precise enough for the correction factor

$(1 + \sigma_y^* / \sigma_x^*)$. We find in Fig. 7 the vertical linear beam-beam tune shift parameter to scale like

$$\xi_y \sim E^{2.4}$$

up to about 2 GeV. Above that energy the tune shift parameter is constant

The limitation seems to be distinctively different for energies below and above 2 GeV. Below 2 GeV, the limit is consistent with the aperture of SPEAR. Above

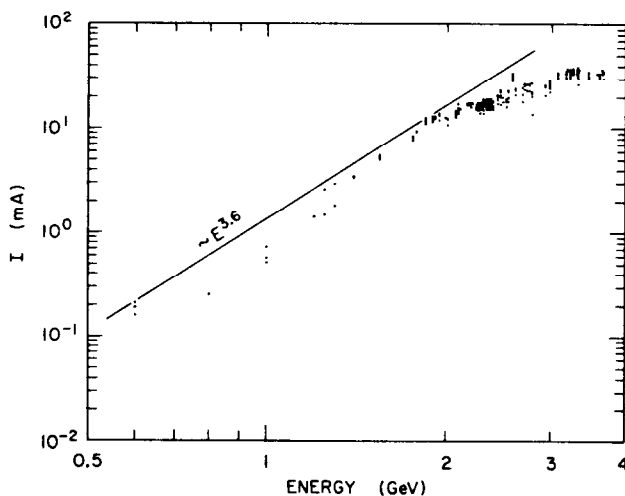


Fig. 6 Maximum colliding beam currents in SPEAR.

achieved in normal runs for high energy physics, as well as in accelerator studies runs, are collected. The maximum luminosity scales like $E^{6.7}$ up to an energy of about 2 GeV. This is in agreement with the $\mathcal{L} \sim E^7$ scaling reported from Adone.⁴⁾ Note that for lack of time the measurements at 0.8 and 1.0 GeV do not yet represent the maximum achievable luminosities. The associated beam currents are shown in Fig. 6 and the

2 GeV we cannot make a

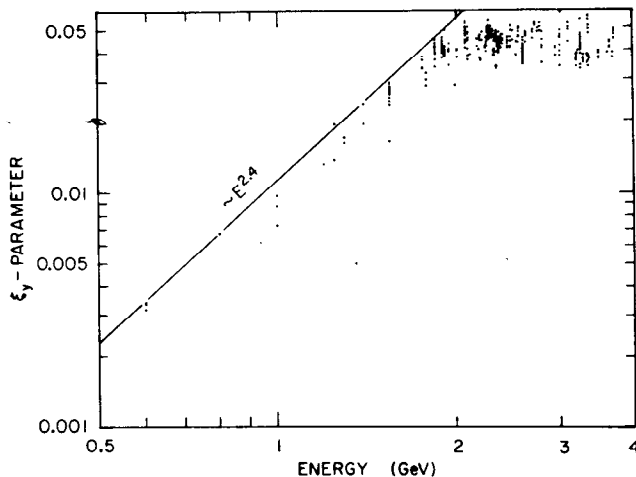


Fig. 7. Maximum tune shift parameter in SPEAR.

and lower energies the tune shift stays constant and only the vertical beam size increases till the limit is reached. In another experiment (Fig. 9) the current and the energy was kept constant but the value of β_y^* was varied. Here again we experience a saturation of values of $\xi_y \approx .06$.

For the design of new storage rings it would be extremely interesting to know what separates the two regimes in order to determine where the new storage ring will operate. Since a similar limit at about the same value for ξ_y has been observed also in Adone⁴⁾ it may very well be a fundamental limitation due to the mere magnitude of the nonlinear perturbation. In this case a proper theory is needed to be able to scale the transition point from one storage ring to another.

So far we have not addressed the horizontal linear tune shift parameter ξ_x . Since we do not observe any significant horizontal beam blow up we conclude that the horizontal tune shift parameter does not take part in the beam-beam limit. In particular, we observed that ξ_x can be much larger than ξ_y . At the beam-beam limit for the

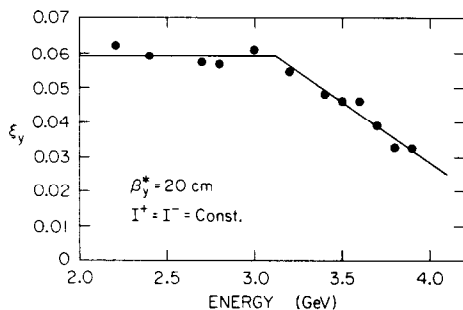


Fig. 8. Tune shift parameter vs. energy for constant beam currents.

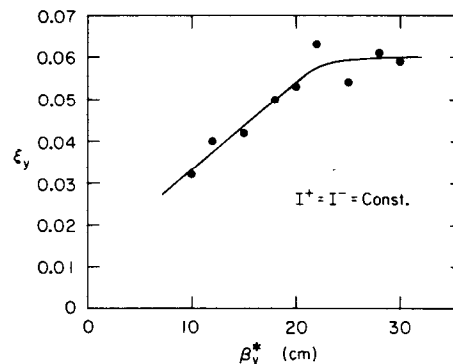


Fig. 9. Tune shift parameter vs. β_y^* for constant beam currents.

similar statement since not enough detailed measurements have been performed. The different behavior is further illustrated in two other measurements. In Fig. 8 the linear tune shift parameter ξ_y is shown as a function of energy for a constant beam current $I^+ + I^- = \text{const}$ and a vertical betatron function at the interaction point of $\beta_y^* = 20$ cm. Above 3 GeV the tune shift parameter drops as expected $\xi_y \sim E^{-3}$. At 3 GeV

following two energies we have:

Energy	600 MeV	2.0 GeV
ξ_x	.016	.040
ξ_y	.0034	.045

This may or may not be a peculiarity of SPEAR since in all cases the beam at the interaction point is rather flat.

3. SCALING OF BEAM-BEAM RELATED PARAMETERS

In the rest of this note we will discuss only the measurements up to 2 GeV, that is in the regime where the maximum linear tune shift parameter changes with energy. From the measurements we obtain the following scaling laws:

$$\begin{aligned} \mathcal{L}_{\max} &\sim E^{6.7 \pm 0.1} \\ I_{\max} &\sim E^{3.6 \pm 0.1} \\ \xi_y \max &\sim E^{2.4 \pm 0.1} \end{aligned}$$

We also observe a threshold current above which the vertical beam size becomes blown up. If we plot $\mathcal{L}/E^{6.7}$ versus $I/E^{3.6}$ in the regime between threshold and beam-beam limit for different energies we find a common behavior (Fig. 10):

$$\frac{\mathcal{L}}{E^{6.7}} = \text{const} \cdot \left(\frac{I}{E^{3.6}} \right)^{1.5 \pm 0.1} \quad (5)$$

From this we can derive a scaling law for the vertical beam size. Using the definition equation of the luminosity, we get

$$\frac{\mathcal{L}}{E^{6.7}} \sim \frac{I^{1.5}}{\sigma_x^* \sigma_y^* E^{1.3}} \left(\frac{I}{E^{3.6}} \right)^{1.5 \pm 0.1}. \quad (6)$$

Since $\sigma_y^* \sim E$ we get

$$\sigma_x^* \sim \frac{I^{1.5}}{E^{2.3 \pm 0.4}} \quad (7)$$

Eq. (7) is in agreement with the observation at PETRA⁵⁾ where $\sigma_y^* \sim I^{1/2}/E^2$ was measured. If we now use the measured scaling for the maximum current from Eq. (4),

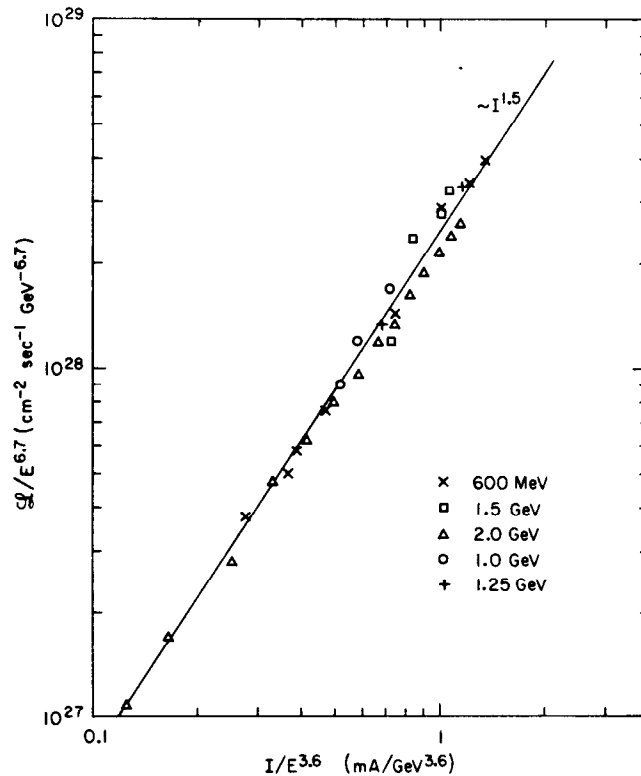


Fig. 10. Normalized luminosity vs. normalized current SPEAR.

we get

$$\sigma_y \text{ max} \sim \frac{I_{\text{max}}^{1/2}}{E^{2.3 \pm 0.4}} \sim E^{-0.5 \pm 0.45} \approx \text{const.} \quad (8)$$

This again is a confirmation that the maximum beam-beam limit in SPEAR is reached at all energies below 2 GeV as soon as the vertical beam size approaches a certain value which is consistent with the SPEAR aperture limit. The total vertical beam size at the beam-beam limit has been measured for a few different energies and configurations and agrees within the errors of the measurement with the acceptance of the SPEAR storage ring.

The scaling of luminosity curves at different energies in SPEAR (Fig. 10) encouraged the author to try for a common scaling for all storage rings. In Fig. 11 the results of such a tryout is plotted. Over many orders of magnitudes the luminosities scale the same way in all storage rings if we normalize the luminosity on the damping and use the number of particles per bunch rather than the beam current. There are certainly more subtle differences between different storage rings as beta functions, tunes, etc. These differences, however, account only for factors two to maybe five in the luminosity.

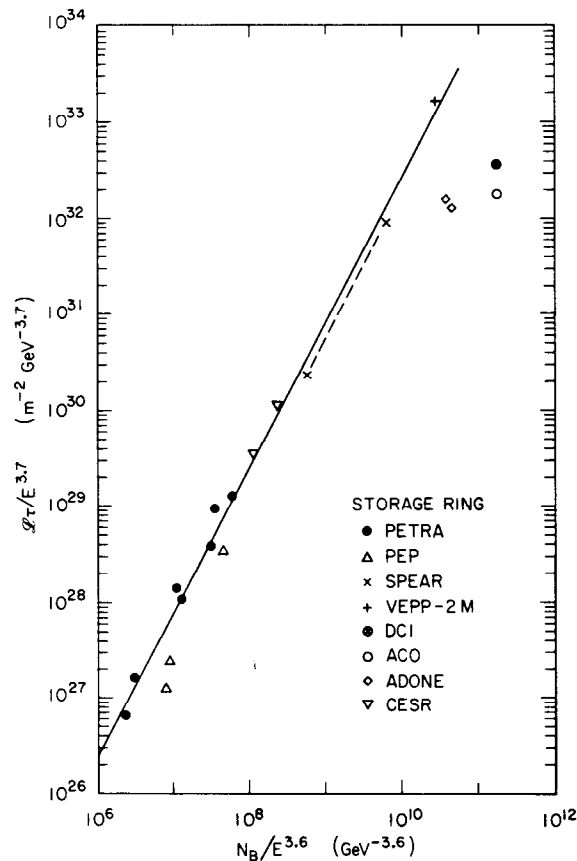


Fig. 11. Luminosity scaling in different storage rings.

On the scale of Fig. 11, these small factors, however, do not show up.

Three storage rings (ACO, ADONE and DCI) seem to behave differently. This might be due to the fact that these storage rings have no beta section and run at the coupling resonance, whereas all the other storage rings have small vertical betatron functions at the interaction point and run at minimum coupling.

The common scaling suggests the same process to be responsible for the beam-beam effect in all storage rings. From Fig. 11 we get

$$\frac{\mathcal{L}\tau}{E^{3.7}} \sim \left(\frac{N_B}{E^{3.6}} \right)^{3/2} \quad (9)$$

where τ is the transverse damping time and N_B the number of particles per bunch.

CONCLUSION

Measurements performed at SPEAR have been discussed and scaling laws for the maximum luminosity and the maximum linear tune shift parameter with energy are shown. We made the following observation: there are two distinct regimes, one below 2 GeV where the linear tune shift parameter scales like $\xi_y \sim E^{2.4}$ and the other regime where this parameter is constant $\xi_y \approx 0.05$ to 0.06. In the lower energy regime the limit is reached when the vertical beam size is blown up to the acceptance of the storage ring. We do not observe a significant (< 10%) horizontal beam blow up and the value of the horizontal linear tune shift parameter ξ_x does not seem to be related to the beam-beam limit.

ACKNOWLEDGEMENT

The author wishes to thank the SPEAR operations group for the continuous help and support in performing the measurements. B. Richter, E. Paterson and J. Harris have given me much support and encouragement during the difficult measurements at very low energies which I am pleased to acknowledge.

* * *

REFERENCES

1. H. Wiedemann, Measurements on Beam-Beam Interaction at SPEAR, IEEE, Vol. NS-20, No. 3, 838-842 (1973).
2. H. Wiedemann, Experiments on the Beam-Beam Effect in e^+e^- Storage Rings, Nonlinear Dynamics and the Beam Beam Interaction, ed. M. Month, American Institute of Physics, New York (1979).
3. M. H. R. Donald and J. M. Paterson, An Investigation of the Flip-Flop Effect in SPEAR, IEEE, Vol. NS-26, No. 3, 3580 (1979).
4. S. Tazzari, Beam-Beam Effects at the 1.5 GeV e^+e^- Storage Ring Adone, Nonlinear Dynamics and the Beam Beam Interaction, ed. M. Month, American Institute of Physics, New York (1979).
5. G. A. Voss, First and Only Partial Analysis of Space Charge Effect in PETRA, DESY M-VM-79/6 (1979).

RECENT EXPERIMENTAL RESULTS ON THE BEAM-BEAM EFFECTS
IN STORAGE RINGS AND AN ATTEMPT OF THEIR INTERPRETATION*

S. Kheifets
Stanford Linear Accelerator Center
Stanford University, Stanford, California 94305

SUMMARY

The latest available experimental results on the luminosity, the space charge parameters, and the beam blowup as functions of particle energy and beam current are reviewed. The comparison with the phenomenological diffusion theory are done and useful scaling laws are derived. Some implications for $\bar{p}p$ storage rings are discussed.

Invited talk presented at
The Seminar on the Beam-Beam Interactions
Stanford Linear Accelerator Center
Stanford University, Stanford, California 94305
May 22 and 23, 1980

(A shorter version of this paper was contributed to the XI International Conference on High Energy Accelerators, CERN, Geneva, Switzerland, July 7 - 11, 1980)

*Work supported by the Department of Energy, contract DE-AC03-76SF00515.

CONTENTS

Introduction

1. Experiment
 - 1.1 Main Relationships and Assumptions
 - 1.1.1 Luminosity
 - 1.1.2 Space charge parameters
 - 1.1.3 Life time
 - 1.1.4 Parameters of interest
 - 1.1.5 Experimental conditions and assumptions
 - 1.2 Recent experimental results
 - 1.2.1 Procedure of calculating values of interest
 - 1.2.2 SPEAR. Dependence on energy (H. Wiedemann)
 - 1.2.3 SPEAR. Dependence on current (M. Cornacchia)
 - 1.2.4 ADONE (S. Tazzari)
 - 1.2.5 PETRA (G. Voss)
2. Theory
 - 2.1 Assumptions
 - 2.2 Beam blowup according to diffusion theory
 - 2.3 Scaling laws
3. Experiment and theory compared
4. Some speculations on $\bar{p}p$ storage rings

Acknowledgments

References

Introduction

Although there are a number of excellent papers^{1-3,14} on the beam-beam phenomena, the importance of the problem which implies the most severe limitation on the beam currents of the storage ring as well as recent availability of new experimental results⁴⁻⁶ and theoretical approach⁷ make it quite feasible to add to the list.

The problem has also an important practical impact on many storage rings of the immediate future. For an electron-positron storage ring it can give, by applying the appropriate scaling laws, some insight on the acceptable magnitude of the space charge parameter. The same is also true for $p\bar{p}$ machine which can be considered, with respect to the beam-beam effect, as e^-e^+ ring with extremely small particle energy.

Although the beam-beam effect itself is rather crude and well pronounced, a theoretical description of it is very difficult to give both analytically and numerically. The main difficulty lies in the nonlinear character of the forces involved and to some extent in the complicated dependence on many beam and machine parameters interlacingly influencing each other.

In this situation a phenomenological approach seems to be adequate. A proper parameterization of the problem and description of many functional dependencies by a few fitting parameters can supply us with needed scaling laws. The behavior of such a fitting parameter with energy for example cannot be explained by a theory. This dependence will be found from an experiment. But after it is established it

can have certain predictive power and will give some insight for the future accelerators.

There is also some hope to find suitable theoretical ground for the accepted dependencies in the numerical analysis of the problem. Much work is needed in this respect.

In this work I suggest some scaling laws for the luminosity, space charge parameters, and beam size as functions of particle energy, maximum beam current, and the number of bunches. These scaling laws are derived from the latest experimental data available now.

The biggest drawback of the description suggested here, as I see it, lies, contrary to the observations, in the complete absence of the fitting parameter dependence on the machine tune. This drawback can be attributed to an averaging procedure needed for a diffusion-like description of the process. By this averaging all resonance structure of the particle motion is completely lost. It is probable that the resonance and diffusion approaches could be complementary to each other. Again much work is needed here.

Section 1 of this work is devoted to the recent experimental results from SPEAR,^{4,8} ADONE,⁵ and PETRA.⁶ In Section 2 the diffusion theory is used to derive main relationships and, together with the experimental results, to get main scaling laws. In Section 3 we summarize these scaling laws, and in Section 4 some predictions for future storage rings are done based upon the scaling laws.

1. Experiment

Before discussing recent experimental results observed on different electron storage rings it is useful to look first at the conditions in which they are obtained and the assumptions under which they are interpreted.

1.1 Main relationships and assumptions

First of all let us discuss relevant storage ring parameters as well as experimental conditions under which they are usually measured. I will list the main parameters and relationships between them although the latter are all well known.

1.1.1 Luminosity of the storage ring for the head-on collision of two identical beams is usually assumed to be

$$\mathcal{L} = \frac{i^2}{4\pi e^2 f B \sigma_x \sigma_y} \quad (1)$$

where i is the current in either of two beams, B is the number of bunches in each of the beams, f is the revolution frequency of the particle with the charge e , σ_x and σ_y are horizontal and vertical dimensions of the bunch (rms widths if the distribution is Gaussian) at the interaction point.

1.1.2 Space charge parameters under the same conditions are given by the following formulae

a) for the vertical motion

$$\xi_y = \frac{e i \beta_y}{2\pi f B E \sigma_y (\sigma_x + \sigma_y)} \quad (2)$$

b) for the horizontal motion

$$\xi_x = \frac{e i \beta_x}{2\pi f B E \sigma_x (\sigma_x + \sigma_y)} \quad (3)$$

In these formulae β_x and β_y are values of horizontal and vertical β -functions at the interaction point, E is particle energy. Both the luminosity \mathcal{L} and the space charge parameters ξ_y and ξ_x depend on the bunch size which is very difficult to measure directly. But it is clear that both values are sensitive to the charge distribution in the core of the beam rather than to the tails of it. At the same time it is known² that tails are affected by the beam-beam interaction much more strongly than the core.

1.1.3 The beam lifetime T for a single Gaussian bunch is given by⁹

$$T = \tau e^{\zeta/2} / \zeta, \quad (4)$$

where τ is the vertical damping time

$$\frac{1}{\tau} = C_Y f E^3 / 2\rho \quad (5)$$

$C_Y = 8.85 \times 10^{-5} \text{ m/GeV}^3$, ρ = bending radius in m, E the energy in GeV.

$$\zeta = \Sigma^2 / \sigma^2 \quad (6)$$

Σ is an effective aperture of the machine. The beam lifetime is sensitive to the distribution of the particles in the tails where the beam-beam interaction changes distributions significantly. That makes

the maximum luminosity strongly dependent upon the value of the maximum beam current which in turn happens to be a fast function of the particle energy.

1.1.4 Parameters of interest. Among the machine parameters entering into expressions (1-6), the energy E , the number of bunches B , and the revolution frequency f are known with great accuracy. The luminosity \mathcal{L} and the beam current i can be measured directly.

On the other hand, several other parameters such as β_x, β_y are very difficult to measure. Although one can expect that β_x, β_y should be modified by the beam-beam force, these functions are changed only in the second order of the perturbation theory and therefore usually are assumed to be equal to their theoretical value at the zero current. The same holds for the horizontal beam emittance ϵ_x and consequently for the horizontal beam size $\sigma_x = \sqrt{\epsilon_x \beta_x}$.

1.1.5 Experimental conditions and assumptions. Experimental data on the beam-beam effect are obtained on different machines virtually in quite different conditions.

- a) The investigation of the beam-beam limitations. Measurements of this kind are done during special machine physics runs. The main goal of these measurements is to achieve the maximum possible luminosity for given parameters by increasing the currents to the point where the lifetime of the beam starts to decrease sharply. To maximize the luminosity of the ring both currents are usually maintained pretty much the same. For the SPEAR measurements⁴

$$2(i_+ - i_-)/(i_+ + i_-) \lesssim (2-3)\%$$

One tries to do the same with the vertical size of the beam. At least at SPEAR this condition was met by means of adjustment of the phase between the rf cavities positioned symmetrically around the interaction point.¹⁰

Experimental data obtained in this situation should be more sensitive to the particle distribution at large amplitudes (to the tails of distribution) rather than to the distribution in the core of the beam.

- b) The investigation of the storage ring performance. Measurements of this kind are usually done during high energy physics runs in a parasitic mode. Maximum luminosity is achieved in this case under a restrained condition of the beam lifetime being unaffected or almost unaffected by beam-beam phenomena. These measurements should be more sensitive to the distribution in the core of the beam.

In all of the storage rings the longitudinal size of the bunch σ_ℓ is much less than β_y . If this condition were not fulfilled, different particles along the bunch would experience different focusing and the results could be distorted by this effect. As we shall see later, it is assumed usually that the distribution of the particles is Gaussian, at least in the core. This assumption one needs to be able to calculate the space charge parameters from the measured luminosity and current.

In some aspects there is also a difference between the strong beam-strong beam and the strong beam-weak beam interactions.

1.2 Recent experimental results

An experimental fact observed on all the machines is that the horizontal size of the bunch is not influenced by the beam-beam interaction^{2,6} with the accuracy $\lesssim 10\%$.

1.2.1 Procedure of calculating values of interest

It is instructive first to see how one can derive the relevant parameters from the measured ones.

a) First of all assuming σ_x to be equal to $\sqrt{\epsilon_x \beta_x}$, one can find beam aspect ratio σ_y/σ_x from the measured luminosity (1):

$$\sigma_y/\sigma_x = i^2/4\pi e^2 f B \sigma_x \mathcal{L} \quad (7)$$

b) Formula (3) then allows us to find the horizontal space charge parameter

$$\xi_x = e i \beta_x / 2\pi f B E \sigma_x^2 (1 + \sigma_y/\sigma_x) \quad (8)$$

c) After eliminating σ_y from (1) and (2) one gets:

$$\xi_y = 2e^3 \mathcal{L} \beta_y / E i (1 + \sigma_y/\sigma_x) \quad (9)$$

Let us review the recent experimental results obtained on different storage rings.

1.2.2 SPEAR. Dependence on energy (H. Wiedemann⁴)

Recently a set of new measurements of the maximum luminosity and the beam current versus machine energy was undertaken by H. Wiedemann. The range of energy variation was from 0.6 to 3.7 GeV and is much wider than in all previous experiments. The data were taken during the special runs of the SPEAR dedicated to machine physics. Much work was done to adjust all the machine parameters to achieve maximum luminosity. Special attention was paid to balance the vertical sizes of electron and positron bunches to avoid the loss of the luminosity due to the flip-flop effect.

The fit by a power law to recent data seems to give quite different slopes, especially for the vertical space charge parameter, than ones in the previous measurements.² The difference may be attributed to the fact that the energy range in the work² was much narrower (from approximately 1.2 to 2.5 GeV). Although the measurements are still in progress, the data are quite reliable in the opinion of the experimenter.⁴ Table 1 summarizes the results of fitting to these measured and calculated data.

1.2.3 SPEAR. Dependence on the beam current

Table 2 summarizes the data picked up from SPEAR logbooks by M. Cornacchia.⁸ The data were mostly taken during regular physics runs of the machine. The fits to the data taken at high energy physics run are recalculated. Instead of fitting data by the least square method the maximum luminosity was fitted.

1.2.4 ADONE (S. Tazzari⁵)

Table 3 summarizes the dependencies of the maximum luminosity and the beam current versus energy which were taken from the report by S. Tazzari.⁵ The space charge parameters of this machine were kept approximately equal to each other. The fit for the space charge parameters is derived from the calculated values plotted in the work.⁵ The number of bunches in ADONE can be and was changed. The data taken with 1 and 3 bunches do not contradict the assumption

$$\xi_y \sim 1/\sqrt{B}$$

1.2.5 PETRA (G. Voss⁶)

The data from the measured specific luminosity \mathcal{L}/i^2 during high energy physics experiments were fitted with the help of the blowup function σ_y assumed to behave according to the following:

$$\sigma_y^2 = \sigma_0^2 + \left(\frac{ai}{\sigma_y}\right)^2 \quad (10)$$

Here σ_0 is the value of σ_y at zero current i and a is a parameter.

From the data taken at different energies, a is found to be:

$$a = \text{const}/E^4 \quad (11)$$

The values of aspect ratio of the beam emittances are estimated to be of the order of several percent at all energies.

2. Theory

The word "theory" is probably an exaggeration in application to the beam-beam phenomena, at least in its present state. What I really mean is a kind of phenomenological theory which helps to make parametrization of the experimental data in a suitable way and to derive some scaling laws by means of a few fitting parameters. The behavior of these fitting parameters is not described by a theory and should be taken from the comparison with an experiment.

It is useful first to go through main assumptions under which the theory is developed as well as those which will be used in the following considerations.

2.1 Assumptions

2.1.1 First of all we shall consider one dimensional model of the beam-beam interaction. Although the phenomenon is essentially multi-dimensional, the justification of this model at least in the first approximation comes from the experimental observations that the vertical size of the bunch is most strongly affected by the interaction while the horizontal size of the bunch seems to be affected very little if any.

One may argue about the loss of some particular multidimensional features like the Arnold diffusion, sideband resonances, and the like. All of these effects seem to be small compared to the main rough effect.

2.1.2 Secondly, we assume that at least some number of particles behave stochastically. The reason for such a behavior can be nonlinearities in the machine lattice, nonlinearity of the electromagnetic

beam-beam force, combined action of many close-lying resonances, presence of a stochastic layer in the phase space of particle motion, etc. Note that I do not include in this list the change of particle amplitude due to radiation quantum fluctuations making thus the consideration equally applicable to proton storage rings.

2.1.3 We shall use in forthcoming considerations an assumption that both beams are identical. This assumption is not mandatory for the derivations but is justified by experimental conditions and makes all formulae more straightforward.

2.1.4 Also everywhere where it is appropriate I will simplify the calculations using Gaussian distribution, linear force, etc. Although more exact calculations can be fulfilled sometimes they do not seem to be necessary due to oversimplifying assumptions made above already.

2.2 Beam blowup according to diffusion theory

At each interaction the vertical coordinate y and the angle in vertical plane y' are changed as follows:

$$\Delta y = 0 \quad (12)$$

$$\Delta y' = 2\pi\xi_y \frac{\sigma_0}{\beta_y} K_b \phi_b(u) \quad (13)$$

where $b = (\sigma_y/\sigma_x)/\sqrt{1 - (\sigma_y/\sigma_x)^2}$, $u = y/\sigma_0$

and $K_b \phi_b$ is a function describing the electromagnetic force of the opposite bunch. For Gaussian distribution⁷

$$K_b = \sqrt{\frac{\sqrt{1+b^2}+b}{\sqrt{1+b^2}-b}} \quad (14)$$

$$\phi_b(u) = u \int_0^1 \frac{dw}{\sqrt{u+b^2}} e^{-wu^2} \quad (15)$$

According to the main assumption a certain part of the motion due to the interaction (13) can be described as stochastic and hence can be considered as an additional source of diffusion (in addition to all other sources which do not depend on the beam-beam force).

We know that at least the linear part of the force cannot cause the stochasticity. It can be considered as an additional focusing force and hence should be included in the regular part of particle motion. Probably the same is true also for some nonlinear parts of the force.

That is why for the purpose of calculating beam blowup as a consequence of a diffusion-like process we should consider not all the force $\phi_b(u)$, but only some nonlinear part of it $\tilde{\phi}_b(u)$. The way to get $\tilde{\phi}_b$ out of ϕ_b is not clear and should be considered here only as a way to introduce in the theory a phenomenological fitting parameter. It can be done in different manners:

$$\tilde{\phi}_b(u) = \begin{cases} \phi_b(u) - (1-h)\phi_b\left(\frac{u}{1-h}\right) & , \quad (\text{S. Kheifets}^7) \\ h\phi_b'(u) & , \quad (\text{A. Ruggiero}^{11}) \end{cases} \quad (16)$$

One can find still other possibilities. For a small value of h both procedures give essentially the same result.

It is reasonable to assume that for particles which behave erratically there is a complete mixing of phases within the bunch and in the long run each particle can be expected to acquire any value of coordinate y . In this case the beam blowup can be found by averaging the value $(\Delta y')^2$ over the distribution function

$$\sigma_y^2 = \sigma_0^2 \left(1 + \eta \langle K_b^2 \phi_b^2 \rangle \right) \quad (17)$$

where the brackets $\langle \rangle$ mean averaging over the distribution function. In expression (17)

$$\eta = 2B \int \tau (2\pi \xi_y)^2, \quad (18)$$

where τ is the vertical damping time (5).

For Gaussian distribution

$$\langle K_b^2 \phi_b^2 \rangle = \frac{K_b^2}{\sqrt{\pi} \sigma_y / \sigma_0} \int_{-\infty}^{\infty} \phi_b^2(u) e^{-\frac{\sigma_0^2 u^2}{\sigma_y^2}} du \quad (19)$$

Instead of doing actual calculations we substitute in the following

$$\phi_b(u) \approx h\phi'(0) = 2h(\sqrt{1+b^2} - b) \quad (20)$$

Then we get:

$$\sigma_y^2 = \sigma_0^2 + \frac{2\pi^2 e^2 \tau \beta_y^2 h^2 \sigma_0^2 i^2}{f B E^2 \sigma_y^2 \sigma_x^2 (1 + \sigma_y/\sigma_x)^2} \quad (21)$$

First of all we see here exactly the same formula (10) that was postulated in the work.⁶ Comparing (21) with (10), we find

$$a = \frac{\pi e \beta_y h \sigma_0}{E \sigma_x (1 + \sigma_y/\sigma_x)} \sqrt{\frac{2\tau}{f B}} \quad (22)$$

An expression similar to (21) can also be found in the paper¹¹ (see Eq. (39) of this work) which gives to parameter h the physical meaning of the probability of finding the particle in a stochastic layer.

Expression (21) was also derived by J. Rees¹² from the assumption

$$\sigma_y^2 = \sigma_0^2 + f B \tau \beta_y^2 \theta_{rms}^2$$

where θ_{rms} is the effective r.m.s. scattering angle of a particle in the vertical plane.

2.3 Scaling laws

Expressions (21,22) contain only one unknown parameter h. Let us consider it as a phenomenological parameter which should be determined from experimental data. One way to do this is to use PETRA results⁶ (11). It is easy to see that to satisfy E^{-4} decrease for the value a we need the following dependence of h on energy:

$$h \sim E^{-3/2} \quad (23)$$

Since we are interested now in maximum values of the luminosity and the current, we derive from (10) that asymptotically at large current i (for the case $\sigma_y \ll \sigma_x$, one can get results for the opposite limit in a similar way) $\sigma_y^4 \approx a i^2$ or

$$\sigma_y \sim \sqrt{i}/E^2 \quad (24)$$

The maximum possible value of σ_y limited by particle losses and beam lifetime should be some constant which can be written as $\sqrt{A_y \beta_y}$ where A_y is an effective vertical acceptance of the storage ring. From formula (4) for Gaussian distribution we would find that σ_y is constant with the logarithmic accuracy. Let us see now what consequences follow from these assumptions.

2.3.1 Dependence on energy

Consider first the situation where the limitation arises from the beam lifetime. Assuming $\sigma_y = \text{const}$ in expression (24) we immediately get

$$i_{\text{max}} \sim E^4 \quad (25)$$

With the help of this expression we also get the following scaling laws (note that for the electron storage ring $\sigma_x \sim E$):

$$\mathcal{L}_{\text{max}} \sim E^7 \quad (26)$$

$$\xi_{y\text{max}} \sim E^2 \quad (27)$$

$$\xi_{x\text{max}} \sim E \quad (28)$$

$$\sigma_y/\sigma_x \sim 1/E \quad (29)$$

2.3.2 Dependence on current

Let us now turn to experiments in which beam lifetime limit has not been reached yet. At a given energy one gets from the same expressions

$$\sigma_x \sigma_y \sim i^{1/2} \quad (30)$$

$$\xi_{y\max} \sim i^{1/2} \quad (31)$$

$$\mathcal{L}_{\max} \sim i^{3/2} \quad (32)$$

2.3.3 Dependence on the number of bunches B

We should distinguish between the strong beam-weak beam and the strong beam-strong beam cases.

- a) For the strong beam-strong beam case an attempt to measure the dependence on B has been made on PETRA.¹³ From expression (21) we have $\sigma_y^4 \approx i^2/BE^8$ or

$$\sigma_y \sim i^{1/2}/E^{2.1/4} \quad (33)$$

Defining in accord with the work¹³ the specific luminosity

$$\mathcal{L}_{\text{sp}} = \frac{\mathcal{L}}{B(i/B)^2} = \frac{\mathcal{L}B}{i^2} \quad (34)$$

we have

$$\mathcal{L}_{\text{sp}} \sim EB^{1/4}/\sqrt{i} \quad (35)$$

The dependence on B seems to be too weak to be in agreement with PETRA observations. The space charge parameters in this case should scale like:

$$\xi_y \sim \sqrt{i/B}^{3/4} \quad (36)$$

$$\xi_x \sim i/E^3 B \quad (37)$$

Data on these dependencies are still not available.

- b) For the strong beam-weak beam case we have observations made on ADONE.⁵ Expression (21) in this case should be rewritten for the blowup of the weak beam by an unperturbed strong beam:

$$\sigma_y^2 = \sigma_0^2 + \frac{2\pi^2 e^2 \tau \beta_y^2 h^2 i^2}{f B E^2 \sigma_x^2 (1 + \sigma_y/\sigma_x)^2} \quad (38)$$

Assuming the same dependence of h on E we have in this case

$$\sigma_y^2 \approx \frac{i^2}{BE^{10}} \approx \text{const} \quad (39)$$

The last equality corresponds to conditions of the ADONE experiment⁵. Hence

$$i_{\max} \sim E^5 \sqrt{B} \quad (40)$$

$$\mathcal{L}_{\max} \sim E^9 B \quad (41)$$

$$\xi_{y\max} \sim E^3 / \sqrt{B} \quad (42)$$

$$\xi_{x\max} \sim E^2 / \sqrt{B} \quad (43)$$

The scaling (40) seems to be in quite good agreement with the experimental data⁵ on the strong beam-weak beam

interaction at ADONE both on E and on B. On the other hand, ξ_y and ξ_x were maintained equal. That makes the comparison of the energy dependence meaningless. The dependence on B is not contradictory to the experiment.

3. Summary of the experiment and theory comparison

Tables 4-6 present the summary of the theoretical and experimental values for different parameters relevant for the beam-beam interaction. Keeping in mind the number of assumptions and the approximations made the agreement seem to be astonishingly good.

4. Some speculations on a $p\bar{p}$ storage ring

There are two main dissimilarities between electron and proton storage rings relevant to our consideration. The first one is the absence of radiation damping of particle oscillations in the latter ring. Consequently the damping time constant τ should be substituted by real time t in the expression for the beam blowup.

The second one is the energy dependence of the beam emittance. In a proton machine both σ_x and σ_y are proportional to $1/\sqrt{E}$.

Hence for a $p\bar{p}$ storage ring we should expect the following relations

$$\mathcal{L} \sim \frac{i^2 \sqrt{E}}{\sigma_y} \quad (44)$$

$$\xi_y \sim i/\sqrt{E}\sigma_y \quad (45)$$

$$\xi_x \sim i \quad (46)$$

$$a^2 \sim h^2 t/E^2 \quad (47)$$

For the case when the blowup is strong enough to influence the lifetime

$$\sigma_y^4 \sim \frac{h^2 i^2 t}{E^2 B} \sim \text{const} \quad (48)$$

If the dependence of h on E is the same as for an electron storage ring

$$i_{\text{max}} \sim E^{5/2} B^{1/2} / t^{1/2} \quad (49)$$

$$\mathcal{L}_{\text{max}} \sim E^{11/2} B / t \quad (50)$$

$$\xi_{y\text{max}} \sim E^2 \sqrt{B} / \sqrt{t} \quad (51)$$

$$\xi_{x\text{max}} \sim E^{5/2} \sqrt{B} / \sqrt{t} \quad (52)$$

The quadratic dependence of ξ_y on energy differs from the 3/2 law which is obtained by L. Teng¹⁵ from fitting the electron ring data.

ACKNOWLEDGMENTS

I am grateful to the members of the Colliding Beams Group of Fermilab and of the Accelerator Studies Group of SLAC for many valuable comments and for the interest in these considerations.

REFERENCES

1. F. Amman, IEEE Trans. on Nucl. Sci., NS-20, 858 (1973). The review of the experimental results up to the beginning of 1973.
2. H. Wiedemann, "Non-Linear Dynamics and the Beam-Beam Interaction (BNL, 1979)," M. Month and J. Herrera, editors, AIP, New York, 1979, pp. 84-98. The review of the more recent results.
3. A. Chao, ibid., see 2, pp. 42-68. This paper has a list of theoretical papers on this subject.
4. H. Wiedemann, private communication.
5. S. Tazzari, ibid., see 2, pp. 128-135.
6. G. Voss, "First and Only Partial Analysis of Space Charge Effects in PETRA," Vorlaufige Mitteilung, M-VM-79/6, November 1979 (DESY, Hamburg).
7. S. Kheifets, IEEE Trans. on Nucl. Sci., NS-26, No. 3, 1979, pp. 3615-3617. See also S. Kheifets, SLAC-PUB-2252 (1979).
8. M. Cornacchia, ibid., see 2, pp. 99-114.
9. M. Sands, "Physics with Intersecting Storage Rings," edited by B. Tuschek, Academic Press, New York, 1971.
10. J. M. Paterson and M. Donald, IEEE Trans. on Nucl. Sci., NS-26, No. 3, 1979, pp. 3580-3582.
11. A. Ruggiero, "The Theory of a Non-Linear System in Presence of Noise (The Beam-Beam Effect)," Fermilab, February, 1980.
12. J. Rees, private communication.
13. D. Degèle et al. (PETRA Group), "Results of Machine Physics Studies on PETRA in 1979," DESY 80/10, February 1980.

14. E. Keil, CERN/ISR/TH/79-32, Geneva, June 25, 1979.
15. L. C. Teng, Fermilab Report TM-938, 1500, January 29, 1980.

Table 1

Dependence of SPEAR parameters on the particle energy E (in GeV). The fit is done⁴ by a function $f = kE^q$.

f	k	q	Comment
\mathcal{L}_{\max}	0.033	6.6	in $10^{30} \text{ cm}^{-2} \text{ sec}^{-1}$
i_{\max}	1.2	3.6	in ma
σ_y/σ_x	0.5	-1.0	--
ξ_x	0.022	0.87	--
ξ_y	0.011	2.3	--

Table 2

Dependence of SPEAR parameters on the beam current i (in ma). The fit is done by a function $f = ki^q$.

f	E GeV	k	q	Comment
\mathcal{L}_{\max} ($10^{30} \text{ cm}^{-2} \text{ sec}^{-1}$)	1.5	0.030	1.95	} high energy physics runs
	2.5	0.046	1.55	
	3.7	0.054	1.45	
	1.95	0.052	1.41	} $\beta_y = 10 \text{ cm}$ } machine } $\beta_y = 20 \text{ cm}$ } physics runs
	1.95		1.45	
σ_y			0.59	
σ_x			0	
ξ_y	2.4		0.33	

Table 3

Dependence of ADONE parameters on the particle energy E (in GeV). The fit is done⁵ by a function $f = kE^q$.

f	k	q	Comment
\mathcal{L}_{\max}	0.64	7	in $10^{30} \text{ cm}^{-2} \text{ sec}^{-1}$
$\xi_x \approx \xi_y$	0.068	1.57	--
i_{\max} (in ma)	105	4.34	3 bunches } strong
	42.4	4.12	1 bunch } weak beam

Table 4

The power q in the power law

$$f(E) \sim E^q$$

Parameter f	Experiment			Theory	Comment
	SPEAR	ADONE	PETRA		
h				$-3/2$	(23)
\mathcal{L}_{\max}	6.6	7		7	(26)
i_{\max}	3.6	4.5		4	strong - strong (25)
i_{\max}		4.12;4.34		5	weak - strong (40)
ξ_y	2.3	1.5		2	(27)
ξ_x	0.9			1	(28)
σ_y/σ_x	-1			-1	(29)
a			-4	-4	(11)

Table 5

The power q in the power law $f(i) \sim i^q$

Parameter f	Experiment			Theory	Comment
	SPEAR	ADONE	PETRA		
\mathcal{L}_{\max}	1.4			1.5	(32)
$\mathcal{L}_{\text{spmax}}$			- 0.5	- 0.5	(35)
$\sigma_x \sigma_y$	0.6			0.5	(30)
ξ_y	0.4			0.5	(31)

Table 6

The power q in the power law $f(B) \sim B^q$.

Parameter f	Experiment			Theory	Comment
	SPEAR	ADONE	PETRA		
\mathcal{L}_{\max}				- 0.25	{ strong beam- (35) strong beam
$\mathcal{L}_{\text{spmax}}$				0.25	
i_{\max}		0.8		0.5	(40) { strong beam- (42) weak beam
ξ_{ymax}		- 0.8		- 0.5	

An Empirical Model for Controlling Beam-Beam Effects in ISABELLE*

G. Parzen

Brookhaven National Laboratory
Upton, N.Y. 11973I. Introduction

The beam-beam interaction may limit the beam intensity in ISABELLE. Although considerable progress has been made in understanding the beam-beam interaction, there appears to be no reliable method at present for computing the effects of the beam-beam interaction. The steps taken at ISABELLE to limit beam-beam effects are based largely on the experience accumulated at the ISR. At the ISR, the beam-beam effects do not appear to be large, and the beam intensity at the ISR does not appear to be limited by beam-beam effects. The beam-beam effects may be much stronger in ISABELLE because of factors like higher intensity and stronger non-linearities.

An empirical model for controlling beam-beam effects in ISABELLE can be arrived at based partly on the experiences at the ISR and based partly on conjecture. Establishing an empirical model may be thought of as consisting of the following steps:

1. Assume a model for the mechanism for beam growth.
2. Establish the critical parameters that lead to beam growth.
3. Establish working tolerances for the critical parameters.

The working tolerances are somewhat different from what one usually means by tolerances. They are based partly on experience, partly on theory, partly on conjecture, and partly on what is doable. They represent a compromise, and provide a useful guide for designing the different components of the accelerator. The working tolerances may change as more information is acquired.

* Work performed under the auspices of the U.S. Department of Energy.

II. Model of Beam Growth

The model for beam growth assumed is

$$\text{Non-Linearities} + \text{"Something"} \rightarrow \text{beam growth}$$

where the "Something" may be

$$\begin{aligned} \text{"Something"} &\rightarrow \text{noise} \\ &\text{ripple} \\ &\text{tune modulation} \\ &\text{randomizing perturbation} \end{aligned}$$

The phrase "randomizing perturbation" indicates some perturbation which in some sense makes the particle forget its history so that it is crossing the non-linear resonances in an almost random way. It is known that multiple crossing of a non-linear resonance will often cause only a limited growth, while random crossing of a non-linear resonance will cause a steady, and often much larger, growth. In the ISR, there is some evidence^{1,6} that the randomizing perturbation may be intra-beam scattering.

In the light of the above model, the steps required to limit beam growth due to the beam-beam interactions are

1. Limit the strength of the non-linearities.
2. Limit the "Something"--noise, ripple, tune modulation or randomizing perturbation.

III. Magnet Non-Linearities

Superconducting magnets are likely to have stronger² non-linear error fields than conventional warm magnets. Recent measurements of the error fields in ISABELLE magnets indicate that the non-linear field errors in ISABELLE magnets may be a factor 10 larger than those found in the ISR magnets.³ At the ISR, magnet non-linearities do not appear to play an

important role in causing beam growth. Because of the larger non-linear fields in ISABELLE, it may not be wise to assume that this will also be the case for ISABELLE. Certainly, one should strive to keep the non-linear fields in ISABELLE magnets as low as possible.

The working tolerances for the non-linear error fields are given in terms of the multipole coefficients Δb_n , and Δa_n which are defined by expanding the error field in the median plane as

$$\begin{aligned}\Delta B_y &= B_0 (\Delta b_0 + \Delta b_1 x + \Delta b_2 x^2 + \dots) \\ \Delta B_x &= B_0 (\Delta a_0 + \Delta a_1 x + \Delta a_2 x^2 + \dots)\end{aligned}$$

The working tolerance for ISABELLE can be roughly and simply stated as

$$\begin{aligned}R^n \Delta b_n &\lesssim (n+1) 2 \times 10^{-4} \\ R^n \Delta a_n &\lesssim (n+1) 2 \times 10^{-4}\end{aligned}$$

where R is the radius of the main coil in the magnets; R = 6.5 cm for ISABELLE. This working tolerance is the expected² rms error multipoles caused by a random rms .005 cm (2 mil.) error in the location of the current blocks of the main coil. In this sense, these tolerances appear to be simply what seems to be achievable. However, it will be seen below that for several known effects they are indeed the tolerances. In this connection, it may be worthwhile recalling what was said about working tolerances in Section I, that they are a useful guide based partly on experience, partly on theory, partly on conjecture, and partly on what is doable.

There are about four known effects which indicate that the above working tolerances are indeed tolerances. These are:

1. Uncorrectable closed orbit error error. The random dipole error field will vary across the aperture⁴ because of the presence of the higher order error multipole fields. Thus, when the closed orbit is corrected at the center using the system of dipole correctors, it will not be corrected at the edges of the aperture. For ISABELLE, this leads to a possible 5 mm orbit error at both edges of the aperture.

2. Vertical dispersion error. The field errors, particularly Δa_1 , generate a vertical dispersion which can change the beam size at the crossing points by about 25% at 30 GeV and about 12% at 400 GeV. This may cause a possible 25% variation in Δv , the beam-beam v -shift, increasing the strength of the beam-beam resonances. Also, the luminosity may be reduced by 25%.

3. Random error in β_y or the crossing points. The field errors cause β_y to vary around the ring by about $\Delta\beta_y/\beta_y = 10\%$. This will cause a beam-beam Δv variation of 5%, and a 5% reduction in luminosity. The random $\Delta\beta_y/\beta_y$ also helps to excite the 1/3 resonances by interacting with the large sextupole required for chromaticity correction.

4. Width of the 1/3 resonance. The field errors excite non-linear resonances. In particular, the 1/3 resonance may have a width of $\Delta v = 1 \times 10^{-3}$.

The above four effects show that if the error fields exceed the working tolerances by very much, some large damaging effects may result.

It is interesting to compare the stop bands of the non-linear resonances generated by the magnet error fields with those generated by the beam-beam interaction. This is done in Table I. The beam-beam resonances listed in Table I are the imperfection resonances generated by orbit errors and random errors in β_y at the crossing points.⁵ One sees that for ISABELLE, the magnet resonances and the beam-beam resonances are comparable for the lower order resonances.

Table I

<u>N Resonance Order</u>	<u>Magnetic Field Error Resonances</u>	<u>Beam-Beam Resonances</u>
2	6.5 E-3	1.6 E-4
3	4.3 E-4	7.6 E-4
4	3.4 E-5	9.1 E-5
5	3.8 E-6	1.2 E-4
6	4.5 E-7	1.3 E-5
7	5.4 E-8	2.0 E-5
8	6.5 E-9	1.3 E-6
9	---	2.5 E-6
10	---	1.5 E-7

IV. Beam-Beam Non-Linearities

In this section, we specify the working tolerances which are intended to limit the strength of the beam-beam non-linearities. These are

1. Beam-beam $\Delta v \leq .005$.
2. Vertical orbit error at crossing points $\lesssim .05$ mm (about 10% of beam size).
3. Vertical dispersion at crossing points

$$Y_p \frac{\Delta p}{p} \lesssim 1\% \text{ of beam size}$$
4. Random $\Delta\beta_y/\beta_y$ at crossing points $\lesssim 1\%$.
5. Periodicity of six is maintained.
6. Control of the working line so as to be able to avoid resonances.

For day one operation of ISABELLE, the periodicity of six is to be maintained. Operation with a lower periodicity may be considered afterward. There is some experience at the ISR that operation with lower periodicities, even a periodicity of 1, is possible. However, it appears to this writer, that it is quite a different matter to suggest operation with a lower periodicity for a machine that is already working, than to suggest it for ISABELLE which will have much stronger non-linearities and whose operation has not been studied.

Present plans for first day operation of ISABELLE will probably not allow the correction of the errors in the vertical dispersion and of β_y at the crossing points to the above tolerance. However, the capability to do so at a later date has been provided.

V. Tune Modulations

According to our model for beam growth, any modulation of the ν -value, ν_x, ν_y with time is of concern. Sources of this modulation include intra-beam scattering,⁶ drift in the power supplies, and ripple in the power supplies.⁷

Drift in the power supplies of the various correction coils and in the main power supply can cause the ν -value to drift. The working tolerance in the amount the ν -value can drift is assumed to be

$$\Delta\nu \leq .001$$

This appears to be the tolerance assumed at the ISR.⁸ The working line in ν -space is constrained to be between the resonances 22.60 and 22.67 and about .01 from the coupling resonance. Part of the beam is usually about .01 from some resonance. Thus, a drift of about .001 can move the beam appreciably closer to some resonance.

There are about 103 correction coil power supplies in each ring of ISABELLE. Power supply errors for each correction coil can cause the ν -value to drift, and one has to choose the power supply accuracies of all these 103 power supplies so that the total ν -drifts due to all of them, plus that due to the main power supply, does not exceed the working tolerance $\Delta\nu \leq .001$. Table II lists all the correction coil power supplies, the full scale accuracy of each power supply, and the peak ν -drift caused by each power supply, and the total ν -drift due to all the power supplies.

Ripple in the main power supply can cause a ν modulation with time. Experiments done at the ISR indicate⁹ that a ripple in ν -value of $\Delta\nu \geq 1 \times 10^{-6}$ can cause appreciable increases in the background rate. The working tolerance assumed for the ν -ripple is

$$\Delta\nu \leq 1 \times 10^{-6}$$

This leads to a required ripple for the main power supply of 1×10^{-7} .

The requirements on the ripple of the correction coil power supplies is almost as severe as it is for the main power supply, primarily because there are many correction coil power supplies. The required ripple for each correction coil power supply is also listed in Table II.

Table II. Accuracy requirements for the correction coil power supplies in order to limit v -drift and ripple.

	Correction Coil	Capacity Required At 400 GeV (cm^{-2})	Current Required At 400 GeV (A)	Power Supply Accuracy At Full Scale	$\Delta v_x/10^{-3}$ (peak)	$\Delta v_y/10^{-3}$ (peak)	Ripple Factor Required (peak)
Quadrupole	$b_{1,H}$	3.0 E-3	129	50 E-6	0.265	0.041	.6 E-6
Quadrupole	$b_{1,V}$	3.0 E-3	129	50 E-6	0.047	0.262	.6 E-6
Sextupole	$b_{2,H}$	6.0 E-4	170	10 E-6	0.262	0.086	.1 E-6
Sextupole	$b_{2,V}$	6.0 E-4	170	10 E-6	0.176	0.286	.1 E-6
Octupole	$b_{3,H}$	8.0 E-5	154	25 E-6	0.294	0.097	.3 E-6
Octupole	$b_{3,V}$	8.0 E-5	154	25 E-6	0.147	0.225	.3 E-6
Decapole	$b_{4,H}$	5.0 E-6	81	50 E-6	0.110	0.036	.6 E-6
Decapole	$b_{4,V}$	5.0 E-6	81	50 E-6	0.041	0.059	.6 E-6
Duodecapole	$b_{5,H}$	1.5 E-6	99	125 E-6	0.092	0.016	1.0 E-6
Duodecapole	$b_{5,V}$	1.5 E-6	99	125 E-6	0.001	0.005	1.0 E-6
Quadrupole	b_1 (bypass I)	9.0 E-3	300	15 E-6	0.326	0.353	.1 E-6
Quadrupole	b_1 (bypass II)	9.0 E-3	300	50 E-6	0.320	0.236	.6 E-6
Insertion Quad.	b_1 (Q9)	4.8 E-3	206	200 E-6	0.140	0.024	2.0 E-6
Insertion Quad.	b_1 (Q8)	4.8 E-3	206	200 E-6	0.024	0.139	2.0 E-6
Insertion Quad.	b_1 (Q7)	4.8 E-3	206	200 E-6	0.137	0.025	2.0 E-6
Insertion Quad.	b_1 (Q6)	4.8 E-3	206	200 E-6	0.026	0.149	2.0 E-6
Insertion Quad.	b_1 (Q5)	4.8 E-3	206	200 E-6	0.155	0.017	2.0 E-6
Insertion Quad.	b_1 (Q4)	4.8 E-3	206	200 E-6	0.011	0.107	2.0 E-6
Insertion Quad.	b_1 (Q2)	4.8 E-3	206	200 E-6	0.446	0.321	2.0 E-6
Insertion Quad.	b_1 (Q1)	4.8 E-3	206	200 E-6	0.184	0.618	2.0 E-6
Skew Quad.	a_1 (Q1)	2.4 E-3	103(?)	200 E-6	--	--	---
Dipole	a_o, b_o	800 G	100	200 E-6	--	--	---
Dipole	a_o, b_o	400 G	50	200 E-6	--	--	---

$$\text{Total } \Delta v_x \text{ (peak)} = 0.88 \text{ E-3}$$

$$\text{Total } \Delta v_y \text{ (peak)} = 0.95 \text{ E-3}$$

VI. Experimental Devices for First Day Operation

An important question is what should be the requirements for experimental devices, such as a spectrometer magnet at a crossing point, that is expected to be in place when the accelerator is first turned on. This problem is still being worked on at present.¹⁰ The following requirements are tentatively suggested.

1. Preserve periodicity. The beam-beam Δv at the crossing point, where the experimental device is located, should be relatively unchanged. The periodicity is actually destroyed by random orbit errors and random β -variations which change the beam-beam Δv . The experimental device should change Δv by an amount which is less than that due to the random errors which are not correctable; in ISABELLE, this is about 2% of the unperturbed Δv .

2. Beam-beam non-linear stop bands introduced by the experimental device should be less than those due to random errors, such as orbit errors, after the random errors have been corrected as well as possible.

3. Magnetic field non-linear stop bands introduced by the experimental device should be less than those due to random magnetic field errors in the accelerator magnets.

After the accelerator has been operating and studied, a more severe perturbation by the experimental device may be considered.

References

1. K. Hubner, Proc. of 1975 ISABELLE Summer Study, p. 562 (1975).
2. G. Parzen, Particle Accelerators, 6, 239 (1975).
3. J. Gareyte and J.P. Gourber, Proc. 1975 ISABELLE Summer Study, p. 395 (1975).
4. M. Month and G. Parzen, Nucl. Instrum. Methods 137, 319 (1976).
5. G. Parzen, Brookhaven National Laboratory Report BNL 51154 (1979).
6. M. Month, Proc. 9th International Conference on High Energy Accelerators, Stanford, p. 402 (1974).
7. G. Parzen, ISABELLE Tech Note 189 and Tech Note 190 (1980).
8. P.J. Bryant, Proc. IX International Conference on High Energy Accelerators, Stanford, p. 80 (1974).
9. J.P. Gourber, E. Keil and P. Proudlock, CERN ISR Performance Report, ISR-TH/EK/amb (1973); K. Hubner, CERN ISR Performance Report, ISR-TH/KH/amb (1973); C. Wyss, CERN ISR Performance Report, ISR-MA/CW/cn (1975); S. Oliver and C. Wyss, CERN ISR Performance Report, ISR-MA-CW/SO/rh (1976).
10. M. Cornacchia and G. Parzen, Brookhaven National Laboratory Report BNL 51103.

BEAM-BEAM STUDIES WITH DCI

J. LeDuff

Lab. de l'Accelérateur Lineaire
Orsay, France

I. INTRODUCTION

An attempt to compensate for the beam-beam effect was done on DCI but did not succeed in yielding higher performances.

The compensation scheme¹ uses four beams stored in two rings having two common straight sections. A residual space charge force appears as a consequence of a non-perfect compensation if the companion beams are not well superposed.

The original aim was to keep the residual linear space charge force one order of magnitude below the corresponding usual beam-beam force in order to get ten times more current per beam for collision. This has been set up experimentally by proper adjustment of the two rings and by correcting the relative orbit displacement between the two rings within a fraction of σ in both common straight sections.

As a reference for the four beam studies, preliminary experiments were performed with one ring or another. Strong increase of the transverse cross section is observed which becomes gradually less as the energy is increased. With four beams, up to the limit, there is no appreciable blow up, but the limit in terms of maximum current per beam is much smaller than in the e^+e^- case.

Each type of interaction shows discrete stable areas in the operating diagram (v_x, v_z) which seem to indicate a strong effect of non-linear resonances of relatively high order.

A few experiments were also performed with three beams in a strong-weak configuration but it merely proved that the incoherent beam-beam limit was partially compensated and more work is required before any conclusion can be drawn.

The data which are presented here were obtained by the DCI study group with the constant help of the DCI operation group, and were recently compiled by M.P. Level and J. LeDuff.²

II. MAIN CHARACTERISTICS OF DCI

The space charge compensation scheme is shown in Fig. 1. It involves one bunch per beam according to the superperiodicity of 2. The

main parameters are:

Ring Energy	: .6 to 1.85 GeV
Revolution Frequency	: 3.169 MHz
Envelope Function at Crossing	: $\beta_x^* = \beta_z^* = 2 \text{ m}$
Operating Point (linear coupling)	: $\nu_x = 2.8, \nu_z = 1.8$
Transverse emittances (full coupling)	: $\epsilon_{\text{mrad}} = 2.5 \times 10^{-7} E^2 \text{ (GeV)}$.

The residual space charge strength and compensation factor were originally defined as follows:

$$\xi_{\text{res}} = \frac{\xi}{K}$$

$$K = \left[\frac{\Delta I}{I} + \left(\frac{\delta}{\sigma} \right)^2 \right]^{-1},$$

where ΔI and δ , respectively, are the current imbalance and the orbit deviation between companion beams.

Conventional monitoring devices make $K \approx 10$ possible.

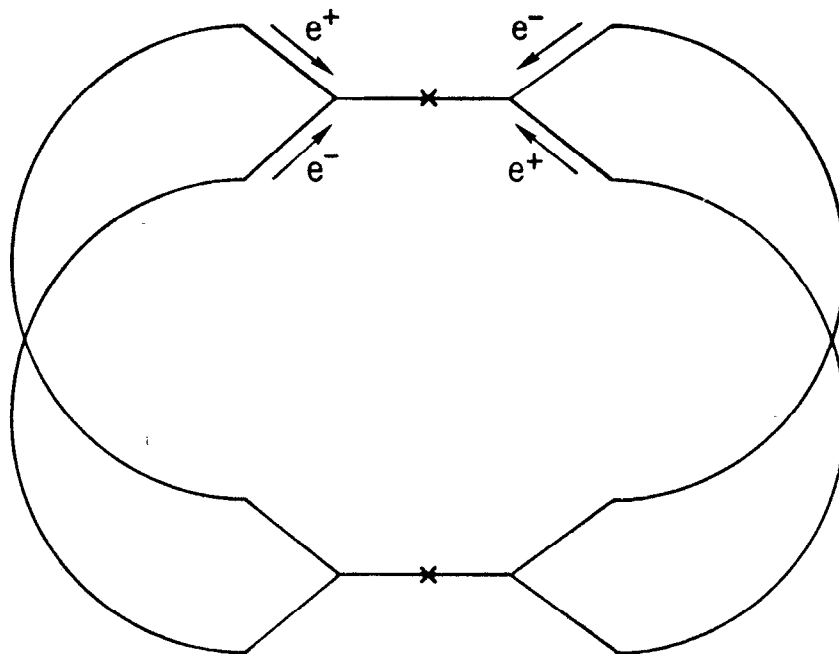


Fig. 1. Space Charge Compensation Scheme

III. SUMMARY OF e^+e^- BEHAVIOR

Most of the experiments have been done with round beams (fully coupled). It is worth mentioning that this is a natural way of increasing the beam cross section and hence the maximum current and luminosity (on the basis of a constant ξ_{\max}). Such configurations were used successfully at ACO and ADONE where enough vertical aperture was available. Apart from slight differences the two DCI rings behave similarly.

As a matter of fact, the luminosity does not vary like I^2 at least above a certain threshold. This is shown in Fig. 2 where the dotted line represents the computed correction according to the linear thin lens approximation. Fig. 3 shows the corresponding relative increase of the effective beam cross section and it becomes more obvious that the linear thin lens correction cannot explain the e^+e^- behavior.

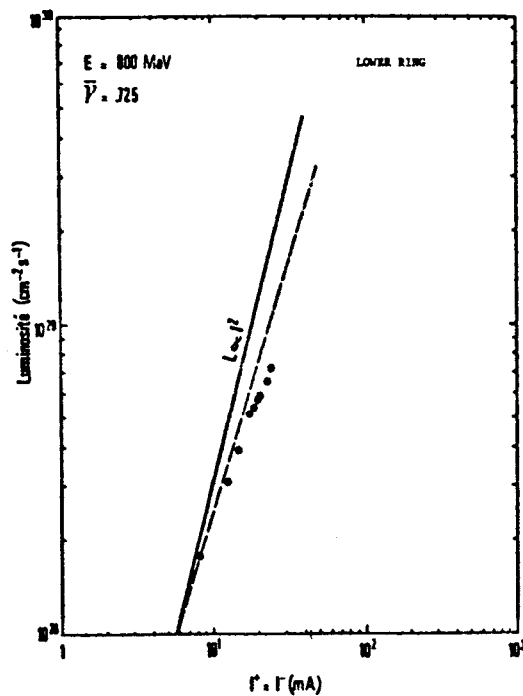


Fig. 2. Luminosity vs. current.
 --- linear thin lens approx.
 ... experimental points

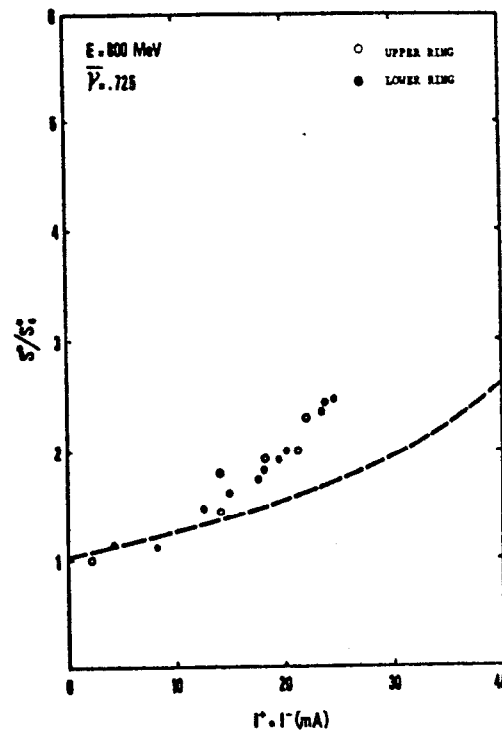


Fig. 3. Beam cross section vs. current.
 ---- linear thin lens approx.

The increase of the transverse cross section may be described in terms of space charge strength versus current. In the present case with round equal beams one gets:

$$\xi = \frac{r_e e \beta_0^*}{\gamma} \times \frac{\mathcal{L}}{I}$$

where β_0^* is the unperturbed envelope function at the crossing. Fig. 4 shows that for a fixed tune the ξ saturates before the limit is reached, the latter being defined as a bad lifetime for at least one of the two beams. Proper adjustment of the tune can increase this saturation level as can be seen on either Fig. 5 or Fig. 6, where ξ_{\max} is plotted as a function of tune along the coupling resonance. As a secondary remark, let's mention that the maximum achievable ξ in DCI was improved by approaching the integer from below.

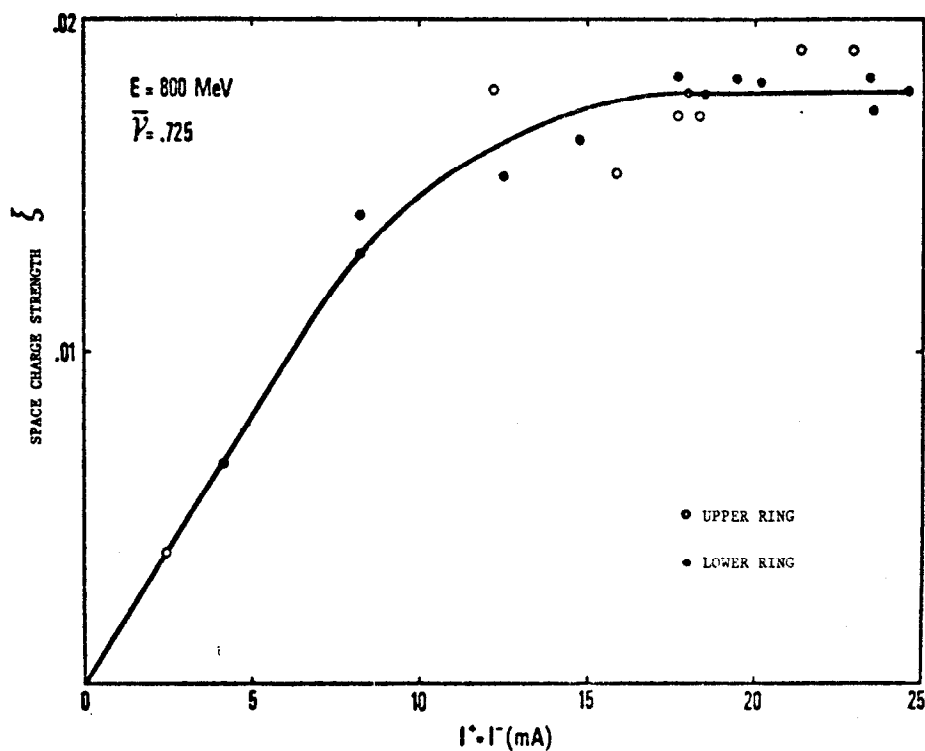


Fig. 4. Space charge strength versus current.

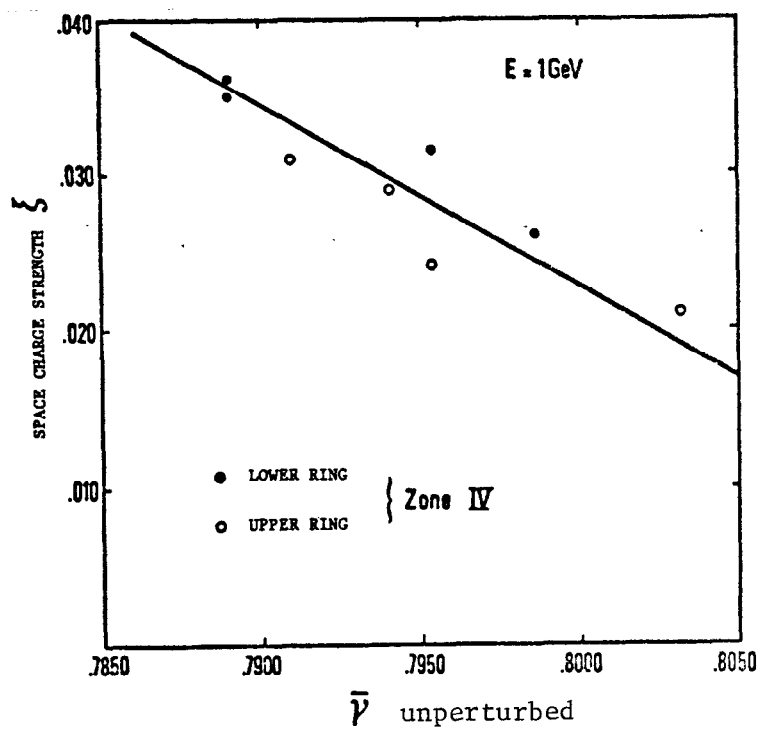


Fig. 5. ξ_{\max} as a function of tune.

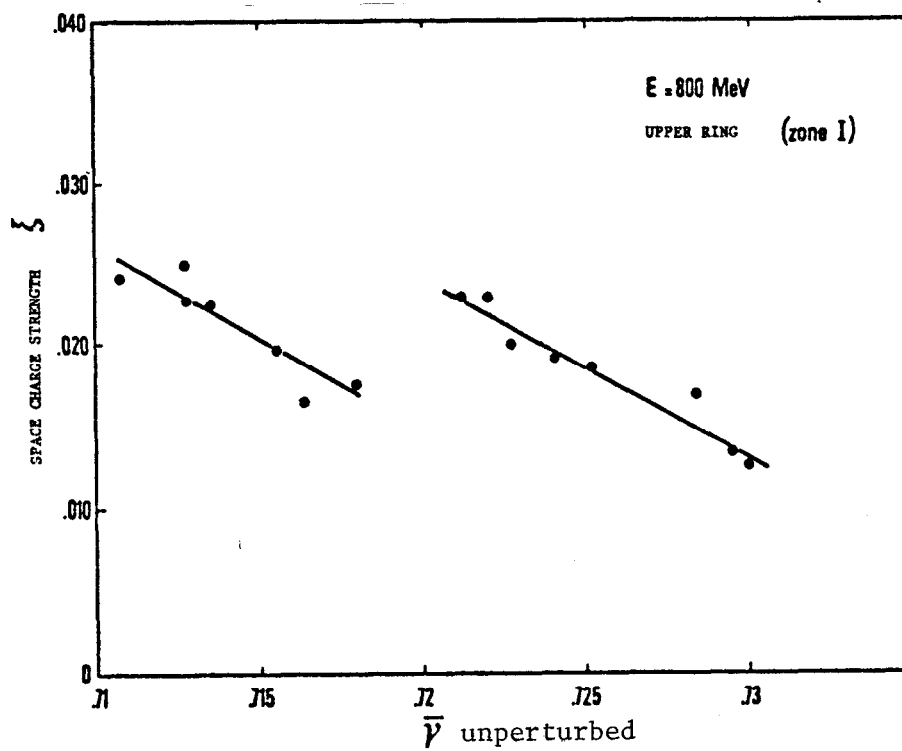


Fig. 6. ξ_{\max} as a function of tune.

An interesting fact which emerges from these two last plots, (Figs. 5 & 6) is that ξ_{\max} goes linearly with the unperturbed tune until it hits a black hole. One has $\bar{\nu} + \xi_{\max} = \text{cte}$ where the "cte" appears to be very close to a rational number p/q . In the cases of Figs. 5 and 6 it is, respectively, $8/11$, $3/4$ and $9/11$ considering only the smaller numbers which give the right ratios.

The discrete behavior is also shown in Figs. 7 and 8.

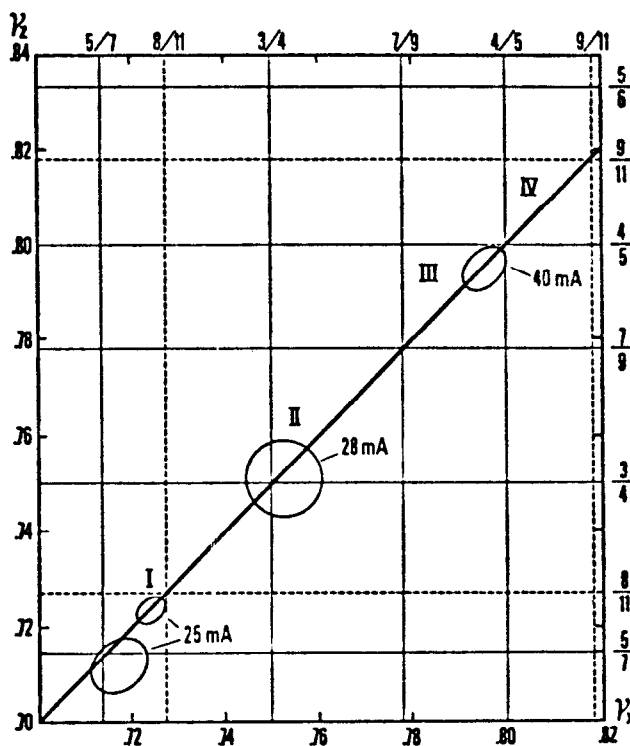


Fig. 7. Stability diagram (Upper Ring) at 800 MeV.

Moreover, it is seen that at high currents close to the limit, the stable region can overlap the left non-linear resonance and even go to the adjacent region, while at low stored current the stable area is much larger and stays in between two resonances. As a matter of fact, on DCI with a single stored beam the $1/4$ resonance is destructive while with two beams of high current the unperturbed tune can be brought on it without damage. Notice that in both cases the unperturbed tune is the one which affects the large amplitude oscillations, so the peculiar effect which has been

mentioned could be an effect of the large tune spread and of the modified particle distribution with two strong beams colliding.

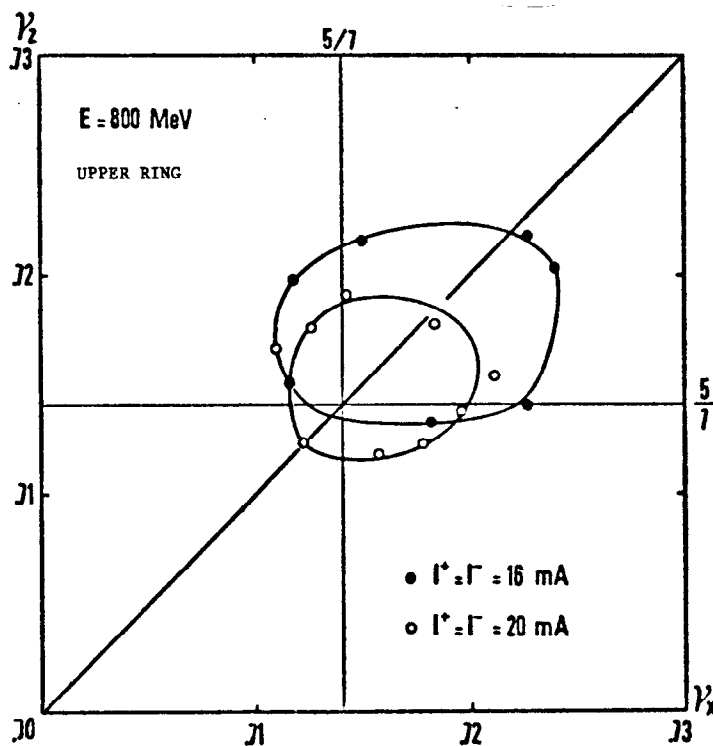


Fig. 8. Stability area versus current.

Each ring has been optimized in the energy range $.8 \leq E \leq 1.2$ GeV, on the coupling resonance at least for two regions: $\bar{\nu} = .714$ and $\bar{\nu} = .800$. Fig. 9 shows that the maximum luminosity varies as E^2 while the corresponding bunch current varies as E . These scaling laws are compatible with a constant ξ_{\max} and a constant maximum cross section at the limit in reasonable agreement with the vertical aperture limit.

The energy range explored is relatively small. However, above 1.2 GeV the vertical aperture does not permit any more work on the coupling resonance, which is why the high energy range was studied with flat beams.

Here again, as shown in Fig. 10, the discrete stability region appears but in a more complicated form where the non-linear coupling resonances seem to play a role. Region M, just below the coupling resonance gives the best results.

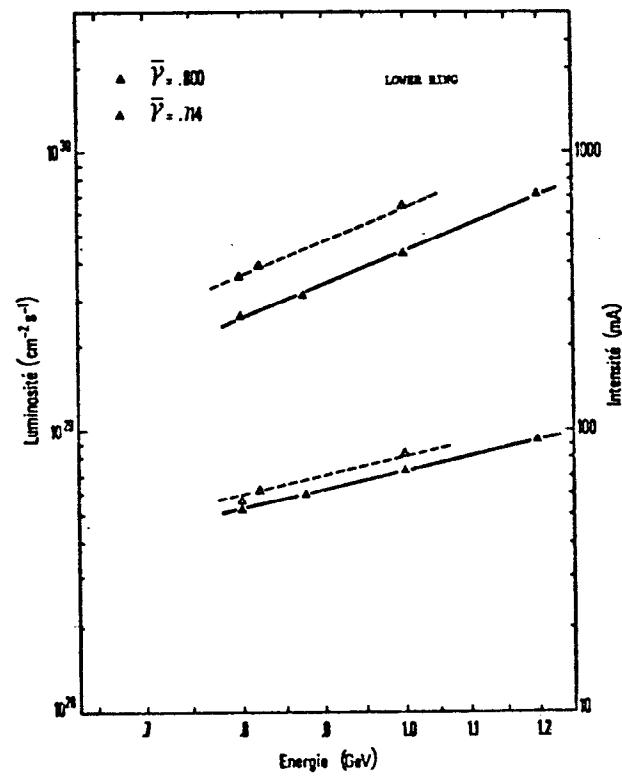


Fig. 9. Maximum luminosity and current versus energy.

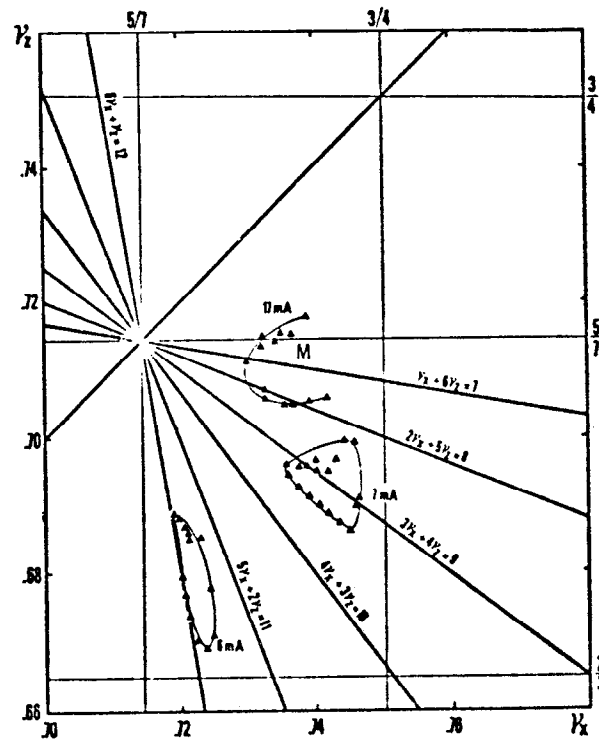


Fig. 10. Stability diagram at: $E = 1$ GeV; $\beta_z^* = 1$ m.

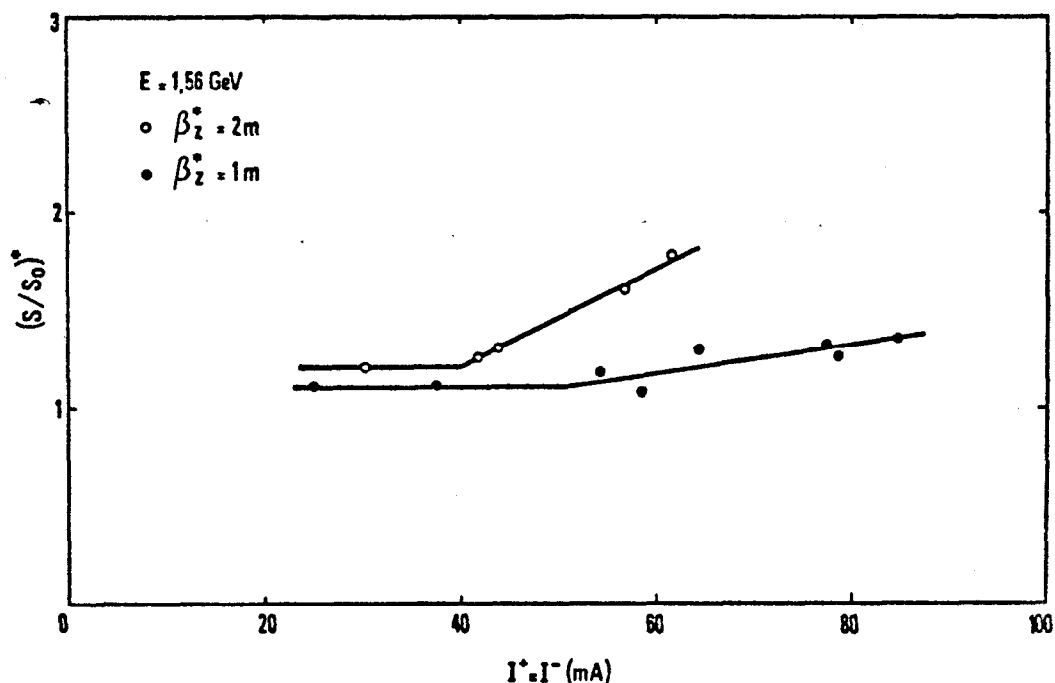


Fig. 11. Beam cross section versus current for two different configurations.

Fig. 11 shows a blow up of the effective cross section at high currents which appears to be smaller as β^* is smaller. However, up to now the beam-beam limit with flat beams, at $E = 1.56$ GeV has not been reached due to high current injection problems and the present ξ is only .015 corresponding to a luminosity of 6.5×10^{29} per ring.

IV. STUDIES WITH FOUR BEAMS (COMPENSATED MODE)

VI. 1. Experimental Conditions and Optimization Procedure

In order to minimize the residual macroscopic space charge forces, the following conditions were achieved for both rings:

- Orbit adjustment of both rings within $.1$ mm for the C.M. and, correspondingly, $.05$ mrd for $1/2$ crossing angle. (At $E = .8$ GeV, $\sigma = .6$ mm).
- Relative rf phase adjustment between rings within 100 ps. (At $.8$ GeV, $V_{rf} = 80$ kV; $\sigma_{\theta}/c = 400$ ps.).

Notice that the current fluctuations in the bending magnets as well as low frequency phase fluctuations lead to a vertical beam

separation of $\leq 50 \mu$ according to the finite dispersion function at crossings ($\pm \eta_z^*$).

The following procedure has been used to optimize the four-beam interaction:

- Identity of the tunes for both rings. This is done with the help of auxilliary quadrupole coils.
- Orbit superposition at both crossings.
- Fine adjustment of tunes with beam colliding; search for stable area.
- Fine adjustment of the closed orbit of one ring with respect to the other one, in both common straights, with colliding beams; search for stable area.

Here again the luminosity and the specific luminosity measurements are of considerable interest. All adjustments together lead to a theoretical compensation factor of the order of 10.

IV. 2. Four-Beam Interaction as a Function of Current

The experiment was performed at the energy $E = .8$ GeV with fully-coupled round beams. With a fixed tune $\bar{\nu} = .725$ halfway between two non-linear resonances which happen to be destructive in the e^+e^- case, it was soon observed that the four-beam interaction had a current limit smaller than the two-beam case. However, no increase of the transverse cross section is observed up to this limit, while for the same current per bunch, the e^+e^- case shows an enlargement by a factor of 1.6. This behavior is shown in Fig. 12 where ξ always represents the space charge strength of each equal bunch colliding. The maximum ξ in the four-beam case is .024 while it saturates at .018 in the two-beam case. As seen earlier, the two-beam case can be improved with a better choice for the tune. It will be shown next that this is not true with four beams.

It is worth noticing that even if the space charge compensation is effective over a small fraction of current it does not help in obtaining more luminosity.

Emphasis can be put also on the fact that the four-beam limit occurs where the two-beam case starts saturating.

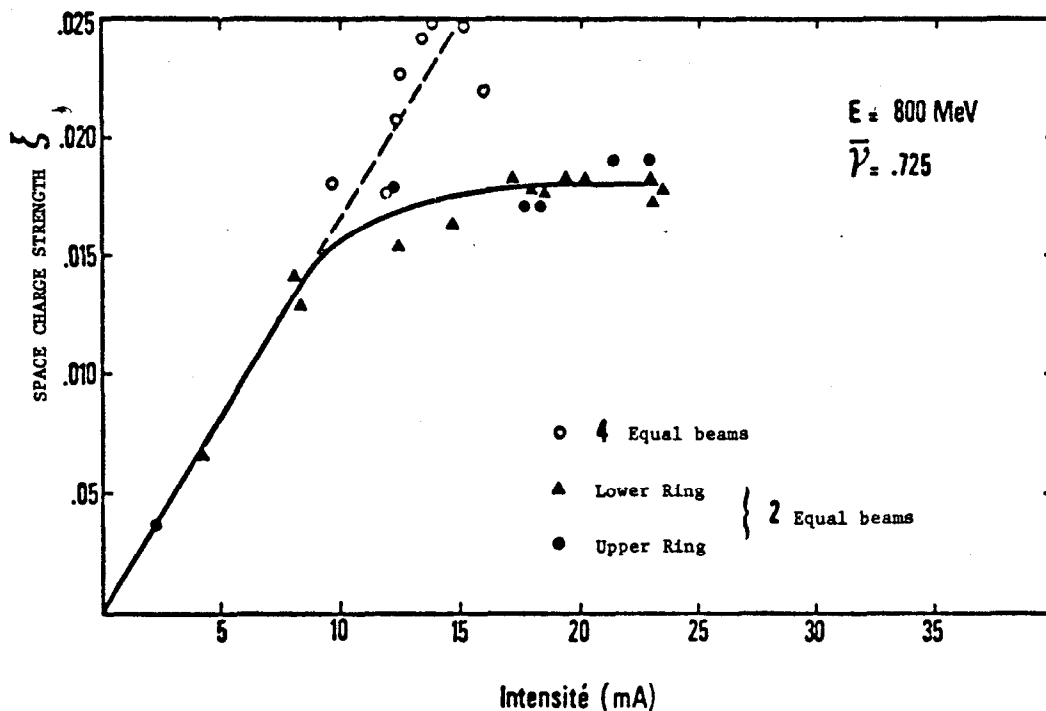


Fig. 12. Comparison between four beams and two beams: ξ versus current at $E = 800$ MeV and $\bar{\nu} = .725$

IV. 3. Stable Regions with Four Beams

With four beams interacting the operating diagram has been systematically investigated on and out of the coupling resonance. In all cases discrete stability areas are found which again seems to result from non-linear resonances with, however, the inconvenience of being smaller than with only two beams. (See Fig. 13).

The stable areas which are seen along the coupling resonance now seem to be located more or less halfway from non-linear resonances which previously appeared to be destructive with two e^+e^- beams also. Quantitatively considering both extremities of each stable area along the coupling resonance, one can roughly say that:

$$\bar{\nu} \pm \xi \approx p/q,$$

which shows again that the ξ value does matter, but not its multiples nor the residual ξ_{res} . It's difficult to perceive any difference in current limit for all the discrete stable zones along the

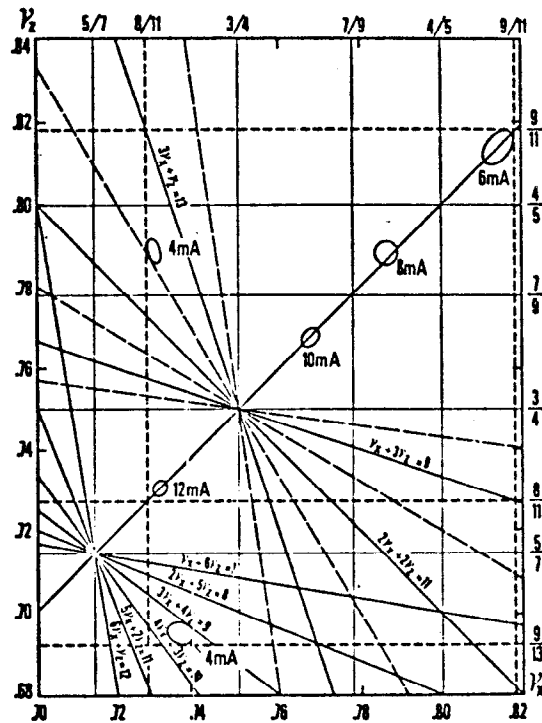


Fig. 13. Stability diagram with four beams and two crossing points at 800 MeV.

coupling resonance.

Again, the flat beam case seems to involve non-linear resonances and leads to a more complicated qualitative analysis.

Non-linear resonance effects could be expected from the following mechanisms: a) Non-Perfect Compensation. The residual linear space charge force decreases as the compensation factor goes up. This is true also for the residual non-linear forces. However, the multipole content of this non-linear part is different from the one which occurs in the two-beam case, unless these two beams are slightly separated which experimentally appears to be more dangerous. Even so it is hardly believable that the current limit with four beams should be lower than with two beams. 2) Perfect Compensation. Collective coherent oscillations can be driven by non-linear resonances if Landau damping (tune spread) is not effective. If so, one would expect the dipole mode to be the most dangerous one as the

corresponding reactive component is higher. That should satisfy the following relation:

$$\bar{\nu} \pm 2 k \xi \approx p/q ,$$

where k is the number of crossing points. Experimental results are more in favor of ξ and not a multiple of ξ .

Higher-order-density oscillations are expected also with four beams which become unstable very close to a rational number p/q^3 . In this model the proximity of the integer is very important which, in fact, means that the linear component gives the major contribution. The non-linear stop band does not vary rapidly with current. As in the previous model the number of crossing is a fundamental parameter. This model would predict as much performance as the hardware could handle anyway (according to the very simple approach based on the residual space charge strength). However, as it appeared to be the major candidate, some more systematic work has been performed, at least to see how far the qualitative agreement applied. This is the object of the following section.

IV. 4. Four-Beam Stability as a Function of Tune-per-Crossing

From the "collective instability model" the expectation is listed in the table below⁴, where the first case is the one which has been considered up to now.

Table 1.

Operating Point		Number of Crossings	ν /Crossing	(ξ_{\max}) Theory
ν_x	ν_z			
3.73	1.73	2	.87	.075
3.73	1.73	1	.73	.15
4.80	2.80	2	.40	.22

The second case is easily obtained by separating the beams vertically at one interaction region. Fig. 14 does not show any appreciable difference as compared to Fig. 13. Notice that from the resonance point of view 7th order remains while 8th has now become 4th

order. Apparently, the beams do not perceive any differences, the limits being roughly the same.

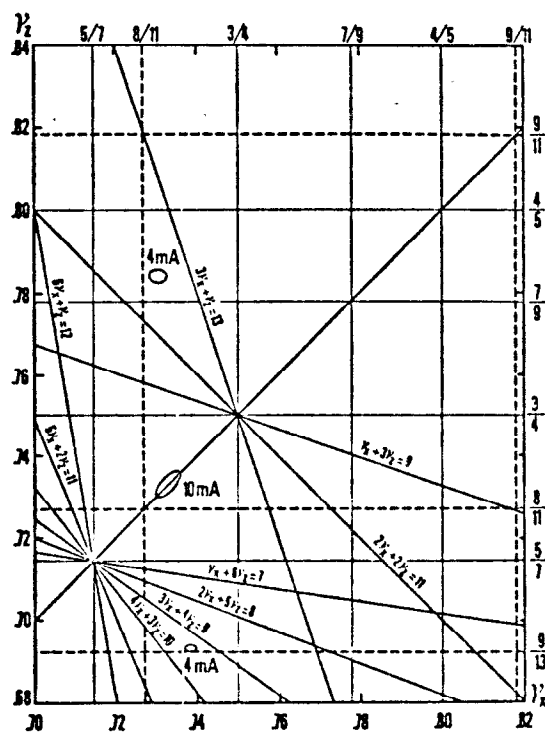


Fig. 14. Stability diagram with four beams and one crossing point at 800 MeV.

The third case corresponds to the initial design operating point of DCI which, however, gave less enthusiasm when it was found that it was impossible to inject there with sextupoles on. According to the small performance that can be obtained with four beams, it has been possible to switch off these sextupoles. A preliminary check showed that the sextupole does not change the stability conditions of the four beams. Moreover, no appreciable difference was found according to the previous cases.

Figs. 15 and 16 show that with four beams the stable area is considerably reduced as compared to two beams only, with the same current per bunch. It becomes more obvious that the four-beam case yields the reverse of what was expected. Finally, neither a transverse feedback nor a detuning of both rings improved the four-beam

case.

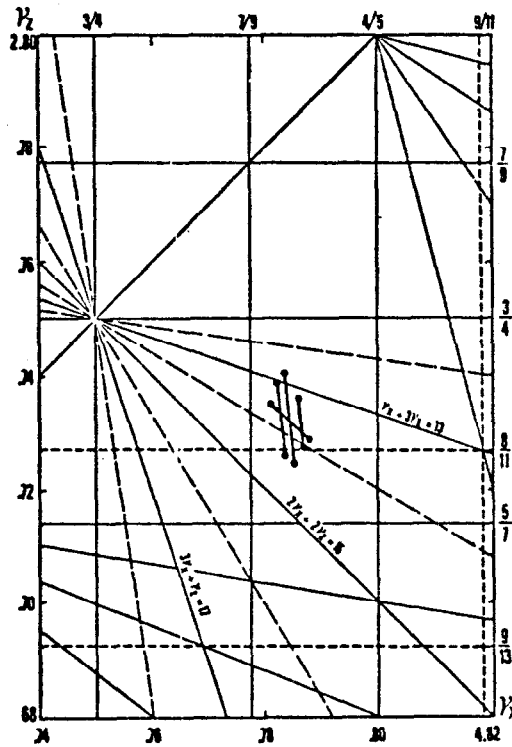


Fig. 15. Stability diagram with four beams ($I_{\text{bunch}} = 2$ mA) at $\nu_x = 4.8$, $\nu_z = 2.8$ with two crossing points. $E = 800$ MeV.

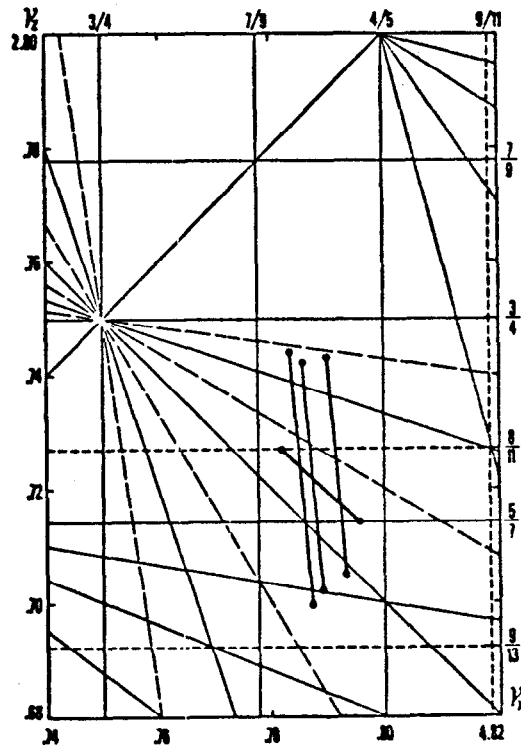


Fig. 16. Stability diagram with two beams ($I_{\text{bunch}} = 2$ mA) at $\nu_x = 4.8$, $\nu_z = 2.8$ with two crossing points. $E = 800$ MeV.

V. THREE-BEAM BEHAVIOR

Experiments with three beams have been done in the strong-weak configuration where a small test beam collides with two strong companion beams. This is a simple way of checking the compensation of the incoherent beam-beam effect.

The test beam was made small enough to not perturb each companion beam, but strong enough to enable luminosity measurements.

The study has been done at $E = 800$ MeV and the main results are summarized in the table below:

Table 2.

Upper Ring		←———— I ₁	I ₂ > I ₁ stable
Lower Ring	→———— i	←———— I ₂	I ₂ ≤ I ₁ unstable
Upper Ring	→———— i	←———— I ₁	I ₁ > I ₂ stable
Lower Ring		←———— I ₂	I ₁ ≤ I ₂ unstable

Whatever sign the test beam is and its location in one of the rings, the interaction is stable when the global sign of the unbalanced companion beams is opposite to the test beam's sign. Otherwise, the interaction is unstable.

Stability here means that no enlargement of the test beam is observable when increasing the strong beam currents. Fig. 17 shows that companion beam intensities up to 55 mA have been achieved with stable configuration while with two beams there is an enlargement factor of 2.5 at 25 mA only. In the unstable case, companion beam intensities of the same order of magnitude as in the stable case have been achieved, but the increase of the effective cross section was considerable above 20 mA. Moreover, there was a visible perturbation of the strong beams. For this reason, it is very difficult to talk about compensation of the incoherent effect rather than stability of coupled bunch modes.

The three-beam experiments were done at a fixed tune, and the stable areas were not investigated in that case.

An attempt to detune the two rings did not succeed in obtaining more stability. However, a proper detuning should include also electric quadrupoles in both rings.

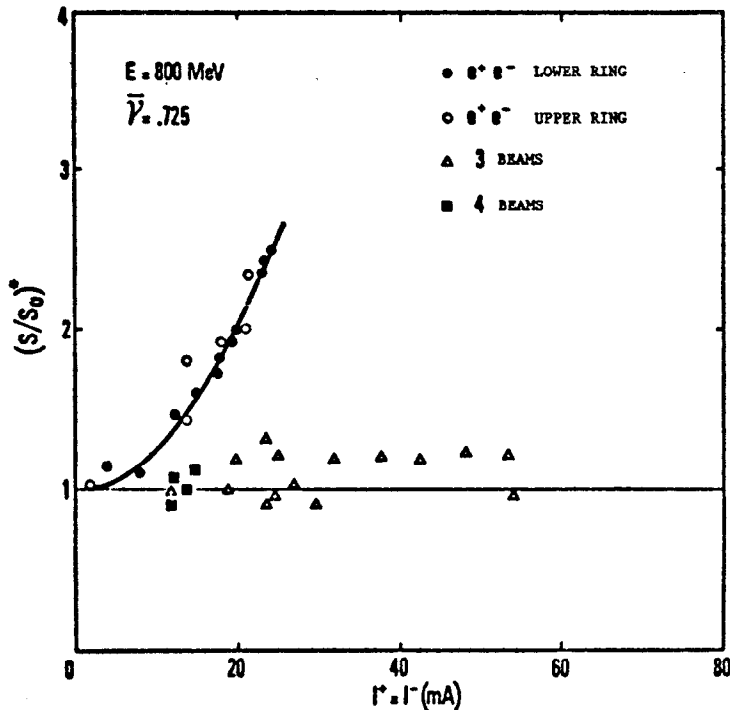


Fig. 17. Beam cross section versus current. Comparison between types of interaction.

VI. COMMENTS AND CONCLUSION

The main fact that comes out of the two-beam experiments on the coupling resonance is the increase of the effective cross section versus current and the corresponding saturation of ξ . A diffusion-like process (Refs. 5, 6, 7, 8, 9) with a threshold would be a good candidate although the effect of the number of crossings could not be checked. The peculiar dependences of the maximum current and luminosity agree very well with a constant maximum beam cross section that remains Gaussian and fills the vertical aperture. Correspondingly, one gets a constant ξ_{\max} , at least over the small energy range considered, which is not in contradiction with a diffusion model for which the ξ value at the threshold would make more sense. The flat beam case remains to be studied more systematically also

as one may expect beam shape distortion close to the limit, leading then to a maximum ξ value that may depend on the energy as observed with other machines. Here notice that the calculation of ξ from luminosity and current measurements is more cautious.

The four-beam behavior definitively kills the simpleminded understanding of the beam-beam effect directly related to the incoherent macroscopic space charge force, linear or even non-linear. There a good candidate appeared to be the collective coherent effect, although present theories look very optimistic and never predicted the present lack of success. Notice that a transverse dipole feedback as well as a detuning of the two rings did not help.

It would be very interesting to know if four-beam and three-beam experiments could help our understanding of two-beam behavior. The tool exists, it would be worth using.

References:

1. J.E. Augustin *et al.*, A MultigeV Electron-Positron Colliding Beam System with Space Charge Compensation, VIIth International Conference on High Energy Accelerators; Vol. 2, p. 113, Yerevan, Aug. 27 - Sept. 2, 1969.
2. J. LeDuff, M.P. Level, Experiences faisceau-faisceau sur DCI, Laboratoire de l'Accélérateur Linéaire, LAL/RT/80-03, Orsay, (Avril 1980).
3. Y.S. Derbenev, Collective Instability of Compensated Colliding Beams, SLAC Translation 151, presented at 3rd All-Union Conference on Accelerators, Moscow, 1972.
4. Nguyen Ngoc Chau, D. Potaux, Stabilité des oscillations transverses dans un anneau à charge d'espace compensée, RT/5-74 and RT/2-75, Groupe "Anneaux de Collisions", LAL, Orsay (1974) and (1975).
5. J. LeDuff, Effet faisceau-faisceau non-linéaire, Diffusion au voisinage des résonances, RT/6-72 "Anneaux de Collisions", Laboratoire de l'Accélérateur Linéaire, Orsay (1972). Also as: PEP Note 65 (1973) and CERN/ISR-AS/74-53 (1974).
6. H.G. Hereward, Diffusion in the Presence of Resonances, CERN/ISR/72-26 (1972).
7. M. Month, Nature of the Beam-Beam Limit in Storage Rings, Proceedings of the Particle Accelerator Conference, Washington, March 12-14, 1975.
8. S.A. Kheifets, Weak Strong Instability as a Diffusion Process, SLAC PUB-2252, PEP Note 278.
9. A.G. Ruggiero, The Theory of a Non-Linear System in Presence of Noise (the beam-beam effect), \bar{p} Note 58, Fermilab (February 1980).



Fermilab

BEAM-BEAM PHENOMENOLOGY

L.C. Teng

June 9, 1980

Introduction

In colliding beam storage rings the beam collision regions are generally so short that the beam-beam interaction can be considered as a series of evenly spaced non-linear kicks superimposed on otherwise stable linear oscillations. Most of the numerical studies on computers were carried out in just this manner. But for some reason this model has not been extensively employed in analytical studies. This is perhaps because all analytical work has so far been done by mathematicians pursuing general transcendental features of non-linear mechanics for whom this specific model of the specific system of colliding beams is too parochial and too repugantly physical. Be that as it may, this model is of direct interest to accelerator physicists and is amenable to (1) further simplification, (2) physical approximation, and (3) solution by analogy to known phenomena.

We define the simplified system as follows:

- (A) head-on collisions of 2 beam bunches at regular intervals, say, once per revolution.
- (B) the weak/strong case in which the strong beam is not affected by collisions with the weak beam. Thus, we have in effect, a single particle colliding with a beam bunch.*
- (C) The strong beam bunch is short compared to the betatron

*Transition to the strong/strong case is similar to the transition from single particle dynamics in an accelerator to the dynamics of a high intensity beam.

wave length of the colliding particle so that it can be approximated by a δ -function in the longitudinal coordinate s .

(D) Close encounters between particles are negligible, hence the beam-beam force is given by a potential. Moreover, since the strong beam is not affected by the colliding particle, the potential is static. The potential depends on the transverse distribution of the beam bunch and can also be approximated by a δ -function in s .

Nature of the Beam-Beam Forces

(A) Extremely non-linear

To get a rough idea of the degree of non-linearity consider a simple round beam with current I . "Outside" the beam at radial location r the magnetic field is

$$B = \frac{2I}{r} . \quad (1)$$

The conventional non-linear field coefficients are

$$b_n \equiv \frac{1}{n!} \frac{1}{B_0} \frac{d^n B}{dr^n} = (-1)^n \frac{2I}{B_0 r^{n+1}} = (-1)^n \frac{B}{B_0} \frac{1}{r^n} \quad (2)$$

where B_0 is the external dipole bending field. For colliding beams the electric and the magnetic forces add, and the non-linear force coefficients are, therefore, approximately $2b_n$. Taking normal values:

$I \sim$ amperes

$r \sim$ millimeters,

$B_0 \sim$ teslas

one gets

$$|b_n| \sim 10^{-4} r^{-n} . \quad (3)$$

This shows that when expressed in units of $[r]^{-n}$ the numerical values of b_n are independent of n , but in bigger units, say cm^{-n} , the numerical

values of b_n increase rapidly with n . This should be compared to the non-linearities arising from errors in the external guide field. Even for the rather poor superconducting dipoles the error non-linear field coefficients fall off rather sharply with increasing n when expressed in units of cm^{-n} .

(B) Non-linear forces are localized to "surface" of beam.

The external error non-linear fields are largest at the coil aperture boundary and decrease rapidly toward the center where the beam resides. The non-linear beam-beam forces behave, however, just in the opposite way. They are largest at the "surface" of the beam and decrease sharply toward the aperture boundary. Hence the beam-beam forces affect the beams much more strongly.

(C) The force potential is periodic in s but very rich in harmonics.

Indeed, if the potential is truly a δ -function of s it will have a "white" harmonic spectrum, i.e. equal harmonic content all the way up to infinite order.

Measure of Beam-Beam Effects

Although many parameters are required to specify the density distribution of the beam bunch and the dynamics of the particle, for simple beam bunch distributions the effects of the beam-beam forces on the colliding particle can be specified by only a few combinations of these parameters. Let us take a bi-Gaussian beam distribution.

$$\rho = \frac{N}{2\pi\sigma_x\sigma_y} \delta(s) \exp\left(-\frac{x^2}{2\sigma_x^2} - \frac{y^2}{2\sigma_y^2}\right) \quad (4)$$

where s is periodic with the periodicity of the ring circumference. The force potential is, then¹

$$\begin{aligned}
V(x,y) &= \frac{r_0 N}{\gamma} \int_0^\infty dt \frac{1 - \exp \left[-\frac{x^2}{2(\sigma_x^2 + t)} - \frac{y^2}{2(\sigma_y^2 + t)} \right]}{\sqrt{(\sigma_x^2 + t)(\sigma_y^2 + t)}} \\
&= \frac{r_0 N}{\gamma} \int_0^\infty d \left(\frac{t}{\sigma_x \sigma_y} \right) G \left(\frac{x^2}{\sigma_x (\sigma_x + \sigma_y)}, \frac{y^2}{\sigma_y (\sigma_x + \sigma_y)} ; \frac{t}{\sigma_x \sigma_y} \left| \frac{\sigma_y}{\sigma_x} \right. \right) \\
&= \frac{r_0 N}{\gamma} F \left(\frac{x^2}{\sigma_x (\sigma_x + \sigma_y)}, \frac{y^2}{\sigma_y (\sigma_x + \sigma_y)} \left| \frac{\sigma_y}{\sigma_x} \right. \right) \tag{5}
\end{aligned}$$

where in the last expressions the parametric dependence on σ_y/σ_x is explicitly indicated. The Hamiltonian for the motion of the particle is

$$H = \frac{1}{2}(p_x^2 + K_x x^2) + \frac{1}{2}(p_y^2 + K_y y^2) + V(x,y) \delta(s). \tag{6}$$

The usual canonical transformation to action-angle variables, namely

$$\begin{cases} x = \sqrt{2\beta_x J_x} \cos \phi_x \\ p_x = -\sqrt{\frac{2J_x}{\beta_x}} \left(\sin \phi_x - \frac{\beta_x'}{2} \cos \phi_x \right) \end{cases} \quad \text{(similar for } y)$$

and $\theta = \frac{s}{R}$ with $2\pi R = \text{circumference}$, gives the transformed Hamiltonian

$$K = v_x J_x + v_y J_y + \frac{r_0 N}{\gamma} F \left(\frac{\beta_x J_x \cos^2 \phi_x}{\sigma_x (\sigma_x + \sigma_y)}, \frac{\beta_y J_y \cos^2 \phi_y}{\sigma_y (\sigma_x + \sigma_y)} \left| \frac{\sigma_y}{\sigma_x} \right. \right) \delta(\theta). \tag{7}$$

Defining the scaled action variables

$$j_x \equiv \frac{\beta_x J_x}{\sigma_x (\sigma_x + \sigma_y)}, \quad j_y \equiv \frac{\beta_y J_y}{\sigma_y (\sigma_x + \sigma_y)}$$

we can write the canonical equations for K as

$$\left\{ \begin{array}{l} \frac{d\phi_x}{d\theta} = \frac{\partial K}{\partial J_x} = v_x - \frac{r_0 N \beta_x}{\gamma \sigma_x (\sigma_x + \sigma_y)} \frac{\partial F}{\partial J_x} \delta(\theta) = v_x - 2\pi \xi_x \frac{\partial F}{\partial J_x} \delta(\theta) \\ \\ \frac{dJ_x}{d\theta} = -\frac{\beta_x}{\sigma_x (\sigma_x + \sigma_y)} \frac{\partial K}{\partial \phi_x} = \frac{r_0 N \beta_x}{\gamma \sigma_x (\sigma_x + \sigma_y)} \frac{\partial F}{\partial \phi_x} \delta(\theta) = 2\pi \xi_x \frac{\partial F}{\partial \phi_x} \delta(\theta). \end{array} \right. \quad (8)$$

(similar for y).

Thus, we see that the motion is uniquely characterized by the five parameters

$$\begin{aligned} v_x, \quad \xi_x &= \frac{1}{2\pi} \frac{r_0 N \beta_x}{\gamma \sigma_x (\sigma_x + \sigma_y)}, \\ & \text{and } \frac{\sigma_y}{\sigma_x}. \end{aligned} \quad (9)$$

$$v_y, \quad \xi_y = \frac{1}{2\pi} \frac{r_0 N \beta_y}{\gamma \sigma_y (\sigma_x + \sigma_y)},$$

Furthermore, we can make the following observations

(a) To the lowest order in x and y or J_x and J_y we have

$$F = 2J_x \cos^2 \phi_x + 2J_y \cos^2 \phi_y \quad (10)$$

and hence the first equation of Eqs. (8) becomes

$$\frac{d\phi_x}{d\theta} = v_x - 2\pi \xi_x (2 \cos^2 \phi_x) \delta(\theta). \quad (11)$$

Since the average value of $2 \cos^2 \phi_x$ is unity we see that to this order ξ_x is just the tune shift.

(b) The betatron wave numbers (tunes) v_x and v_y enter only to relate the phases of the kicks given by $V(x,y)\delta(s)$ in the Hamiltonian (6). If the kicks are random (We shall discuss later what random means here.) v_x and v_y become irrelevant in so far as the overall

characteristics of the motion is concerned.

(c) If there are more than one collision points around the ring and the perturbing kicks at these collision points are random the tune advances between collisions are again irrelevant and the beam-beam effects can be measured by $\langle \xi_x \rangle$ and $\langle \xi_y \rangle$ averaged over all the collision points.

(d) The maximum tolerable beam-beam effects are generally reached when one of the two tune-shifts ξ_x and ξ_y reaches its limiting value. Hence if one is only interested in the beam-beam limits the parameter σ_y/σ_x is irrelevant and only one of the two values ξ_x and ξ_y is crucial.

Semi-Quantitative Features of the Beam-Beam Effect

We consider only the equation for one degree-of-freedom x ,

$$\frac{d^2x}{ds^2} + K(s)x = -\frac{dV(x)}{dx} \delta(s) \quad (12)$$

where the independent variable s is periodic with a period equal to the ring circumference. The following observations are important.

(A) Unperturbed ($\frac{dV}{dx} = 0$) oscillation is linear and long-time stable. Hence accelerators are built to be "linear". Non-linearity can arise from imperfections in design and construction, and from beam-beam interactions. As was seen above, the latter is much larger and is unavoidable in principle. The beam-beam forces impart "kicks" on the colliding particle equal to

$$\Delta x_i' = -\frac{dV(x_i)}{dx_i} \quad (13)$$

on the i^{th} revolution.

(B) If the kicks $\Delta x_i'$ are random the oscillation amplitude will grow. The increment of the Courant-Snyder invariant² $W \equiv \gamma x^2 + 2\alpha x x' + \beta x'^2$ caused by all the $\Delta x_i'$ is

$$\Delta W = \sum_i \left[2(\alpha x_i + \beta x_i') \Delta x_i' + \beta (\Delta x_i')^2 \right] = n\beta (\Delta x')_{\text{rms}}^2. \quad (14)$$

Where the terms linear in $\Delta x_i'$ sum to zero for random $\Delta x_i'$ and where n is the total number of kicks received. The corresponding increment in amplitude A is given by

$$\Delta(A^2) = \beta \Delta W = n\beta^2 (\Delta x')_{\text{rms}}^2. \quad (15)$$

The values assumed for Eq. (3) gives a magnetic field on the "surface" of the beam of ~ 1 gauss. With a beam bunch length of, say, 10^{-1} m and a particle rigidity of 10^{-6} gauss-meter (~ 30 GeV proton) we get

$$(\Delta x')_{\text{rms}} \sim \frac{(1 \text{ gauss})(10^{-1} \text{ m})}{10^6 \text{ gauss-m}} = 10^{-7}. \quad (16)$$

Taking a typical value of $\beta = 10 \text{ m} = 10^4 \text{ mm}$ we get

$$\Delta(A^2) = 10^{-6} n \text{ mm}^2. \quad (17)$$

Thus it takes only 5×10^6 kicks to increase A from 2 mm to 3 mm which is very rapid indeed. This is why a beam transport line with a length equivalent to more than 10^7 kicks of this magnitude (not very long compared to the distance travelled by a particle in a storage ring) can not possibly work.

(C) If the kicks are periodic all evils are concentrated into resonances. On resonance, $\Delta x_i'$ add coherently and A grows proportional to n . Off resonance, $\Delta x_i'$ cancel systematically to give zero amplitude growth.

(D) For perturbations arising from external field errors only low order non-linearities are sizeable. Therefore only low order resonances are excited in appreciable strength. As long as these

resonances are avoided the amplitude growth should be negligible. The drop-off of high order non-linearity is a general characteristic of all fields generated by charges and currents outside the aperture and is a consequence of the vacuum Maxwell equations. This discussion shows also that the resonance expansion is useful only when the resonances excited are limited to low orders.

(E) When the perturbations arise from the field generated by a beam bunch through which the colliding particle travels, the non-linearity and the harmonics of the forces extend to extremely high orders. The tune-space is covered dense (density of rational numbers) by resonances and the unperturbed tune ν_0 sits in a continuum of high order resonances even when all strong low order resonances are avoided. This means that the part of $\Delta x_1'$ which contributes to the continuum of resonances in the neighborhood (within the "line width") of ν_0 appears to be random, the corresponding part of the motion is ergodic, and the oscillation amplitude grows*. This is similar to the statement that a signal which is random in the time domain has a continuous "white" spectrum in the frequency domain. The "natural line width" is rather small, but since ν_0 is always wobbled by some random noises in the external field, with this ν_0 -wobble included the "total line width" could be substantial.

*It may be objected that this is contrary to the KAM theorem which states that for 1 degree-of-freedom when the non-linear perturbation is sufficiently small well behaved KAM surfaces exist and prevent the growth of the oscillation amplitude. There is indication, however, that KAM theorem holds only for extremely small perturbations, much smaller than any physically realistic values. In any case we can always consider the motion in 1 degree-of-freedom as the projection of a motion in 2 degrees-of-freedom for which Arnol'd diffusion does occur and cause unrestricted growth in oscillation amplitude.

(F) Following the reasonings given above and using the bi-Gaussian potential, Eq. (5), we can derive a semi-quantitative formula for the amplitude growth. Putting $\sigma_x = \sigma_y \equiv \sigma$ (round beam) and $y = 0$ in Eq. (5) we get

$$\begin{aligned}
 V(x) &= \frac{r_0 N}{\gamma} \int_0^{\infty} dt \frac{1 - \exp\left[\frac{-x^2}{2(t+\sigma^2)}\right]}{t+\sigma^2} \\
 &= \frac{r_0 N}{\gamma} \sum_{n=0}^{\infty} \frac{(-1)^n}{2^n (n+1)!} \frac{1}{2(n+1)} \left(\frac{x^2}{\sigma^2}\right)^{n+1} \quad (18)
 \end{aligned}$$

and

$$\Delta x' = - \frac{dV}{dx} = \frac{r_0 N}{\gamma \sigma^2} \left[\sum_{n=0}^{\infty} \frac{(-1)^{n+1}}{2^n (n+1)!} \left(\frac{x^2}{\sigma^2}\right)^n \right] x. \quad (19)$$

If only resonances of order m (a large integer) and above can fall inside the ν_0 line-width, the random part of $\Delta x'$ contains only terms with $n > m$. Thus, in the expression for $(\Delta x')_{\text{rms}}$ the summation should only be from m to ∞ . The amplitude growth is, then, given by Eq. (14) to be

$$\frac{dW}{dt} = f\beta (\Delta x')_{\text{rms}}^2 = 8\pi^2 f\xi^2 \left[\sum_{n=m}^{\infty} \frac{(-1)^{n+1}}{(n+1)!} \left(\frac{W}{\epsilon/\pi}\right)^n \right]^2 W \quad (20)$$

where we have used the relations

$$\xi \equiv \frac{1}{4\pi} \frac{r_0 N \beta}{\gamma \sigma^2}$$

$$\left(\frac{x^2}{\beta}\right)_{\text{rms}} \sim \frac{W}{2}$$

$$\frac{4\pi\sigma^2}{\beta} = \epsilon = \text{emittance of beam}$$

and

$f = \frac{dn}{dt}$ = rate of collision between particle and beam bunch.

Generally, the first term in the summation is the largest and we have approximately

$$\frac{dW}{dt} = kf\xi^2 \left(\frac{W}{\varepsilon/\pi} \right)^{2m} W, \quad k \equiv 2 \left[\frac{2\pi}{(m+1)!} \right]^2 \quad (21)$$

Two comments are useful.

(1) The line-width cannot be derived from this crude model. Thus, m must be considered an adjustable parameter. Furthermore, depending on how much reliance one puts on the measured beam emittance ε and on the validity of the approximations, it may be well to consider k also as an adjustable parameter.

(2) Larger line-width corresponds to lower m , hence larger k and larger dW/dt . Thus, the effect of external noise in increasing dW/dt is magnified by the non-linear beam-beam forces through a widening of the line-width.

Comparison of Different Systems

(A) According to the beam and collision geometry

(1) Continuous beams

(a) Crossing at an angle - Kicks are one dimensional (only in direction perpendicular to the crossing plane), hence the motion should be relatively stable.

(b) Colliding head-on - Kicks are two dimensional, hence the motion is expected to be more unstable.

(2) Long bunched beams - The force potential is identical to that of the corresponding case of continuous beams except at the ends of the beam bunches which constitute only a negligible part of the long bunches. The synchrotron motion of particles in the beam bunch will, however, enhance the instability. This can be understood

simply by noting that the number of resonances is increased by the synchro-betatron side-bands and the continuum of resonances is therefore much denser than without the synchro-betatron resonances.

(3) Short bunched beams - If the length of the beam bunches is comparable to their widths the kicks from the beam-beam forces are three dimensional whether the beams are crossing at an angle or colliding head-on. This plus the synchrotron oscillation will make this the most unstable geometry.

(B) According to the particle type

(1) Electrons (positrons)

At the present storage ring energies the synchrotron radiation from these particles is sizeable. The synchrotron radiation produces two major effects on the particle oscillations: (i) damping and (ii) quantum fluctuation which acts as random kicks to blow up the oscillation. In terms of the Courant-Snyder invariant W defined in Eq. (14) we can write

$$\frac{dW}{dt} = Q - \frac{W}{\tau} \quad (22)$$

where $Q(>0)$ is the blowup due to quantum fluctuation and τ is the damping time due to synchrotron radiation. With some modification and reinterpretation the beam-beam effect can be obtained from Eq. (19). The electron beams are not round but flat ribbons with $\sigma_x \gg \sigma_y$, hence the vertical (y) effect is larger and gives the limitations. We first rewrite Eq. (19) as

$$\begin{aligned} \Delta y' &= \frac{r_0 N}{\gamma \sigma_y (\sigma_x + \sigma_y)} (\sigma_x + \sigma_y) \sum_{n=0}^{\infty} \frac{(-1)^{n+1}}{2^n (n+1)!} \left(\frac{y^2}{\sigma_y^2} \right)^{n+\frac{1}{2}} \\ &\cong \frac{2\pi \xi_y}{\beta_y} \sigma_x \sum_{n=0}^{\infty} \frac{(-1)^{n+1} \sqrt{2}}{(n+1)!} \left(\frac{y^2}{2\sigma_y^2} \right)^{n+\frac{1}{2}}. \end{aligned} \quad (23)$$

Eq. (20) then becomes

$$\frac{dW}{dt} = f\beta(\Delta y')_{\text{rms}}^2 = 8\pi^2 f\xi^2 \left(\frac{\sigma_x^2}{\beta}\right) \left[\sum_{n=m}^{\infty} \frac{(-1)^{n+1}}{(n+1)!} \left(\frac{W}{\epsilon/\pi}\right)^{n+\frac{1}{2}} \right]^2 \quad (24)$$

where the subscript y is omitted. Again, taking only the largest term $n = m$ in the summation we get

$$\frac{dW}{dt} = kf\xi^2 \left(\frac{\sigma_x^2}{\beta}\right) \left(\frac{W}{\epsilon/\pi}\right)^{2m+1}, \quad k = 2 \left[\frac{2\pi}{(m+1)!} \right]^2. \quad (25)$$

In addition to the beam-beam effect we can also add an external noise term P . Altogether Eq. (22) is modified to

$$\frac{dW}{dt} = P+Q-\frac{W}{\tau} + kf\xi^2 \left(\frac{\sigma_x^2}{\beta}\right) \left(\frac{W}{\epsilon/\pi}\right)^{2m+1}. \quad (26)$$

The maximum tune shift ξ_{max} that can be obtained is given by the condition $\frac{dW}{dt} = 0$ at a value of W of the order of and proportional to ϵ/π , since the two beams are approximately equal in height. This gives

$$kf\xi_{\text{max}}^2 \left(\frac{\sigma_x^2}{\beta}\right) \left(\frac{W}{\epsilon/\pi}\right)^{2m+1} = \frac{W}{\tau} - Q - P. \quad (27)$$

This leads immediately to the energy (E) dependence of ξ_{max} because we have

$$W \propto \epsilon/\pi \propto E^2, \quad \text{hence } \frac{W}{\epsilon/\pi} \propto E^0;$$

$$\frac{1}{\tau} \propto E^3, \quad \text{hence } \frac{W}{\tau} \propto E^5,$$

$$Q \propto E^5, \text{ coupled over from horizontal;}$$

$$\sigma_x \propto E^0, \text{ because } \sigma_x \text{ is likely aperture limited, and}$$

$$P \propto E^0.$$

The energy dependence of ξ_{\max} can, thus, be

$$\xi_{\max} = (aE^5 - b)^{\frac{1}{2}}. \quad (28)$$

In actuality the measured data from SPEAR³ can be fitted quite well with $b=0$, i.e. no external noise. Fig. 1 shows the fit with

$$\xi_{\max} = 0.01 E^{\frac{5}{2}} \quad (E \text{ in GeV}). \quad (29)$$

The energy dependence of the maximum luminosity L_{\max} is related to that of ξ_{\max}^2 by⁴

$$L_{\max} \propto E^2 \xi_{\max}^2 \propto E^7. \quad (30)$$

Figure 2 shows the fit to SPEAR data with

$$L_{\max} = 0.03 E^7 \quad (E \text{ in GeV}). \quad (31)$$

(2) Protons (antiprotons)

For present storage rings at energies less than tens of TeV the synchrotron radiation for these particles is negligible and the amplitude (or W) growth equation is given by Eq. (21) for round beams to be

$$\frac{dW}{dt} = P + kf\xi^2 \left(\frac{W}{\epsilon/\pi} \right)^{2m} W. \quad (32)$$

Several conclusions can be drawn from this equation.

(a) With all terms positive on the right-hand-side there cannot be any threshold behavior as in the case of electrons. The beam growth rate will simply increase with increasing ξ .

(b) If the beam growth rate is measured by the beam loss on a collimator aperture, the collimator has to be fitted

rather tightly around the beams. As was stated at the beginning, the non-linear beam-beam forces are localized to the "surface" of the beam and fall off rapidly going away from the beam.

(c) Unlike electron beams, proton (antiproton) beams generally do not have Gaussian transverse density distributions. The distribution tends to be more squarish and more truncated. Nevertheless, the qualitative or perhaps even the semi-quantitative features of the development given above should still be valid.

(d) Eq. (32) indicates a beam growth rate proportional to ξ^2 . The same quadratic dependence in Eq. (27) led to the fit shown in Eq. (29). Experiments by Keil⁵ and Zotter⁶ on the CERN-ISR seem, however, to indicate an exponential dependence. This discrepancy must be resolved.

References

1. B.W. Montague, "Calculation of Luminosity and Beam-Beam Detuning in Coasting Beam Interaction Regions", CERN/ISR-GS/75-36 (1975).
2. E.D. Courant and H.S. Snyder, "Theory of the Alternating-Gradient Synchrotron", Annals of Physics, Vol. 3, No. 1, pp. 1-48 (1958).
3. H. Wiedemann, Private communications, also paper given in this seminar.
4. L.C. Teng, "Parametric Fits for the Maximum Luminosity and Tune Shift in e^{\pm} Colliding Beams", Fermilab report TM-938 (1980)
5. E. Keil and G. Leroy, "Effects of a Nonlinear Lens on the Stored Proton Beam in the ISR", IEEE Trans. on Nucl. Sci., Vol. NS-22, No. 3, p. 1370 (1975).
6. B. Zotter, "Experimental Investigation of the Beam-Beam Limit of Proton Beams", Proc. of Xth Int. Conf. on High Energy Accelerators (Protvino) Vol. 2, pp. 23-28 (1977).

BEAM-BEAM TUNE SHIFT IN SPEAR

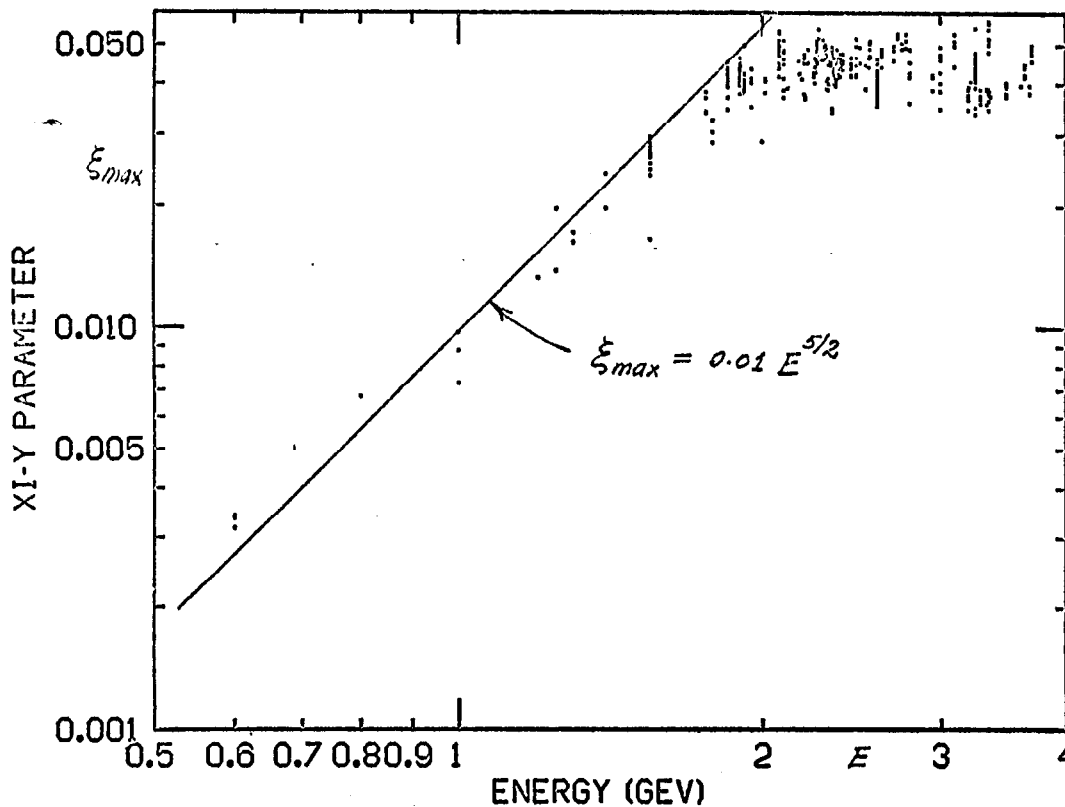


Fig. 1. Maximum vertical tune-shift versus energy in SPEAR

LUMINØSITY IN SPEAR

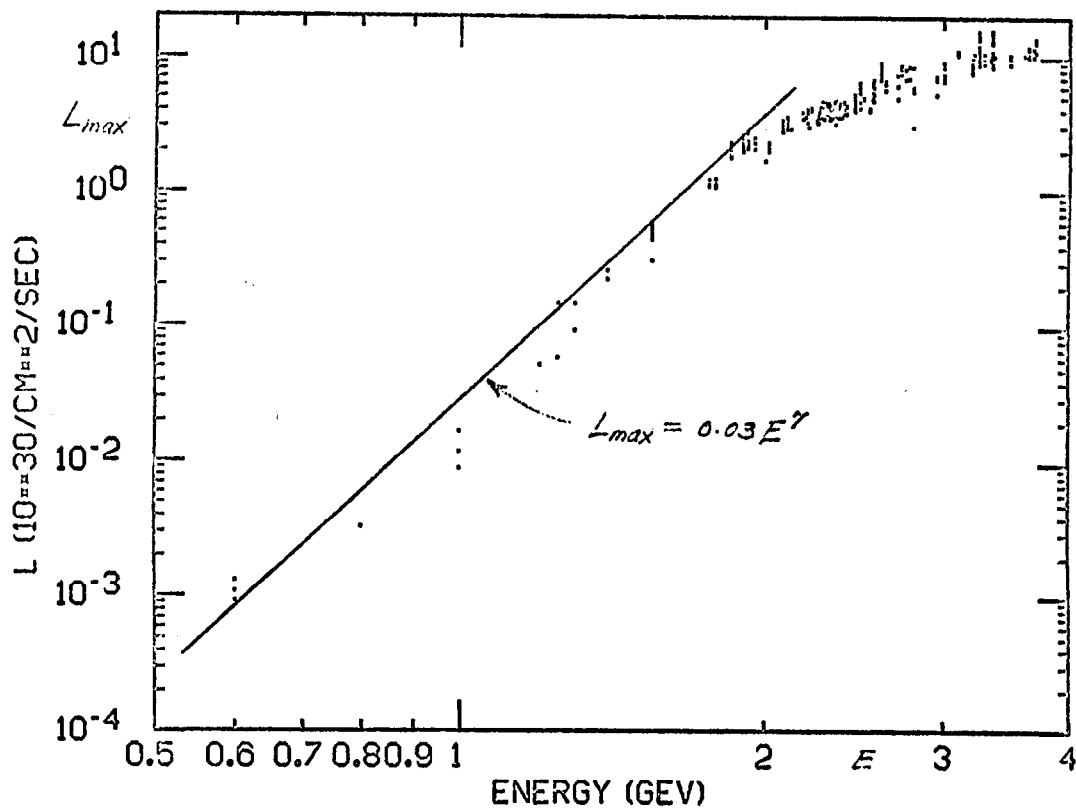


Fig. 2. Maximum luminosity versus energy in SPEAR.

PLASMA INSTABILITY IN ELECTRON AND POSITRON
COLLIDING BEAMS IN STORAGE RING

Han S. Uhm
Naval Surface Weapons Center
White Oak, Silver Spring, Maryland 20910

and

Chuan S. Liu
Department of Physics and Astronomy
University of Maryland
College Park, Maryland 20742

Manuscript Submitted for Seminar on the
Beam-Beam Interaction SLAC, May 22-23, 1980

PLASMA INSTABILITY IN ELECTRON AND POSITRON
COLLIDING BEAMS IN STORAGE RING

Han S. Uhm
Naval Surface Weapons Center
White Oak, Silver Spring, Maryland 20910

and

Chuan S. Liu
Department of Physics and Astronomy
University of Maryland
College Park, Maryland 20742

ABSTRACT

The filamentation instability of the electron and positron colliding beams in a storage ring are investigated within the framework of the rigid beam model and the Vlasov-Maxwell equations, and closed algebraic dispersion relations for the complex eigenfrequency ω are obtained. It is shown that the typical growth rate of instability is a substantial fraction of the electron plasma frequency ω_{pe} , thereby severely limiting the electron density in a storage ring. Moreover, the influence of collective self-field effects on the electron and positron colliding beams in the storage ring is investigated. The analysis is carried out, distinguishing the cases, where (a) the particle motions are in a very coherent orbit, and (b) the randomness dominates the operational condition of a storage ring (e.g., the incoherent collision location by small fluctuation, etc.) In

either case, it is shown that the self-fields effects play a dominant role in the stability behavior of transverse orbit or the expansion of the beam cross section.

INTRODUCTION

There is a growing interest in the equilibrium and stability properties of the electron-positron colliding beams in a storage-ring facility.¹⁻³ A recent experiment⁴ with colliding electron-positron beams at DESY has shown the broadening of the beam cross section, thereby leading to reduction of luminosity. To address this serious problem, we examine the filamentation instability³ of electron-positron beams and the influence of the collective self-field⁵ on the electron-positron colliding beams in the storage ring. For the analytic simplicity, we assume that beams have cylindrical shape and are azimuthally symmetric in the equilibrium state. Equilibrium and stability properties of planar geometric beams are to be presented in a subsequent publication.

In Sec. II, we treat the filamentation instability³ of colliding electron-positron beams with finite-geometry effects included. Stability analysis of dipole oscillation is carried out in Sec. II.A, within the framework of a rigid beam model, which provides a simple instructive description. In Sec. II.B, the analysis for the high harmonic perturbations with $\ell \gg 2$ (where ℓ is azimuthal harmonic number) is carried out within the framework of the Vlasov-Maxwell equations. An important conclusion of the present analysis is that the typical growth rate of the filamentation instability is of the order of the electron plasma frequency ω_{pe} , thereby severely limiting the electron density in a storage ring. However, the analysis of broadening of beam cross section by repeating interaction between electron and positron beams is not completed yet.

The influence of the collective self-fields⁵ on the electron and positron colliding beams in the storage ring is investigated in Sec. III. The

theoretical analysis is carried out, distinguishing the two cases, where (a) the particle motions are in a very coherent orbit and (b) the randomness dominates the operational condition of storage ring (e.g., incoherent collision location by fluctuation, etc.). In either case, it has been found that the self-fields effects play a dominant role in the stability behavior of transverse orbit and the expansion of beam cross section.

II. FILAMENTATION INSTABILITY

Electron and positron colliding beams in storage ring are likely subject to various macro- and micro-instabilities.^{3,6} Perhaps one of the most important instabilities of the electron and positron colliding beam in a storage ring is the filamentation instability. The unstable modes propagates nearly perpendicular to the beam with mixed electrostatic and electromagnetic components, the latter destabilizing and the former stabilizing. The perturbed magnetic field is mostly in the plane perpendicular to the beam and the Lorentz force causes the beam to filamentate, similar to the Weibel instability. Unlike the Weibel modes, which are purely electromagnetic for counter-streaming electron beams, the linear perturbations of colliding electron-positron beams cause both charge and current perturbations giving rise to mixed polarizations. Furthermore, for the case of colliding-beams with radial dimension smaller than the collisionless skin depth c/ω_p , the finite geometry becomes important and the usual assumption of infinite, homogeneous medium is no longer valid. In this paper, we treat the filamentation instability of colliding electron-positron beams with finite geometry effects included. For simplicity, we assume in this section that this colliding beam is straight and infinite along the axial direction.

The analysis is carried out within the framework of both the rigid beam model and the Vlasov-Maxwell equations. As illustrated in Fig. 1, the equilibrium configuration consists of intense relativistic electron and positron beams propagating opposite to each other with axial velocity

$\beta_p c \hat{\xi}_z$ for the positron beam and $\beta_e c \hat{\xi}_z$ for the electron beam, where $\hat{\xi}_z$ is a unit vector along the z-direction and c is the speed of light in

vacuo and $\beta_p = -\beta_e$. Moreover, both beams have the same radius R_b and the same characteristic energy $\gamma_b mc^2$. It is also assumed that the ratio of the beam radius to the collisionless skin depth c/ω_p is small, i.e.,

$$\frac{\nu_j}{\gamma_b} = N_j \frac{e^2}{mc^2} \frac{1}{\gamma_b} \ll 1, \quad (1)$$

where $j=e,p$ denote electrons and positrons, respectively, ν_j is Budker's parameter, $N_j = 2\pi \int_0^\infty dr r n_j^0(r)$ is the number of particles per unit axial length, $n_j^0(r)$ is the equilibrium particle density of beam component j , $-e$ and m are the charge and rest-mass, respectively, of electron. As shown in Fig. 1, we introduce a cylindrical polar coordinate system (r, θ, z) . All equilibrium properties are assumed to be azimuthally symmetric ($\partial/\partial\theta=0$) and independent of axial coordinate ($\partial/\partial z=0$).

A. Rigid Beam Model

In order to illustrate the physical mechanism of this filamentation instability, we carry out the stability analysis in this section within the framework of a "rigid beam" model. For the purpose of analytic simplification, we also specialize to the case of sharp-boundary profiles in which the equilibrium density profiles are rectangular, i.e.,

$$n_j^0(r) = \begin{cases} \hat{n}_j = \text{const}, & 0 < r < R_b, \\ 0, & \text{otherwise,} \end{cases} \quad (2)$$

where $j=e$ and p . Making use of Eq. (2), it is straightforward to show that the equilibrium radial electron field produced by particles of species j is given by

$$E_{jr}(r) = \begin{cases} 2\pi e_j \hat{n}_j r, & 0 < r < R_b, \\ 2\pi e_j \hat{n}_j R_b^2 / r, & r > R_b, \end{cases} \quad (3)$$

where e_j is the charge of particles of beam component j (i.e., $e_j = -e$ for $j=e$ and $e_j = e$ for $j=p$). Similarly, the equilibrium azimuthal magnetic field produced by particles of species j can be expressed as

$$B_{j\theta}(r) = \begin{cases} 2\pi e_j \hat{n}_j \beta_j r, & 0 < r < R_b, \\ 2\pi e_j \hat{n}_j \beta_j R_b^2 / r, & r > R_b, \end{cases} \quad (4)$$

where $V_j = \beta_j c$ is the axial drift velocity and c is the speed of light in vacuo.

In the subsequent analysis, we introduce the center of mass coordinates (X_j, Y_j) for the beam component of species j . In the equilibrium state, we assume that

$$(X_j, Y_j) = (0, 0), \quad (5)$$

for $j=e$, and p . It is also assumed that

$$X_j^2 + Y_j^2 \ll R_b^2. \quad (6)$$

The restriction to small perturbation amplitudes makes the subsequent stability analysis tractable. The transverse motion of a single particle of species j is determined approximately from

$$m_j \frac{d^2}{dt^2} \mathbf{x}_j = e_j \left(\mathbf{E} + \frac{1}{c} \frac{d}{dt} \mathbf{x}_j \times \mathbf{B} \right), \quad (7)$$

where $\underline{x}_j = (x_j, y_j)$ is the position coordinate for a particle of species j and \underline{E} and \underline{B} are the total electric and magnetic fields, and $m_j = \gamma_b m$ is the relativistic mass. Assuming \underline{E} and \underline{B} can be approximated by their equilibrium values, we substitute Eqs. (3) and (4) into Eq. (7). The equation of motion for the x direction can be expressed as

$$m_j \frac{d^2}{dt^2} x_j = 2\pi e_j \sum_k \hat{n}_k e_k (1 - \beta_j \beta_k) (x_j - x_k) . \quad (8)$$

Neglecting momentum spread, Eq. (8) can be averaged over the beam cross section. After some straightforward algebra, we obtain the approximate equation for average motion on the x direction,

$$m_j \frac{d^2}{dt^2} X_j = 2\pi e_j \sum_k \hat{n}_k e_k (1 - \beta_j \beta_k) (X_j - X_k) . \quad (9)$$

Similarly, the equation for average motion in the y direction is given by

$$m_j \frac{d^2}{dt^2} Y_j = 2\pi e_j \sum_k \hat{n}_k e_k (1 - \beta_j \beta_k) (Y_j - Y_k) . \quad (10)$$

Defining

$$Z_j = X_j + iY_j \quad (11)$$

and making use of Eqs. (9) and (10), we obtain

$$\frac{d^2}{dt^2} Z_j = \frac{2\pi e_j}{m_j} \sum_k \hat{n}_k e_k (1 - \beta_j \beta_k) (Z_j - Z_k) . \quad (12)$$

We seek oscillatory wave solutions to Eq. (12) of the form

$$Z_j = \hat{Z}_j \exp \{i[k_z(z + \beta_j c t) - \omega t]\} \quad (13)$$

where ω is the complex eigenfrequency, $\hat{Z}_j = \text{const}$ is the perturbed amplitude, and the axial wavenumber k_z is limited to the range

$$k_z^2 R_b^2 \lesssim 1 \quad . \quad (14)$$

Equation (14) assures the approximate validity of Eq. (12) for wave perturbations with $\partial/\partial z \neq 0$. Substituting Eq. (13) into Eq. (12), we obtain

$$\left[(\omega - k_z \beta_j c)^2 + \frac{2\pi e_i}{m_j} \sum_k \hat{n}_k e_k (1 - \beta_j \beta_k) \right] \hat{Z}_j = \frac{2\pi e_i}{m_j} \sum_k \hat{n}_k e_k (1 - \beta_j \beta_k) \hat{Z}_k \quad (15)$$

Equation (15) gives two homogeneous equations relating the amplitudes \hat{Z}_e and \hat{Z}_p . Setting the determinant of the coefficients of \hat{Z}_j equal to zero gives 2×2 matrix dispersion equation that determines the complex eigenfrequency ω . After some straightforward algebra, we obtain the dispersion relation

$$\left[(\omega + k_z c)^2 - \omega_{pe}^2 \left(\frac{\hat{n}_p}{\hat{n}_e} \right) \right] \left[(\omega - k_z c)^2 - \omega_{pe}^2 \right] = \omega_{pe}^4 \left(\frac{\hat{n}_p}{\hat{n}_e} \right) \quad , \quad (16)$$

where $\omega_{pe}^2 = 4\pi e^2 \hat{n}_e / \gamma_b m$ is the electron plasma frequency-squared and use has been made of $\beta_e = -\beta_e \approx 1$, which is consistent with present experimental parameters.

Assuming that both electron and positron beams have the same density,

and defining

$$a = k_z c + \omega_{pe} , \quad b = k_z c - \omega_{pe} , \quad (17)$$

we simplify the dispersion relation in Eq. (16) as

$$(\omega^2 - a^2)(\omega^2 - b^2) = \omega_{pe}^4 , \quad (18)$$

which provides a necessary and sufficient condition

$$\omega_{pe}^4 > a^2 b^2 = (k_z^2 c^2 - \omega_{pe}^2)^2 \quad (19)$$

for instability. For the unstable branch, the perturbation is purely growing with the growth rate

$$\omega_i = \text{Im}\omega = \left\{ \left[\left(\frac{a^2 - b^2}{2} \right)^2 + \omega_{pe}^4 \right]^{1/2} - \frac{a^2 + b^2}{2} \right\}^{1/2} . \quad (20)$$

The maximum growth rate of instability can occur at $a=0$ or $b=0$, thereby giving

$$(\omega_i)_m = (5^{1/2} - 2)^{1/2} \omega_{pe} \approx 0.5 \omega_{pe} . \quad (21)$$

For colliding beams interacting over a finite distance L , the axial wavenumber k_z is $k_z = 2\pi n/L$ where $n=1,2,\dots$. In this case, the condition for $a=0$ becomes $L\omega_{pe}/c = 2\pi n$. The finite interaction length also imposes a severe condition for the instability to grow significantly before the beam exit. Although a small growth of perturbations during one individual

interaction of electron and positron beams, we expect that due to this filamentation instability, the repating interactions between both beams eventually convert the longitudinal energy of the beams into the transverse energy of beams and the field energy of perturbations, thereby broadening the beam cross section and leading to reduction of luminosity. However, the analysis of broadening of beam cross section is particularly difficult and is currently under investigation by the authors.

B. Vlasov Description

In the previous section, we have investigated the stability properties of dipole oscillation in the transverse instability for the electron and positron colliding beams, within the context of rigid beam model. Although a dipole oscillation in a rigid beam model provides a simple instructive description, it is necessary to investigate stability properties for perturbations with high azimuthal harmonic number $\ell > 2$ within the framework of the Vlasov-Maxwell equations.

For beams of well-defined energy and momentum, an equilibrium associated with the steady-state ($\partial/\partial t=0$) beam distribution function,

$$f_j^0(H, P_\theta, P_z) = \frac{\hat{n}_j}{2\pi\gamma_b m} \delta(H - \omega_j P_\theta - \hat{\gamma}_j m c^2) \delta(P_z - \gamma_b m \beta_j c) , \quad (22)$$

is particularly suited for stability analysis, where the total energy,

$$H = (m^2 c^4 + c^2 P^2)^{1/2} + e_j \phi_0(r) , \quad (23)$$

the canonical angular momentum,

$$P_\theta = r p_\theta , \quad (24)$$

and the axial canonical momentum

$$P_z = p_z + (e_j/c)A_z^S(r) , \quad (25)$$

are the three single-particle constants of the motion in the equilibrium fields, and ω_j is the beam rotational frequency of species j and $\hat{\gamma}_j$ is a constant. In Eqs. (23)-(25), $\phi_0(r)$ is the equilibrium self-electric potential, $A_z^S(r)$ is the axial component of vector potential for the azimuthal self-magnetic field, and $\mathbf{p} = (p_r, p_\theta, p_z)$ denotes mechanical momentum and is related to the particle velocity \mathbf{v} by $\mathbf{v} = (\mathbf{p}/m)(1 + p^2/m^2 c^2)^{-1/2}$.

Since the r - θ kinetic energy of particles is small in comparison with the characteristic energy $\gamma_b m c^2$, it is straightforward to show that the term $H - \omega_j P_\theta$ in Eq. (22) can be approximated by⁷

$$H - \omega_j P_\theta = \gamma_b m c^2 + \frac{p_\perp^2}{2\gamma_b m} + \frac{1}{2} \gamma_b m \Omega_j^2 r^2 , \quad (26)$$

where

$$\gamma_b^2 = (1 - \beta_p^2)^{-1}, \quad p_\perp^2 = p_r^2 + (p_\theta - \gamma_b m \omega_j r)^2 ,$$

and

$$\Omega_j^2 = (\hat{\omega}_j - \omega_j)(\omega_j + \hat{\omega}_j) = -\omega_j^2 - \frac{2\pi e}{\gamma_b m} \sum_k \hat{n}_k e_k (1 - \beta_j \beta_k) . \quad (27)$$

In Eq. (27), the laminar rotation frequency $\hat{\omega}_j$ is defined by

$$\hat{\omega}_j = \left[-\frac{2\pi e j}{\gamma_b m} \sum_k \hat{n}_k e_k (1 - \beta_j \beta_k) \right]^{1/2}. \quad (28)$$

Substituting Eq. (26) into Eq. (22), we find the equilibrium particle density profile

$$\begin{aligned} n_j^o(r) &= \int d^3 p f_j^o(H, P_\theta, P_z) \\ &= \begin{cases} \hat{n}_j, & 0 \leq r < R_b, \\ 0, & \text{otherwise,} \end{cases} \end{aligned} \quad (29)$$

where the beam radius R_b is defined by

$$R_b^2 = 2c^2 (\hat{\gamma}_j - \gamma_b) / \gamma_b \Omega_j^2 \quad (30)$$

for $j=e,p$. Equation(30) ensures that the electron and positron beams have the common beam radius R_b . It is important to note from Eqs. (27) and (30) that the radially confined equilibrium exists only for the rotational frequency ω_j satisfying

$$-\hat{\omega}_j < \omega_j < \hat{\omega}_j. \quad (31)$$

Additional equilibrium properties associated with the distribution function in Eq. (22) are discussed in Ref. 7.

In order to obtain the dispersion relation for filamentation instability of the electron and positron beams, we make use of the linearized Vlasov-Maxwell equations. For perturbations with azimuthal

harmonic number ℓ and axial wavenumber k_z , a perturbed quantity $\delta\phi(\underline{x},t)$ can be expressed as $\delta\phi(\underline{x},t)=\hat{\phi}(r)\exp\{i(\ell\theta+k_z z-\omega t)\}$, where ω is the complex eigenfrequency. The present stability analysis is carried out in long parallel wavelength and low frequency perturbation satisfying $k_z^2 R_b^2 \ll \ell^2 + 1$, $|\omega R_b/c|^2 \ll \ell^2 + 1$. With this assumption, the axial components of perturbed field $E_z(r)$ and $B_z(r)$ are negligible and the Maxwell equations of perturbed potentials can be expressed as

$$\left(\frac{1}{r} \frac{\partial}{\partial r} r \frac{\partial}{\partial r} - \frac{\ell^2}{r^2}\right) \hat{\phi}(r) = -4\pi\hat{\rho}(r) \quad (32)$$

and

$$\left(\frac{1}{r} \frac{\partial}{\partial r} r \frac{\partial}{\partial r} - \frac{\ell^2}{r^2}\right) \hat{A}(r) = -\frac{4\pi}{c} \hat{J}_z(r) \quad (33)$$

where $\hat{\phi}(r)$ is the perturbed electrostatic potential, $\hat{\rho}(r)$ is the perturbed charge density, $\hat{A}(r)$ and $\hat{J}_z(r)$ are the axial components of the perturbed vector potential and current density, respectively. Components of perturbed fields can be expressed in terms of $\hat{\phi}(r)$ and $\hat{A}(r)$ as $\hat{E}_\theta = -i\ell\hat{\phi}(r)/r$, $\hat{E}_r(r) = -(\partial/\partial r)\hat{\phi}(r)$, $\hat{B}_r(r) = i\ell\hat{A}(r)/r$, and $\hat{B}_\theta(r) = -(\partial/\partial r)\hat{A}(r)$.

In order to calculate perturbed charge and current densities, we solve the linearized Vlasov equation to obtain the perturbed distribution function⁷

$$\begin{aligned} \hat{f}_j(r,p) &= \frac{e_j \gamma_j b_j^m}{p_\perp} \frac{\partial f_j^0}{\partial p_\perp} \left\{ \hat{\psi}_j(r) + (\omega - \ell\omega_j - k_z \beta_j c) \right. \\ &\times \left. \int_{-\infty}^0 d\tau \ i \hat{\psi}_j(r') \exp[i\ell(\theta' - \theta) - i(\omega - k_z \beta_j c)\tau] \right\}, \end{aligned} \quad (34)$$

where the perturbed electrostatic potential $\hat{\psi}_j(\mathbf{r})$ in the frame of reference moving with velocity $\beta_j c$ is defined by $\hat{\psi}_j(\mathbf{r}) = \hat{\phi}(\mathbf{r}) - \beta_j \hat{A}(\mathbf{r})$ and use has been made of $p_z / \gamma_b m \approx \beta_j$ consistent with Eq. (1). It is useful to introduce the polar momentum variables (p_\perp, ϕ) in the rotating frame defined by $p_x + \gamma_b m \omega_j y = p_\perp \cos \phi$, $p_y - \gamma_b m \omega_j x = p_\perp \sin \phi$. Note also that the Cartesian coordinates (x, y) are related to the polar coordinates (r, θ) by $x = r \cos \theta$ and $y = r \sin \theta$. In this context, the transverse equation of motion of particles can be expressed as⁷

$$\begin{aligned} x'(\tau) &= (1/\hat{\omega}_j) [(p_\perp/\gamma_b m) \cos \phi \sin \hat{\omega}_j \tau - r \omega_j \sin \theta \sin \hat{\omega}_j \tau + r \hat{\omega}_j \cos \theta \cos \hat{\omega}_j \tau] \\ y'(\tau) &= (1/\hat{\omega}_j) [(p_\perp/\gamma_b m) \sin \phi \sin \hat{\omega}_j \tau + r \omega_j \cos \theta \sin \hat{\omega}_j \tau + r \hat{\omega}_j \sin \theta \cos \hat{\omega}_j \tau]. \end{aligned} \quad (35)$$

where $\tau = t' - t$, and the harmonic frequency $\hat{\omega}_j$ is defined in Eq. (28).

Upon integration of Eq. (34), the perturbed charge density can be found to be

$$\hat{\rho}(\mathbf{r}) = 2\pi e^2 \sum_j \gamma_b m \int_0^\infty dp_\perp p_\perp \int_{-\infty}^\infty dp_z \frac{1}{p_\perp} \frac{\partial f_j^0}{\partial p_\perp} [\hat{\psi}_j(\mathbf{r}) + (\omega - \ell \omega_j - k_z \beta_j c) I_j]. \quad (36)$$

where the orbit integral I_j is defined by

$$I_j = i \int_0^{2\pi} \frac{d\phi}{2\pi} \int_{-\infty}^0 d\tau \hat{\psi}_j(\mathbf{r}') \exp \{ i [\ell (\theta' - \theta) - (\omega - k_z \beta_j c) \tau] \}. \quad (37)$$

Similarly the perturbed axial current density can be obtained. For analytic traceability, we will consider here a class of special solutions

for which the perturbed charge and current density are localized on the beam surface, i.e., equal to zero except at $r=R_b$. More general perturbations, particularly the body wave perturbations, are to be presented in a subsequent publication. In this case, it follows from Eqs. (32) and (33) that the function $\psi_j(r)$ has the simple form $\hat{\psi}_j(r) = \hat{\phi}(r) - \beta_j \hat{A}(r) = C_j r^\ell$ for $0 < r < R_b$. Substituting Eq. (35) into Eq. (37) it is readily shown that

$$I_j = \frac{i\hat{\psi}_j(r)}{(2\hat{\omega}_j)^\ell} \int_{-\infty}^0 d\tau \exp[-i(\omega - k_z \beta_j c)\tau] [(\omega_j + \hat{\omega}_j) \exp(i\hat{\omega}_j \tau) - (\omega_j - \hat{\omega}_j) \exp(-i\hat{\omega}_j \tau)]^\ell. \quad (38)$$

After some straightforward algebra that utilizes Eqs. (22), (36) and (38), Eq. (32) can be expressed as

$$\left(\frac{1}{r} \frac{\partial}{\partial r} r \frac{\partial}{\partial r} - \frac{\ell^2}{r^2} \right) \hat{\phi}(r) = - \sum_j \hat{\psi}_j(r) \frac{\omega_j^2}{\Omega_j^2 R_b} \Gamma_j(\omega) \delta(r - R_b), \quad (39)$$

where $\omega_{pj}^2 = 4\pi e^2 n_j / \gamma_b m$ is the plasma frequency - squared of beam component j , $\Omega_j^2 = (\hat{\omega}_j - \omega_j)(\omega_j + \hat{\omega}_j)$ is defined in Eq. (27) and $\Gamma_j(\omega)$ is defined by

$$\Gamma_j(\omega) = -1 + \left(\frac{\hat{\omega}_j - \omega_j}{2\hat{\omega}_j} \right)^\ell \sum_{n=0}^{\ell} \frac{\ell!}{n!(\ell-n)!} \frac{\omega - \ell\omega_j - k_z \beta_j c}{\omega - k_z \beta_j c + \ell\hat{\omega}_j - 2n\hat{\omega}_j} \left(\frac{\omega_j + \hat{\omega}_j}{\hat{\omega}_j - \omega_j} \right)^n \quad (40)$$

Similarly, Eq. (33) can be expressed as

$$\left(\frac{1}{r} \frac{\partial}{\partial r} r \frac{\partial}{\partial r} - \frac{\ell^2}{r^2} \right) \hat{A}(r) = - \sum_j \beta_j \hat{\psi}_j(r) \frac{\omega_j^2}{\Omega_j^2 R_b} \Gamma_j(\omega) \delta(r - R_b). \quad (41)$$

where use has been again made of the approximation $p_z / \gamma_b m \approx \beta_j c$ consistent with Eq. (1).

As the right-hand sides of the coupled differential equations (39) and (41) are equal to zero except at the surface of the beam $r=R_b$, they can be solved in a straightforward manner to give

$$C_k = \sum_j (1 - \beta_k \beta_j) \frac{\omega_{pj}^2}{2\ell\Omega_j^2} \Gamma_j(\omega) C_j. \quad (42)$$

In the case when the beams are located inside the cylindrical conducting wall with radius R_c , the term C_k in the left-hand side of Eq. (42) is replaced by $[1 - (R_b/R_c)^2]^{-1} C_k$. Note that the absolute value of $\omega_{pj}^2 \Gamma_j(\omega) / \Omega_j^2$ in Eq. (42) is of the order of unity or less. It follows from Eq. (42) that the condition for a nontrivial solution (C_j not all zero) is given by

$$1 - (\omega_{pp}^2 \omega_{pe}^2 / \ell^2 \Omega_p^2 \Omega_e^2) \Gamma_p(\omega) \Gamma_e(\omega) = 0, \quad (43)$$

where use has been made of $\beta_p = -\beta_e \approx 1$ and $\gamma_b^{-2} \ll 1$, which is consistent with present experimental parameters. Equation (42), when combined with Eq. (40), constitutes one of the main results of this paper and can be used to investigate filamentation stability properties for a broad range of system parameters.

As an example, we restrict the investigation of dispersion relation (43) to the case, where both beams are in a cold fluid rotational equilibrium characterized by $\omega_j \rightarrow \pm \hat{\omega}_j$. A careful examination of expression for $\Gamma_j(\omega)$ show that⁷

$$\lim_{\omega_j \rightarrow \pm \hat{\omega}_j} \left[\frac{\omega_{pj}^2}{2\ell\Omega_j^2} \Gamma_j(\omega) \right] = \frac{\omega_{pj}^2}{2(\omega - k_z \beta_j c \mp \ell \hat{\omega}_j) [\omega - k_z \beta_j c \mp (\ell - 2) \hat{\omega}_j]} \quad (44)$$

Therefore, in a cold fluid limit, the dispersion relation in Eq. (43) can be considerably simplified. After some algebraic manipulation we can show that for the fundamental mode perturbation (i.e., $\ell=1$), the dispersion relation in Eq. (43) is identical to Eq. (16) obtained within the framework of rigid beam model. The stability analysis of Eq. (43) for a broad range of harmonic number ℓ and rotational frequency ω_j is currently under investigation by the authors. Nonlinearly the beams become filamentated first, then the current filaments of the same sign attract each other to form a broader beam. Finally, we conclude this section by pointing out that the understanding in broadening in beam cross section by repeating interactions of beams is not completed yet. And this area is currently under investigation by the authors.

III. COLLECTIVE SELF-FIELD EFFECTS

In this section, we examine the influence of the collective self-fields⁵ on the electron and positron colliding beams in the storage ring. While the forces of the self-generated electric and magnetic field of a highly relativistic electron (positron) beam on an electron (positron) cancel out to order $O(\gamma^{-2})$, i.e., $E_r + \beta_c B_\theta \approx O(\gamma^{-2})$ the forces of the electric and magnetic fields of the electron beam on the colliding positrons are additive leading to radial acceleration. This effect of the collective self-fields of one species on the other species of the colliding beams imparts considerable transverse energy, thereby substantially increasing the beam transverse dimensions upon collision. In order to make the problem simple, we assume that the colliding section of the storage ring is straight. The theoretical analysis is carried out, distinguishing the two cases, where (a) the particle motions are in a very coherent orbit and (b) the randomness dominates the operational condition of storage ring (e.g., incoherent collision location by fluctuation, etc.). In either case, it is found that the self-fields effects play a dominant role in the stability behavior of transverse orbit or the expansion of beam cross section. For present experimental parameters⁴ at DESY, the cross section of the beam can be expanded to ten times of its original area within 5 milliseconds operational time. Without loss of generality, we assume in Fig. 1 that the front edges of both beams arrive in $z=0$ at time $t=0$.

The axial orbit of particles of beam component j is given by

$$z = z_j + \beta_j ct \quad (45)$$

where the initial position z_j is restricted to satisfy

$$z_j(z_j + \epsilon_j L) < 0 . \quad (46)$$

Here $\epsilon_j = \text{sgn } e_j$ and e_j is the charge of the particles of beam component j .

The particle density profile of beam component j is expressed as

$$n_j^0(r, z, t) = n_j(r, z) U[(\beta_j ct - z)(z + \epsilon_j L - \beta_j ct)] , \quad (47)$$

where the Heaviside step function $U(x)$ is defined by

$$U(x) = \begin{cases} 0, & x < 0 , \\ 1, & x > 0 . \end{cases} \quad (48)$$

For a specific choice of the beam density $n_j(r, z)$ in Eq. (47), the potentials for the self-fields are to be calculated from the Maxwell equations. The Poisson equation can be approximated by

$$\frac{1}{r} \frac{\partial}{\partial r} r \frac{\partial}{\partial r} \phi(r, z, t) = - 4\pi \sum_j e_j n_j^0(r, z, t) , \quad (49)$$

where $\phi(r, z, t)$ is the self-electric potential. In obtaining Eq. (49), we neglect the term proportional to $\partial^2 \phi / \partial z^2$, under the assumption that the axial length L of the beam is much larger than the beam radius and the effects of the leading edge of the beams are thus neglected. Furthermore, the z -component of the $\nabla \times \mathbf{B}^S(\mathbf{x})$ Maxwell equation is expressed as

$$\frac{1}{r} \frac{\partial}{\partial r} r \frac{\partial}{\partial r} A_z^S(r, z, t) = - 4\pi \sum_j e_j \beta_j n_j^0(r, z, t) , \quad (50)$$

where $A_z^S(r, z, t)$ is the z -component of the self-vector potential. Other components of the vector potential are negligible because of Eq. (1). Defining the effective self-potential $\psi_j^S(r, z, z_j) = \phi - \beta_j A_z^S$, and making use of Eqs. (45) (47), (49), and (50), we have

$$\begin{aligned} \frac{\partial}{\partial r} \psi_j^S(r, z, z_j) &= - 8\pi e_k \frac{1}{r} \int_0^r dr' r' n_k(r', z) \\ &\times U[(z_j - 2z)(2z - z_j + \epsilon_k L)] , \end{aligned} \quad (51)$$

where $k \neq j$. In obtaining Eq. (51), use has been made of $\gamma_b^{-2} = (1 - \beta_p^2) \ll 1$.

In order to make the problem simple, we carry out the analysis in the average applied field provided externally by the periodic quadrupole magnetic field, similar to that used in the previous study⁶. In this regard, the applied focussing force can be obtained from the axial component of the effective vector potential

$$A_z^{\text{ext}}(r) = -(\gamma_b m / 2e\beta_p) \omega_f^2 r^2 \quad (52)$$

where ω_f is the focussing oscillation frequency determined by the quadrupole field gradient.

The total energy of particles of the beam component j is given by

$$H = (m^2 c^4 + c^2 \tilde{p}^2)^{1/2} + e_j \phi(r, z, t), \quad (53)$$

where the lower case p denotes mechanical momentum and is related to the particle velocity \tilde{v} by $\tilde{v} = \tilde{p} / m(1 + \tilde{p}^2 / m^2 c^2)^{1/2}$. Since the r - θ kinetic energy of particles is small in comparison with the characteristic energy $\gamma_b m c^2$ and $v_j / \gamma_b \ll 1$ in Eq. (1), it is straightforward to show that Eq. (53) can be approximated by

$$H = \gamma_b m c^2 + \frac{p_x^2 + p_y^2}{2\gamma_b m} + e_j \psi_j^s(r, z, z_j) + \frac{1}{2} \gamma_b m \omega_f^2 r^2, \quad (54)$$

where $\gamma_b^2 = (1 - \beta_j^2)^{-1}$. From Eq. (54), we obtain the equation of motion for

$$Z(t) = x(t) + iy(t) \quad (55)$$

where $i = (-1)^{1/2}$. Making use of Eqs. (45) and (55), and $\beta_j^2 \approx 1$, the equation of motion for particles of the beam component j is given by

$$\frac{d^2 Z}{dz^2} + \frac{8\pi e^2}{\gamma_b m c^2} \cdot \frac{Z}{r^2} \int_0^r dr' r' n_k(r', z) U[(z_j - 2z)(2z - z_j + \epsilon_k L)] + \frac{\omega_f^2}{c^2} Z = 0 \quad (56)$$

where $k \neq j$ and z_j is defined in Eq. (45). Equation (56) determines the transverse position of particles of beam component j , thereby providing the information of the particle density $n_j(r, z)$, which in turn governs the equations of motion for particles of the beam component k . In this regard, the coupled differential equation (56) for $j=e$ and p can be used to investigate the temporal profile evolutions of various beam properties for a broad range of initial parameters.

As an example, we consider a tenuous positron beam satisfying

$$\bar{\omega}_{pp}^2 \ll (c/L)^2, \quad (57)$$

where $\bar{\omega}_{pp}^2 = 4\pi\bar{n}_p e^2 / \gamma_b m$ is the average positron plasma frequency-squared in the laboratory frame. Equation (57) assures that all the electrons move on the straight paths with constant radius r during the collision. Assuming the electron density profile as

$$n_e(r, z) = \begin{cases} \hat{n}_e, & r < R_b, \\ 0, & \text{otherwise,} \end{cases} \quad (58)$$

the transverse equation of motion for positron can be expressed as

$$\frac{d^2 Z}{dz^2} + \frac{\omega_{pe}^2}{c^2} Z U[(z_p - 2z)(2z - z_p - L)] + \frac{\omega_f^2}{c^2} Z = 0, \quad (59)$$

where $\omega_{pe}^2 = 4\pi\hat{n}_e e^2 / \gamma_b m$ is the electron plasma frequency-squared.

Without loss of generality, we assume that there is one pair of electron and positron beams in the entire system, thereby indicating that the whole storage ring can be represented by two focusing sectors. Each sector consists of a self-beam focusing set (the region in which beams collide) and an applied focusing set. The subsequent analysis is carried out distinguishing the two cases: (a) the positrons move on a very coherent orbit, and (b) the

axial location of collision as well as the beam length fluctuates incoherently, thereby the ensemble average can be feasible.

A. Stability Analysis of Coherent Positron Orbit

The stability properties of individual particle orbit can be determined from the transformation matrix of one sector⁸ for a very coherent positron orbit. Assuming that a positron has an initial condition $Z=Z_1$ and $Z' = (dZ/dz) = Z'_1$ at $z = z_p/2$, it can be shown from Eq. (59) that the transverse orbit of this positron is given by

$$Z = Z_1 \cos[(\omega_T/c)(z - z_p/2)] + (Z'_1 c / \omega_T) \sin[(\omega_T/c)(z - z_p/2)] , \quad (60)$$

for $z_p/2 < z < z_p/2 + L$. Here the frequency $\omega_T = (\omega_{pe}^2 + \omega_f^2)^{1/2}$. From Eq. (60) it is also straightforward to show that the transverse position Z_2 and orbit slope Z'_2 of positron, when it emerges from the right-hand side of the electron beam, is given by

$$\begin{pmatrix} Z_2 \\ Z'_2 \end{pmatrix} = \begin{pmatrix} \cos(\omega_T L / 2c) & (c / \omega_T) \sin(\omega_T L / 2c) \\ -(\omega_T / c) \sin(\omega_T L / 2c) & \cos(\omega_T L / 2c) \end{pmatrix} \begin{pmatrix} Z_1 \\ Z'_1 \end{pmatrix} \quad (61)$$

Similarly, when the applied focusing section has been traversed, the position and orbit slope are given by

$$\begin{pmatrix} Z_3 \\ Z'_3 \end{pmatrix} = \begin{pmatrix} \cos\phi & (c / \omega_f) \sin\phi \\ -(\omega_f / c) \sin\phi & \cos\phi \end{pmatrix} \begin{pmatrix} Z_2 \\ Z'_2 \end{pmatrix} \quad (62)$$

where the phase shift $\phi = \omega_f(S-L)/2c$ and S is the length of the whole circumference of storage ring.

Therefore, from Eqs. (61) and (62), we obtain the trace of the transformation matrix M for a sector

$$\text{Tr } M = 2 \cos\phi \cos\left(\frac{\omega_T L}{2c}\right) - \left(\frac{\omega_T}{\omega_f} + \frac{\omega_f}{\omega_T}\right) \sin\phi \sin\left(\frac{\omega_T L}{2c}\right), \quad (63)$$

which is the sum of the elements of the principal diagonal of the transformation matrix M . The necessary and sufficient condition for stable transverse orbit is⁸

$$\left|\frac{1}{2} \text{Tr } M\right| \leq 1. \quad (64)$$

As a typical example in the present experiment,⁴ we consider the system parameters $\omega_{pe} = 10^9$ rad/sec, $L = 2$ cm, and $\omega_f = 2 \times 10^7$ rad/sec. Substituting these parameters into Eq. (63) gives approximately $\text{Tr } M/2 \approx \cos\phi - \sin\phi$, which violates the inequality in Eq. (64) for the range $(n-0.5)\pi < \phi < n\pi$, where n is an integer. We therefore conclude that the collective self-fields effects (ω_{pe}) of the electron and positron colliding beams play a significant role in the stability behavior of transverse particle orbit.

B. Expansion of Beam Cross Section with Ensemble Average

In order to investigate the expansion of beam cross section for uncontrollable collision (incoherent collision location, etc.), we define

$$r_1^2 = Z_1 Z_1^* + (c/\omega_f)^2 Z_1' Z_1'^*, \quad (65)$$

which represents the maximum radial deviation from the axis of symmetry before collision. In Eq. (65), the asterisk (*) denotes the complex conjugate. During the collision ($z_p/2 < z < z_p/2 + L$), the transverse orbit of a positron in Eq. (60) can also be expressed as

$$Z = A \cos[(\omega_T/c)(z - z_p/2) + \alpha], \quad (66)$$

where A is the maximum amplitude and α is the initial phase angle which is

defined by $\alpha = \tan^{-1}[-(c/\omega_T)Z_1'/Z_1]$. The maximum radial deviation for range z satisfying $z_p/2 < z < z_p/2 + L$ is determined from

$$AA^* = r_1^2/[1 + (\omega_{pe}/\omega_f)^2 \sin^2 \alpha] , \quad (67)$$

where use has been made of Eqs. (65) and (66), and $\omega_T = (\omega_{pe} + \omega_f^2)^{1/2}$. From Eq. (66), the positron position Z_2 and orbit slope Z_2' can be expressed as

$$Z_2 = A \cos[(\omega_T L/2c) + \alpha] ,$$

$$Z_2' = -A(\omega_T/c) \sin[(\omega_T L/2c) + \alpha] ,$$

thereby giving the relation

$$\left(\frac{r_2}{r_1}\right)^2 = \frac{1 + (\omega_{pe}/\omega_f)^2 \sin^2[(\omega_T L/2c) + \alpha]}{1 + (\omega_{pe}/\omega_f)^2 \sin^2 \alpha} , \quad (68)$$

from which the maximum radial deviation r_2 after collision is determined.

Depending on the phase angle α , positrons gain (or lose) the transverse energy by the collision according to $r_2/r_1 > 1$ (or $r_2/r_1 < 1$). The net gain of the transverse energy (or temperature) by the collision is determined from the phase angle average of Eq. (68). We therefore define

$$\langle r_2^2/r_1^2 \rangle = \frac{1}{2\pi} \int_0^{2\pi} d\alpha \frac{1 + (\omega_{pe}/\omega_f)^2 \sin^2[(\omega_T L/2c) + \alpha]}{1 + (\omega_{pe}/\omega_f)^2 \sin^2 \alpha} f(\alpha) \quad (69)$$

for future notational convenience. In Eq. (69), the phase angle distribution $f(\alpha)$ is a positive definite function normalized by $\int_0^{2\pi} d\alpha f(\alpha) = 2\pi$. For uniform distribution ($f=1$), we obtain

$$\langle r_2^2/r_1^2 \rangle = \cos\left(\frac{\omega_T L}{c}\right) + \frac{1 + \omega_{pe}^2/2\omega_f^2}{(1 + \omega_{pe}^2/\omega_f^2)^{1/2}} [1 - \cos\left(\frac{\omega_T L}{c}\right)] . \quad (70)$$

Evidently, we note from Eq. (70) that the value $\langle r_2^2/r_1^2 \rangle$ approaches unity

when the beam length (L) or density (ω_{pe}) decreases to zero. Moreover, the value $\langle r_2^2/r_1^2 \rangle$ is always greater than unity.

As a typical example in the present experiment, we evaluate Eq. (70) for $\omega_{pe} = 10^9$ rad/sec, $L = 2$ cm and $\omega_f = 2 \times 10^7$ rad/sec. Substituting these parameters into Eq. (70), we find $\langle r_2^2/r_1^2 \rangle \approx 1.025$. Therefore, in these particular parameters, the cross section of the beam is increased by 2.5 percent of its original area after each collision. However, we assume that the positrons are uniformly distributed in the phase angle α whenever beams start collision, which is consistent with the ensemble average scheme. The cross section of the positron beam can be expanded to ten times of its original area for $\langle r_2^2/r_1^2 \rangle = 1.025$ after 100 times collisions, which corresponds to the operational time $(S/2c) \log 1.025 = 5$ milliseconds for the circumferential length $S = 3 \times 10^6$ cm of storage ring.

IV. CONCLUSIONS

In this paper, we have examined the filamentation instability and the influence of the collective self-fields on the electron-positron colliding beams in the storage ring. In Sec. II, we have investigated the stability properties of filamentation instability of electron-positron colliding beam. An important conclusion of this stability analysis is that the typical growth rate of the filamentation instability is order of the electron plasma frequency, thereby severely limiting the electron density in a storage ring. Influence of collective self-field effects on the electron and positron colliding beams has been investigated in Sec. III. The theoretical analysis has been carried out, distinguishing the two cases, where (a) the particle motions are in a very coherent orbit and (b) the randomness dominates the operational condition of storage ring (e.g., incoherent collision location by fluctuation, etc.). In either case, it has been found that the self-fields effects play a dominant role in the stability behavior of transverse orbit and the expansion of beam cross section.

ACKNOWLEDGMENTS

We wish to thank Professor Ming Chen and Professor Gus Zorn for informing us about the experimental observation of beam broadening at DESY, and Professor R. C. Davidson for useful discussions. This work was supported in part by the Independent Research Fund at the Naval Surface Weapons Center and in part by the Office of Naval Research under the auspices of a University of Maryland-Naval Research Laboratory joint program (Contract N-00014-77-C-0590).

REFERENCES

1. J. R. Rees, IEEE Trans. Nucl. Sci. NS-24, 1836 (1977).
2. G. A. Voss, IEEE Trans. Nucl. Sci. NS-24, 1842 (1977).
3. H. S. Uhm and C. S. Liu, Phys. Rev. Lett. 43, 914 (1979).
4. G. A. Voss, Bull. Am. Phys. Soc. 24, 142 (1979).
5. H. S. Uhm and C. S. Liu, "Collective Self-Field Effects on the Electron and Positron Colliding Beams in Storage Ring," TR-79-112, Univ. of Maryland (1979).
6. R. L. Gluckstern, Proc. 1970 Proton Linac Conf., edited by N. R. Tracy, (National Accelerator Lab., Batavia, Illinois, 1970), p. 811.
7. H. S. Uhm and R. C. Davidson, "Kinetic Description of Coupled Transverse Oscillations in an Intense Relativistic Electron Beam-Plasma System," Phys. Fluids 23, 813, (1980).
8. J. J. Livingood, Principles of Cyclic Particle Accelerators, (D. Van Nostrand Company, Inc., Princeton, N.J., 1961), Chap. 3.

FIGURE CAPTION

Fig. 1 System configuration and coordinate system.

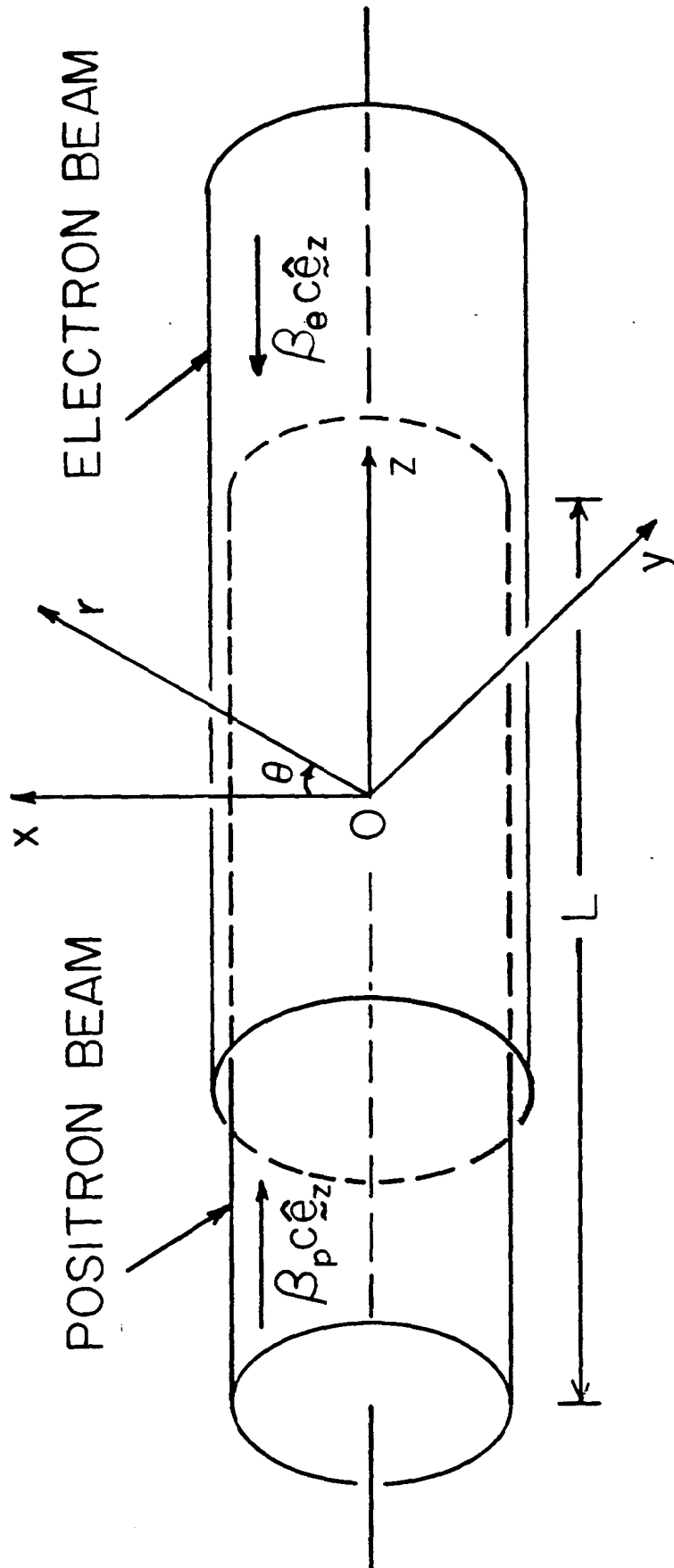


Figure 1

A BEAM-BEAM SIMULATION
FOR THE SINGLE-PASS LINEAR COLLIDER

R. SAH
Lawrence Berkeley Laboratory
Berkeley, California

The beam-beam interaction for the single-pass linear collider has been simulated by means of a computer calculation. This work is similar to that done by Robert Hollebeek at SLAC, but the two simulations were done independently.

The Computer Program - SMASH

A computer program named SMASH has been written to perform the beam-beam simulation. A "macroparticle" approach was selected in that the calculation tracks the trajectories of a number of macroparticles, each of which represents a large number of electrons or positrons. This approach was favored because it permits the greatest flexibility in simulating cases of different density distributions, cases without azimuthal symmetry, etc. Also, the coarseness inherent in the use of a relatively small number of macroparticles is not a serious drawback for simulations of the single-pass linear collider, since the particles do not return again and again. In contrast, beam-beam simulations for PEP must contend with the problem associated with the repeated collisions of the bunches. That is, small simulation errors for PEP can cause severe artificial effects when these errors are compounded during the repeated collisions. In order to provide a useful simulation of the single-pass linear collider, however, SMASH only has to reveal the overall characteristics of the beam-beam interaction.

When highly-relativistic particles or macroparticles pass near one another, their electromagnetic interaction is very simple. See Figure 1. As particle 1 (with charge q_1 and velocity v) passes particle 2 at a distance of b meters, the transverse momentum imparted to particle 1 is given by the following formula:

$$\Delta p_1 = \left(\frac{1}{4\pi\epsilon_0} \right) \frac{2q_1q_2}{bv}, \text{ where}$$

$$\left(\frac{1}{4\pi\epsilon_0} \right) = 8.99 \times 10^9 \frac{\text{nt} - \text{m}^2}{\text{coulomb}^2} \text{ (MKS units)}$$

q_1, q_2 in coulombs

b in meters

v in meters/sec

"2" comes from the evaluation of a definite integral

All the dynamics in SMASH is contained in the above equation, except for a form factor which is used to avoid the infinity when the impact parameter approaches zero. The forces are attractive for electrons passing positrons.

Since the above transverse kick occurs only at the point of closest approach, it is convenient to arrange the macroparticles in each bunch in a series of "slices", as shown in Figure 2. Then the particles in a given slice of bunch 1 interact with the particles in a slice in bunch 2 when and only when it passes through that slice.

In program SMASH the interactions between pairs of macroparticles (one from each bunch) are calculated directly. For large numbers of macroparticles, this approach is slower than the usual technique of calculating fields from particle distributions and then using the fields to integrate particle trajectories. However, the direct calculation is simpler and avoids possible problems in calculating the intermediate fields.

As it turns out, SMASH can simulate a collision of a 600-macroparticle bunch with another 600-macroparticle bunch in 40 computing units on the CDC 7600, at a cost of \$6.00. A 1200-macroparticle calculation is adequate to reveal many aspects of the beam-beam interaction, but it is not suited to the investigation of very detailed questions, such as those concerning the extreme tails of angular distributions.

Disruption Parameter and Luminosity

The disruption parameter D has been defined as follows for a round bunch¹:

$$D = \frac{\sigma_z}{F} = \frac{r_e \sigma_z N}{\gamma \sigma_y^2}$$

If we interpret σ_z and σ_y^* as the half-length (Δz) and the edge radius (Δr) of a cylindrical bunch of uniform density, we can write the following in MKS units:

$$D = \left(\frac{e^2}{4\pi\epsilon_0} \right) \frac{(\Delta z)N}{E(\Delta r)^2} ,$$

where e = electron charge

E = electron energy in joules

N = number of electrons (or positrons) in one bunch

The significance of the parameter D can be easily understood by considering Figure 3. Here, two cylindrical bunches of particles collide with one another. Bunch 2 is artificially kept unperturbed, but bunch 1 is pinched by the electromagnetic forces caused by bunch 2. Figure 3 shows cross-sectional views of the collision, the average edge-radius $\bar{\Delta r}$ being used as the half-width of each slice. The time evolution of the collision is revealed by the three views plotted from top to bottom. As is shown in the figure, a disruption parameter of 1 corresponds to the case when bunch 1 gets focussed to a point just as it passes through bunch 2. Actually, the focus of bunch 1 occurs slightly outside of bunch 2, because the definition of D does not take into account the reduction of focussing forces as bunch 1 particles approach the central axis of the cylindrical bunch 2.

To calculate luminosities, it is necessary to perform a distribution smoothing in order to calculate the area of a slice or, equivalently, the particle density. This is because truly pointlike macroparticles never hit one another and the luminosity is zero. For slices with uniform density, the area can easily be calculated by first finding the RMS half-widths σ_x and σ_y . Then we have

$$\bar{\Delta r} = 2 \sqrt{\sigma_x \sigma_y}, \text{ and}$$

$$\text{Area} = \pi (\bar{\Delta r})^2.$$

Figure 4 shows what happens when two cylindrical uniform bunches collide, and both bunches are pinched. The parameters of this case correspond to the single-pass linear collider.

$$E = 50 \text{ GeV}$$

$$N = 5 \times 10^{10}$$

$$\sigma_x = \sigma_y = (\Delta r)/2 = 0.6 \text{ } \mu\text{m}$$

$$\sigma_z = (\Delta z)/\sqrt{3} = 0.58 \text{ mm}$$

$$\sigma_{x'} = \sigma_{y'} = 0.12 \text{ mrd}$$

595 macroparticles, 17 slices

$$D = 1$$

For this case (Figure 4) we find a luminosity of $1.11 \times 10^{29}/\text{cm}^2$ per collision, and for the particle angular distribution after the collision we find $\sigma_{x'} = 1.17 \text{ mrd}$.

Figure 5 shows a very similar case where the bunches have gaussian distributions in x , y , z , x' , and y' . The parameters are as follows:

$$E = 50 \text{ GeV}$$

$$N = 5 \times 10^{10}$$

$$\sigma_x = \sigma_y = 0.6 \text{ } \mu\text{m}$$

$$\sigma_z = 0.58 \text{ mm}$$

$$\sigma_{x'} = \sigma_{y'} = 0.12 \text{ mrd}$$

590 macroparticles, 19 slices

$$D = 1$$

I have chosen to generalize the disruption parameter D to gaussian distributions by noting that, for uniform distributions, we have

$$\Delta z = \sqrt{3} \sigma_z$$

$$\Delta r = 2\sigma_x = 2\sigma_y$$

Therefore I define

$$D_{\text{gaussian}} = \left(\frac{e^2}{4\pi\epsilon_0} \right) \frac{(\sqrt{3} \sigma_z) N}{E(2\sigma_y)^2}$$

by analogy with the uniform-distribution case.

In Figure 5 the bunch radius which is plotted is calculated by the following:

$$\overline{\Delta r} = 2 \sqrt{\sigma_x \sigma_y}$$

Therefore the cross-sections of the bunches exhibit azimuthal symmetry. The luminosity calculation proceeds somewhat differently than for the uniform-density case. For cases using gaussian distributions, the particle density is approximated by a gaussian distribution with the RMS widths σ_x and σ_y which are actually found. For the case in Figure 5 we find a luminosity of $1.13 \times 10^{29}/\text{cm}^2$ per collision, and for the particle angular distribution after the collision we find $\sigma_{x'} = 1.26$ mrd. Clearly, there are no profound differences between gaussian and uniform-density bunches.

Number of Slices

The number of slices which should be used in a simulation was investigated in a series of simulations summarized in Figure 6. For $D = 1$ it was found that about 10 slices was adequate for an accurate calculation of luminosity, but $D = 5$ required 17 slices or more. This can be understood easily because the cases with higher disruption parameter D exhibit stronger pinch effects so that the bunches are focussed in shorter longitudinal distances. Therefore, more slices are required to reveal the details of an interaction which has more longitudinal structure.

For the rest of the cases in this report, $D \leq 6$; and 19 slices are always used.

It should be noted that if the total number of macroparticles were held constant, and if the number of slices N_s were varied, then the statistical error associated with each slice is proportional to $\sqrt{N_s}$ and the error reduction due to many slices is proportional to $1/\sqrt{N_s}$. Therefore, at least to first order the statistical errors of these simulations depend on the total number of macroparticles and not on the number of slices.

Varying D

In order to investigate the effects of different values of the disruption parameter D , a series of simulations were run in which D was varied by varying N . In interpreting the results, luminosities were compared after scaling by $1/N^2$ to remove the effect of varying N . Figure 7 and 8 show two representative cases. It can be seen that increasing D from 1 to 6 does not cause the character of the beam-beam interaction to change dramatically. The stronger pinch effect is visible even in the top plot of Figure 8. Then the bunches are focussed to a quasi-stable pinched configuration (central plot). Finally the bunches leave one another with large angular divergences.

Comparing the behavior of the two bunches in Figure 8 is quite revealing. The fact that the two bunches behave generally similarly indicates that the simulation is not dominated by the statistical fluctuations inherent in using a random number generator to place a finite number of macroparticles in each slice. On the other hand, the differences between the bunches are clearly growing with time, which I believe indicates an inherent instability in the interaction. Of course, by using a small number of macroparticles, SMASH simulations exhibit far greater statistical fluctuations than an actual beam-beam collision involving 10^{11} particles would exhibit.

Figure 9 shows that as D is increased from 0 to 6, the luminosity rises to a peak at $D = 2$ and then drops off slowly. Notice the luminosity enhancement of about 2.3 times over the $D = 0$ value.

Figure 10 shows that for the $D = 1$ case, the width of the angular distribution is increased from ± 0.12 mrd to ± 1.3 mrd by the collision of the bunches. However, the final angular distribution is considerably wider (± 2.0 mrd) for the $D = 6$ case. The cross-hatched bins are overflow bins. Note that the presence of significant numbers of particles between 3 and 5 milliradians means that shielding the experimental detector is considerably more difficult

for $D = 6$. The wider angular distributions at $D = 6$ can be explained easily. As the two bunches pass through one another, the pinch effect causes individual particles to oscillate about the symmetry axis. For cases with stronger focussing (i.e., larger D), the particles cross the axis at steeper angles. When the particles emerge from the opposing bunch, those particles which happen to be crossing the axis are also the ones with the largest angular divergences.

Offset Bunches

A series of simulations were performed to investigate the effect of bunches colliding at small offsets instead of directly head-on. Figures 11 and 12 show the beam profiles of two representative collisions. Here, because of the lack of azimuthal symmetry, the beam radius which is plotted is

$$\Delta r = 2\sigma_x$$

The parameters of these simulations are the same as previous calculations except $\bar{x} = 3.0 \sigma_x$ for bunch 1. The vertical scale has been compressed 4 times more than in previous plots. Note that in the $D = 1$ case, an offset of $3.0 \sigma_x$ causes the bunches to miss one another for the most part. However, the stronger attraction between the bunches in the $D = 6$ case causes the bunches to collide with a considerable luminosity. This effect is clearly seen in Figure 13, where the luminosity loss is seen to be much more pronounced (at offsets around $4.0 \sigma_x$) for the $D = 1$ case as compared with the $D = 6$ case.

Figure 14 reveals a somewhat insidious problem with larger values of D . What is plotted is the average final angle x' , with the error bars representing $\pm \sigma_x$. The lack of azimuthal symmetry leads to non-zero values of x' , since the entire bunches are deflected as they pass one another. If the bunch-positioning system does not operate properly for the $D = 1$ case, most of the particles would remain within a cone of ± 2.5 mrd as the bunches collide not quite head-on. In contrast, off-center collisions would be mostly contained in a cone of about ± 10.0 mrd in the $D = 6$ case. The probable presence of significant numbers of particles at angles as great as ± 13 mrd might be very inconvenient for the design of detectors and masks.

Incoming Angles

One can conceive of cases where the external focussing of beam-line magnets produces a pronounced waist during the collision of the two bunches. When $\sigma_z > \beta^* y$, we have collisions which would appear much like the one shown in Figure 15. Here, the pinch effect is intense only near the $z = 0$ plane, so the effects of the beam-beam interactions upon luminosities or angular distributions are less pronounced than in the earlier cases where $\sigma_z \ll \beta^* y$.

Conclusions

The choice of parameters corresponding to D greater than 1 or 2 leads to a luminosity enhancement of about 2. However, the choice of larger values of D (say 5 or 6) leads to much larger final particle angles, especially if the bunches do not collide exactly head-on.

1. J.-E. Augustin, et al., "Limitation on Performance of $e^+ e^-$ Storage Rings and Linear Colliding Beam Systems at High Energy", Proceedings of the Workshop on Possibilities and Limitations of Accelerators and Detectors held at Fermi National Accelerator Laboratory, October 15-21, 1978, p. 87.

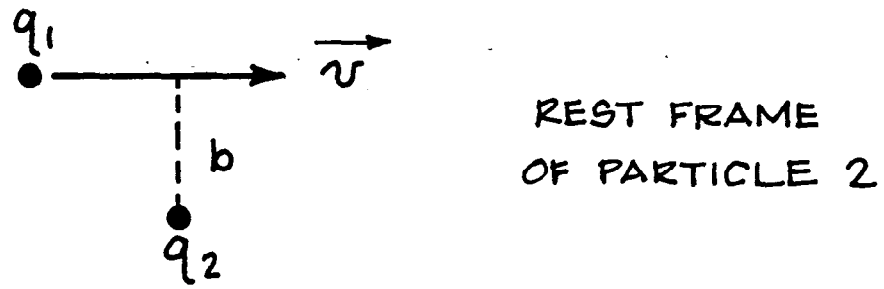


FIGURE 1

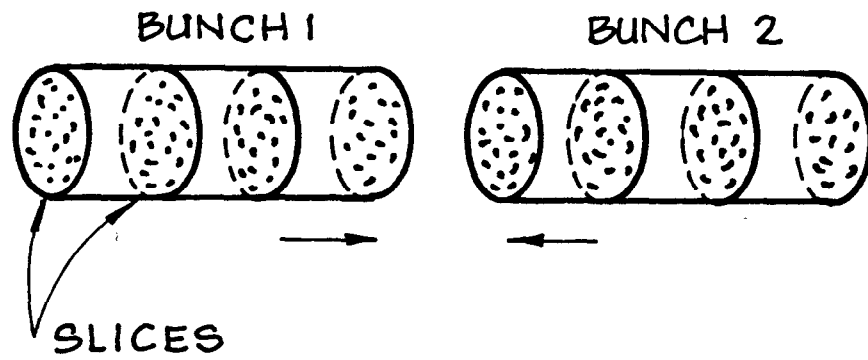


FIGURE 2

SMASH 268

SPLC

 $D = 1.0$

UNIFORM ROUND BUNCHES

BUNCH 2 NOT PERTURBED

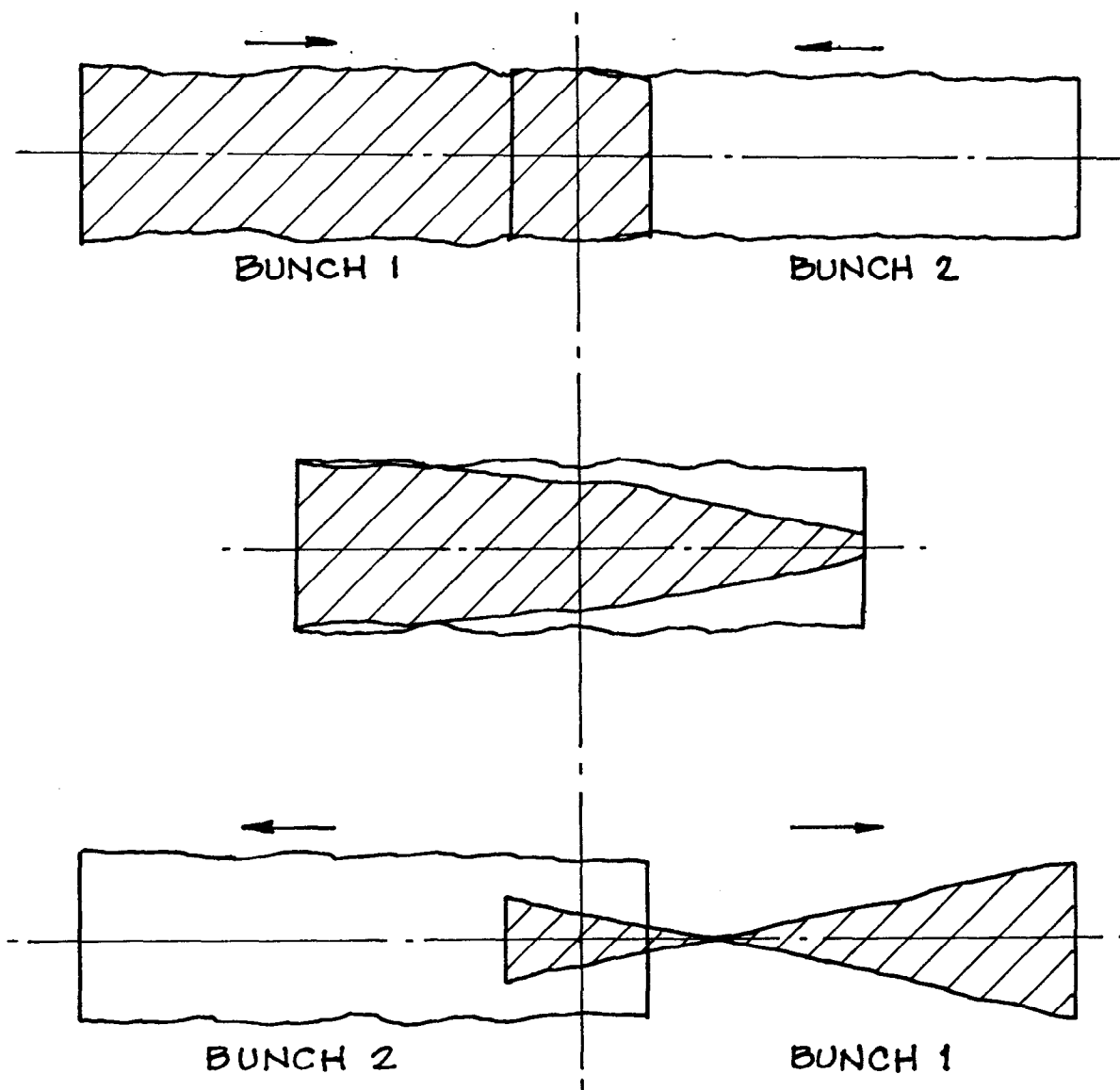


FIGURE 3

GMASH 267

SPLC

 $D = 1.0$

UNIFORM ROUND BUNCHES

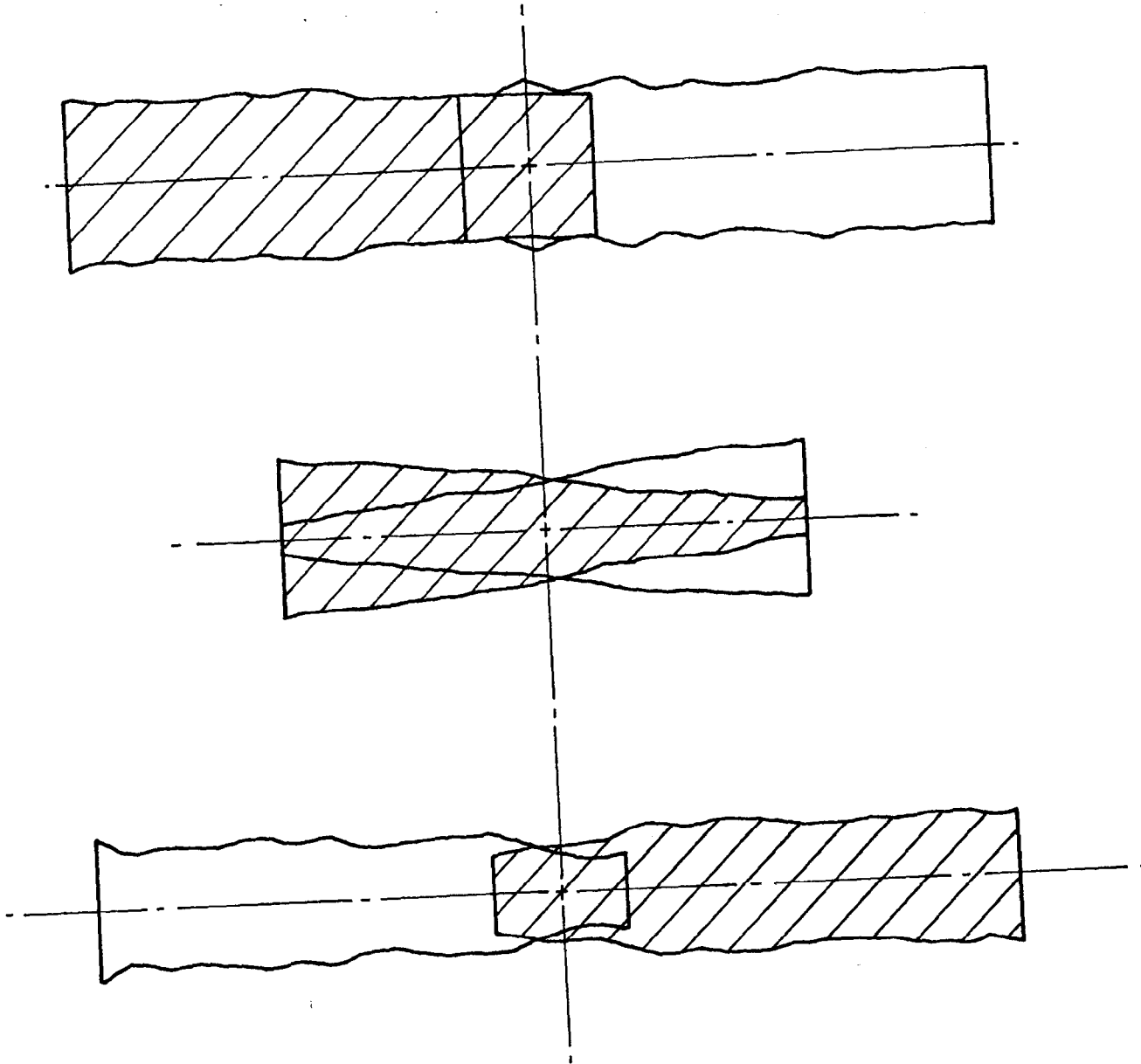


FIGURE 4

SMASH 255

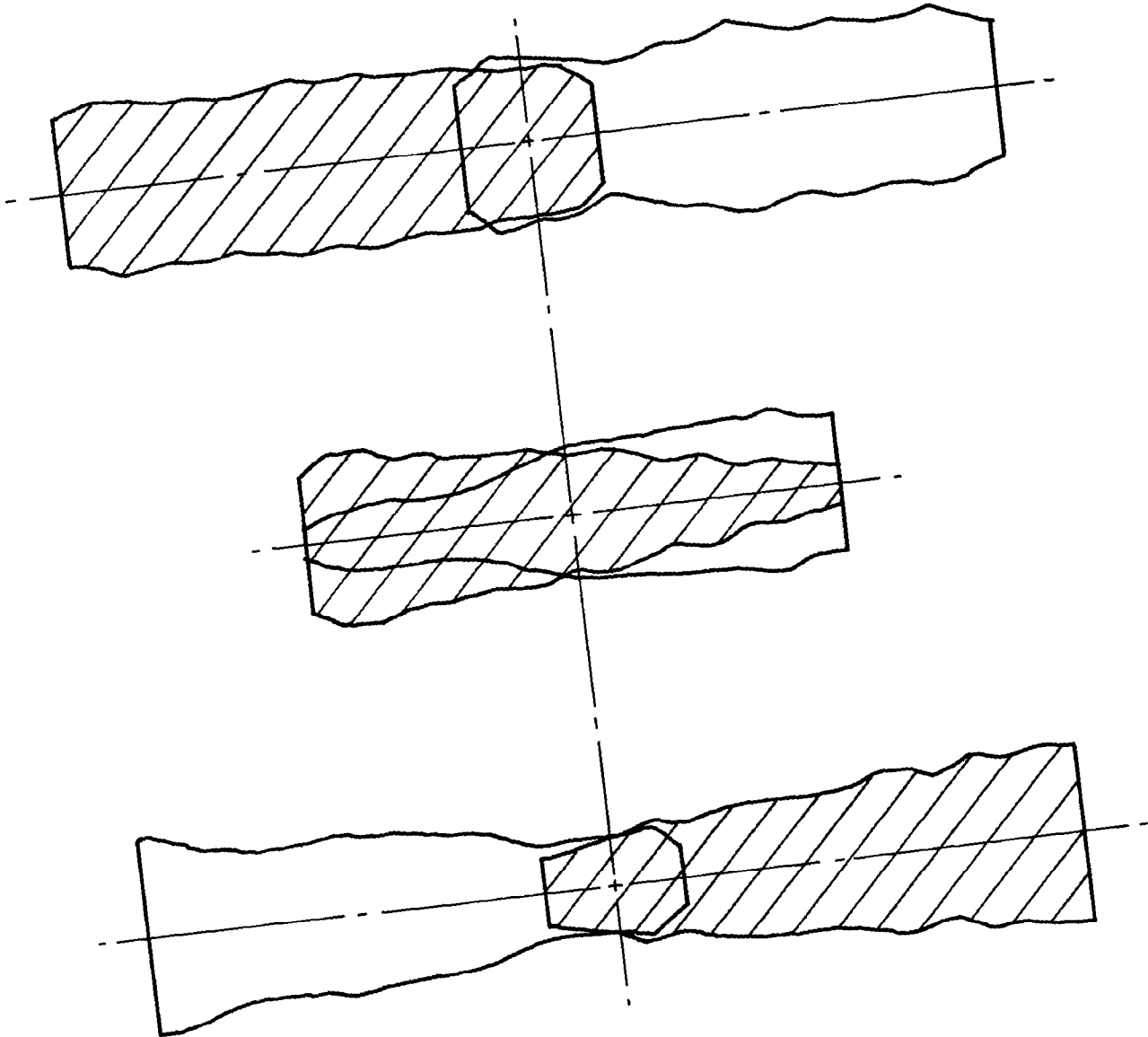
SPLC
D=1.0
GAUSSIAN BUNCHES

FIGURE 5

SMASH 233-243

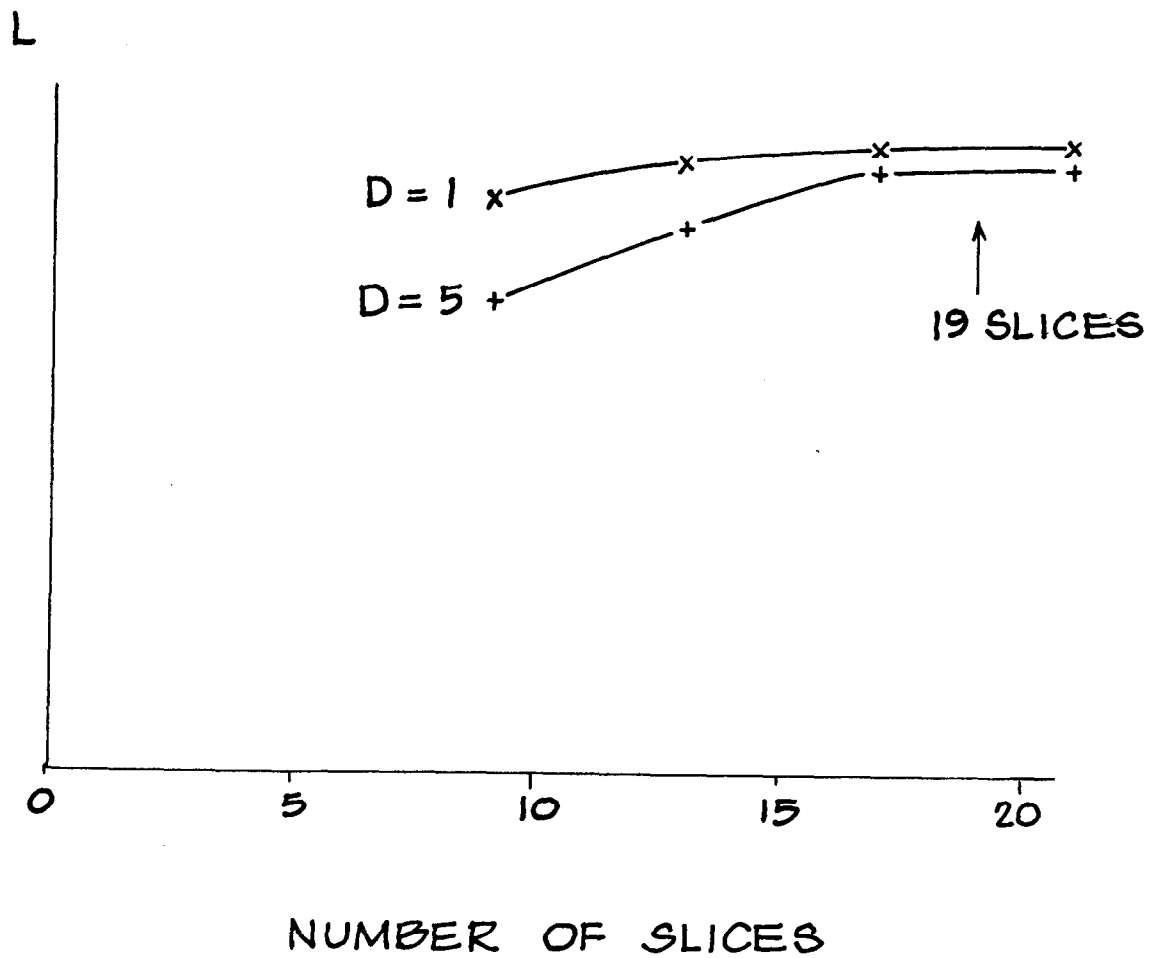
SPLC, GAUSSIAN BEAMS, $\sigma_{x'} = \sigma_{y'} = 0$.

FIGURE 6

SMASH 244

SPLC
D = 1.0
GAUSSIAN

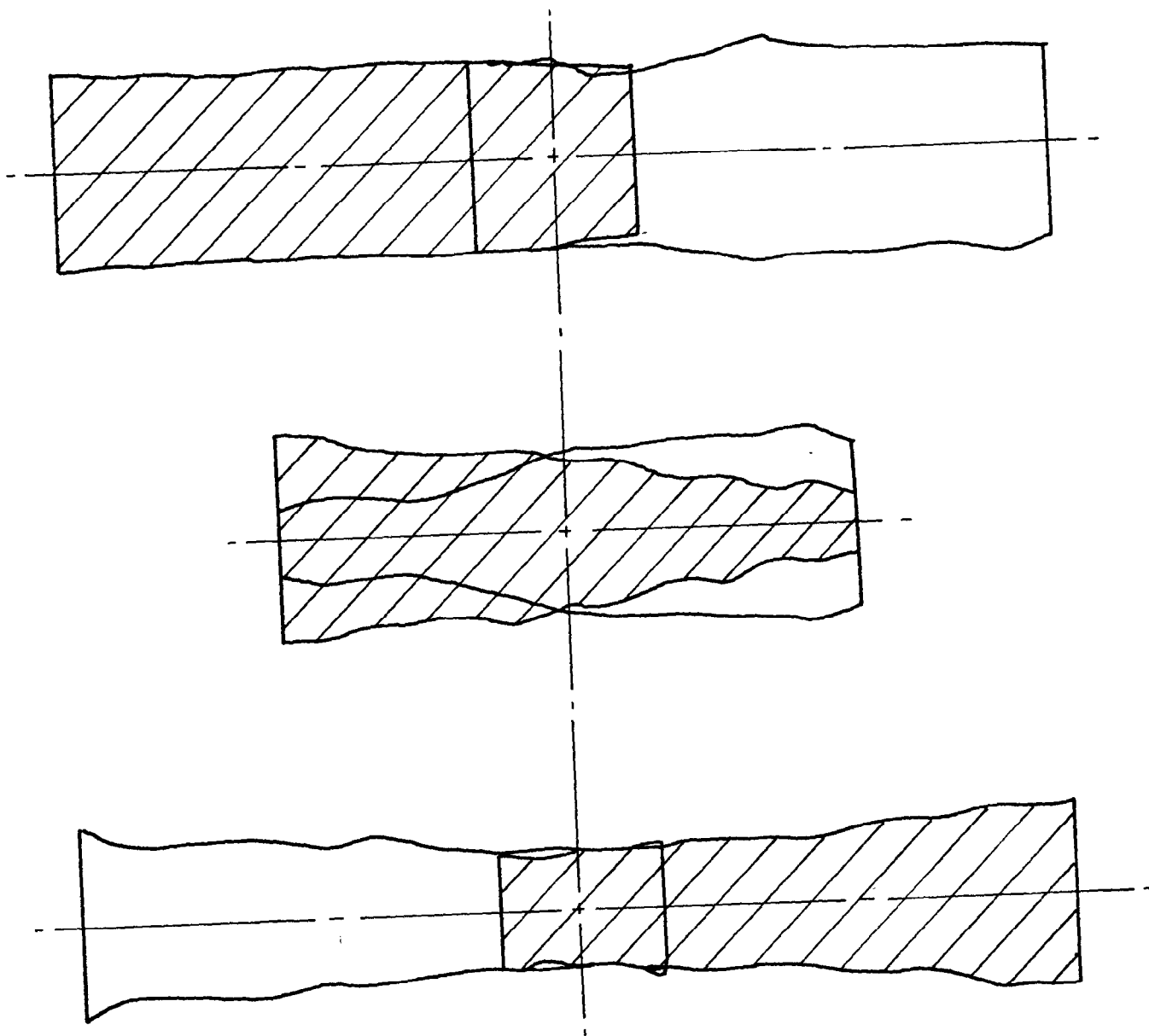


FIGURE 7

SMASH 251

SPLC
D = 6.03
- GAUSSIAN

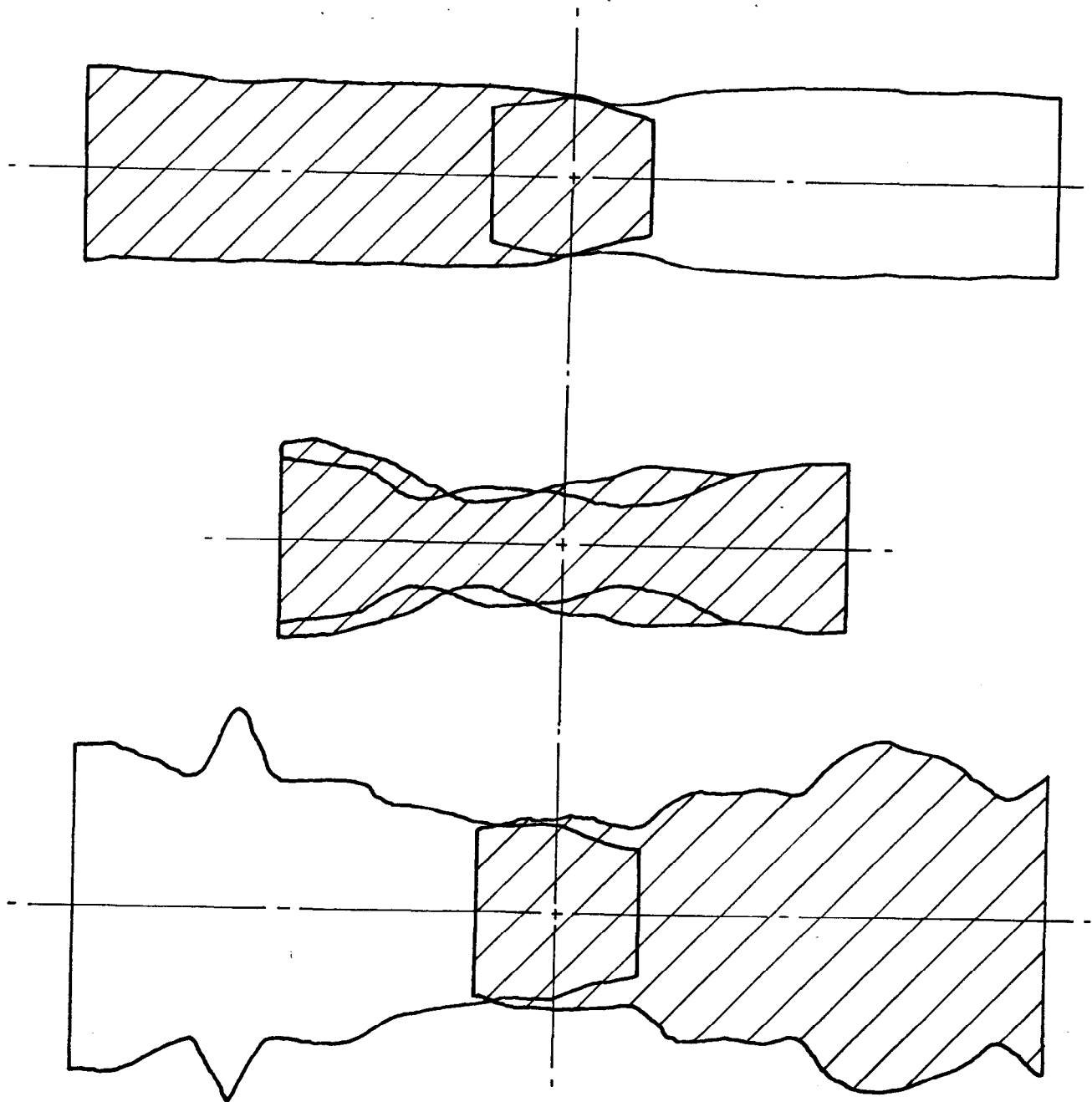


FIGURE 8

SMASH 244-251

SPLC

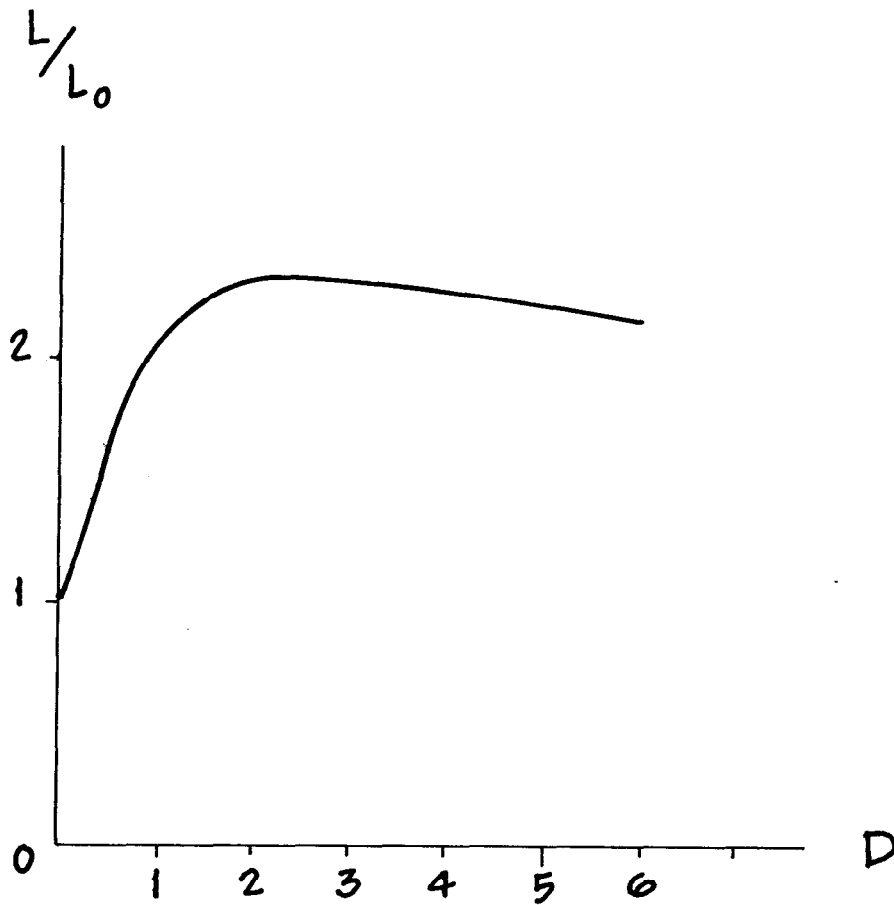


FIGURE 9

FINAL PARTICLE ANGLES

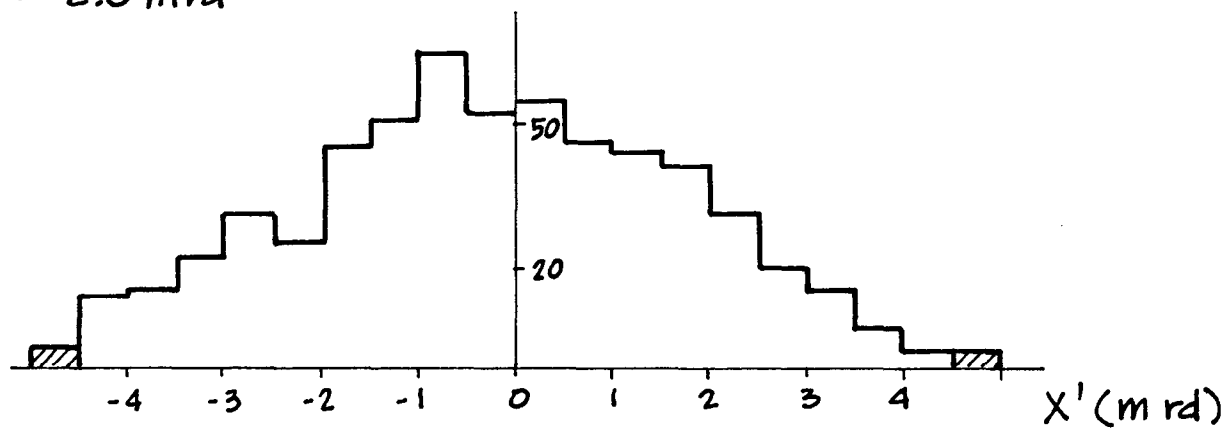
$$\sigma_{x'} = \sigma_{y'} = 0.12 \text{ m rd} \text{ ORIGINALLY}$$

GAUSSIAN

SMASH 251

$$D = 6$$

$$\sigma_{x'} = 2.0 \text{ mrd}$$



SMASH 244

$$D = 1$$

$$\sigma_{x'} = 1.3 \text{ mrd}$$

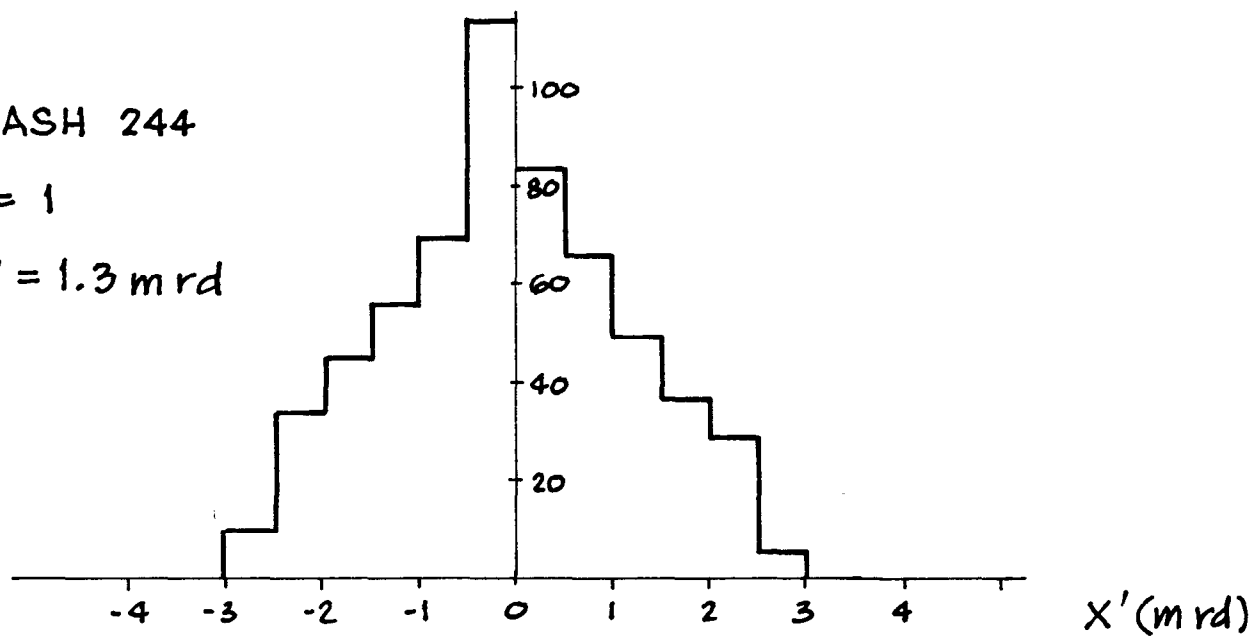


FIGURE 10

SPLC
D = 1.0
GAUSSIAN BUNCHES
OFFSET/ σ_x = 3.0

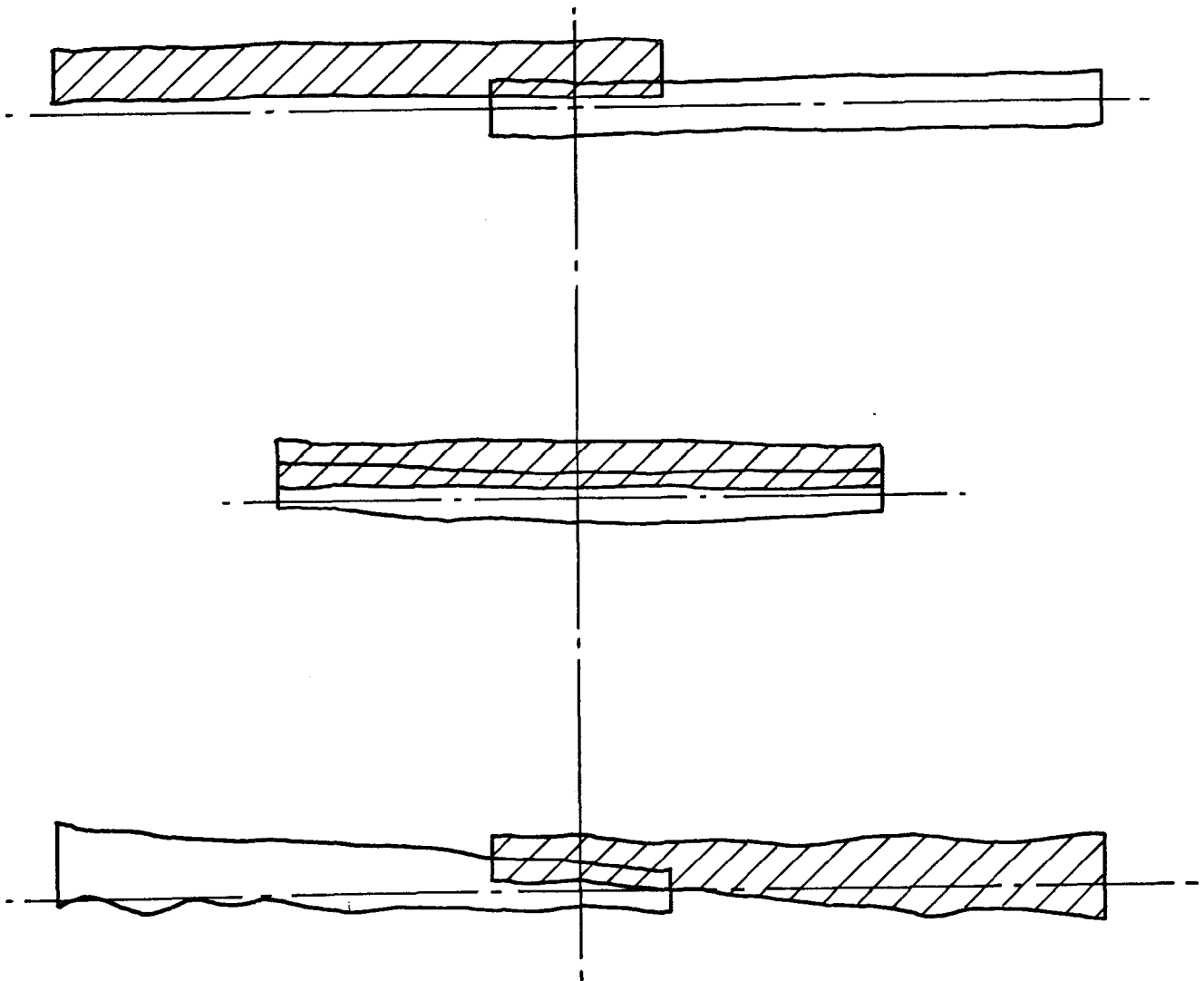


FIGURE 11

SPLC
D = 6.03
GAUSSIAN BUNCHES
OFFSET/ $\sigma_x = 3.0$

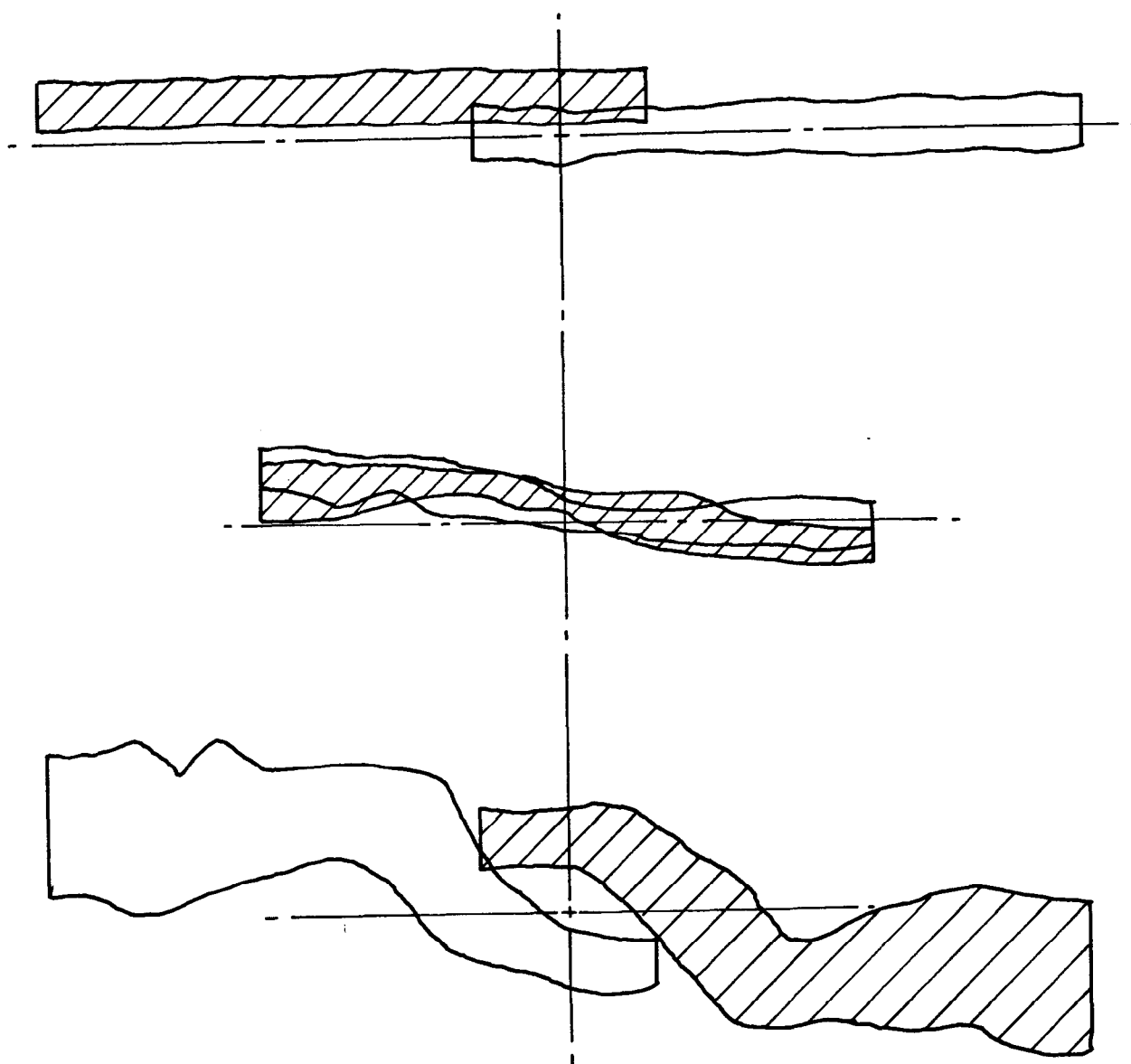


FIGURE 12

SMASH 255 - 266

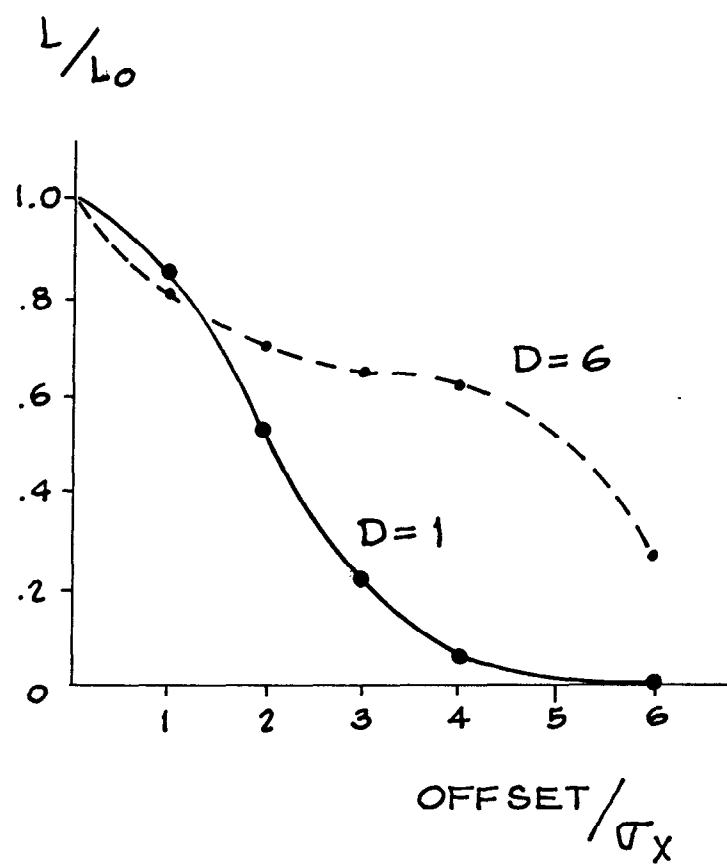


FIGURE 13

SMASH 255-264, 306-311

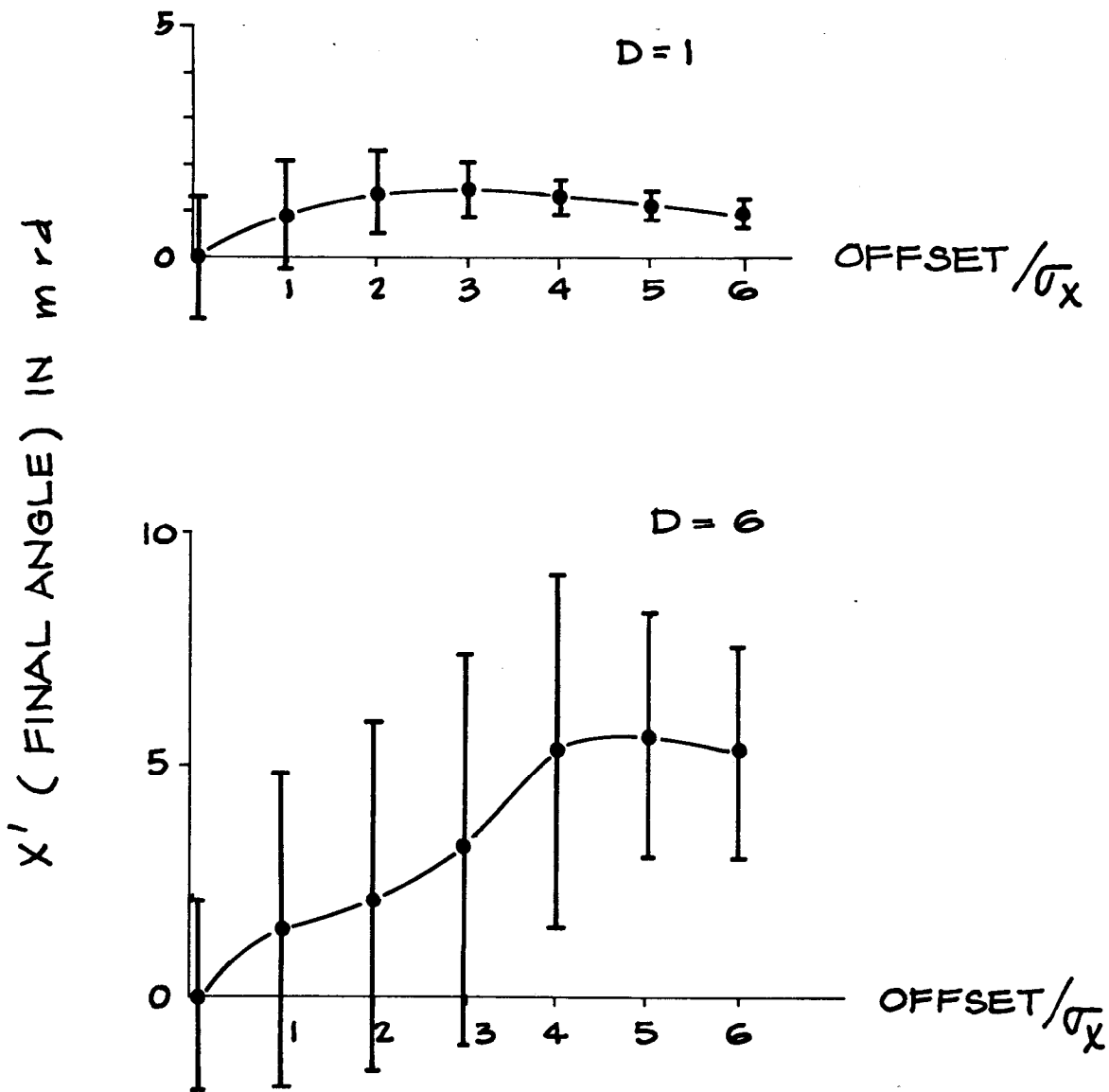


FIGURE 14

$$D = 1.0$$
$$\sigma_z = G\beta y^*$$

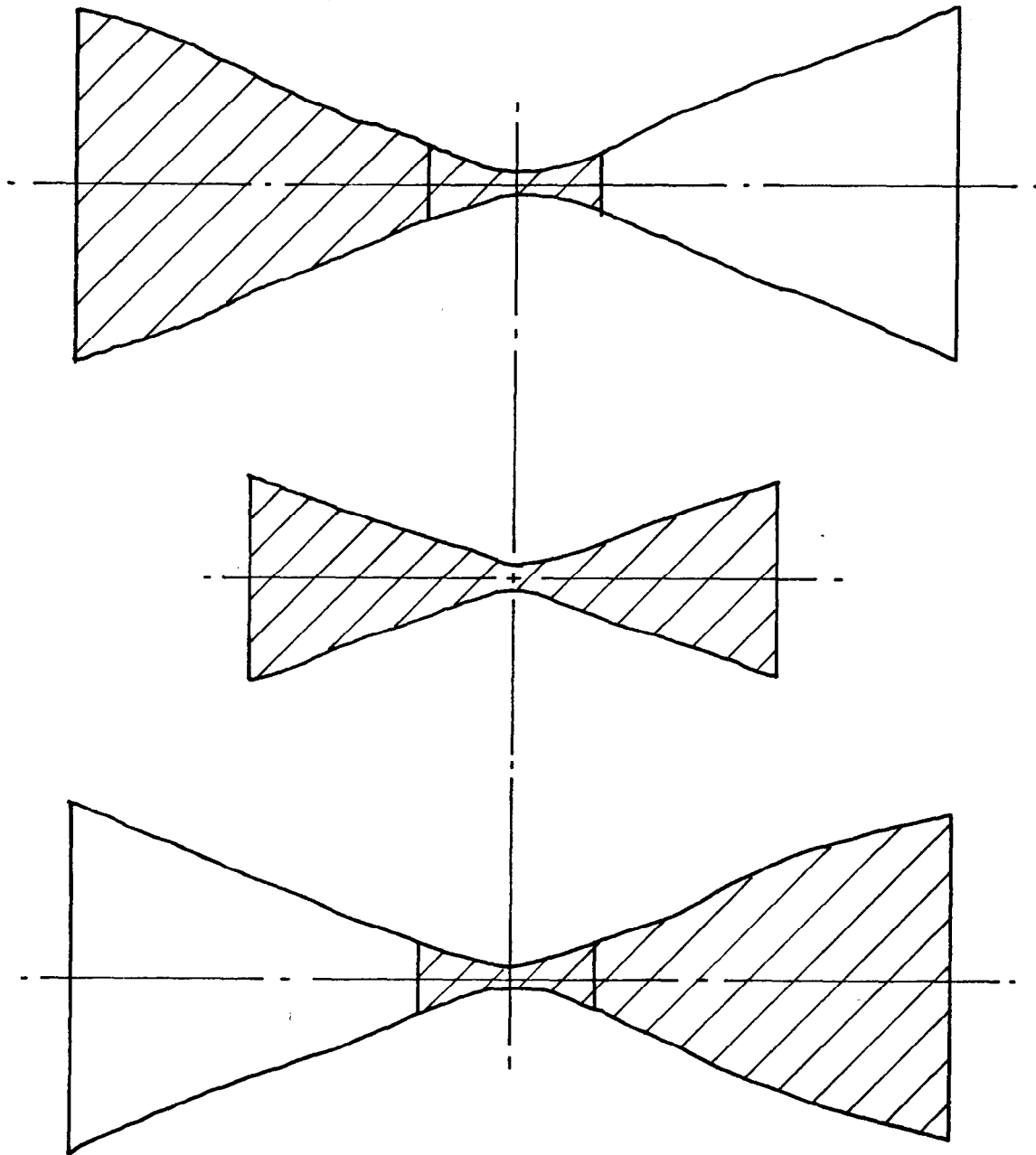


FIGURE 15

DISRUPTION LIMITS FOR LINEAR COLLIDERS*

Robert Hollebeek
Stanford Linear Accelerator Center
Stanford University, Stanford, California 94305

ABSTRACT

Beam behavior in a single-pass collision device has been investigated using a cloud-in-cells plasma simulation code. The intense electromagnetic fields of the beams produce mutual focusing effects whose strength is determined by the disruption parameter D . The consequent decrease in the beam radii causes an increase in the luminosity of a single collision. The dependences of the beam behavior on beam profiles and current density are described. The beam behavior is stable for several plasma oscillations and indicates that high luminosity can be achieved in single-pass collision devices by using intense beams.

Submitted to Nuclear Instruments and Methods

* Work supported by the Department of Energy, contract DE-AC03-76SF00515.

I. Introduction

The idea of using two linear accelerators firing beams of particles at each other for the study of high energy interactions has been suggested by several authors.¹⁾ This type of device is called a linear collider and is of particular importance in the area of high energy electron-positron physics where the energy loss in a circular machine has become a dominant consideration in the design of new storage rings. For circular machines, modest increases in beam energy are accompanied by large increases in either the power required to run the machine, the size of the machine, or both. Linear colliders can reduce these problems if the beams can be made sufficiently dense at the collision point.

The small emittance of linear accelerator beams allows the beam to be focused to a very small spot (several square microns). For a linear collider, one would like to decrease the spot size as much as possible to increase the luminosity or rate at which interesting interactions occur. However, when two such beams collide, the intense electromagnetic fields of the two beams will cause the beams to be disrupted. If this disruption destroys the beam focus, the luminosity will be decreased.

If the beams consist of short pulses, and each pulse is discarded after a collision (single-pass collision device), then the growth of instabilities due to this beam-beam interaction will be limited by the short duration of the interaction. The limitations on beam intensity in a single-pass collision device will be determined by the plasma effects which occur during the short collision time.

This paper presents the results of investigations into the behavior of the two beams in a single-pass collision device. There are two issues

which must be addressed in considering the beam-beam interaction in such a device. The first is, how large can the transverse density of the beams be before plasma instabilities increase the size of the beams during the collision and thereby reduce the luminosity? The second question is, what is the effect of the beam-beam dynamics without instabilities on the average luminosity of a collision?

The beam-beam dynamics have been investigated using a modified three-dimensional cloud-in-cells (CIC) plasma simulation program. These studies indicate that the number of plasma oscillations during beam passage is of order

$$n \approx \frac{1}{3} \sqrt{D} \quad (1)$$

where D is the dimensionless disruption factor (discussed later) which is related to the initial beam density. Typical instability growth rates are such that n values of one or two can be achieved allowing quite large values of D .

The second result of these studies is that the pinch effect due to the attraction of the oppositely charged beams enhances the luminosity. Figure 1 shows the changes which occur in two such beams as they collide. The luminosity is related to an overlap integral of the density distribution of the two beams. The behavior of the luminosity as a function of initial beam density and beam profile can be studied with plasma simulation techniques and can be reliably calculated for small numbers of plasma oscillations.

The definition of the disruption factor is discussed in Section II and its relation to the plasma frequency and bunch instabilities in Section III. Section IV discusses the computer simulation of the beam-

beam interaction. Section V gives the results of the simulations for the enhancement of the luminosity due to beam pinch. Section VI discusses the case where the beams are offset or have uniform transverse profiles. The conclusions are summarized in Section VII.

II. Beam-Beam Disruption Factor

To investigate the interaction of the two beams as they collide, one must start by looking at the electrodynamics of two relativistic particles traveling in opposite directions. In the rest frame of particle 1, particle 2 approaches with

$$\gamma' \simeq 2\gamma^2 . \quad (2)$$

The fields at the position of particle 1 can be calculated by transforming the Coulomb field of particle 2 in its rest frame to the frame moving with

$$\beta' = \left(1 - \frac{1}{\gamma'^2}\right)^{1/2} . \quad (3)$$

If particle 2 travels along the z axis and has a minimum displacement from particle 1 of b in the x direction (see fig. 2), the electric and magnetic fields are²⁾

$$\begin{aligned} E_x &= \frac{\gamma' qb}{(b^2 + \gamma'^2 \frac{v^2}{c^2} t^2)^{3/2}} \\ E_z &= \frac{-q\gamma' vt}{(b^2 + \gamma'^2 \frac{v^2}{c^2} t^2)^{3/2}} \\ B_y &= \beta' E_x \end{aligned} \quad (4)$$

The time dependence of the fields is shown in fig. 3. Note that, as γ increases, E_x increases and Δt decreases in such a way that the total impulse given to particle 1 is proportional to $1/v$. For electrons with $E = 50$ GeV, $\gamma = 10^5$ so that at high energies an impulse approximation for the effect of the transverse fields is justified. The impulse is just

$$F\Delta t \sim \frac{e^2}{bc} \quad (5)$$

The total impulse in the longitudinal direction (due to E_z) is zero.

Consider now a test particle with displacement b from the collision axis incident on a charge distribution as shown in fig. 4. For simplicity, let the distribution be a uniform density cylinder with

N = number of particles of charge e

R = radius of the bunch

L = length of the bunch

Then the incident particle sees a magnetic field H_ϕ due to the current caused by the passage of the other beam. The current enclosed by a circular contour of radius b is

$$I = \frac{Ne}{L} \cdot c \cdot \frac{\pi b^2}{\pi R^2} \quad (6)$$

and amperes law gives

$$\oint \vec{H} \cdot d\vec{l} = \frac{4\pi}{c} I = 2\pi b H_\phi, \quad H_\phi = \frac{2Ne b}{LR^2} \quad (7)$$

For oppositely charged beams the force is radial and directed inwards

$$F_r = - \frac{2Ne^2 b}{LR^2} \quad (8)$$

and is experienced for a time $\Delta t = \frac{L}{2c}$.

The effect of the electric field of the passing relativistic bunch is equal to that of the magnetic field ($E_x = \frac{1}{\beta} B_y$) hence the total deflection is given by

$$\Delta r' = \frac{\Delta p_l}{p} = \frac{2F_r \Delta t}{\gamma mc} = - \frac{2Nr_e b}{\gamma R^2} \quad (9)$$

A similar analysis applied to a bi-Gaussian distribution gives³⁾

$$\begin{aligned}\Delta x' &= -\frac{2N r_e x}{\gamma \sigma_x (\sigma_x + \sigma_y)} \\ \Delta y' &= -\frac{2N r_e y}{\gamma \sigma_y (\sigma_x + \sigma_y)}\end{aligned}\tag{10}$$

for displacements $x \ll \sigma_x$ and $y \ll \sigma_y$.

The focal length of a thin lens is given by

$$\Delta x' = -\frac{1}{f} x\tag{11}$$

and comparing this to eqs. (9), (10), one can define a dimensionless parameter, called the disruption factor, which is the ratio of the length of the bunch to the focal length near the center. For a Gaussian distribution,

$$D = \frac{\sigma_z}{f}.\tag{12}$$

If the charge distribution is uniform, then it is easy to see that test particles incident on the bunch with $b < R$ will be focused to the axis after traveling a distance σ_z/D . As will be discussed in Section III, the behavior of the test particles is actually periodic with a wavelength $\lambda \simeq 4f$ which is related to the bunch plasma frequency. For small values of D , however, viewing the collision in terms of a thin lense with a fixed focal length gives a good physical picture of the test particle dynamics.

A test particle traveling through a non-uniform charge distribution sees a focal length which may change as a function of time due to the variation of the charge density along the collision axis. The effective focal length can also depend on the initial position and angle of the test particle trajectory. If the charge distribution does not differ too

much from a uniform one, this represents a lens with small aberrations, and the point focus of the uniform lens becomes a line focus or a diffuse focus. The disruption factor can still be defined in terms of the focal length for small displacements from the collision axis or equivalently the focal length determined by the central density. For a Gaussian distribution in x , y , and z one has

$$D_x = \frac{2N r_e \sigma_z}{\gamma \sigma_x (\sigma_x + \sigma_y)}$$

$$D_y = \frac{2N r_e \sigma_z}{\gamma \sigma_y (\sigma_x + \sigma_y)}$$
(13)

Note that if the aspect ratio of the beam is not one, the focal lengths in the x and y directions are not equal and one must define two disruption parameters. For the Gaussian case with aspect ratio $\sigma_x/\sigma_y = 1$, the disruption parameter is simply

$$D = \frac{N r_e \sigma_z}{\gamma \sigma_x^2}$$
(14)

The problem becomes much more complex when one considers the collision of two charge distributions. The complication arises because each distribution will be modified during the collision by its interaction with the other one. The disruption factors of the two beams can still be defined in terms of their initial density distributions and the results discussed previously for test particles are obtained when one of the beams is weak and its disruption of the strong beam can be neglected. For the general case however, the focal strength experienced by particles varies with time both because of the variation of charge density along the collision axis and because of the variation in density due to the time dependence of the charge distribution.

The object of colliding intense relativistic beams of positrons and electrons is, of course, to study the fundamental interactions of these particles. When an individual positron and electron annihilate or have a close collision, new particles are produced with a rate that is given by the interaction cross section times the incoming flux. The rate of particle production per unit interaction cross section is called the luminosity and is the quantity which together with the energy determines the usefulness of the machine for the experimenters. The total luminosity is the luminosity per collision multiplied by the number of collisions per second. Hence

$$\mathcal{L} = f \int \rho_1(x, y, z, t) \rho_2(x, y, z', t) dx dy dz dt \quad (15)$$

where $z' = z - ct$ and $f =$ collision frequency. Neglecting the dynamic changes in the beam density distributions, one can define a luminosity for the limit in which the disruption parameters are zero which is

$$\mathcal{L}_0 = f \int \rho_1(x, y, z, t=0) \rho_2(x, y, z', t=0) dx dy dz dt \quad (16)$$

For two Gaussian distributions with $\sigma_{x1} = \sigma_{x2}$, $\sigma_{y1} = \sigma_{y2}$, $\sigma_{z1} = \sigma_{z2}$ we get the well known result

$$\mathcal{L}_0 = \frac{N^2 f}{4\pi \sigma_x \sigma_y} \quad (17)$$

The factor $1/4\pi \sigma_x \sigma_y$ comes only from the x and y integration.

In order to calculate the effects of beam dynamics for arbitrary initial density distributions and investigate any shape dependence, one needs to define the collision strength in a shape independent way. If the charge distribution is characterized by the scale parameters λ_x , λ_y , and λ_z , the variables in the problem can be scaled since we are dealing essentially with a collisionless plasma (point-like scattering). If the variables are now scaled such that

$$\begin{aligned}\xi_x &= x/\lambda_x \\ \xi_y &= y/\lambda_y \\ \xi_z &= z/\lambda_z\end{aligned}\tag{18}$$

and a shape distribution ρ_ξ is defined using

$$\int \rho_\xi d\xi_x d\xi_y d\xi_z = 1 ,\tag{19}$$

the luminosity becomes

$$\mathcal{L} = \frac{f N_1 N_2}{\lambda_x \lambda_y} I_0\tag{20}$$

where I_0 is the overlap integral in x and y and the convolution in z of ρ_ξ with itself. For a Gaussian distribution

$$\rho_\xi = \frac{1}{(2\pi)^{3/2}} e^{-\left(\xi_x^2/2 + \xi_y^2/2 + \xi_z^2/2\right)}\tag{21}$$

and $\lambda_x = \sigma_x$, and $I_0 = 1/4\pi$.

We now must consider the way in which the dynamics scales. For a unit charge, the scattering angle per unit length is given by

$$\frac{dx'}{dz} = \frac{-r_e}{\gamma} \int \rho(x,y,z) \frac{\underline{b} \cdot \hat{x}}{b^2} dx dy\tag{22}$$

where b is the impact parameter of the test charge relative to the element $dx dy$. This equation can be rewritten in terms of the scale independent variables and the shape distribution as

$$\frac{d^2 \underline{x}}{dz^2} = \frac{-r_e}{\gamma} \frac{N}{\lambda_x \lambda_y \lambda_z} \frac{\lambda_x \lambda_y}{\lambda_b} \int \rho_\xi \frac{\underline{\xi}_b \cdot \hat{x}}{\xi_b^2} d\xi_x d\xi_y\tag{23}$$

and

$$\frac{d^2 \xi_x}{d\xi_z^2} = \frac{-r_e}{\gamma} \frac{N \lambda_z}{\lambda_x \lambda_b} \int \rho_\xi \frac{\underline{\xi}_b \cdot \hat{x}}{\xi_b^2} d\xi_x d\xi_y\tag{24}$$

where

$$\xi_{\sim b} = \left((x - b_x)/\lambda_x, (y - b_y)/\lambda_y \right)$$

which is in the form of a dimensionless constant times a shape dependent function. For a Gaussian distribution this has the simple form

$$\frac{d^2 \xi_x}{d\xi_z^2} = -D \xi_x e^{-\xi_x^2/2} \quad (25)$$

for $\xi_x \ll 1$ and $\xi_y \ll 1$, or

$$\frac{d^2 \xi_x}{d\xi_z^2} = -D \xi_x$$

near the bunch center. D is now defined to be

$$D_x \equiv \frac{r_e}{\gamma} \frac{N \lambda_z}{\lambda_x \lambda_b} \quad (26)$$

The unperturbed luminosity is related to D by

$$\mathcal{L}_0 = \frac{D_y P}{8\pi mc^2 r_e \sigma_z} \left(\frac{1+R}{R} \right) \quad (27)$$

where P is the power required to accelerate the beam

$$P = f N \gamma mc^2$$

and R is the aspect ratio

$$R = \frac{\sigma_x}{\sigma_y} .$$

Expressing the luminosity as a function of D in this way is only approximate because the effect of the beam dynamics on the overlap integral (i.e., the difference between \mathcal{L}_0 and \mathcal{L}) has been neglected in calculating the luminosity, but it does point out that if the amount of beam power available is fixed, one must increase the severity of the collision in order to achieve higher luminosities. Note that increasing D by increasing

σ_z without affecting the transverse dimensions has no effect on \mathcal{L} except through beam dynamics.

For the Gaussian shape, the numerical value of the disruption parameter is

$$D = \frac{14.4 N \sigma_z}{E \sigma_x \sigma_y} \quad (28)$$

where

N = number of particles in units of 10^{10}

σ_z = bunch length in mm

E = beam energy in GeV

$\sigma_x \sigma_y$ = transverse dimensions in microns.

For oppositely charged beams, the first order effect of the beam dynamics is to decrease the transverse dimensions of the beam. Since $\delta r/r$ is proportional to D and the luminosity is proportional to $1/\langle r \rangle^2$ we expect the luminosity to be modified by a factor

$$\frac{\mathcal{L}}{\mathcal{L}_0} \sim \frac{r_0^2}{\langle r \rangle^2} \quad (29)$$

After a distance l , $\delta r/r = -Dl/\sigma_z$ for $Dl/\sigma_z < 1$. The dimensions of the opposite beam are also changing so that $D(t) \simeq D_0(r_0/r)^2$. We have

$$r^2 \simeq r_0^2 \left(1 - \frac{Dl}{\sigma_z}\right), \quad \frac{Dl}{\sigma_z} < 1 \quad (30)$$

and if L is the total length,

$$\begin{aligned} \langle r \rangle &= \frac{1}{L} \int_0^L r_0 \left(1 - \frac{Dz}{\sigma_z}\right)^{1/2} dz \\ &\simeq r_0 \left(1 - \frac{3}{8} \frac{DL}{\sigma_z}\right). \end{aligned} \quad (31)$$

Hence for $D \sim 1/2$, $L/\sigma_z \sim 2$, and $DL/\sigma_z \sim 1$, the luminosity is enhanced by

$$\frac{\mathcal{L}}{\mathcal{L}_0} \sim 2.5.$$

From eq. (10), the scattering angle distribution for $\sigma_x = \sigma_y$ and impact parameter b is

$$N(\theta) \simeq \frac{N r_e b}{\gamma \sigma_x^2} \frac{N(b)}{N} = \frac{b}{\lambda_z} D \frac{N(b)}{N} \quad (32)$$

which has a maximum near $b \approx \lambda_x$ since for larger impact parameters $N(b)/N$ is decreasing and the scattering angle is less than D/λ_z due to the non-uniformity of the current density. The scattered beam will have a maximum opening angle near $\lambda_x/\lambda_z D$. This opening angle is not a scaling parameter, and its value will depend on the way in which D is increased. If D is increased by increasing λ_z , then θ_{\max} will remain roughly constant. If D is increased by increasing the current or decreasing the transverse scale, then θ_{\max} will increase proportional to N or $1/\lambda_x$, respectively. Furthermore, if the value of D is larger than one, the particle trajectories are oscillatory and the distribution of scattering angles must be found by simulation.

III. Relation of D to the Plasma Frequency and Instabilities

It is interesting to compare D to the relativistic transverse plasma frequency of the bunch ω_p which is defined as

$$\omega_p^2 = \frac{4\pi \rho r_e c^2}{\gamma} \quad (33)$$

For a three-dimensional Gaussian distribution with charge Ne , ρ varies with position and so does ω_p . Using ρ_{\max} and comparing to D defined in terms of the central density (for simplicity $\sigma_x = \sigma_y$).

$$\begin{aligned} \rho_{\max} &= \frac{N}{(2\pi)^{3/2} \sigma_x \sigma_y \sigma_z} \\ \omega_{p\max}^2 &= \frac{4\pi \rho_{\max} r_e c^2}{\gamma} \end{aligned} \quad (34)$$

and one finds

$$D = \frac{N r_e \sigma_z}{\gamma \sigma_x^2} = \frac{\omega_p^2 \sigma_z^2}{c^2} \sqrt{\frac{\pi}{2}} \quad (35)$$

The number of plasma oscillations which occur while traveling a distance L is $n = L/\lambda_p$ and using $L \sim \sqrt{2\pi} \sigma_z$ and eq. (35) yields

$$D \sim 8n^2. \quad (36)$$

Thus, \sqrt{D} is a measure of the number of plasma oscillations which occur during the collision. This conclusion could also have been reached from the form of the scaled equation of motion, eq. (25).

The results of a full simulation (see Section V) indicate that the effective phase shift for particles near the axis of a Gaussian beam is actually related to D by

$$D = 10.4 n^2. \quad (37)$$

If the beam behavior was stable for two full plasma oscillations, then D could be as large as 32 for Gaussian beams. Beam growth due to plasma instabilities typically requires several plasma oscillations so that values of D less than 10 are certainly stable. The value of numerical coefficient is somewhat shape dependent.

The collision strength parameter used for storage ring machines is the linear tune shift³⁾

$$\Delta\nu_y = \frac{r_e}{2\pi} \frac{N \beta_y^*}{\gamma \sigma_y (\sigma_x + \sigma_y)} \quad (38)$$

where β^* is the betatron function at the collision point. Using eq. (4) one finds

$$\Delta\nu_y = \frac{D}{4\pi} \frac{\beta_y^*}{\sigma_z} \quad (39)$$

Maximum luminosity is achieved when $\beta^* \sim \sigma_z$ and the observed limitation for the tune shift of $\Delta\nu \sim 0.06$ corresponds roughly to a disruption

parameter of one. This low value is probably a consequence of the fact that there are many collisions in a storage ring per damping time. For this case, Uhm and Liu⁴⁾ have derived a dispersion relation for the linearized Vlasov-Maxwell equations which predicts a maximum growth rate of $0.6 \omega_p$. As pointed out by B. Zotter,⁵⁾ this value agrees well with the observed limitation of Δv using an effective bunch length $L = 2\sqrt{\pi} \sigma_z$ but does not explain the fact that the limit is independent of β^* .

The growth of the kink (or hose) instability for the linear collider case has been analyzed by Fawley and Lee⁶⁾ who find that the growth factor is limited by the finite length of the interaction to

$$g < \frac{1}{1 + \alpha/2} \frac{\omega_\beta \ell}{2c} \quad (40)$$

where $\alpha \approx 0.18$ is a term used to model phase mix damping, ℓ is the effective length and ω_β is the effective betatron frequency of the collision. Since $\omega_\beta \ell/2c = 2\pi n$, we can use $n \approx \sqrt{D}/3.22$ to get (for the Gaussian)

$$g < 1.8\sqrt{D} \quad (41)$$

For a given fractional transverse offset δ , the condition $g\delta < 1$ places a limit on D which is

$$D < \left(\frac{1}{1.8\delta} \right)^2 \quad (42)$$

For a 10% offset this requires that D be less than 31, and for a 25% offset, D must be less than 5.

The effect of the beam emittance on the collision depends on the ratio of the beam envelope size to the Debye length. The Debye length λ_D is the average distance which a particle travels in the transverse dimension during a time $1/\omega_p$.

$$\lambda_D = \frac{\langle v_1^2 \rangle^{1/2}}{\omega_p} \quad (43)$$

Hence, if the transverse size of the beam is comparable to λ_D and the collision time is of order $1/\omega_p$, particles will traverse the beam due to emittance effects during the collision, and this will damp any change in the beam envelope due to the coherent focusing effect of the beams. The emittance is the area of the phase space ellipse $\pi\langle x\rangle\langle x'\rangle$ and hence

$$\epsilon^2 = \pi^2 \lambda_x^2 \frac{\langle p_{\perp}^2 \rangle}{p^2} = \frac{\pi^2 \lambda_x^2 \langle v_{\perp}^2 \rangle}{2c^2} \quad (44)$$

The velocity distribution also defines an effective temperature for the beam which is

$$k T_{\text{eff}} = \frac{p_{\perp}^2}{2\gamma m} = \frac{\epsilon^2 \gamma m c^2}{2\pi^2 \lambda_x^2} \quad (45)$$

The temperature and the rms velocity actually vary with position within the beam since they depend on the phase space distribution function. Usually the temperature falls to zero on the edges of the beam envelope (where $\langle v_{\perp} \rangle \approx 0$) and reaches a maximum on the beam axis. For a uniform radial dependence of the temperature

$$\begin{aligned} \langle kT \rangle &\simeq \frac{\epsilon^2 \gamma m c^2}{4\pi^2 \lambda_x^2} = 1/2 \gamma m \langle v_{\perp}^2 \rangle \\ \langle v_{\perp}^2 \rangle^{1/2} &= \frac{\epsilon}{\pi} \frac{c}{\sqrt{2} \lambda_x} \end{aligned} \quad (46)$$

The relationship between the beam size and the Debye length for a fixed disruption parameter is found using $D = 1/4\pi \omega_p^2 \lambda_z^2 / c^2$ and eq. (43)

$$\frac{\lambda_D}{\lambda_x} = \frac{\epsilon}{\pi} \frac{\lambda_z}{2\sqrt{2\pi} \lambda_x^2 \sqrt{D}} \quad (47)$$

When λ_D is much smaller than λ_x the emittance of the beam can be ignored.

IV. Computer Simulation

The computer simulation of the beam-beam effect in a single pass collider is considerably simplified by the fact that the beams are highly relativistic and that the collision occurs only once. For the relativistic beam, the effect of the longitudinal excitation is unimportant, and the transverse motion is given by integrating the effect of the kicks defined by eq. (24). In contrast, the computer investigation of beam-beam effects in a storage ring requires that one follow the evolution of the bunches for a time comparable to the damping time. This time is typically much longer than the time between collisions, and in this case, small perturbations in the initial configuration of the bunches can grow with time and eventually become important. This is difficult to study with a computer because numerical approximations and truncation errors lead to a cumulative loss of information about the beam behavior. The long-time scale also means that longitudinal modes in the beam can be important. The single pass beam-beam effect at high energy can be reliably calculated because of the validity of the impulse approximation and the small number of plasma oscillations for reasonable collision strengths.

The computer simulation used here starts by distributing the charge on a three-dimensional lattice which defines typically 8000 cells for each beam. The central position and trajectory of each cell is advanced using time symmetric difference equations derived from eq. (24). The advantages of time symmetric equations have been discussed by Buneman.⁷⁾ In this application, they allow one to verify that the code is reversible and increase the accuracy of the simulation. Any irreversibility is due to round-off errors and coarse binning of the density or time step.

The cells are advanced longitudinally at a uniform velocity equal to the speed of light. For each time step, the transverse kick given to each cell of one beam is calculated from the charge in the cells of the other beam which are at the same longitudinal position. The charge distribution of each beam is modified due to the cumulative effect of all the transverse kicks which have been applied previously.

To further increase the accuracy of the simulation, the charge in each cell is treated as a cloud of charge rather than as a point charge. Simulations in plasma physics often use the particle-in-cell method⁸⁾ which simulates the motion of the plasma by having many particles within the cell which share the charge. The number of such particles must be large enough to reduce the particle or shot noise introduced by statistical fluctuations. Real plasmas contain large numbers of particles, and such fluctuations are unphysical. The major advantage of such an approach is that the simulation of temperature effects is simplified since the particles can be given an initial velocity distribution within the cell. The cell is used in these calculations to bin continuous quantities like pressure, density and electromagnetic fields. The density distribution, for example, is calculated by simply counting the number of particles which are found in a given cell at each time step.

The shot noise contributions of the particle-in-cell model can be eliminated by treating each particle as a cloud of charge. As pointed out by Birdsall and Fuss,⁹⁾ this cloud-in-cells method also reduces many fictitious effects which come about because of the finite cell size. Errors in time due to the early or late arrival of a particle in a cell and errors in the forces due to the uncertainty of the particle's position

within the cell are smoothed. The finite size cloud also smooths the interactions between particles and eliminates the necessity of cutting off the singularity in the interaction which occurs when point particles approach zero separations.

The cloud size does not have to be equal to the cell size. If it is larger than a cell size or if the cloud is not centered on a cell, the charge is spread out over several cells in proportion to the fraction of the total cloud's area which falls in that cell. If the cloud is smaller than a cell, the model is very similar to the particle-in-cell model with a particular choice for the cutoff distance for the interaction of the charges.

In this simulation, the cloud size is changed as the interaction progresses. The size of a cloud at any given time is determined by the distance to adjacent clouds on a lattice. Using the nearest neighbors to determine the cloud size is equivalent to a first order Taylor series expansion of the motion about the center of the cloud. A fixed cell size is used to calculate the density distribution and the luminosity overlap integral. The cloud's charge is apportioned to the cells using an area weighting scheme.

By dividing each cell into four subcells, the gradient of the density distribution within a cell can be adjusted to match the local gradient measured by the positions of the nearest neighbor clouds. This increases the number of effective cells in the calculations for the purpose of calculating density distributions and overlap integrals of the type given by eq. (15) without increasing the number of clouds which must be followed in the simulation of the dynamics. At the expense of increased computing

time, several clouds can be superimposed at the same positions but with differing velocities to simulate temperature effects, but we concentrate here on the cold beam limit. The cell size is usually equal to the original cloud size since the behavior of the beam is not followed on a scale smaller than a subcell. A cell size larger than the original cloud size would decrease the accuracy of the luminosity calculation.

V. Results of the Simulations

Consider the collision of two beams with Gaussian profiles and scale factors σ_x , σ_y , and σ_z . One can begin studying the effect of the collision by looking at the motion of a test charge in one beam whose position (x,y,z) relative to the center of the beam is $(\sigma_x, 0, 0)$. The trajectories in the x,z projection for increasing values of the collision strength are shown in fig. 5. As can be seen in fig. 5 for the case $D = 1$, the effect of beam 2 on this test charge is well represented by a focal length which is equal to the bunch length σ_z . For large values of D , it is best to think in terms of the number of betatron oscillations which a particle executes as it passes through the other beam.

The case $D = 1$ corresponds roughly to a quarter betatron oscillation and $D = 10$ is slightly more than one full oscillation. Because of the form of eq. (24), the equation of motion for small offsets from the beam center is given by

$$\Delta \xi_x' \simeq -D \xi_x \quad (48)$$

so that the betatron wave length will be proportional to the square root of D . The observed values for the phase shift of the test particle at $x = \sigma_x$ are shown in fig. 6 and the phase shift is found to be $\Delta\phi \simeq 0.62\pi\sqrt{D}$.

This relationship for the focal strength of the beam works well up to quite large values of the collision strength and agrees reasonably with the rough calculation of Section III, eq. (36). The corrections due to the changes which occur in the other beam are small. The exit angle versus position of the test charge for D between 0 and 32 is shown in fig. 7. The position is that which occurs when the longitudinal separation between the two beams is $2.5 \sigma_z$. This corresponds to a position for beam 1 of $z/\sigma_z = 1.25$ in fig. 5. As D increases from 0 to 1, the exit angle increases. The maximum exit angle occurs when D is between 1 and 2. The values of test charge exit angle and position for increasing values of D form an approximate ellipse similar to a phase ellipse. The rotation of the ellipse is related to the effective thickness of the lens. The positions of the points for $D = 16$ and $D = 32$ are close to those for $D = 3$ and $D = 8$ respectively and indicate that the nonlinearities of the interaction are not very important.

Due to the fact that the charge distributions of the beams change during the collision, the dynamics of the leading and trailing parts of the beam are not quite the same as those of the central part. Figure 8 shows a superposition of the trajectories in the xz plane of all the lattice points with $y = 0$ for the case where $D = 2.4$. The lattice is 10×20 in this projection and the distance between lattice points is $0.5 \sigma_z$. The trajectories should be compared to fig. 5 for the case $D = 2$. Particles within 1σ of the beam center are scattered through the maximum angle. The particles scattered through small angles come predominantly from the trailing part of the beam which scatters off a partially disrupted charge distribution and therefore sees a smaller charge density.

Figures 9a-c show the density in the $y = 0$ plane of one of the beams for the case $D = 1, 3,$ and 5 . The times shown are in arbitrary units corresponding to a beam center-to-center separation of $10 \sigma_z$ at $T = 0$ and $T = 40$. The longitudinal positions of the beam centers coincide when $T = 20$ and the luminosity overlap integral (eq. (15)) receives most of its contributions from $15 < T < 25$.

By comparing fig. 9a, 9b, and 9c, one can see that as D is increased from 1 to 5, the focal point of the beam moves toward smaller times. For $D = 1, 3$ and 5 , the focus occurs near $T = 26, T = 18,$ and $T = 16$ respectively. In all cases the focus is diffuse because of the non-uniform charge distribution. As expected, the transverse tails have longer focal lengths.

The luminosity will reach a maximum when the focal spots of the two beams overlap most completely, i.e., when the central focus occurs near $T = 20$. This happens near $D = 2.4$. The harmonic motion of particles near the center for $D > 2$ (see fig. 5) can yield several diffuse foci during beam collisions (see fig. 9c, $T = 25$).

As discussed in Section II, the luminosity overlap integral will be a function of D because of the time dependence of the density distribution caused by the beam disruption. For oppositely charged beams which are not too severely disrupted, the dynamics lead to an enhancement of the luminosity. Using the time dependent density distributions found by the simulation, this enhancement can be studied as a function of the collision strength. The enhancement is defined as the ratio between the actual luminosity (eq. (15)) and the unperturbed luminosity (eq. (16)) and is

shown in fig. 10. In order to accurately calculate the overlap integral, the number of lattice points used in the simulation must be large enough to follow the density variations during the collision. The integral is calculated directly from the density distribution of the two beams at each step. The dependence of the enhancement factor on the cell size was investigated and the number of cells was increased until no further effect of the cell size could be seen.

VI. Offset Beams and Uniform Transverse Profiles

For the case where the density distributions do not change (the limit as D goes to zero), one can calculate the effect of an initial offset of $n\sigma$ in the transverse plane on the luminosity. The overlap integral (eq. (16)) gives a luminosity

$$\mathcal{L} = \frac{e^{-n^2/4}}{4\pi} = \mathcal{L}_0 e^{-n^2/4} \quad (49)$$

for Gaussian beams. The luminosity as a function of D for $n = 2$ is shown in fig. 11. From eq. (49) one can see that for a two sigma offset the $D = 0$ luminosity is reduced by a factor of 0.37. However, the enhancement still occurs and the ratio of maximum luminosity to $D = 0$ luminosity is almost the same as in the zero offset case. The enhancement drops off more rapidly with D however.

Similar results have been obtained for the case where the beam has a uniform density profile in the transverse direction and a Gaussian profile in the longitudinal direction. The collision strength is from eq. (26)

$$D = \frac{r_e N \sigma_z}{\gamma \lambda^2} \quad (50)$$

and the unperturbed luminosity is $\mathcal{L}_0 = 1$. The trajectories for test particles are shown in fig. 12 and the enhancement is shown in fig. 13.

For the uniform profile, the enhancement falls off rapidly as the collision strength is increased leading to a net loss of luminosity for D greater than 16. The local peaks in the enhancement correspond to values of the collision strength yielding trajectories which tend to focus the two beams when the maximum charges overlap. (This is the point $Z = 0$ in fig. 12.)

The more rapid fall-off of luminosity with collision strength for the uniform case can be understood in terms of the plasma properties of the charge distributions. In the leading and trailing parts of a Gaussian beam and in the transverse tails, the charge density is less than the density in the central part of the beam. Since the plasma frequency squared is proportional to the density, this means that the corresponding plasma wavelength λ_p is longer in the tails and that the tails are more stable than the beam core. When beam dynamics are neglected, the tails of the beam contribute little to the luminosity of the collision. The luminosity is proportional to the integral of the density squared and in the Gaussian case, for example, it receives very little contribution from those parts of the beam which are more than one sigma from the center or times when the beams are separated longitudinally by more than one sigma.

When beam dynamics are included, one expects that the cumulative focusing effect of the head of the beam on the central core will be important in determining the approximate transverse dimensions of the beam core and its profile when it overlaps with the core of the other beam. Thus, the charge distribution in the head of the beam is an important factor in determining the enhancement factor or ratio of the actual luminosity to the luminosity expected for undisturbed beam profiles. The

Gaussian transverse profile has a larger enhancement for $D > 10$ than the uniform profile because the non-uniform density distribution leads to a spread in the plasma frequencies and this together with the longer plasma wavelength in the tails helps stabilize the enhancement factor.

VII. Conclusions

The energy lost per turn by a particle stored in a magnetic ring grows as the fourth power of the particle's energy and this power loss has become a significant constraint in the design of machines to produce high energy electron-positron collisions. This problem has led to the consideration of the properties of alternative systems which collide linearly accelerated beams of electrons with similar beams of positrons. The required luminosity is achieved in a linear system by having very tight focusing at the beam collision point. Spot sizes of several square microns can be achieved.

The beam-beam effect which limits the current which can be stored in a circular machine is still expected to be the limiting factor in linear systems. However, the limitation comes not from the cumulative effect of many small perturbations but from the disruptive nature of a single collision. Particle densities several orders of magnitude higher can be achieved in the single collision case. In addition, the strong disruption of the beams leads to an enhancement of the luminosity due to the net focusing effect which the two oppositely charged beams have on each other (see fig. 1).

The strength of the interaction between the beams \sqrt{D} , is related to the number of plasma oscillations which occur during the collision. The plasma frequency however grows only as the square root of the incoming current, and this means that very high beam densities can be tolerated.

Typical instability growth rates would allow several plasma oscillations. For Gaussian beam profiles, two full plasma oscillations occur for $D \approx 32$.

The interaction of two such beams for small numbers of plasma oscillations can be reliably calculated using plasma simulation techniques. The magnitude of the luminosity enhancement and the relation between beam density and effective plasma wavelength have been investigated using a computer simulation. The luminosity enhancement grows proportional to D^2 and reaches a maximum value when the focal spots of the two beams overlap most completely. This occurs after one-quarter plasma oscillation. For Gaussian bunches, the enhancement reaches a maximum for $D \approx 2.4$ and remains constant to large values of D ($D \approx 20$). The value of the enhancement is approximately 6 for a Gaussian beam which is mismatched at insertion, and 2.5 for a matched beam (i.e., emittance dominated minimum waist). The non-uniformity of the Gaussian charge density helps stabilize the beam dynamics. For more uniform shapes, the enhancement drops off more rapidly with D .

Suggestions for linear colliding beam machines have been limited to small values of the disruption parameter.^{10,11)} In future designs it should be possible to greatly increase the design luminosity by increasing the collision strength and taking advantage of the luminosity enhancement. A disruption limit $D = 32$ with a luminosity enhancement $\mathcal{L}/\mathcal{L}_0 = 6$ yields an increase in luminosity of

$$D^2 \frac{\mathcal{L}}{\mathcal{L}_0} = 6 \times 10^3$$

if the current is increased or

$$D^2 \frac{\mathcal{L}}{\mathcal{L}_0} = 2 \times 10^2$$

if the beam spot is decreased compared to a design with $D = 1$ and $\mathcal{L}/\mathcal{L}_0 = 1$.

Acknowledgements

The author would like to thank T. Solazzo for assistance with the analysis of the simulation results and B. Richter, E. Lee, and W. Fawley for useful discussions.

This work was supported by the Department of Energy under contract DE-AC03-76SF00515.

References

1. M. Tigner, *Nuov. Cim.*, Vol. 37, No. 3 (1965), 1228; U. Amaldi, *Phys. Lett.* B61, 313; J.-E. Augustin et al., *Proceedings of the Workshop on Possibilities and Limitations of Accelerators and Detectors (Batavia, 1978)* 87.
2. J. D. Jackson, *Classical Electrodynamics* (John Wiley & Sons, Inc., New York, 1962).
3. A. Chao, PEP NOTE 279; B. W. Montague, "Calculation of Luminosity and Beam-Beam Detuning in Coasting Beam Interaction Regions," CERN/ISR-GS/75-36 (1975).
4. H. S. Uhm, C. S. Liu, *Phys. Rev. Lett.* 43 (1979) 914.
5. B. Zotter, LEP-Note 194, CERN (1979).
6. William M. Fawley, Edward P. Lee, Lawrence Livermore Report, UCID-18584.
7. O. Buneman, *Journal of Computational Physics*, 1 (1967) 517.
8. R. W. Morse, *Methods in Computational Physics* 9 (1970) 312.
9. C. Birdsall, D. Fuss, *Journal of Computational Physics* 3 (1969) 494.
10. J.-E. Augustin et al., *Proceedings of the Workshop on Possibilities and Limitations of Accelerators and Detectors (Batavia, 1978)* 87.
11. SLAC LINEAR COLLIDER DESIGN REPORT, SLAC Report 229.

Figure Captions

1. Computer simulated collision of intense relativistic beams illustrating the pinch effect.
2. In the rest frame of particle 1, particle 2 travels along the z axis and has a minimum displacement from particle 1 of b in the x direction.
3. Time dependence of the electric and magnetic fields due to the passage of particle 2 as seen at the position of particle 1.
4. Test particle incident with displacement b from the axis of a charge distribution.
5. Trajectory of a test charge incident on a Gaussian bunch with displacement σ_x from the axis for the case $D = .5, 1, 2, 5, 10, 32$. The test charge is within a Gaussian charge distribution.
6. Phase shift of the test particle versus disruption parameter.
7. Exit angle versus position of the test charge incident at $(\sigma_x, 0, 0)$ for values of D between 0 and 32.
8. Trajectories of the lattice points in the yz plane for the case $D = 2.4$.
9. (a), (b), (c) Simulation of the density distributions during the collision of two Gaussian beams for $D = 1, 3, \text{ and } 5$.
10. Luminosity enhancement versus disruption factor.
11. Luminosity versus disruption factor for two Gaussian beams colliding with an initial offset of $2\sigma_x$.
12. Trajectory of a test charge incident on a uniform transverse profile, Gaussian longitudinal profile beam. The test charge is initially at the boundary of the transverse distributions and is within a uniform transverse profile beam.
13. Luminosity enhancement versus disruption factor for uniform transverse profile beam collisions.

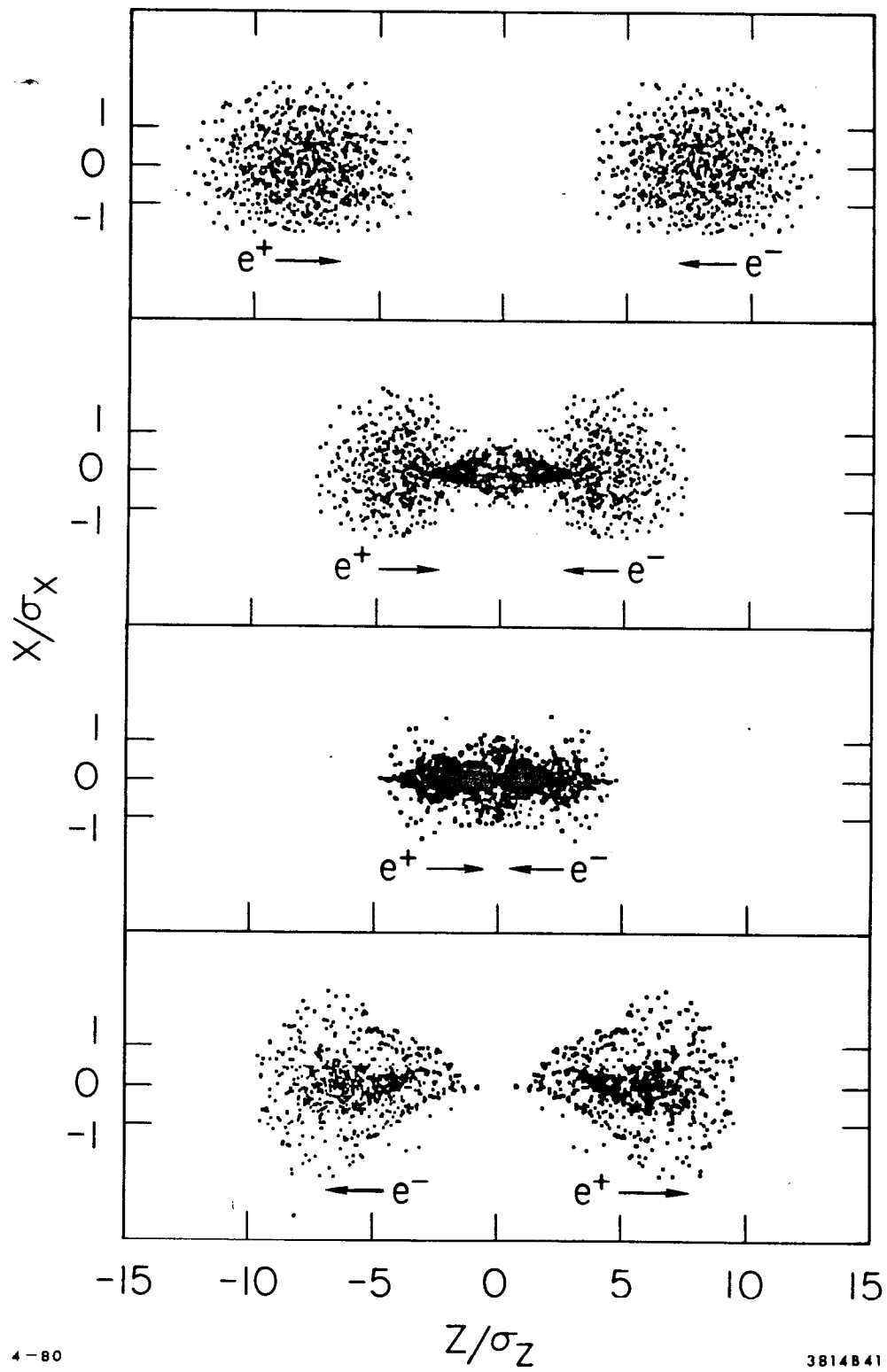


Fig. 1

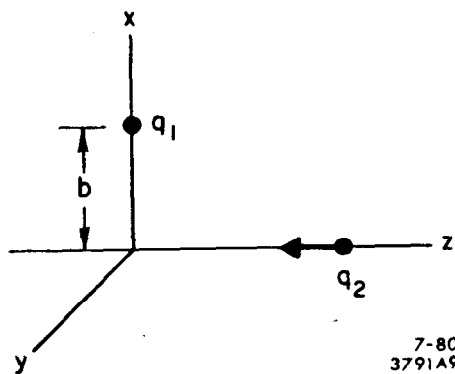


Fig. 2

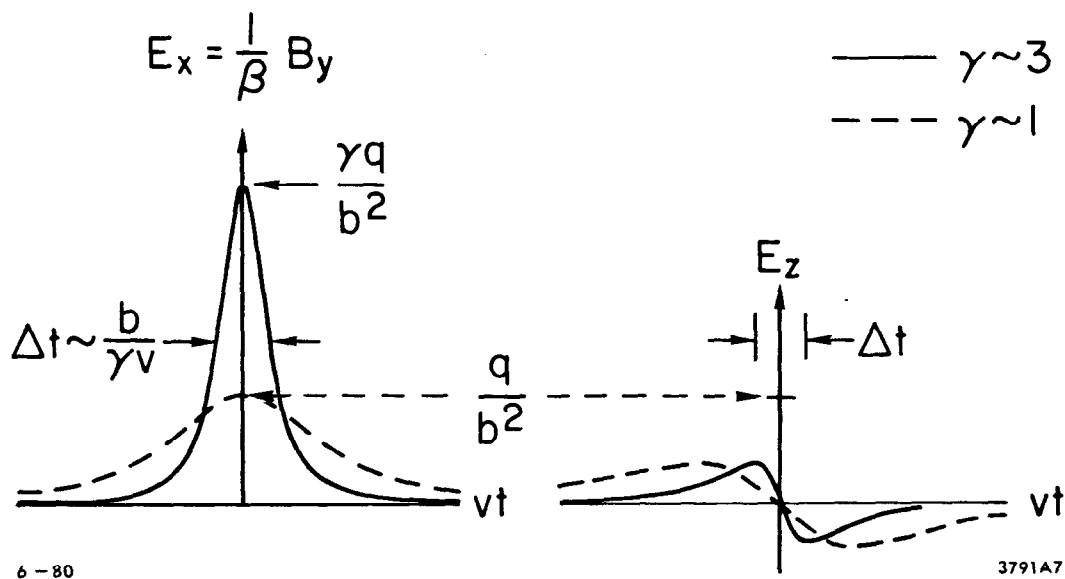


Fig. 3

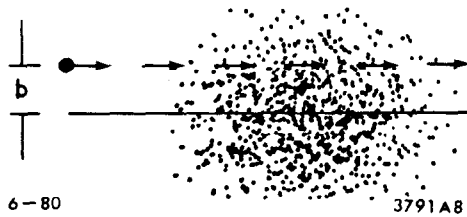


Fig. 4

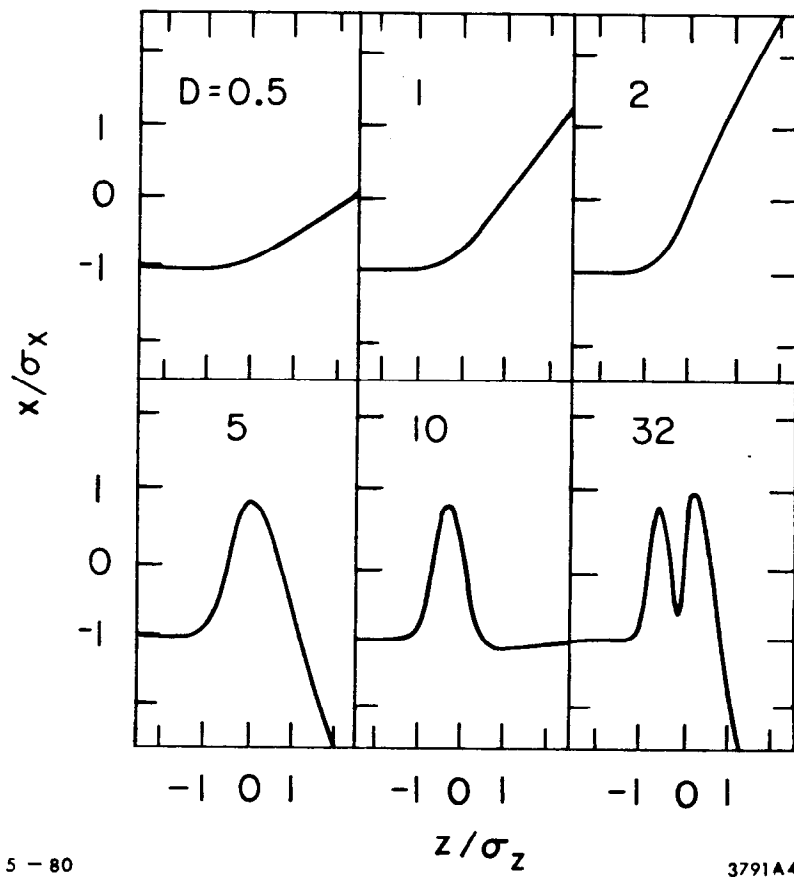
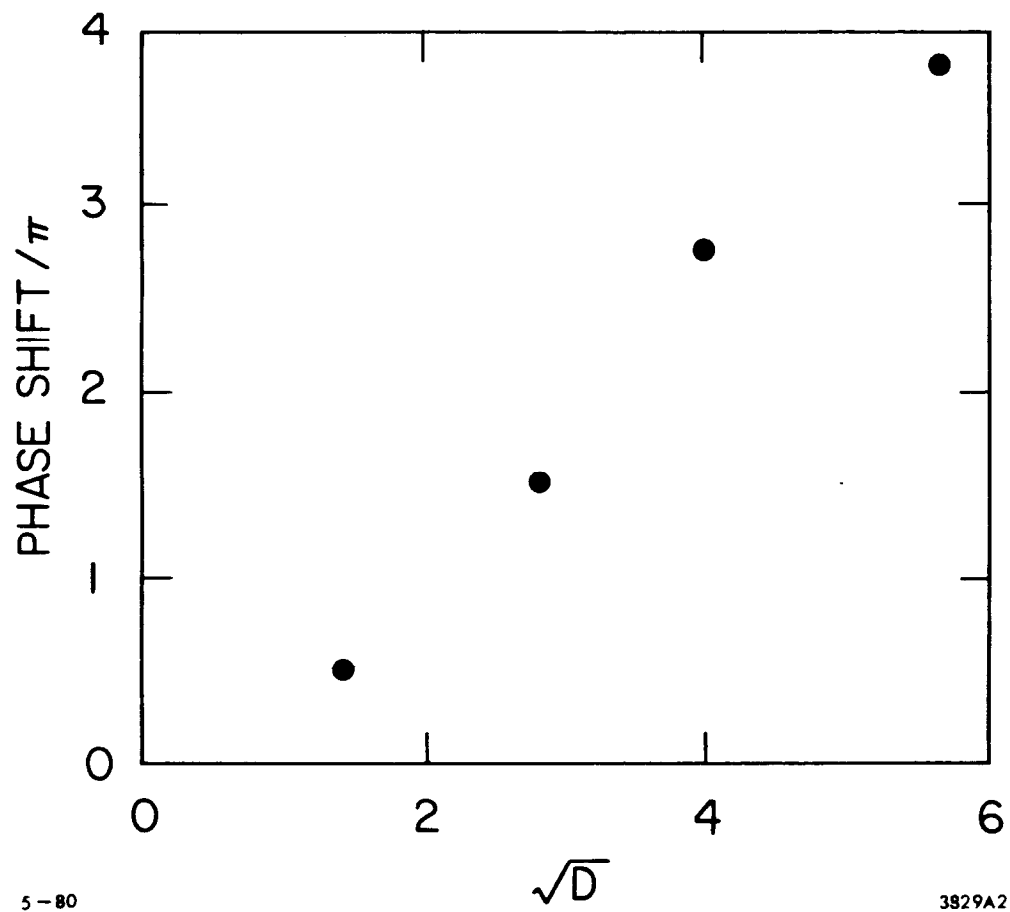
PARTICLE TRAJECTORIES
FOR 1σ INITIAL OFFSET

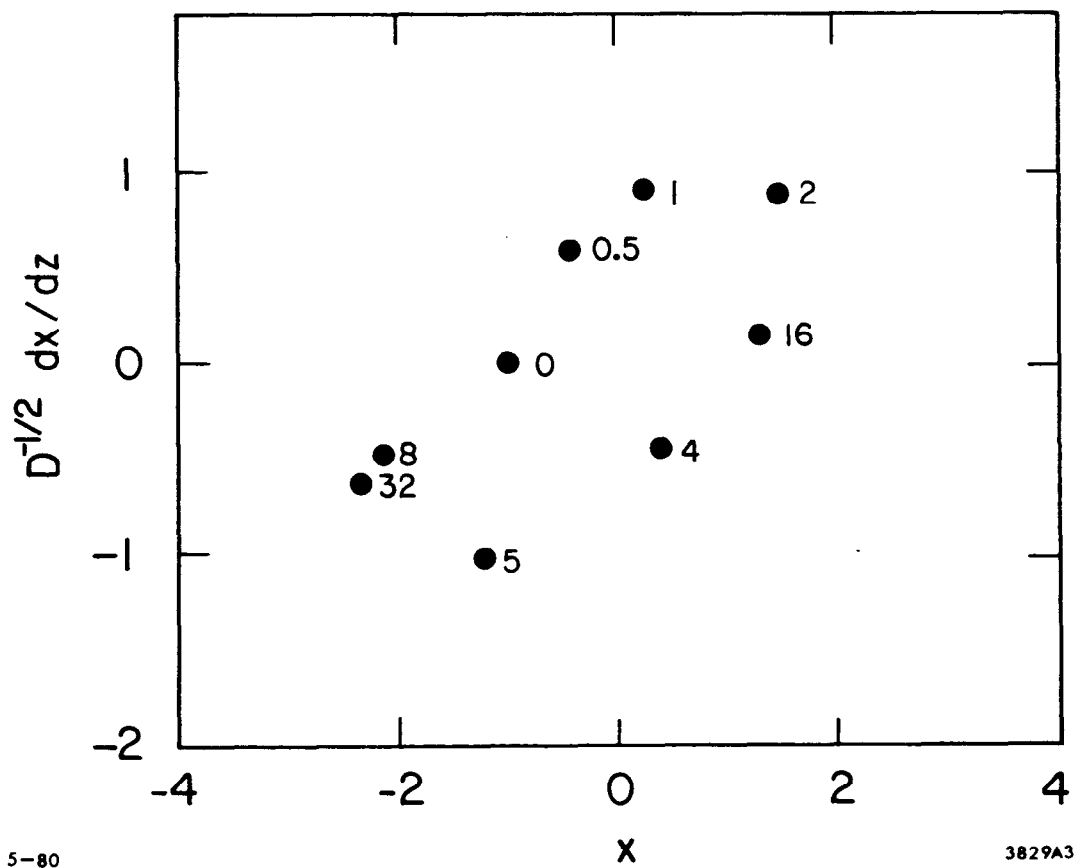
Fig. 5



5-80

3829A2

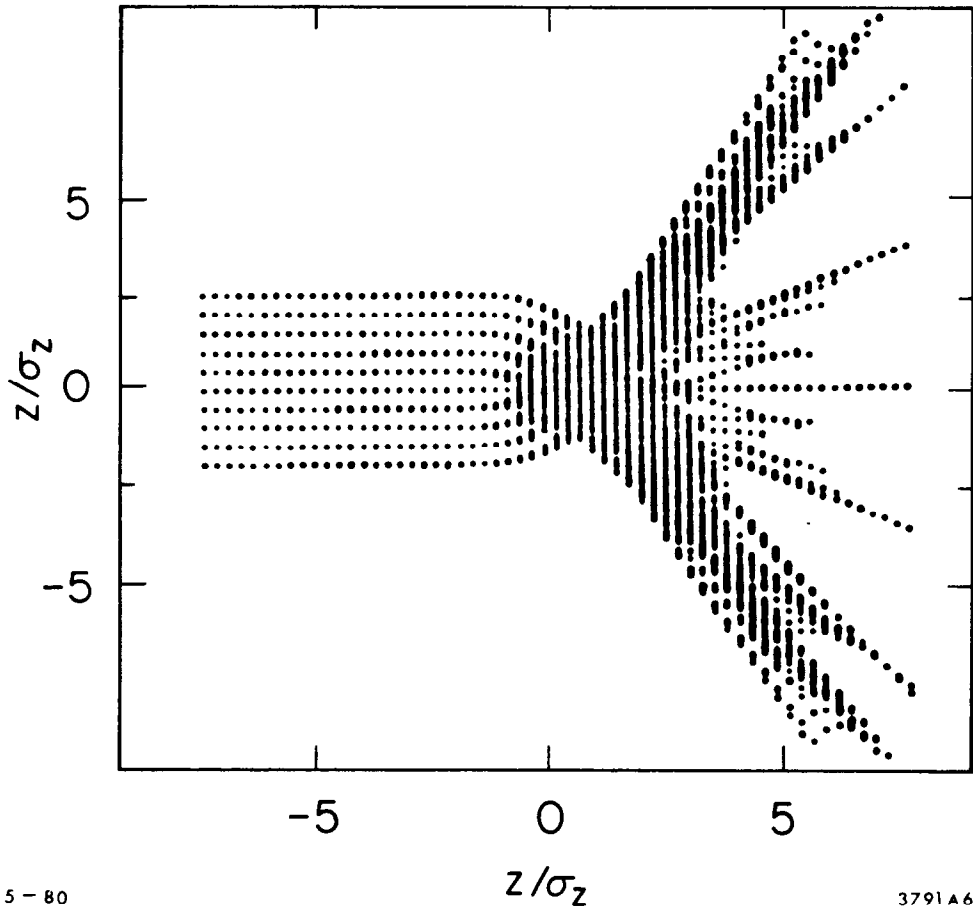
Fig. 6



5-80

3829A3

Fig. 7



5-80

3791A6

Fig. 8

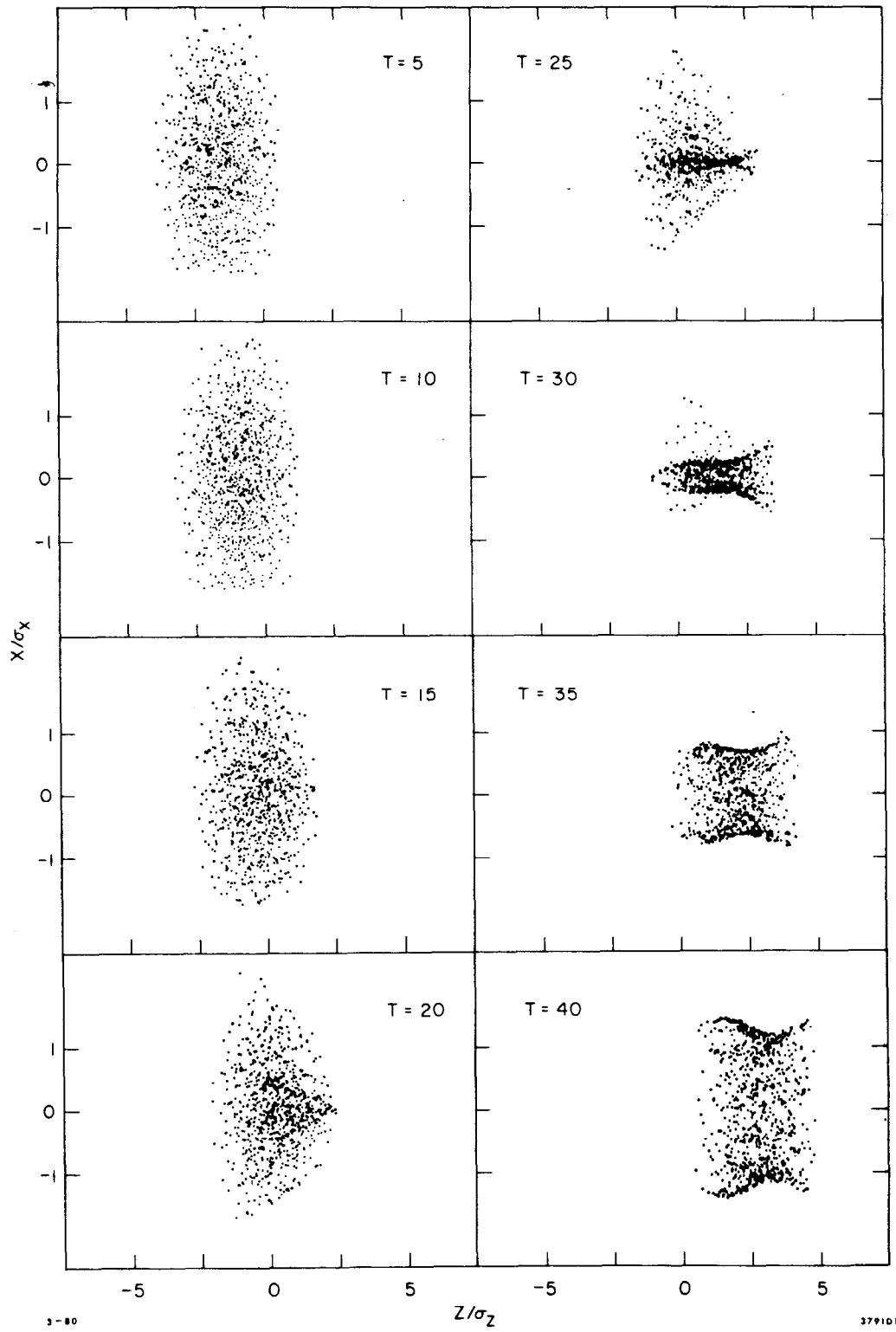


Fig. 9(a)

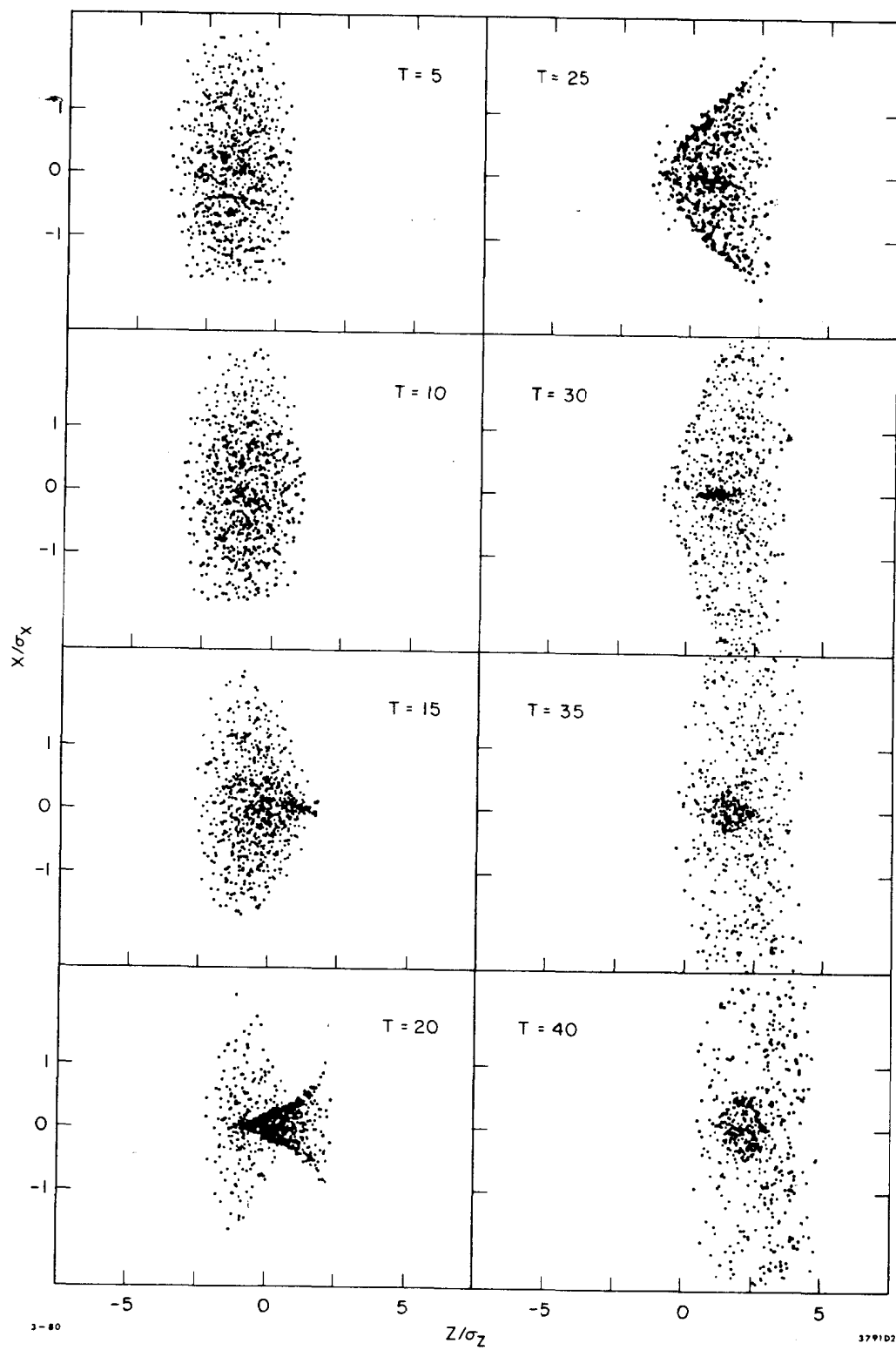


Fig. 9(b)

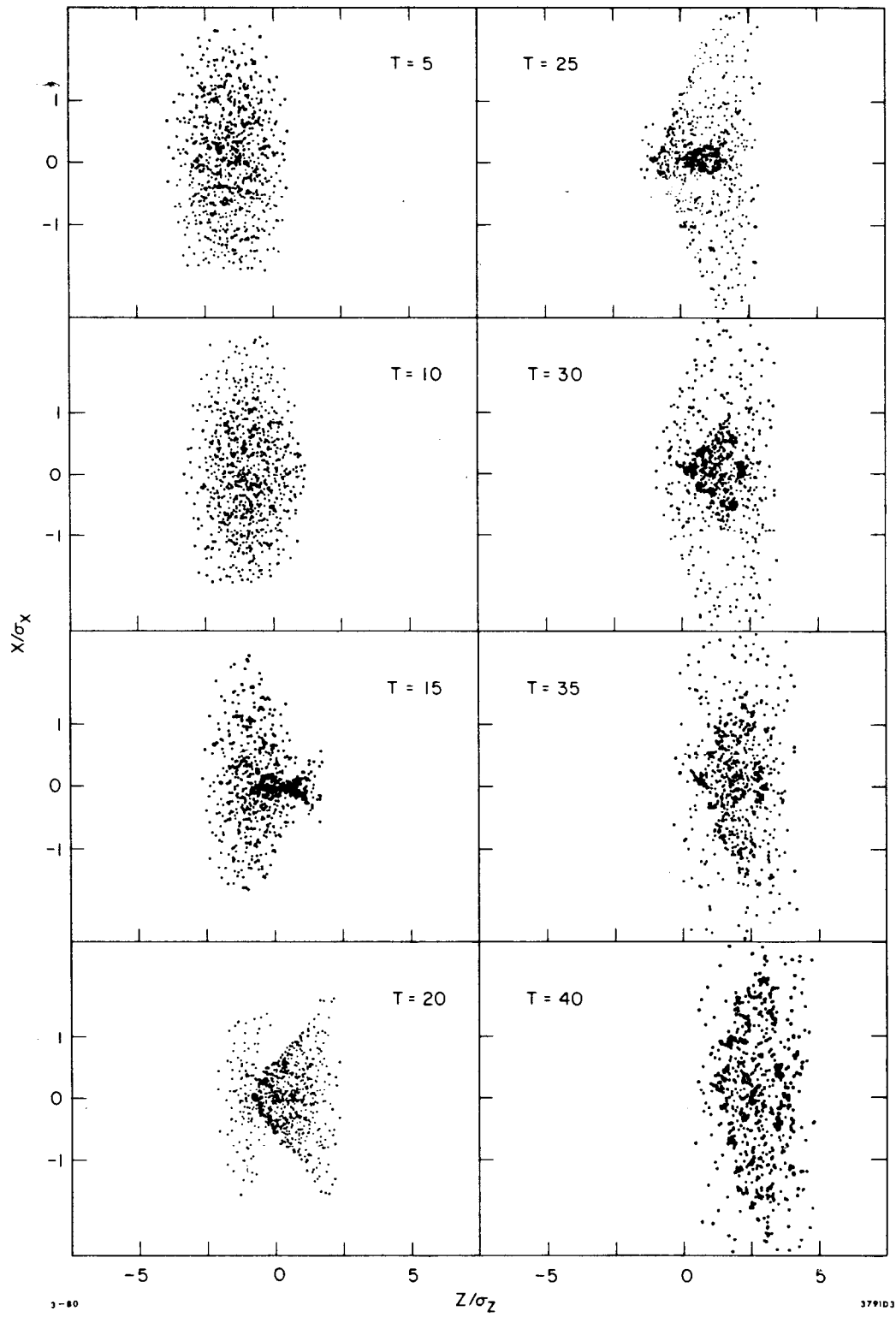


Fig. 9(c)

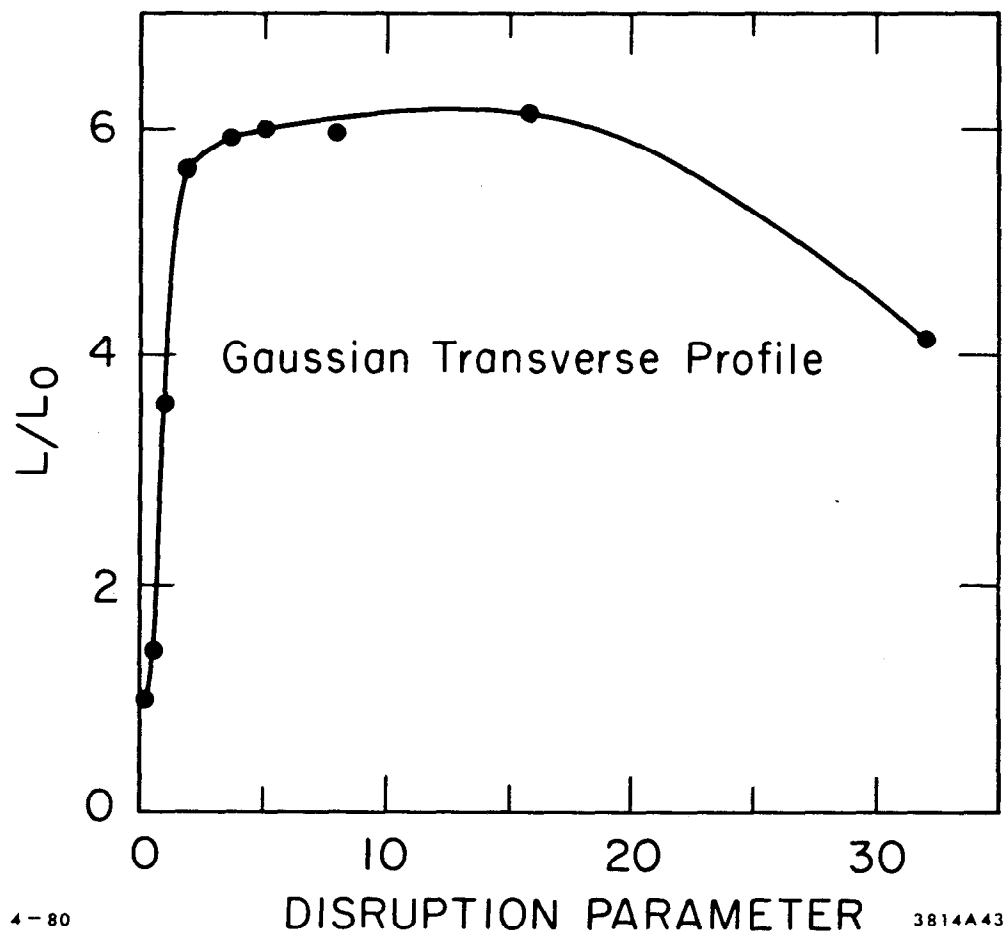
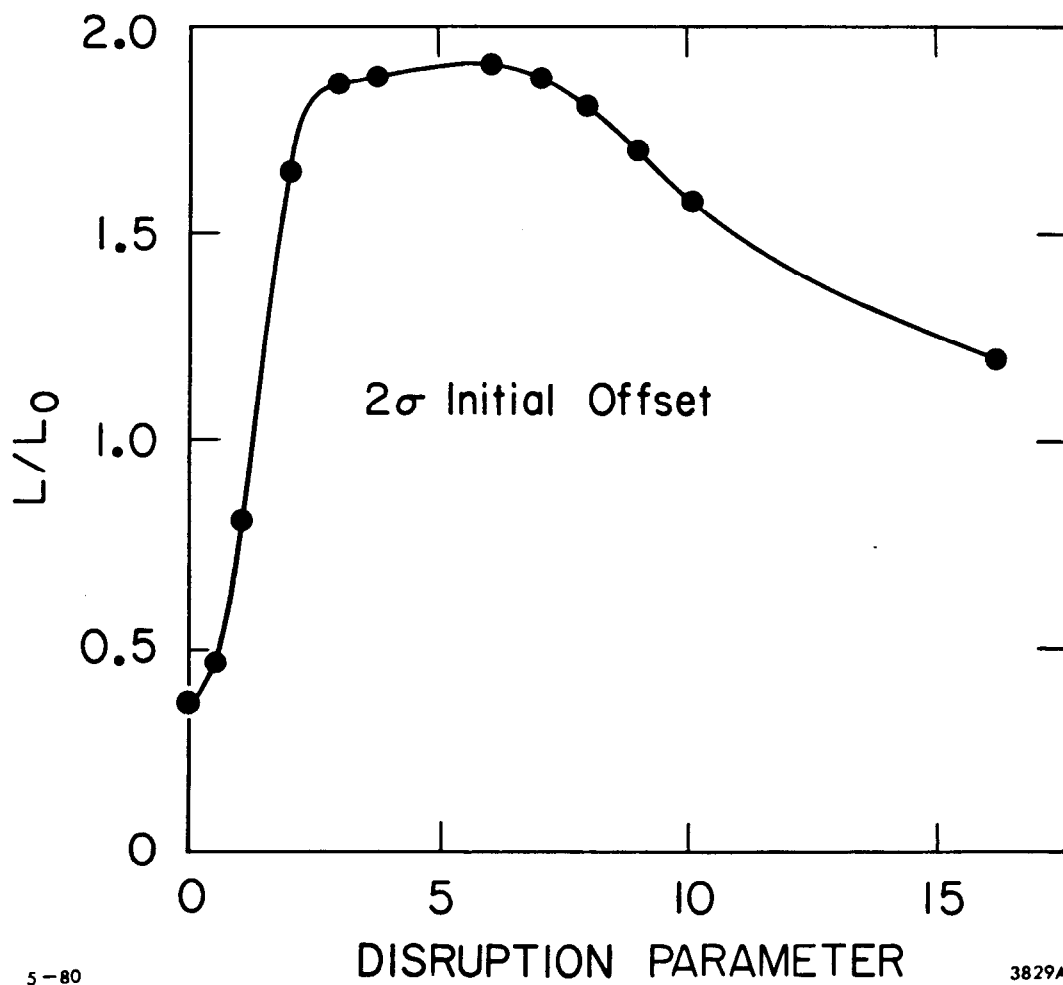


Fig. 10



5-80

3829A1

Fig. 11

PARTICLE TRAJECTORIES
FOR UNIFORM TRANSVERSE PROFILE

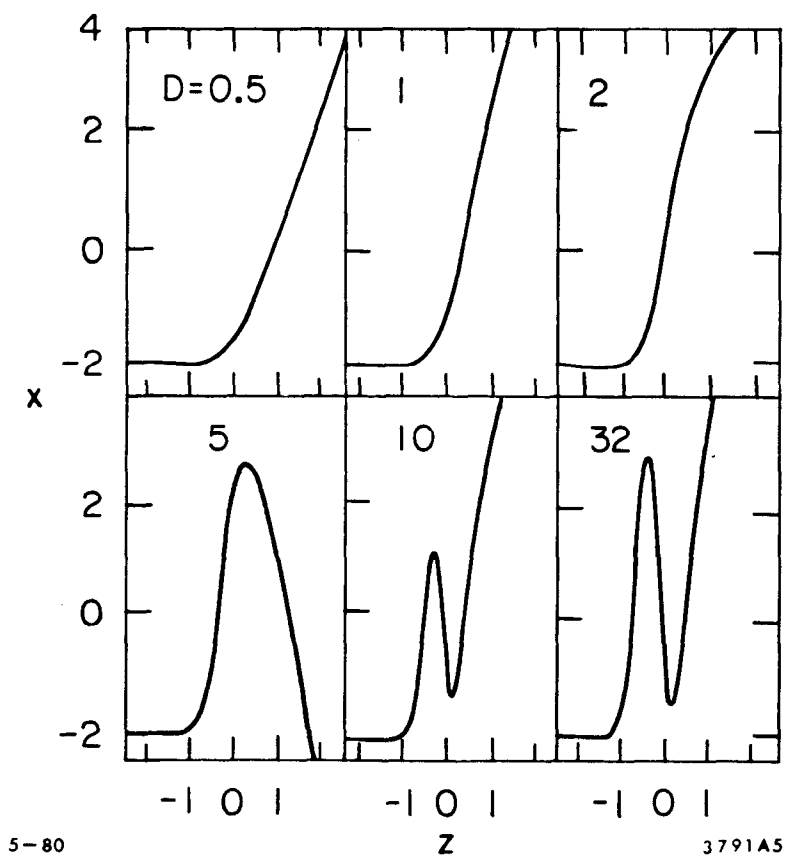


Fig. 12

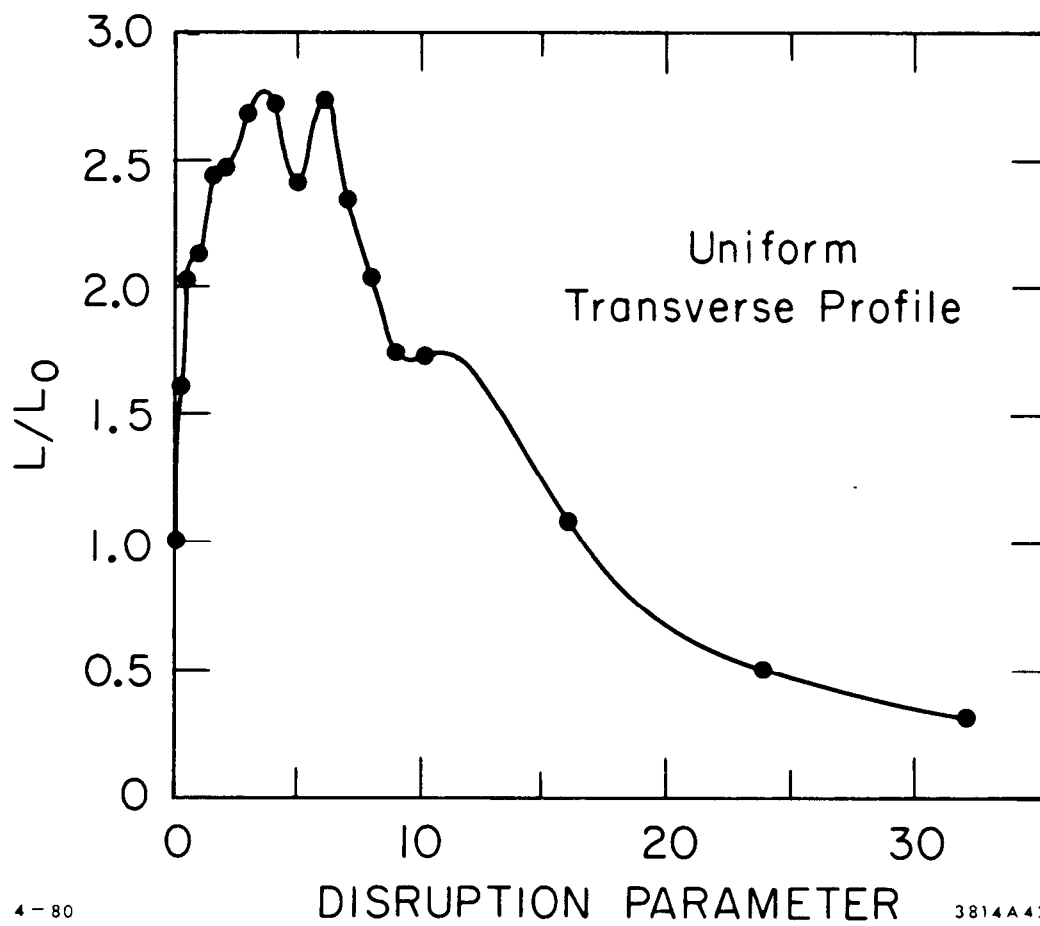


Fig. 13

ANALYSIS OF THE BEAM-BEAM INTERACTION
USING TRANSFER MAPS

Alex J. Dragt* and Oleg G. Jakubowicz
Department of Physics and Astronomy
University of Maryland
College Park, Maryland 20742

*Supported in part by Department of Energy
Contract #DE-AS05-80ER10666.A000

ABSTRACT

The method of transfer maps is used to develop generalized Courant-Snyder invariants in the presence of the beam-beam interaction for both nonresonant and resonant tunes. Numerical evidence is presented to illustrate that the generalized invariants are indeed constant through terms of first order in the beam-beam interaction strength. The invariants are next used as a "magnifying glass" to search for irregularities and evidence of stochastic behavior. It is found that within the model employed, the beam-beam interaction at its contemplated strengths shows no evidence of producing particle loss in ISABELLE.

1. Introduction

The beam-beam interaction for ISABELLE, in the weak beam-strong beam model of Herra, Month, and Peierls⁽¹⁾, can be studied by the method of Transfer Maps^(2,3). In this approach, the transfer map M for passage of a particle in the weak beam through its storage ring followed by passage through the strong beam is given by the product⁽⁴⁾

$$M = \exp(F_2)\exp(F_b). \quad (1.1)$$

Here F_2 is the Lie operator associated with the quadratic polynomial

$$f_2 = -\pi w(z_1^2 + z_2^2), \quad (1.2)$$

where

$$z_1 = q, \quad z_2 = p. \quad (1.3)$$

The Lie transformation $\exp(F_2)$ describes passage through the weak-beam storage ring with tune w . The quantity F_b is the Lie operator associated with the function

$$f_b(z) = \int_0^{z_1} u(q) dq, \quad (1.4)$$

where u is proportional to the electrostatic force exerted by the strong beam,

$$u(q) = 4\pi D/\sqrt{3} \int_0^{q\sqrt{3}} dt e^{-t^2}. \quad (1.5)$$

The Lie transformation $\exp(F_b)$ describes passage of a particle in the weak beam through the strong beam. The effect of the strong beam is normalized in such a way that the beam-beam interaction depresses the tune of the weak beam, for infinitesimal betatron oscillations, by an amount D when D is small.

Introduce polar coordinates in phase space by using action-angle variables a, ϕ defined by the relations

$$q = z_1 = (2a)^{1/2} \sin \phi \quad (1.6a)$$

$$p = z_2 = (2a)^{1/2} \cos \phi. \quad (1.6b)$$

In these variables f_b has the Fourier expansion

$$f_b = \sum_{-\infty}^{\infty} c_n(a) \exp(i2n\phi). \quad (1.7)$$

The coefficients c_n will be computed explicitly in the next section.

Suppose the tune w of the weak-beam storage ring is not near a resonant value. Then, using the Campbell-Baker-Hausdorff formula^(2,3,4), it can be shown that the quantity h given by the expression

$$h = -2\pi w a + c_0(a) + 2 \sum_1^{\infty} c_n(a) \left[\frac{2n\pi w}{\sin(2n\pi w)} \right] \cos[2n(\phi + \pi w)] \quad (1.8)$$

generalizes the Courant-Snyder invariant through first order in the beam-beam interaction strength D .

In the case of resonant or near-resonant tunes, it is necessary to work with powers of M . Consider an m 'th order resonance. Then tunes near an m 'th order resonance value can be written in the form

$$w = k/m + \delta \quad (1.9)$$

where δ measures departure from exact resonance. Now consider the iterated transfer map M^m . Again, using the Campbell-Baker-Hausdorff formula, it can be shown that the quantity h_r given by the expression

$$h_r = -2\pi\delta a + c_0(a) + 2 \sum_1^{\infty} c_n(a) \left[\frac{2n\pi\delta}{\sin(2n\pi w)} \right] \cos[2n(\phi + \pi w)] \quad (1.10)$$

generalizes the Courant-Snyder invariant through first order in D for the map M^m .

The purpose of this paper is to use the non-resonant and resonant invariants, h and h_r , as a kind of "magnifying glass" to study numerical results in fine detail. Section 2 derives expansions for the coefficients $c_n(a)$ suitable for numerical use. Section 3 shows that h and h_r do indeed generalize the Courant-Snyder invariant through order D in the beam-beam interaction strength. Section 4 illustrates how magnifying glass methods have been applied to problems in other areas of physics to detect the presence of small-scale homoclinic oscillations and associated stochastic behavior. A final section applies these methods to the beam-beam interaction, and demonstrates that within the model employed, the beam-beam interaction at its contemplated strengths shows no evidence of producing particle loss in ISABELLE.

2. Evaluation of Expansion Coefficients

The purpose of this section is to compute the expansion coefficients $c_n(a)$. We begin by observing that the function $\exp(-t^2)$ appearing in the integrand of equation (1.5) can be expanded in a Taylor series having an infinite radius of convergence. Therefore, this expansion can be integrated term by term to provide an expansion for $u(q)$. Similarly, the expansion for $u(q)$ can be inserted into equation (1.4) and integrated term by term to provide an expansion for f_b . Carrying out these substitutions and integrations, we find the result

$$f_b(z) = 4\pi D \sum_{\ell=0}^{\infty} (-3)^\ell z_1^{2\ell+2} / [(\ell!)(2\ell+2)(2\ell+1)]. \quad (2.1)$$

Next, substitute into the expansion (2.1) the expression (1.6a) for the quantity z_1 . Making this substitution gives the result

$$f_b = 4\pi D \sum_{\ell=0}^{\infty} (-3)^\ell (2a)^{\ell+1} (\sin \phi)^{2\ell+2} / [(\ell!)(2\ell+2)(2\ell+1)]. \quad (2.2)$$

Our task, now, is to rearrange the series (2.2) into a Fourier series of the form (1.7).

By employing the binomial formula, we find the result

$$\begin{aligned} (\sin \phi)^{2\ell+2} &= (e^{i\phi} - e^{-i\phi})^{2\ell+2} / (2i)^{2\ell+2} = \\ &= [1/(2i)]^{2\ell+2} \sum_{r=0}^{2\ell+2} (-1)^r \binom{2\ell+2}{r} e^{2i(\ell+1-r)\phi}. \end{aligned} \quad (2.3)$$

Introduce a new summation variable n defined by the relation

$$n = \ell+1-r. \quad (2.4)$$

With this substitution, the expansion (2.3) takes the more convenient form

$$(\sin \phi)^{2\ell+2} = [1/(2i)]^{2\ell+2} \sum_{n=-(\ell+1)}^{\ell+1} (-1)^{\ell-n+1} \binom{2\ell+2}{\ell-n+1} e^{2in\phi}. \quad (2.5)$$

To proceed further, we insert the expression (2.5) into the expansion (2.2) to find the result

$$\begin{aligned} f_b &= 2\pi D \sum_{\ell=0}^{\infty} (-3/2)^\ell (a)^{\ell+1} / [\ell!(2\ell+2)(2\ell+1)] \sum_{n=-(\ell+1)}^{\ell+1} (-1)^n \\ &\quad \times \binom{2\ell+2}{\ell-n+1} e^{2in\phi}. \end{aligned} \quad (2.6)$$

The expansion coefficients $c_n(a)$ can now be read off from equation (2.6) simply by exchanging orders of summation. We find the results

$$c_0(a) = 2\pi Da \sum_{\ell=0}^{\infty} (-3a/2)^{\ell} (2\ell!) / \{(\ell!) [(\ell+1)!]^2\} \quad (2.7)$$

and

$$c_n(a) = -(4\pi/3)D (3a/2)^n \sum_{m=0}^{\infty} (-3a/2)^m (2n+2m-2)! / [m!(n+m-1)!(m+2n)!] \\ \text{when } n > 0. \quad (2.8)$$

Here use has been made of the relation

$$\binom{s}{r} = s! / [(s-r)!r!], \quad (2.9)$$

and some rearrangement of the summation index has been made in writing (2.8).

In order to do numerical work, it is necessary to truncate the series (1.8), (1.10), (2.7), and (2.8) at some point. Explicit evaluation shows that the coefficients in these series (the terms not involving D or powers of a) are less than 10^{-9} provided that $\ell > 25$ in (2.7), and $n > 15$ or $m+n > 25$ in equation (2.8). Also, the normalization employed for q , p , and a in setting up the beam-beam problem is such that the value $a = 1/2$ corresponds to the outside of the beam. Therefore, even in the extreme case $a = 1$, which is well outside the beam, at least eight significant figure accuracy is obtained by restricting sums in ℓ , m and n to the range $\ell \leq 25$, $n \leq 15$, $m+n \leq 25$. This level of accuracy is certainly sufficient, for the quantities h and h_r as given by equations (1.8) and (1.10) omit all terms of order D^2 , and $D^2 \sim 10^{-4}$ for cases of practical interest.

3. Numerical Behavior of h and h_r

The purpose of this section is to illustrate numerically the claim that the quantities h and h_r act as generalized Courant-Snyder invariants. Our procedure is to iterate numerically the transfer map (1.1) a large number of times for a variety of initial conditions, and to then verify that h and h_r remain approximately constant as the iterations proceed.

At this point, it is necessary to remark on the numerical method used to evaluate the integral (1.5) since the beam-beam portion of the transfer map involves the transformation

$$\begin{aligned} q'' &= q' \\ p'' &= p' + u(q') \end{aligned} \quad (3.1)$$

at each iteration of the map.⁽³⁾ The integral (1.5) can be evaluated in terms of the error function with the result

$$u(q) = (4\pi D/\sqrt{3})(\pi/\sqrt{2}) \operatorname{erf}(q\sqrt{3}). \quad (3.2)$$

The problem is to find a good approximation to the error function which can be readily evaluated over and over again by a computer. We have found it convenient to use the approximation⁽⁵⁾

$$\operatorname{erf}(x) = 0, \text{ for } x = 0 \quad (3.3a)$$

$$\operatorname{erf}(x) = 1 - \exp(-x^2) \sum_{n=1}^5 b_n t^n, \text{ for } x > 0 \quad (3.3b)$$

$$\operatorname{erf}(x) = -\operatorname{erf}(-x), \text{ for } x < 0 \quad (3.3c)$$

where

$$t = 1/(1 + b_6 x) \quad (3.3d)$$

and the constants b_1 through b_6 have the values

$$\begin{aligned} b_1 &= .254829592, \quad b_2 = (-.284496736) \\ b_3 &= (1.421413741), \quad b_4 = -1.453152027 \\ b_5 &= 1.061405429, \quad b_6 = .3275911 \end{aligned} \quad (3.3e)$$

The above approximation is accurate to within an error less than or equal to 1.5×10^{-7} . This error is certainly far smaller than the expected accuracy of the model, because there is no reason to believe that the charge distribution in the strong beam is exactly Gaussian as (1.5) and (3.2) would imply.

With this explanation, we turn first to a study of the behavior of h in the nonresonant case. Figure 1 shows typical phase-space plots obtained by iterating the transfer map numerically for the case of a nonresonant tune. Correspondingly, figure 2 shows plots of the two quantities $(-2\pi wa)$ and h as a function of $(\phi/2\pi)$ for each of the three curves in figure 1. It is evident that the quantity $(-2\pi wa)$, which is proportional to the ordinary Courant-Snyder invariant, can, in some cases, show substantial variations. By contrast, the quantity h is more nearly constant in all cases.

To exhibit the behavior of h in more detail, figure 3 shows in expanded scale the variations of h corresponding to the case of curve C in figure 1. Observe that h has an average value of ~ 5.665 and variations of about ± 0.053 above and below the average.

Presumably these variations come from the order D^2 terms which have been omitted in the expression for h . Now suppose that the value of D were halved from the value $D = .01$ which was used to generate figures 1 through 3. Then the variations in h , if they are proportional to D^2 , should be reduced by a factor of four. Figure 4 illustrates that this is indeed the case. It shows the variations in h for a phase space plot having a beam-beam interaction strength of $D = .005$, but otherwise having the same initial conditions and tune as curve C of figure 1. Now h has an average value of ~ 5.5405 with variations of about ± 0.0125 from the average. Note that there is indeed a reduction in the variation by about a factor of four.

We turn next to a briefer study of a resonant case. Figure 5 shows a sample of phase space-plots for the resonant case of a nearly half-integer tune. Note that the plots now are far from the near-circular shapes pertaining to the non-resonant case of figure 1. Correspondingly, figure 6 shows values of h_r plotted as functions of q for each of the curves in figure 5. Observe that the quantity h_r remains remarkably constant. Thus, the curves of figure 5 are very nearly level lines of h_r , and the major features of figure 5 can be predicted by studying

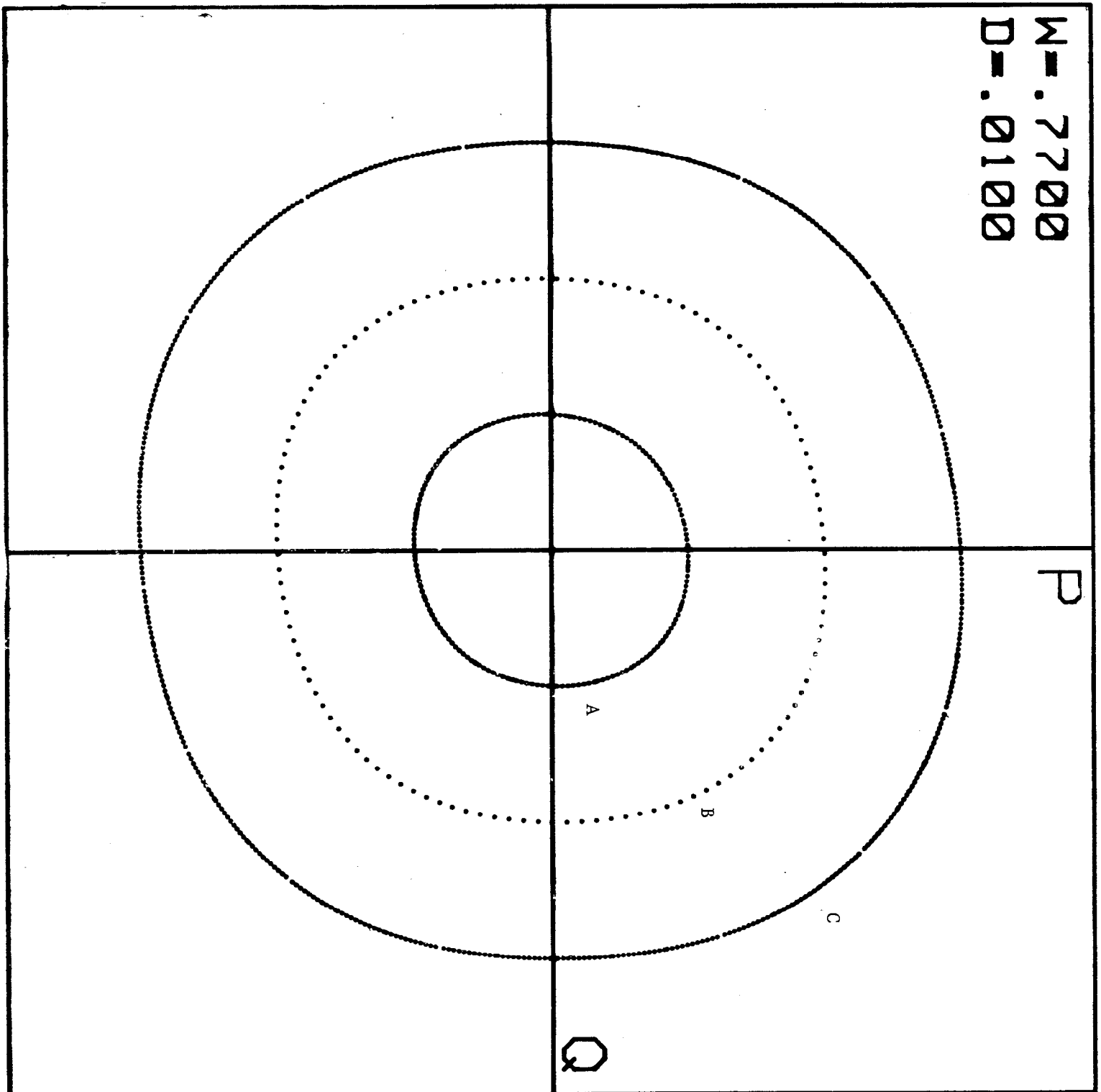


Figure 1. Phase-space plot generated by successive iterations of the transfer map M for various initial conditions. The coordinates extend from -2 to 2 , and are normalized in such a way that the beam will be within the unit circle under actual operating conditions. The tune is $.77$, and the beam-beam interaction strength is 10^{-2} .

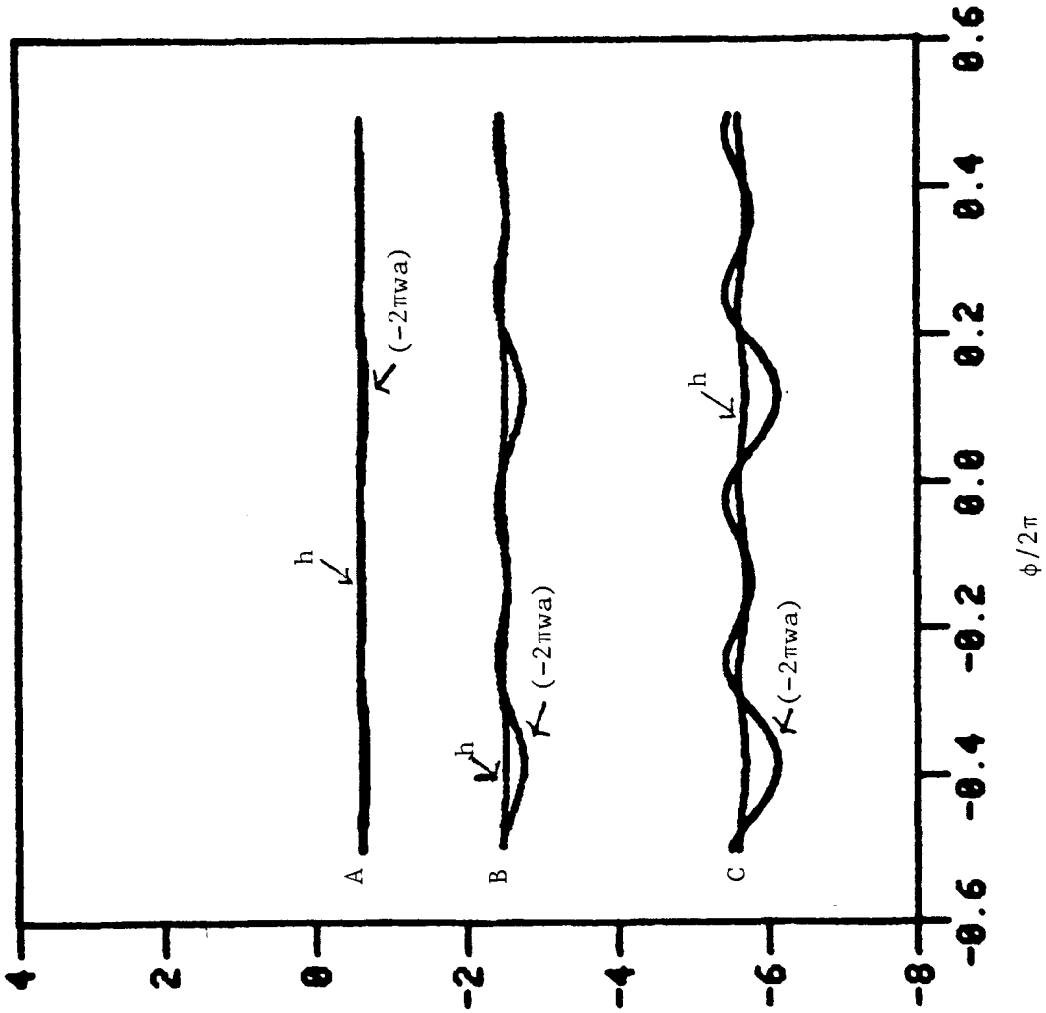
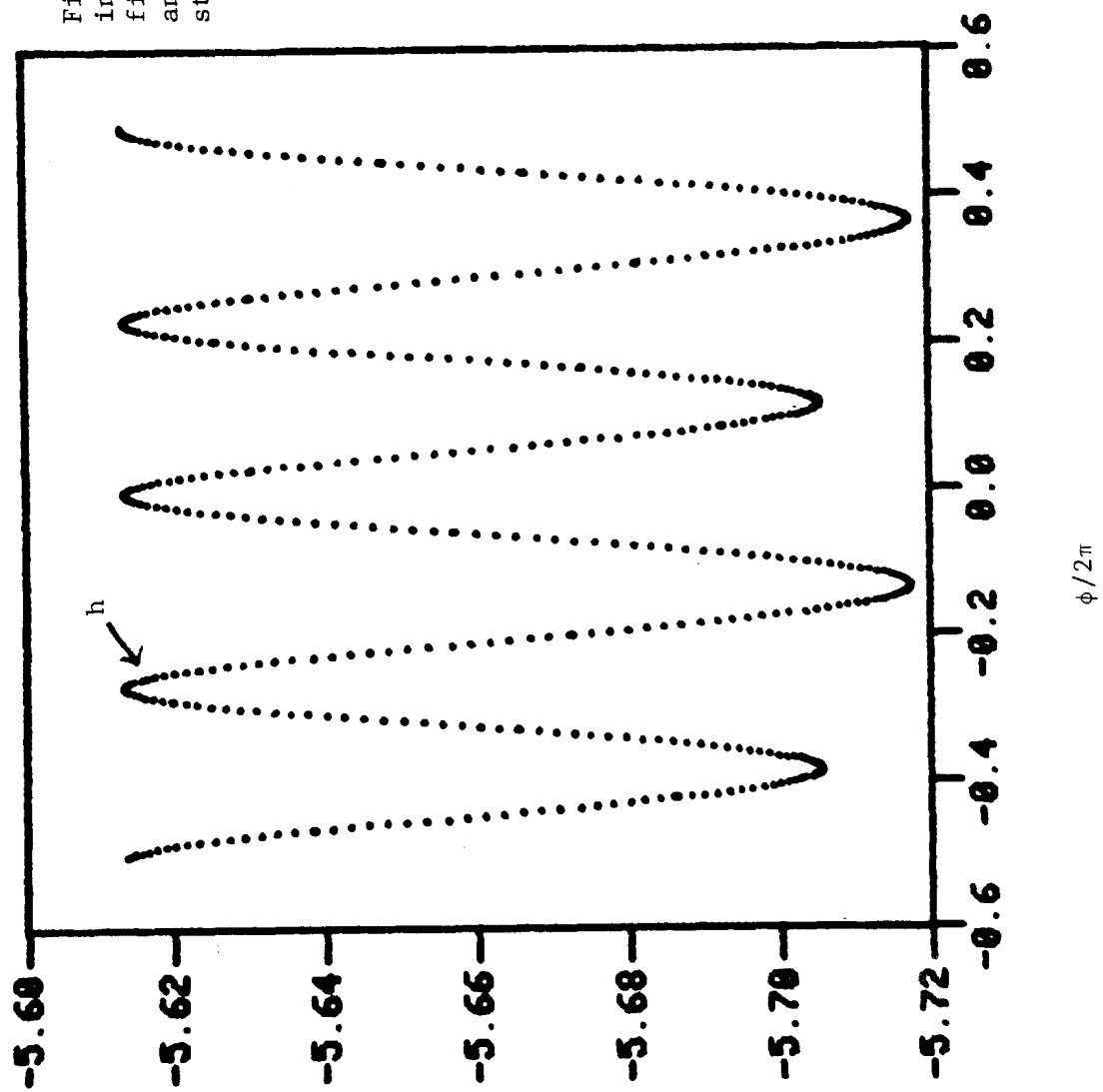


Figure 2. Plots of the quantities $(-2\pi wa)$ and h for each of the three cases of figure 1. Observe that h is more nearly constant than the ordinary Courant-Snyder invariant $(-2\pi wa)$. Observe also that the larger variations in the ordinary Courant-Snyder invariant occur in the cases with the larger betatron amplitudes, i.e., the cases where nonlinearities are more important.

Figure 3. Variations in h shown in expanded scale for case C of figures 1 and 2. The tune is .77 and the beam-beam interaction strength is 10^{-2} .



**NORMAL EXIT. EXECUTION TIME:
6500 MILLISECONDS.**

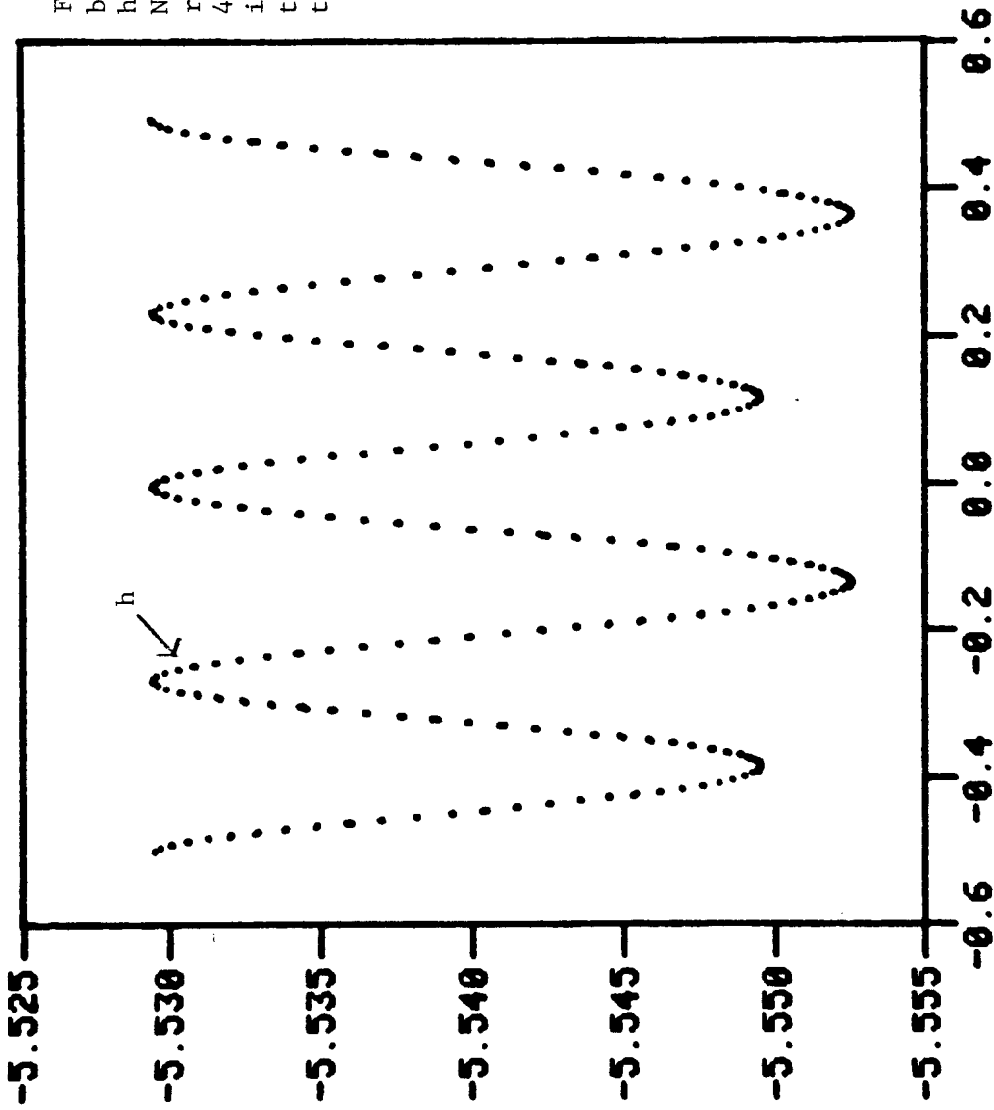


Figure 4. Variations in h when the beam-beam interaction strength is halved from its value in figure 3. Note that the variations in h are reduced by approximately a factor of 4, thereby indicating that variations in h are caused primarily by omitted terms proportional to the square of the beam-beam interaction strength.

$\phi/2\pi$

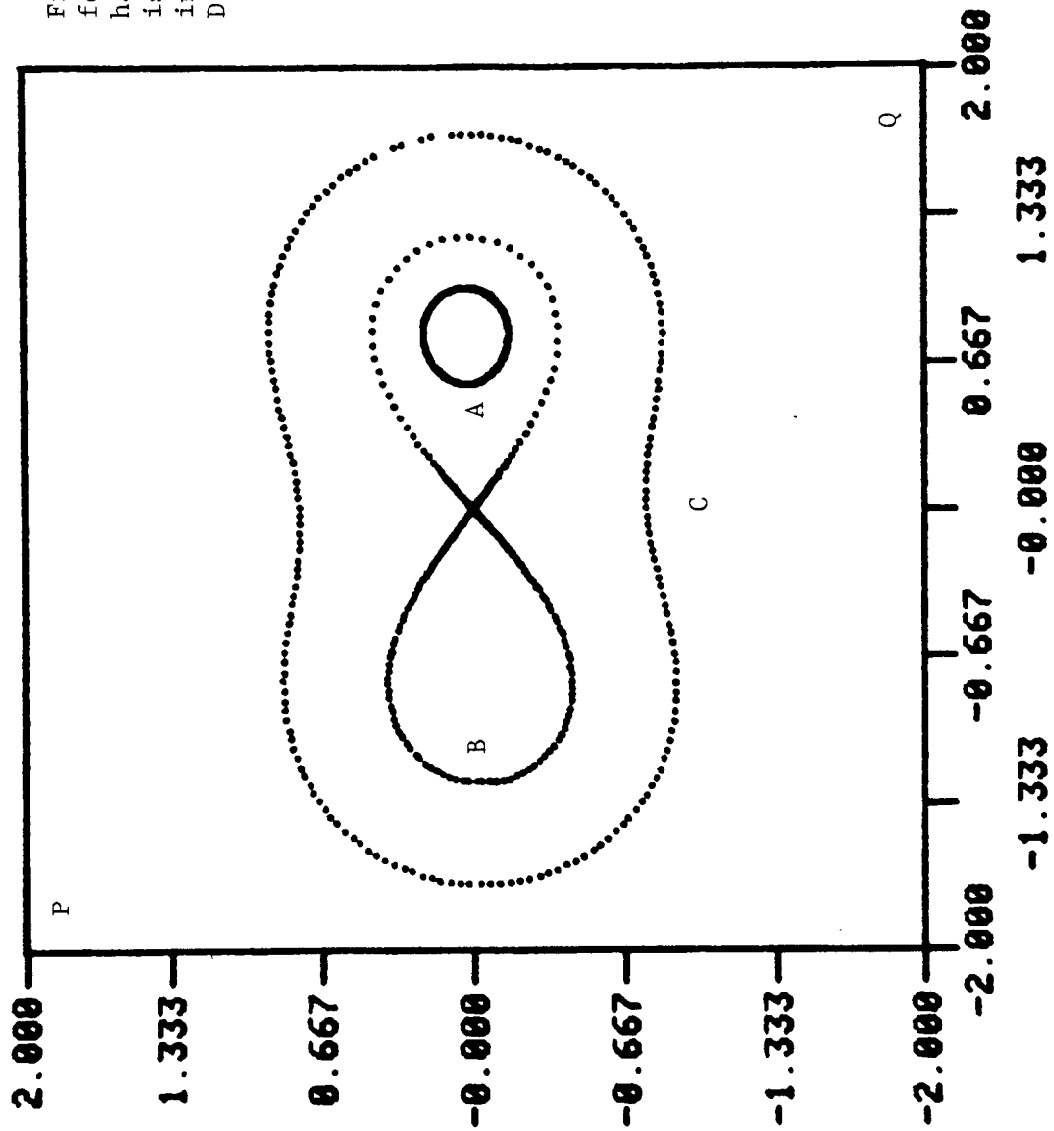
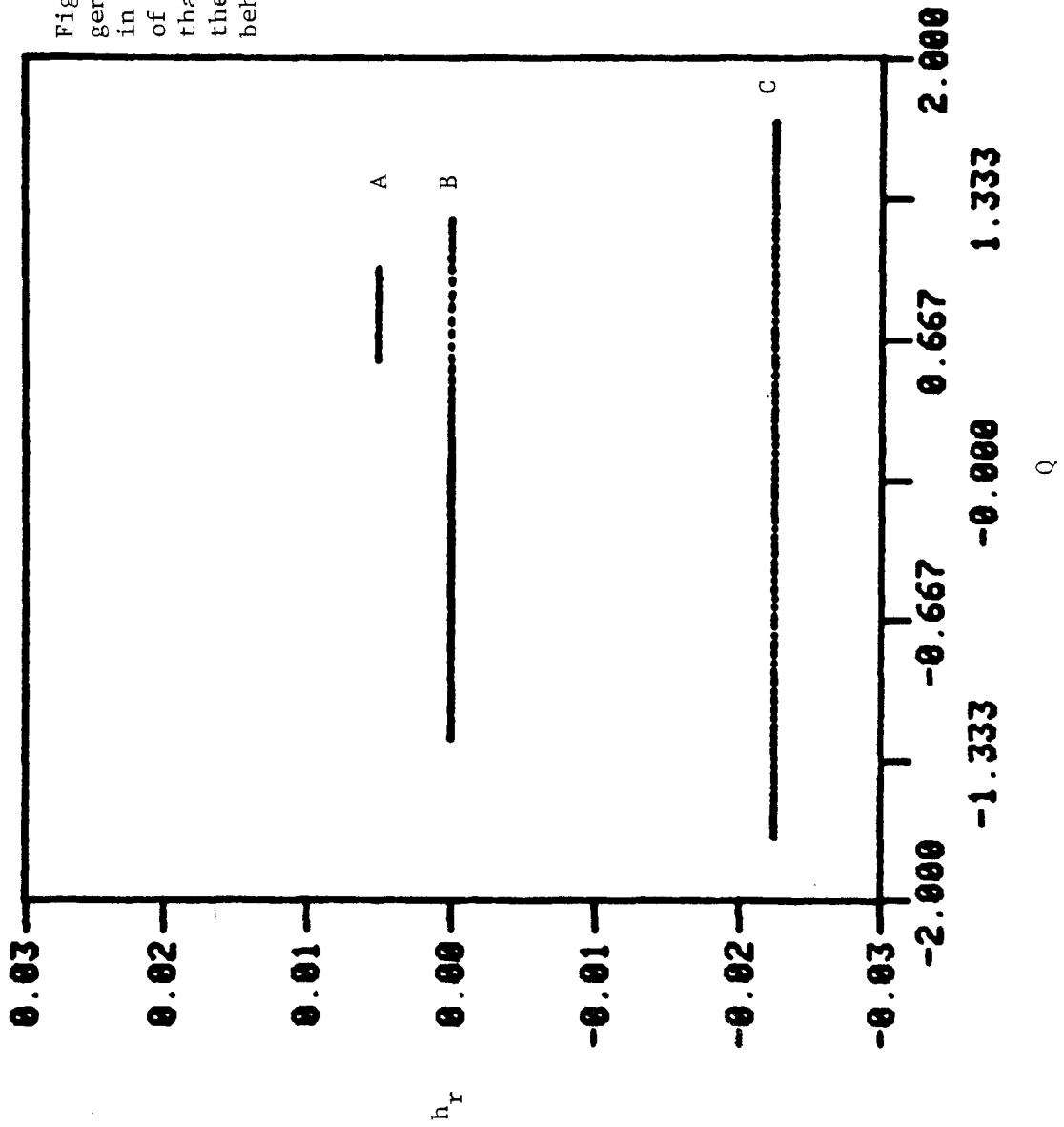


Figure 5. Sample phase-space plots for the resonant case of a near half-integer tune. The tune value is $w = .5122$, and the beam-beam interaction strength is again $D = 10^{-2}$.

Figure 6. Values of h_r , the generalized Courant-Snyder invariant in the resonant case, plotted for each of the three cases of figure 5. Note that h_r is remarkably constant despite the large distortions from circular behavior evident in figure 5.



the level lines of h_r and the points at which the gradient of h_r is zero. These latter points correspond to fixed points of M , and give the initial conditions for periodic orbits.

4. Magnifying Glass Methods

A standard procedure for studying the long-time behavior of a dynamical system is to make phase-space plots of the motion, and to then examine these plots for evidence of stochastic or unstable behavior. This procedure has the virtue of giving a good qualitative picture of the motion. However, it has the disadvantage that much of the resolution of the graph is devoted to displaying regular features of the motion. Consequently, small-scale irregularities in the motion may not be readily apparent if their scale is much smaller than the scale required to display the regular features of the motion.

This difficulty can be overcome by making additional plots of some quantity which takes into account the regular features of the motion. This quantity should have the property that it is expected to be nearly constant if the motion is regular. Departure from constancy could then reflect irregularities in the motion, and the full scale of the plot could then be devoted to displaying departures from constancy.

Such quantities in the case of the beam-beam interaction could be the generalized Courant-Snyder invariants h and h_r . The purpose of this section is to illustrate briefly how these methods, which will be called "magnifying glass" methods, have been applied to two other problems: the study of a simple mapping and the study of the Van Allen radiation. The section after this will apply the same methods to the beam-beam interaction.

We begin with a study of the simplest nontrivial canonical mapping, called a quadratic Cremona map, given by the relations⁽⁶⁾

$$\begin{aligned} x' &= \lambda [x + (x-y)^2] \\ y' &= (1/\lambda) [y + (x-y)^2] . \end{aligned} \tag{4.1}$$

Here λ is some fixed parameter, and the properties of the map are to be studied for various values of λ .

It is readily verified that this mapping has two fixed points. One of these fixed points is the origin. This fixed point is evidently hyperbolically unstable for real positive λ , and hence we write its coordinates in the form

$$\begin{aligned}x^h &= 0 \\y^h &= 0.\end{aligned}\tag{4.2}$$

The other fixed point is also readily found. Its location is given by the equation

$$\begin{aligned}x^e &= -\lambda(\lambda-1)/(\lambda+1)^2 \\y^e &= (\lambda-1)/(\lambda+1)^2\end{aligned}\tag{4.3}$$

This fixed point is elliptically stable, for certain ranges of the parameter λ , as the notation is meant to suggest. Indeed, if the mapping (4.1) is expanded about the fixed point (4.3), it can be shown to be equivalent to the mapping associated with a storage ring having a short sextupole insertion.⁽²⁾ The tune of this ring is given by the relation

$$2\cos(2\pi\nu) = -(\lambda^2 - 4\lambda + 1)/\lambda.\tag{4.4}$$

It is easily verified that the fixed point (4.3) is elliptically stable provided λ lies in the range

$$1 < \lambda < (3 + \sqrt{8}).\tag{4.5}$$

Associated with every hyperbolic fixed point is a stable and unstable manifold. If these manifolds, when followed away from the fixed point, intersect each other with a nonzero angle at some other point, this point is called a homoclinic point. If one such homoclinic intersection occurs, then it can be shown that the two manifolds must go into wild oscillation about each other. These oscillations result in the irregular behavior of trajectories over at least a portion of phase space⁽⁷⁾. Figures 7, 8 and 9 illustrate a homoclinic intersection and the ensuing oscillations when $\lambda = 3$ for the case of the quadratic Cremona map.

The size of the angle of intersection of the stable and unstable manifolds at the homoclinic point, and correspondingly the amplitude of the ensuing oscillation, depends very sensitively on the size of the parameter λ . Figure 10 shows that the homoclinic angle becomes very small as λ approaches the value 1. In the range of very small angle, its size was inferred by studying the behavior of an invariant of the map. This invariant was found by employing the Campbell-Baker-Hausdorff formula in a manner similar to that used to find the generalized Courant-Snyder invariants.⁽⁸⁾

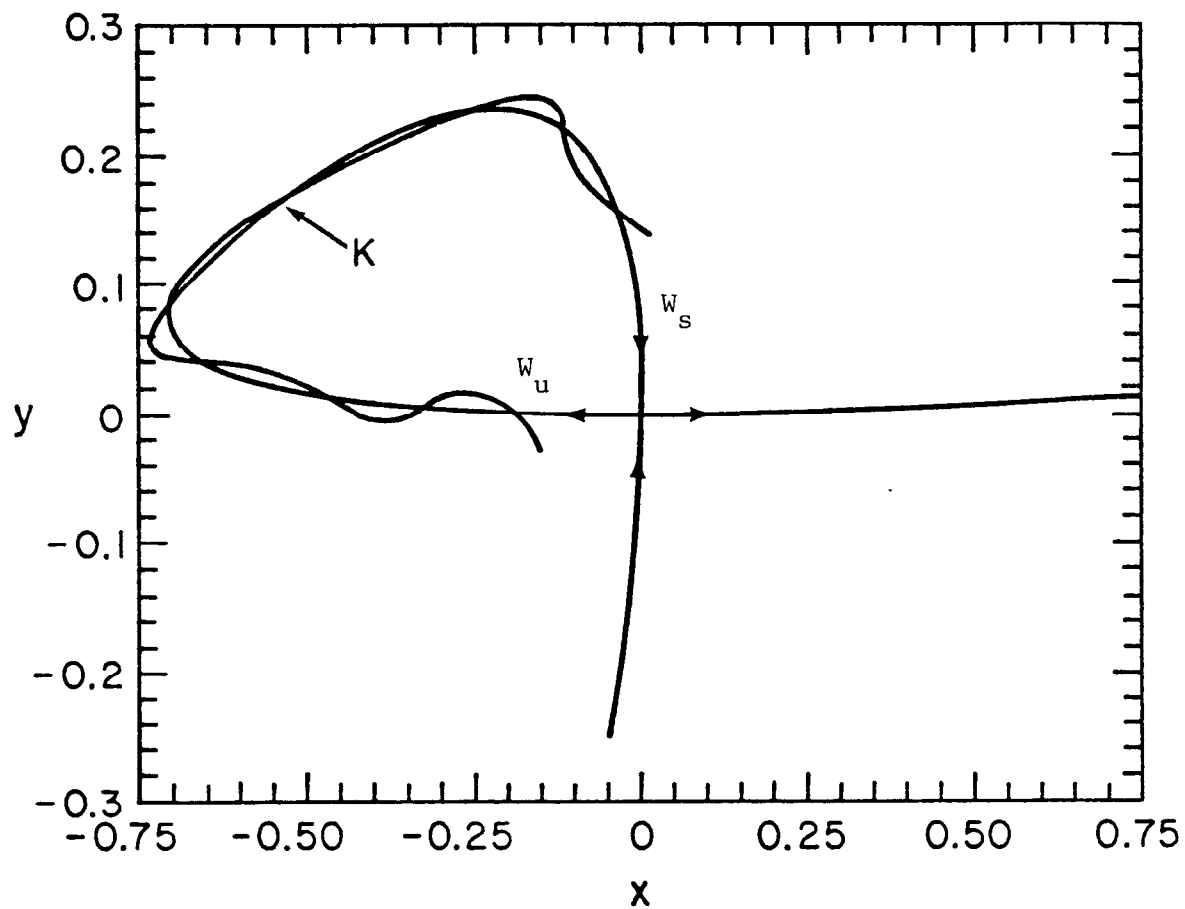


Figure 7. Behavior of the stable and unstable manifolds, W_s and W_u , for the hyperbolic fixed point of the quadratic Cremona map in the case $\lambda = 3$. Note the homoclinic intersection at the point K .

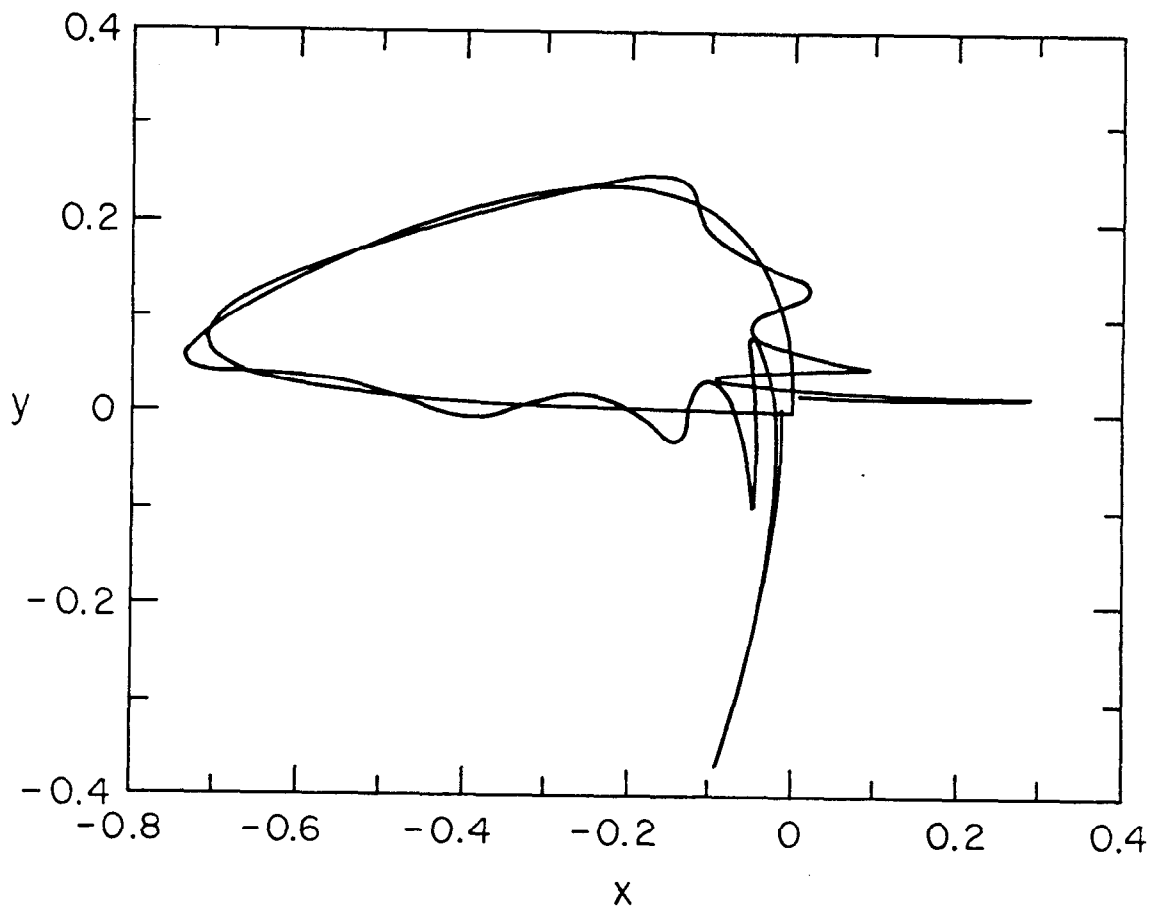


Figure 8, Continued homoclinic oscillations of the stable and unstable manifolds about each other. Note that the amplitude of oscillation grows in the vicinity of the hyperbolic fixed point.

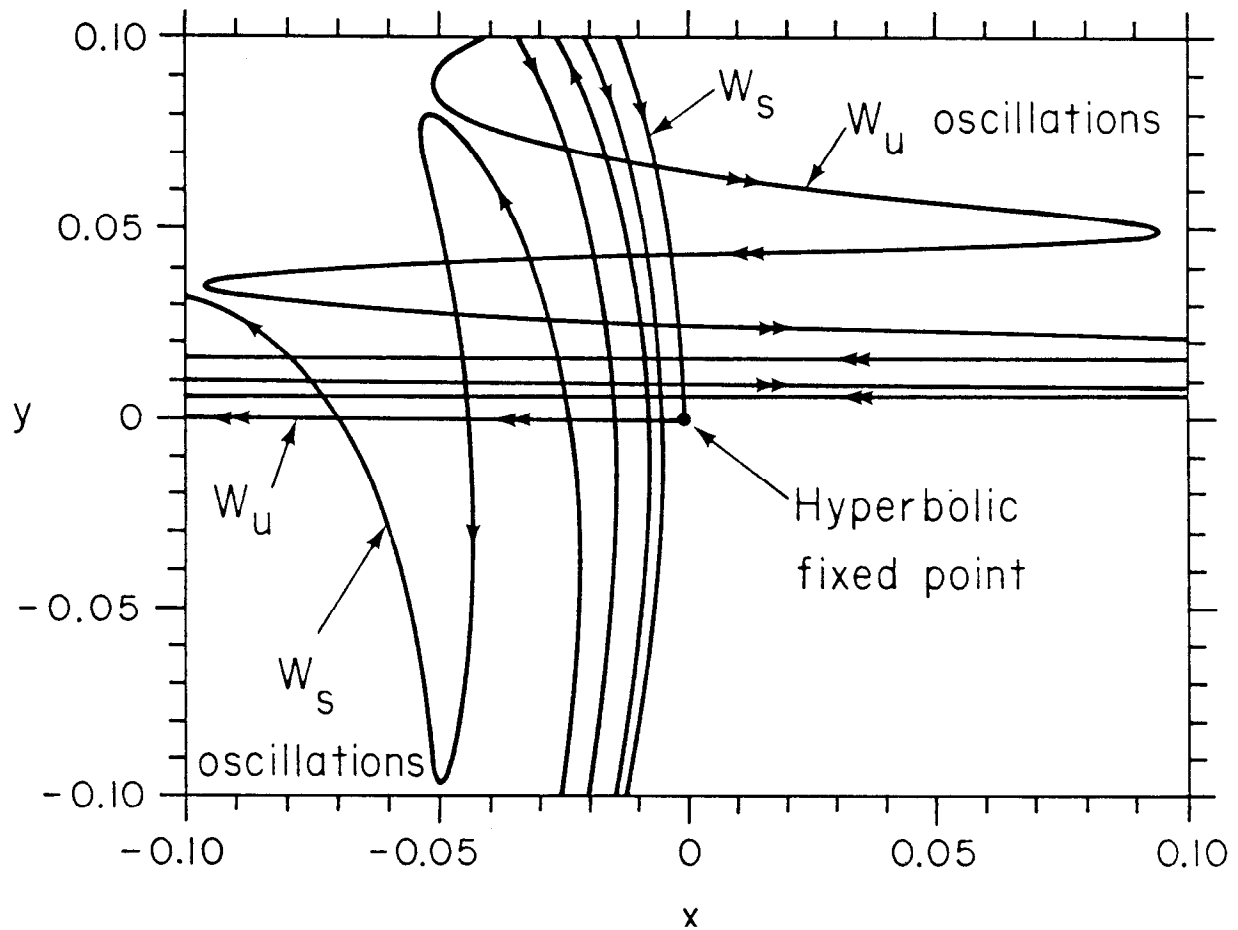
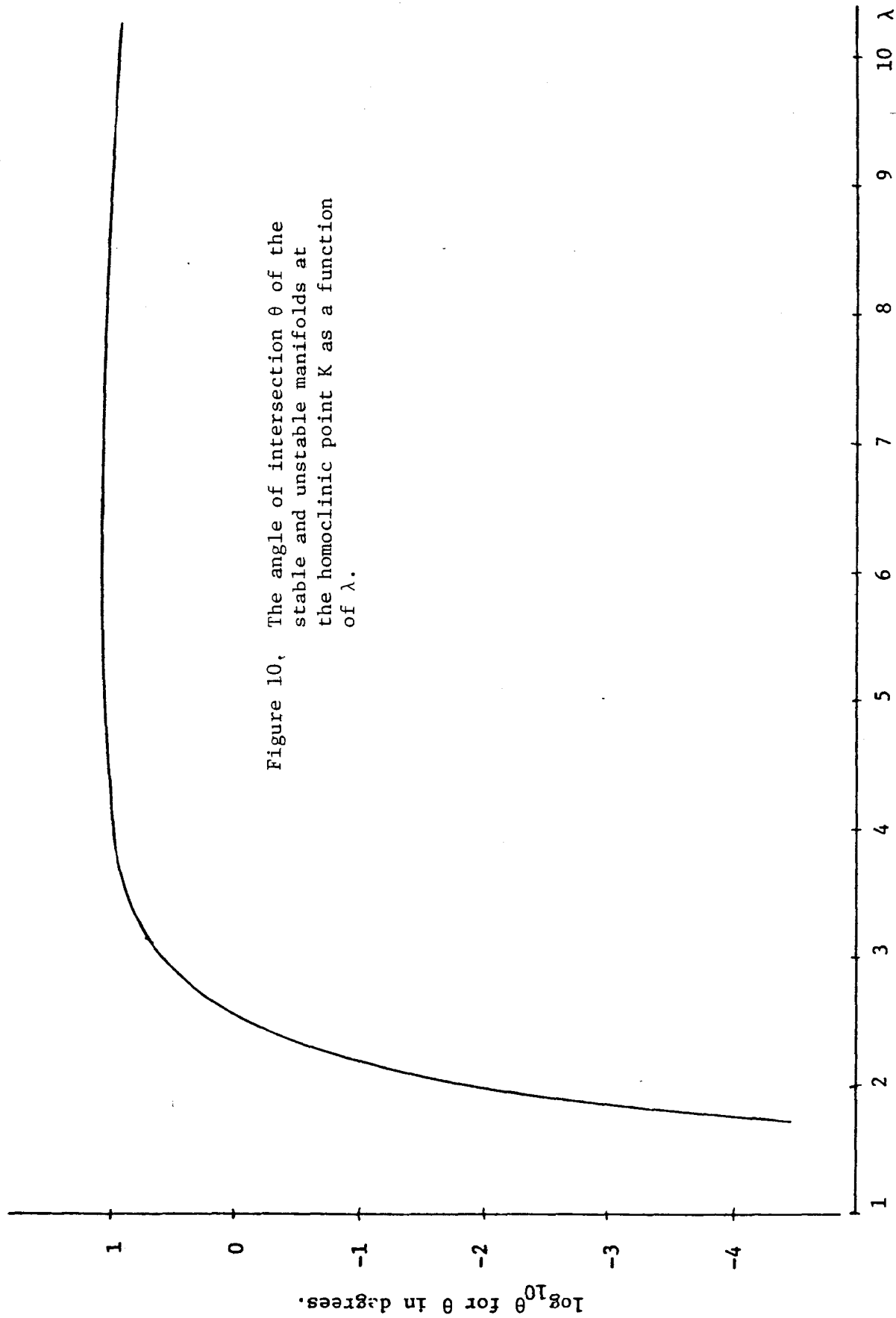


Figure 9. A continuation of figure 10 near the origin showing the formation of a grid of intersecting lines. The spacing of the grid becomes finer and finer as it approaches the hyperbolic fixed point. Each grid intersection is a homoclinic point. The result of all these intersections is an ever denser cloud of homoclinic points which has the hyperbolic fixed point as a limit point.



Because the homoclinic angle varies so rapidly with λ , the nature of phase-space plots appears to change abruptly as λ is varied. Thus, many authors speak of a threshold for stochastic behavior. In reality, at least for the map (4.1), there is no threshold. Homoclinic oscillations are always present. However, unless λ is large, the amplitude of these oscillations is too small to be seen in ordinary phase-space plots.

A second problem for which magnifying glass methods have proved useful is that of analyzing the motion of particles in the Van Allen radiation⁽⁶⁾. In simplest approximation, this problem is idealized to that of studying the so-called Stormer problem, the problem of determining the motion of a charged particle in a dipole magnetic field. By the use of a Poincare surface of section, the Stormer problem can also be reduced to the study of a certain map M of a two-dimensional phase space onto itself. And, as in the case of storage rings, the real problem is to determine the behavior of M^n for large n .

Figure 11 displays schematically a hyperbolic fixed point for the Stormer map and a conceivably possible behavior for the stable and unstable manifolds in which there are two postulated homoclinic intersections. Figure 12 shows actual results obtained by numerical integration. Evidently, within the resolution provided by ordinary plotting, there appears to be no sign of homoclinic oscillation, and the postulated homoclinic angles are very small, and could well be nonexistent.

In the case of the Stormer problem, by using Lie transformation and normal form procedures, it is possible to find a formal power series for an integral of motion⁽⁹⁾. This series, when truncated, can be used to account for most of the regular features of the motion as exhibited by figure 12. Thus, this truncated series can be used to look for irregularities in the motion that are not apparent on the scale required to represent the regular motion. Figure 13 shows how this works out in practice. It displays the behavior of the truncated series near the hyperbolic point. It is now apparent that there are indeed homoclinic oscillations, and there must be a nonzero homoclinic angle. These oscillations and the homoclinic angle are just too small to be seen on an ordinary phase-space plot.

Figure 11. A hyperbolic fixed point \vec{h} for the Stormer map, and a possible behavior for the stable and unstable manifolds for which there are two homoclinic intersections.

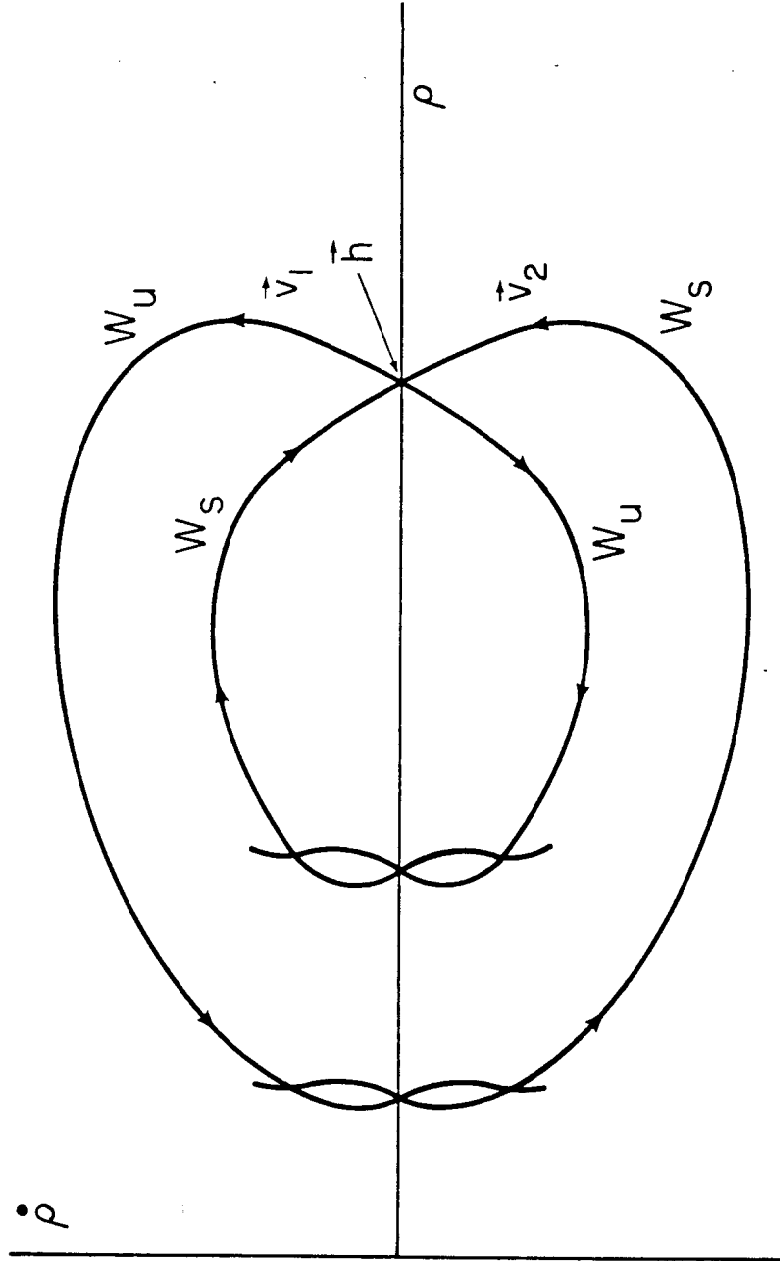


Figure 12. Actual behavior of the Stormer map near a hyperbolic fixed point as determined by numerical integration. Note that there is no visible evidence for homoclinic intersections or oscillations.

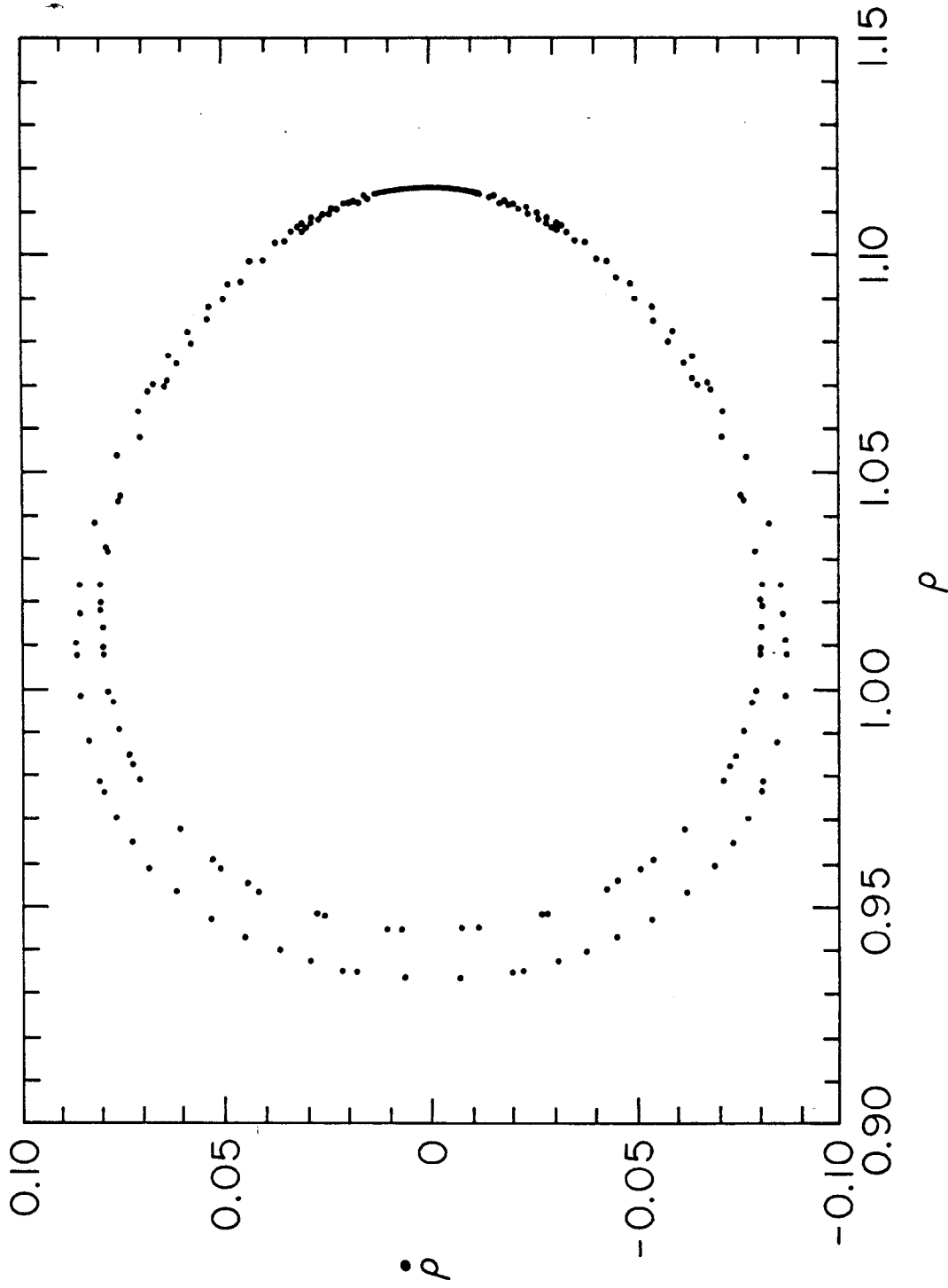
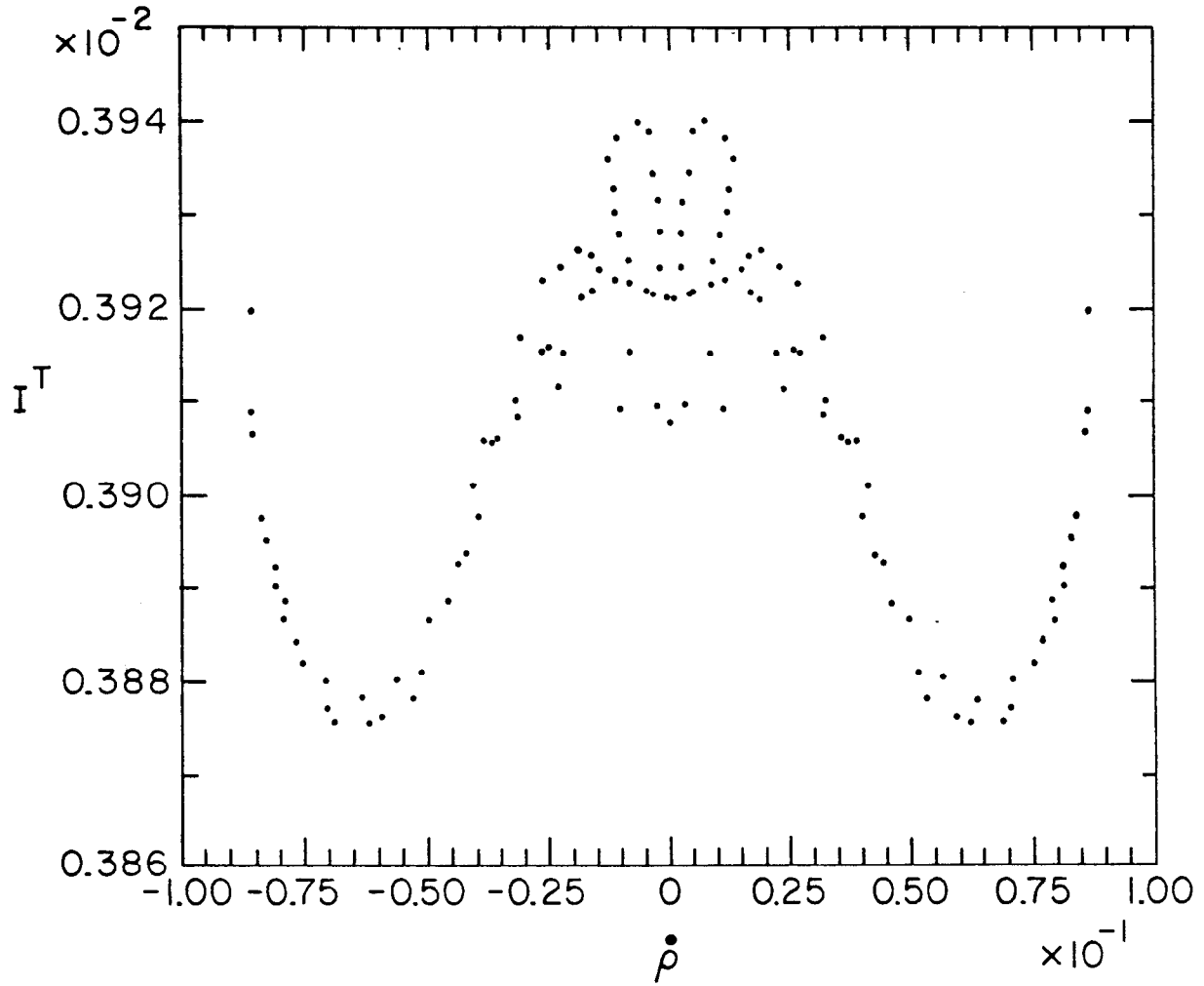


Figure 13. The points of the outer curve of figure 12 which are also near the hyperbolic fixed point are replotted here to display the truncated invariant series I^T versus $\dot{\rho}$. The presence of homoclinic oscillations near the hyperbolic fixed point ($\dot{\rho} = 0$) is now apparent.



5. Application to the Beam-Beam Interaction

The purpose of this section is to apply magnifying glass methods to the beam-beam interaction in order to search for evidence of small-scale irregularities in the motion.

We begin with the nonresonant case. Figure 14 shows a plot of h for conditions identical to those for figure 3 except that the mapping has been carried out for 100,000 iterations with every two hundredth point plotted. All calculations were carried out in double precision with an accuracy of approximately 16 significant figures. Evidently, even with the magnification provided by plotting h rather than the customary q, p variables of figure 1, there is no evidence of irregular behavior. We conclude that within the model employed, the beam-beam interaction at its contemplated strengths shows no evidence, even under magnification, of producing particle loss in ISABELLE. This conclusion is consistent with earlier conclusions based on less stringent tests⁽⁴⁾.

We turn next to a brief examination of the resonant case. Figure 15 illustrates that stochastic behavior can indeed occur, due to homoclinic oscillations, for large values of the beam-beam interaction. In the case shown, the origin is hyperbolically unstable, corresponding to a half-integer resonance, and the stable and unstable manifolds associated with this fixed point intersect in homoclinic points as illustrated schematically in figure 16. This behavior can be followed to smaller values of the beam-beam interaction providing the tune w is also suitably adjusted. It is readily apparent, with and without magnification, for the parameter pairs $(w = .80, D = .30)$, $(w = .70, D = .20)$, and $(w = .60, D = .10)$. However, when D is decreased to the value $D = .05$, and below, (for example the case $w = .55, D = .05$), homoclinic behavior is no longer visible even in plots of h_r . Thus, for example, the case of figure 5 shows no evidence of homoclinic behavior despite the hyperbolic instability of the origin. It is presumably still there, but has a scale too small to be presently seen. Perhaps if the expressions for h and h_r were calculated in more detail to provide the corrections of order D^2 , and perhaps even beyond, which is in principle possible using the Campbell-Baker-Hausdorff formula⁽³⁾, sufficient magnification might become available to again detect homoclinic oscillations. Such an effort is beyond the scope of this paper. Suffice it to say that the apparent lack of visible homoclinic oscillations, even in the hyperbolically unstable case, is further evidence for the benign nature of the beam-beam interaction at its presently contemplated strength.

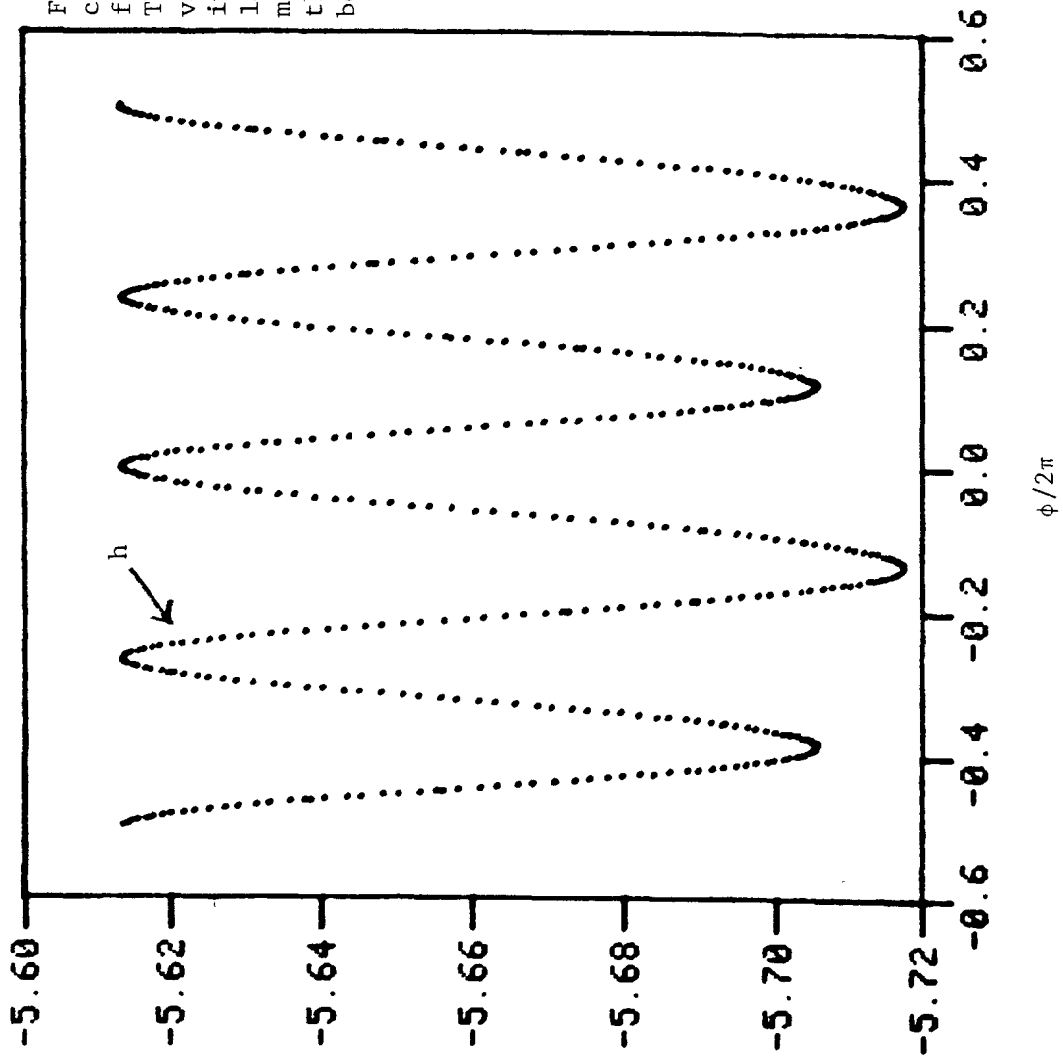


Figure 14. Variations in h over the course of 100,000 iterations. Results for only every 200'th point are plotted. The initial conditions and parameter values are the same as those for curve C in figures 1, 2, and 3. Despite the large number of iterations and the magnification provided by the use of h , there is no evidence of irregular behavior.

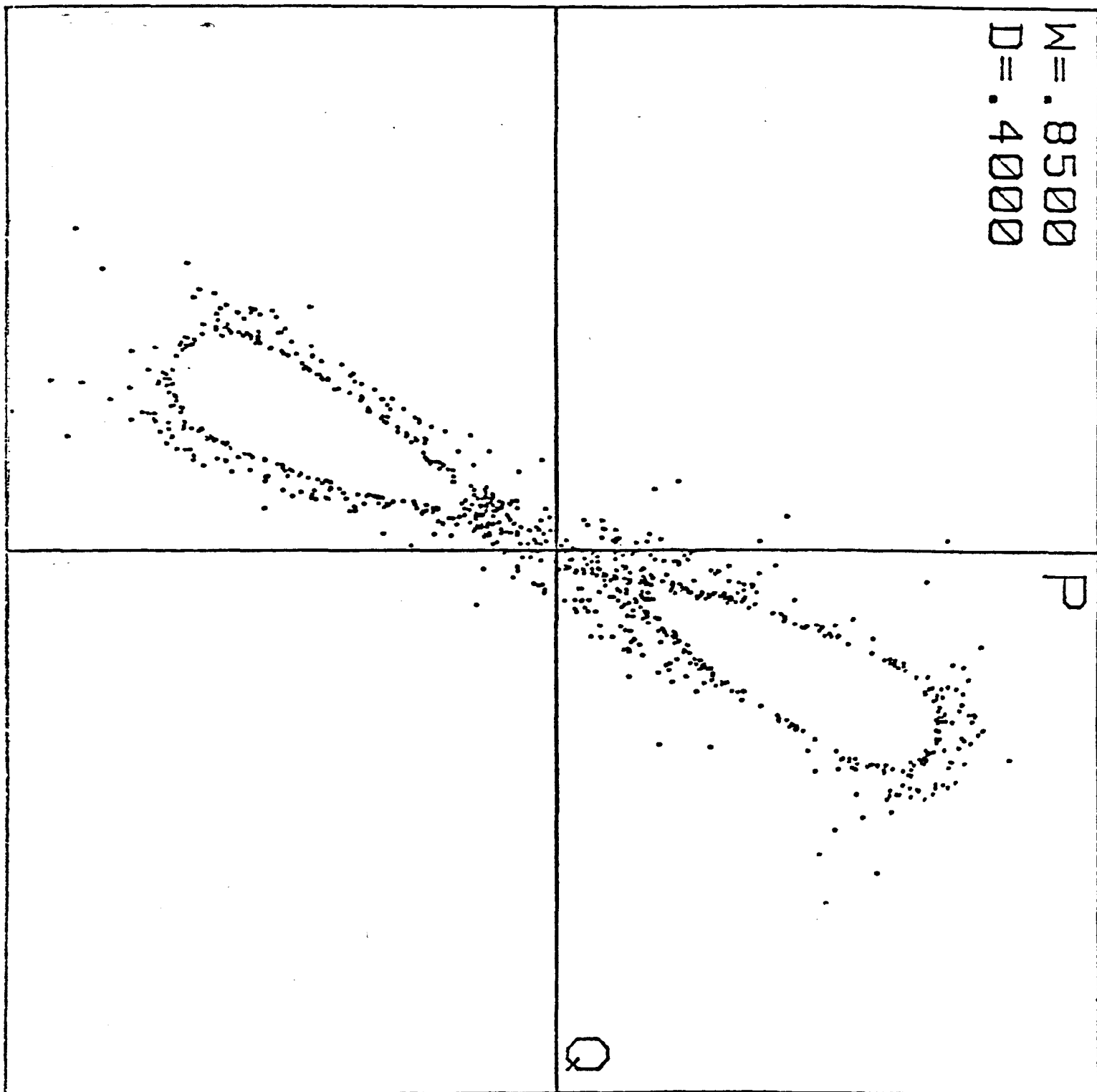


Figure 15. A phase-space plot showing stochastic behavior for a large value of the beam-beam interaction strength.

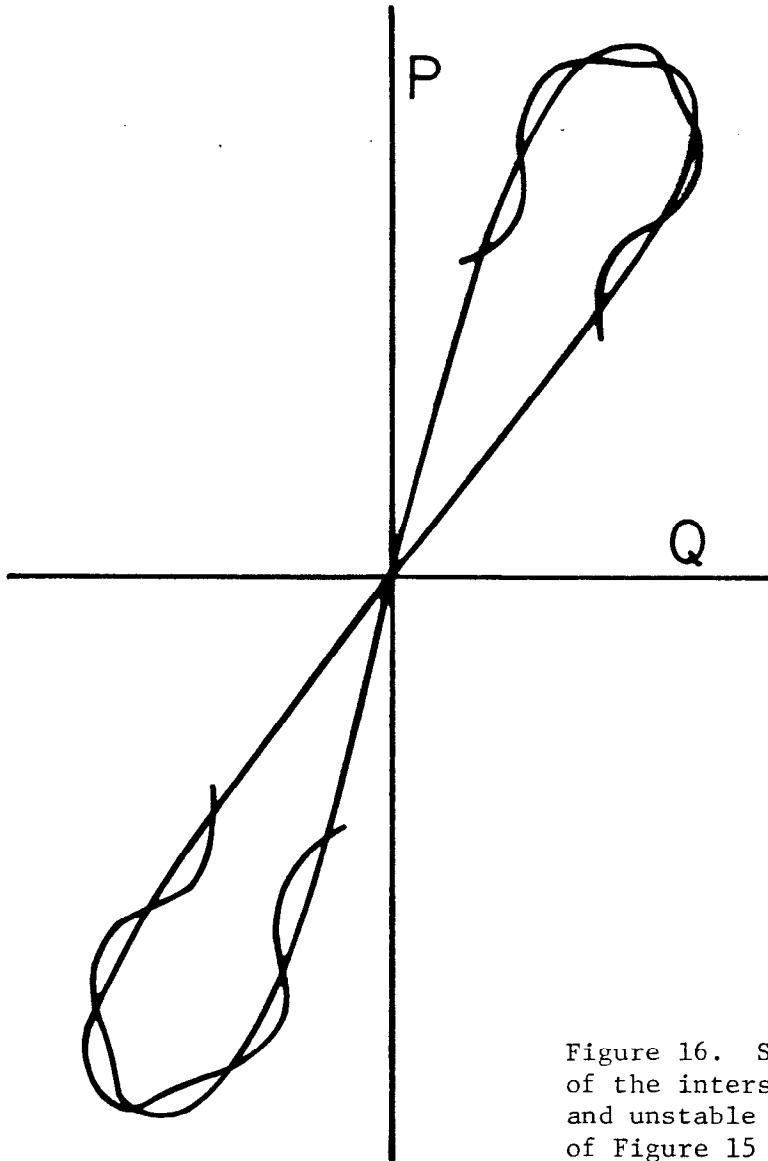


Figure 16. Schematic presentation of the intersection of the stable and unstable manifolds in the case of Figure 15 leading to stochastic behavior.

Conclusion

It has been shown in section 3 that the generalized Courant-Snyder invariants h and h_r reproduce well, for sufficiently small values of the beam-beam interaction strength D , the regular features of phase-space plots. In section 5 these invariants were used to search for evidence of small-scale irregularities in the motion. No evidence was found for beam-beam interaction strengths of physical significance. Consequently, within the model employed, the beam-beam interaction at its contemplated strengths shows no evidence, even under magnification, of producing particle loss in ISABELLE.

References

1. J.C. Herrera, M. Month, and R.F. Peierls, Simple Computer Model for the Nonlinear Beam-Beam Interaction in ISABELLE, Nonlinear Dynamics and the Beam-Beam Interaction, AIP Conference Proceedings Number 57, M. Month and J.C. Herrera, Edit., American Institute of Physics, p. 202 (1979).
2. A. Dragt, A Method of Transfer Maps for Linear and Nonlinear Beam Elements, IEEE Transactions on Nuclear Science, Vol. NS-26, No. 3, p. 3601 (June 1979).
3. A. Dragt and J. Finn, J. Math. Phys. 17, pp. 2215-2227 (1976).
4. A. Dragt, Transfer Map Approach to the Beam-Beam Interaction, Nonlinear Dynamics and the Beam-Beam Interaction, AIP Conference Proceedings Number 57, M. Month and J.C. Herrera, Edit., American Institute of Physics, p. 143, (1979). See this paper for derivations of the results quoted in section 1 of the present paper.
5. M. Abramowitz and I. Stegun, Eds., Handbook of Mathematical Functions, National Bureau of Standards Applied Mathematics Series 55 (1966).
6. A. Dragt and J. Finn, J. of Geophys. Res. 81, pp. 2327-2339 (1976).
7. J. Moser, Stable and Random Motions in Dynamical Systems, Princeton University Press, Princeton, N.J., (1973).
8. J.M. Finn, Integrals of Canonical Transformations and Normal Forms for Mirror Machine Hamiltonians, Ph.D. thesis, Univ. of Maryland, College Park, MD (1974).
9. A. Dragt and J. Finn, J. Math. Phys. 20, pp. 2649-2660 (1979).

Measures of Nonintegrability in Two-Dimensional Mappings

John M. Greene

Princeton University, Plasma Physics Laboratory

Princeton, N.J. 08544

Over the past few years I have been studying Hamiltonian systems, and particularly the simplest nontrivial example which is the area preserving mapping of a plane onto itself. Such deterministic Hamiltonian systems provide a useful model for a wide variety of phenomena. That is such common knowledge that it sounds trivial. Thus, it is good to remember that these models completely ignore both dissipation and random perturbations, and that Hamiltonian systems are so delicately balanced that the smallest non-Hamiltonian effects completely dominate the behavior after a long time. One advantage of the widespread use of Hamiltonian models is the variety of experience and points of view of the workers in this field. It has been pleasurable and profitable to learn about the beam-beam interaction in the last few months. In return, I am happy to share what I know about two-dimensional mappings.

It is outside my expertise to review the physics of the beam-beam interaction, but it is in order to provide a few paragraphs setting the context for some two-dimensional mappings. The phase space in which the beam-beam interaction takes place is multi-dimensional. Nevertheless, there may be an effective decoupling of the various degrees of freedom of a particle traversing an accelerator and interacting with another beam. The two-dimensional mappings considered here are an abstraction of the behavior of a single degree of freedom with a periodic external forcing term.

Many of the two-dimensional mappings that are useful for understanding the beam-beam interaction can be written¹

$$x_{n+1} = x_n \cos 2\pi\nu - p_n \sin 2\pi\nu$$

$$p_{n+1} = x_n \sin 2\pi\nu + p_n \cos 2\pi\nu - 8\pi k F(x_{n+1}) \quad (1)$$

Here x_n and p_n are the orbit displacement and momentum in the degree of freedom that is being studied, evaluated at a point in the orbit just after the particle has experienced a beam interaction, and (x_{n+1}, p_{n+1}) are the phase space coordinates after the next interaction. The force function, $F(x)$, is taken to be odd, so that it vanishes at zero. Then the origin, $(0,0)$, maps into itself. This represents the central periodic orbit that closes after one trip around the accelerator. Neighboring orbits exhibit betatron oscillations, which are represented by a rotation in this phase space mapping. Thus ν is the tune of the degree of freedom that is being studied. When the interaction parameter, k , vanishes, the betatron oscillations of different orbits all have the same frequency, independent of the amplitude of the oscillation, in this approximation. Thus, they contribute a rigid rotation to the mapping.

The beam-beam interaction is represented here as an impulsive force, $F(x)$, that instantaneously displaces the particle momentum without affecting its position. This paper concentrates on two of the important effects of this force. In the first place, it changes the betatron frequency of small amplitude orbits. Then the mapping is not approximately a rigid rotation, but exhibits shear, with inner orbits revolving around the central periodic orbit more slowly than the outer orbits. Secondly, this force provides a perturbation that resonates, to some degree, with every rational tune. Thus,

the beam-beam force impresses a range of rational tunes on the system, and resonates with all of them.

In the linear, rigid rotation approximation, orbits lie on concentric circles in the (x,p) plane. Under the influence of the beam-beam force, $F(x)$, several new types of orbits appear. Corresponding to each rational tune, a resonance, or island structure is born. This consists of a central periodic orbit surrounded by an orbit system that rotates around it. This system thus reproduces, on a smaller scale, the orbit system around the primary central periodic orbit at $(0,0)$. One characteristic of these secondary islands is that their central orbits close only after many trips around the accelerator so a number cross sections of each resonance system are displayed in pictures of the mapping of Eq. (1).

Surrounding each such system, there is generally a region where a single orbit appears to fill a portion of the (x,p) plane randomly. This will be called a stochastic sea.

In and around these orbits, some distorted circular orbits continue to exist, according to a theorem of Kolmogorov, Arnol'd and Moser. Such closed curves in the (x,p) plane that are filled by a single orbit are called KAM surfaces.

With orbits no longer lying on circles, and particularly as some orbits can wander over regions of phase space, the problem of stability arises. By this will be meant here, the problem of whether orbits can wander indefinitely far from the origin, $(0,0)$. At least two stability questions can be distinguished. Does the model exhibit stability or instability? Is the real system stable?

The existence or absence of KAM surfaces is strongly relevant to the first question. These surfaces divide the (x,p) plane. By continuity and

uniqueness orbits in one region can never cross over into another. Thus, if KAM surface can be proven to exist the orbits inside can be said to be stable. A large part of my efforts for the past few years have been devoted to investigating criteria for the existence of KAM surfaces in mappings such as those studied here.

A study of this mapping may also be of assistance toward the question of whether a real system is stable. A real system contains the features of Eq. (1), and additional terms spanning the entire frequency range from sixty-cycle hum to the time of interaction of a high energy particle with a neutral gas atom. Nevertheless, Eq. (1) would be important toward the understanding of the full system when the true orbit follows a model orbit for a significant distance. For example, the effect of small random perturbations can be much enhanced if much of an increase in amplitude is due to rotation around the secondary central periodic orbit in a resonance zone. Equivalently, consider the evolution of an ensemble of particles that satisfy Eq. (1) plus additional small perturbation terms. Equation (1) will force the distribution function to be relatively flat in resonance and stochastic zones, and thus steep in the inbetween regions. This steepness can much enhance the effect of small perturbations. Thus even when Eq. (1) predicts stability, the widths of resonances and stochastic regions may be important in determining the containment properties of real systems.

Several different measures have been used to estimate the degree to which resonances and stochastic seas are important in a given mapping. Since integrable systems lack these characteristics, they will be called measures of nonintegrability.

A first such measure is the size of the resonance structures. However, experience has shown that systems for which the tune is a slowly varying

function of the amplitude of the betatron oscillations, resonances are far apart, interact only to a small degree, and have small associated stochastic seas. Thus, a second measure of nonintegrability is the resonance overlap parameter, the ratio of island width to island separation. The overlap criterion implies that large stochastic regions exist when the overlap parameter is of order unity, and resonances are over crowded.²

These measures of nonintegrability can be evaluated in perturbation theory, but have major deficiencies when utilized with numerical work at finite values of the perturbations. Since the islands float in stochastic seas, their width is poorly defined, particularly for the interesting cases where the stochastic seas are a significant component of the mapping. A third measure of nonintegrability that avoids this problem is related to the periodic orbits at the center of the resonances, and particularly to the tune of the oscillations in the vicinity of these orbits. Specifically, the mapping can be linearized and represented by a 2 x 2 matrix in the vicinity of each of these orbits, exactly as around the primary periodic orbit. The local tune is related to the trace of the corresponding matrix. I find it convenient to introduce a quantity called the residue that is a linear transformation of the trace,³

$$R = \frac{1}{4} (2 - \text{Trace}) = \sin^2 \pi \nu_R \quad (2)$$

where ν_R is the local tune around the secondary periodic orbit.

It has been shown that the residue is directly related to the overlap parameter in perturbation theory.^{4,5} It has the advantage that it is well defined and can be evaluated numerically with arbitrary accuracy for systems with finite or large perturbations. When the residue is larger than one, the corresponding periodic orbit is unstable. Thus, the picture associated with the residue criterion is that stochastic seas appear where residues are larger than unity and nearly all periodic orbits are unstable.³ There are indications of coming developments that will reinforce this concept.⁶

To illustrate the utility of the residues in understanding given mappings, I undertook to estimate the amplitude dependence of the degree of nonintegrability introduced by different beam-beam force functions, $F(x)$. As a random example, I chose to study the $2/5$ resonance.

This resonance has some peculiarities, and is seen in different ways by different people, so some explanation is in order to illuminate my attitude. Because of symmetry, odd resonances do not appear in lowest order of perturbation theory. Closely coupled to this is the fact that there are two symmetrically placed stable periodic orbits with the appropriate tune. Thus, the two $2/5$ orbits yield a picture with a chain of ten resonances. Nevertheless, I call this resonance $2/5$, since I use the denominator of the resonance label to indicate the length of its central periodic orbit. None of this leads to any difficulty in calculating either the orbit or its residue.

The perturbation parameter was fixed at $k = 0.05$, and the position of the resonance in the phase plane was changed by varying ν . Thus, the resonance

is forced to sample different ranges of the force $F(x)$.

As discussed previously,³ a dominant feature of the magnitude of the residues is their exponential dependence on orbit length. To compare orbits of different length, it is useful to introduce a mean residue for the resonance P/Q by

$$f \equiv (4R)^{1/Q}$$

Thus in Fig. 1, f , the mean residue, is the measure of nonintegrability, and x_m , the maximum value of x around the orbit, is a measure of the orbit amplitude.

Three different functions have been evaluated for Fig. 1,

$$\begin{aligned} F_G &= [1 - \exp(-x^2/2)]/x \\ &\approx \frac{1}{2} x \left(1 - \frac{1}{4} x^2 + \frac{1}{24} x^4 + \dots \right) \end{aligned}$$

$$\begin{aligned} F_H &= \frac{1}{\sqrt{3}} \tanh \sqrt{3} x/2 \\ &\approx \frac{1}{2} x \left(1 - \frac{1}{4} x^2 + \frac{3}{40} x^4 + \dots \right) \end{aligned}$$

$$\begin{aligned} F_A &= \frac{1}{\sqrt{3}} \tanh^{-1} \sqrt{3} x/2 \\ &\approx \frac{1}{2} x \left(1 - \frac{1}{4} x^2 + \frac{9}{80} x^4 + \dots \right) \end{aligned} \tag{4}$$

In each case they are normalized to have a slope of 1/2 at zero. Then k is the tune shift for small amplitude orbits, when k is small, with some nonlinear corrections for larger values of k .

The scale of the x variation was adjusted so that the first nonlinear term in the Taylor series agreed for each of the force functions. When different scalings were used, so that

$$F(x) \approx \frac{1}{2} x \left(1 - \frac{a^2}{4} x^2 + \dots \right) \quad (5)$$

then, for small values of x_m , the mean residue depended only on the combination ax_m . Thus the mean residue depended only on the nonlinearity. Further, the mean residue had a relatively weak dependence on the beam force parameter, k , $f \approx \sqrt{k}$. A perturbation calculation, taking the limit of small k and varying the tune ν simultaneously to fix the position of the resonance, would be useful to confirm this result. Finally, other resonances gave rather similar curves. The mean residue was somewhat larger for even resonances, consistent with the fact that they exist in lower orders of perturbation theory, but the difference was not large.

A number of conclusions can be drawn from this calculation, at various levels of abstraction.

The values of the residues and mean residues illustrated in Fig. 1 are quite small. According to previous results,³ KAM surfaces disappear in regions where the mean residues are greater than unity. Thus, while this calculation was designed to test methods rather than to design experiments, it

seems clear that significant KAM surfaces should exist, within this model, for values of the tune shift, k , up to 0.1 or greater. Thus, the loss of the KAM surfaces of this model is unlikely to be a physically important effect.

A second conclusion that can be drawn from this figure is that the beam-beam interaction forces significant nonintegrability at very large amplitudes. Its effect on the tune shift is small at these amplitudes, but its effect on the resonances is large. This is rather independent of the shape of the force function.

At another level, the primary purpose of this calculation was to demonstrate the utility of the mean residues as a measure of nonintegrability. This measure is consistent since Fig. 1 can be essentially reproduced using a variety of different resonances. That it yields a good criterion for the existence of KAM surfaces has been shown previously.³ It is a good way to organize computational data, since it concentrates on short orbits that can be evaluated accurately.

One of the delicate problems that this method might be useful for arises when perturbations added to Eq. (1) have periods from several to a few hundred times that of the basic interaction period embedded in Eq. (1). Multiple interaction regions or periodic variations of beam intensity are two possibilities of this type. A more complicated two-dimensional mapping, taken over the full period of the perturbation, might still be an appropriate model. The existence of KAM surfaces would determine the stability of this super-period model.

There may be some relations between the size of stochastic seas and the residues of nearby orbits, but this has not been explored yet in any detail.

Finally, this work is another effort to achieve a balance between computational and analytic, perturbation methods. These two approaches are

sometimes seen to be competitive. In fact, they tend to be complementary. Perturbation calculations tend to work best when the various parameters of a problem have significantly different values, so that something can be taken to be small. Numerical calculations are most difficult in such regimes. On the other hand, the care required for accuracy and convergence is about the same in either case, though over the years there has been considerably more experience with perturbation theory. It seems appropriate for our generation to concentrate on sorting out the concepts and methods that yield the best computational results. Since the tradition of excellence is younger in this field, opportunities are greater.

ACKNOWLEDGEMENTS

I am particularly grateful to Drs. S. Ohnuma, A. Ruggiero, and their colleagues at Fermilab for introducing me to the world of accelerators and the beam-beam interaction. The encouragement of, and many useful conversations with Drs. Month, Ford, Tennyson, Bountis, and Helleman have also been very useful.

This work was supported by the U.S. Department of Energy Contract No. DE-AC02-76-CH03073.

REFERENCES

- (1) For example, see: Helleman, R. H. G., 1979 in "Nonlinear Dynamics and the Beam-Beam Interaction," eds. M. Month and J. C. Herrera, AIP Conf. Proc. 57, (AIP, New York), P. 236.
- (2) Chirikov, B. V., 1979 Physics Reports 52, 263.
- (3) Greene, J. M., 1979, J. Math. Phys. 20, 1183.
- (4) Lichtenberg, J. A., 1980 in "Intrinsic Stochasticity in Plasmas" ed. D. Gresillon (Editions de Physique, Orsay, France), P. 13.
- (5) Greene, J. M. 1980, to be published in the Proceedings of the New York Academy of Sciences.
- (6) Feigenbaum, M., 1980, private communication.

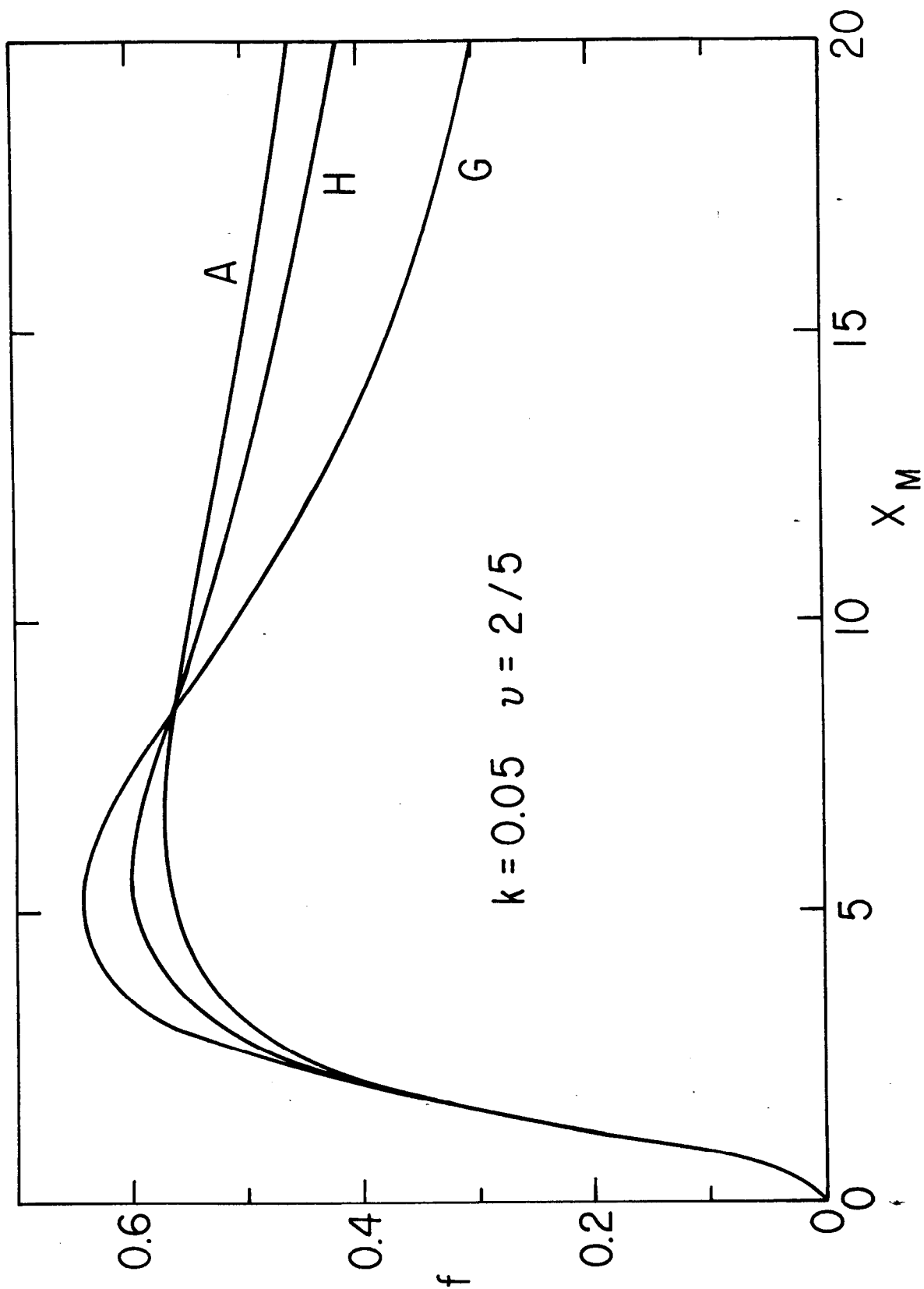


Fig. 1. Dependence of mean residue on amplitude for three different beam-beam interaction forces, given in Eq. (4).

THE ROLE OF RESONANCES, "STOCHASTICITY"
AND ARNOL'D DIFFUSION IN MODELS OF
THE BEAM-BEAM INTERACTION

BY

TASSOS C. BOUNTIS

DEPARTMENT OF MATHEMATICS AND COMPUTER SCIENCE

CLARKSON COLLEGE

POTSDAM, N.Y. 13676

TABLE OF CONTENTS

Section Number	Page Number
1. Introduction.....	1
2. Hamiltonian Dynamics and Nonlinear Resonances.....	2
3. Motion in "Stochastic" Regions	
A. The Resonance Overlap Criterion.....	7
B. Diffusion in Large Scale "Stochastic" Regions.....	10
4. Arnol'd Diffusion in 4-Dimensional Mappings	
A. The Tennyson-Lieberman-Lichtenberg Model.....	12
B. The Chirikov-Ford-Vivaldi Model.....	16
5. Future Plans, Work in Progress.....	19
6. Acknowledgements.....	21
7. References.....	22

ABSTRACT

We review here some recent results on the long time behavior of the orbits of two- and four-dimensional mappings which display, in a qualitative way, most of the complicated features of the Beam-Beam Interaction. We conclude that this behavior depends crucially on the location of the initial conditions of the orbits with respect to the "largest" (i.e. lowest order in perturbation theory) resonances of the system. In the "stochastic" regions, where these resonances overlap, the properties of the motion are well described by classical diffusion processes. In 4-dimensional mappings, where Arnol'd diffusion occurs, various theoretical and empirical methods proposed by Chirikov yield estimates of the rates of particle diffusion which are in good agreement with experimental evidence.

1. Introduction

This paper is a brief review of a number of recent results illustrating some basic concepts of Nonlinear Hamiltonian Dynamics: Resonances, "stochasticity" and Arnol'd Diffusion. These concepts are of direct relevance to the long term stability of colliding beams in the intersecting storage rings of high energy accelerators.¹

The models and the results reviewed here are, admittedly, far from a realistic description of actual, true to life machines. They do offer, however, a lucid picture and considerably enhance our understanding of the nonlinear phenomena associated with the so-called Beam-Beam Interaction.¹

Our aim in reviewing these results here is to emphasize and discuss their main features in a unified way so as to help researchers in this field better analyze and assimilate a rapidly growing collection of experimental evidence.

In section 2 we briefly introduce the fundamental ideas of Nonlinear Hamiltonian Dynamics referring the reader to the literature for more details. A general Hamiltonian is written down in Action-Angle variables and the motion near a (nonlinear) resonance is discussed. The appearance of large scale (resp. small scale) "stochastic" regions is pictorially explained as a result of the overlapping of low order (resp. high order) resonances, an idea originally due to B.V. Chirikov.²

In section 3, Chirikov's Resonance Overlap Criterion is illustrated on a widely studied two dimensional model, the so-called Standard Mapping.^{2,13-15} Two dimensional mappings can accurately represent periodically "kicked" one degree of freedom systems which describe Beam-Beam effects in the direction vertical to the plane of revolution ignoring all coupling with the horizontal motion. In the "stochastic" regions a theoretical description of the motion in terms of a classical diffusion process agrees well with the experimental results.

Section 4 is devoted to four dimensional mappings which do take into account the coupling between vertical and horizontal motion. Such mappings represent periodically "kicked" two degree of freedom systems, in which phase space orbits can wander (for sufficiently long times) over most of the energy "surface" for arbitrarily small coupling parameter ϵ ! This universal (i.e. for all $\epsilon \neq 0$) instability, often referred to as Arnol'd Diffusion^{2,3}, is discussed here with the aid of two models, one due to Tennyson et al.⁴ and one due to Chirikov et al.⁵.

Finally, we conclude with some remarks on work currently in progress^{6,22} on a four dimensional mapping involving a realistic Beam-Beam force. Our eventual goal is to implement as well as develop further the results reviewed here on more realistic models of the Beam-Beam Interaction.

* * * * *

2. Hamiltonian Dynamics and Nonlinear Resonances

In the last two decades, the field of Nonlinear Hamiltonian Dynamics has experienced considerable growth. There has been a number of rigorous results primarily in the area of integrable (i.e. "separable" or "solvable") systems^{7,8}, with the notable exception of the celebrated theorem of Kolmogorov, Arnol'd and Moser^{2,7-9} (KAM). The KAM theorem, however, even though it has stimulated many theoreticians and provided new insight, is essentially an existence result, whose applicability has so far been very limited.

Faced with serious analytical difficulties many physicists and mathematicians - starting with E. Fermi and S. Ulam in the early fifties¹⁰! - turned to numerical computation in order to study the properties of non-integrable⁷⁻⁹ systems. In particular, they asked the question: How can a deterministic system described by Newton's equations of motion exhibit "statistical" behavior? (By "statistical" behavior we mean, here a set of properties which can be well described by the laws of

statistics, random processes etc.).

It is well known that all the orbits of an integrable system lie on invariant "surfaces" or "tori"⁷⁻⁹ and hence are not allowed to wander freely over all the available phase space. Integrable systems, however, are in some sense highly exceptional¹¹ and thus, in practice, we deal more often with non-integrable systems. KAM theory, on the other hand, together with a great number of numerical experiments¹² indicate that the behavior of a non-integrable system closely resembles the behavior of an integrable system "nearby"! To be precise let us write the Hamiltonian of a non-integrable system of N degrees of freedom in the form

$$H(I, \theta) = H_0(I) + \epsilon \sum_n V_n e^{i(n, \theta)} \quad (2.1)$$

where $I \equiv (I_1, I_2, \dots, I_N)$ and $\theta \equiv (\theta_1, \theta_2, \dots, \theta_N)$ are the usual Action-Angle coordinates and the summation proceeds, in general, over all N dim. integers $n \equiv (n_1, \dots, n_N)$ [we omit here, for simplicity, a possible explicit time dependence of H , which often takes the form of an extra $e^{i(n, \tau)}$ in (2.1), where $\tau \equiv \Omega t + \tau_0$].

For $\epsilon=0$, the I_k reduce to the Action variables of the integrable system $H_0(I^{(0)})$, which satisfy

$$\dot{I}_k^{(0)} = \frac{\partial H_0}{\partial \theta_k^{(0)}} = 0 \quad (2.2)$$

whence

$$I_k^{(0)} = \text{const.}; k=1, 2, \dots, N. \quad (2.3)$$

These N constants determine the location and shape of the N -dim. invariant tori associated with H_0 . The motion on these tori is quasi-periodic with frequencies

$$\omega_k(I^{(0)}) = \dot{\theta}_k^{(0)} = \frac{\partial H_0}{\partial I_k^{(0)}}, k=1, 2, \dots, N. \quad (2.4)$$

For $\epsilon \neq 0$, KAM theory tells us that "most" of these tori will survive though somewhat distorted

$$I = I^{(0)} + \epsilon I^{(1)} + \epsilon^2 I^{(2)} + \dots \quad (2.5)$$

Using first order perturbation theory we find that this distortion is more pronounced in the neighborhood of a resonance^{7,12}:

$$(n, \omega) \equiv n_1 \omega_1 + n_2 \omega_2 + \dots + n_N \omega_N = 0. \quad (2.6)$$

It is very important that $H_0(I)$ be nonlinear i.e. that the frequencies depend on the amplitude, ($\partial \omega_k / \partial I_\ell \neq 0$ for some k, ℓ) so that the motion near a resonance will be bounded as in the case of the familiar phase space plots of a simple pendulum, cf. fig. 1b below. We then call (2.6) a nonlinear resonance.

For definiteness, consider a free particle moving in two dimensions x_1, x_2 under the influence of a single spatial periodic perturbation⁴:

$$H = \frac{1}{2m}(p_1^2 + p_2^2) + \epsilon V_n e^{i(n, x)} + \text{c.c.} \quad (2.7)$$

where $x \equiv (x_1, x_2)$ and c.c. refers to the complex conjugate of the perturbation term. For $\epsilon=0$, the Action-Angle variables (omitting superscripts) are

$$I_k \equiv p_k / \sqrt{m}; \quad \theta_k \equiv x_k, \quad k=1, 2. \quad (2.7a)$$

The (constant) energy "surface" is a circle in Action space

$$H_0 = \frac{1}{2} (I_1^2 + I_2^2) = \text{const.} \quad (2.8)$$

In this example the frequencies are equal to the Action variables:

$$\omega_k = \frac{\partial H_0}{\partial I_k} = I_k, \quad k=1, 2,$$

c.f. (2.4), and thus the resonance

$$(n_1 \omega) \equiv n_1 \omega_1 + n_2 \omega_2 = 0 \quad (2.9)$$

is represented by a straight line through the origin in the $I_1, I_2 (\omega_1, \omega_2)$ plane, c.f. also fig. 2.

For $\epsilon \neq 0$ the circle (2.8) becomes an annulus of thickness $2\epsilon V_n$, c.f. (2.7) and fig. 1 below. In that annulus the motion is vertical to the resonance line as I_k changes only in the direction of the vector n :

$$\dot{I}_k = \frac{\partial H}{\partial \theta_k} = i n \epsilon V_n e^{i(n, \theta)} + \text{c.c.} \quad (2.10)$$

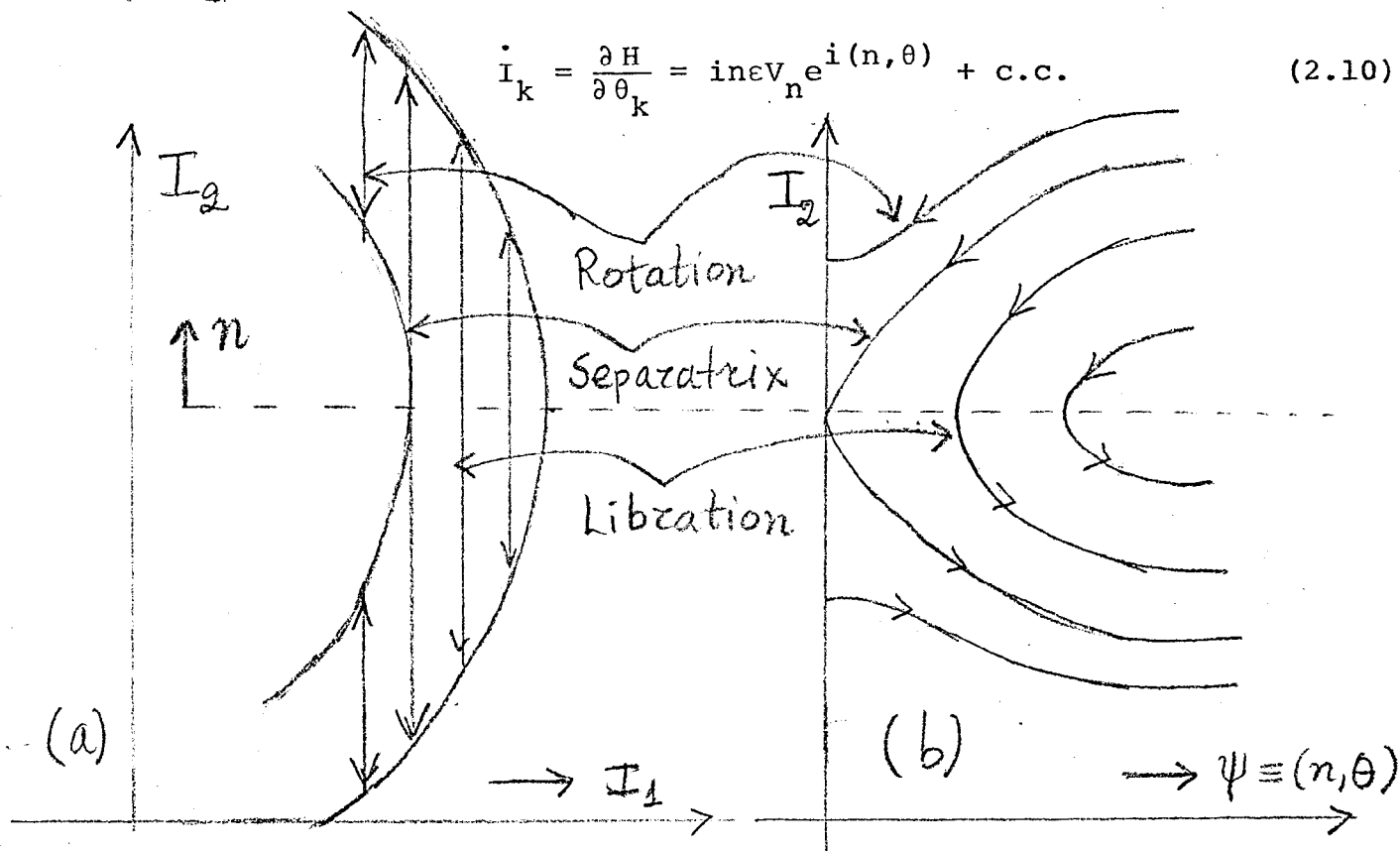


Fig. 1 Motion near resonance (2.9) (a) in Action space
(b) In Action-Angle space, see also reference 4.

In the presence of a second resonance

$$(\ell, \omega) \equiv \ell_1 \omega_1 + \ell_2 \omega_2 = 0 \quad (2.11)$$

the Hamiltonian (2.7) takes the form

$$H = \frac{1}{2} (I_1^2 + I_2^2) + \epsilon V_n e^{i(n, \theta)} + \epsilon V_\ell e^{i(\ell, \theta)} + \text{c.c.}, \quad (2.12)$$

c.f. (2.7a). The two resonance lines (2.9), (2.11) are plotted in fig. 2 below. The angle between the vectors n and ℓ and the magnitude of the perturbation parameter ϵ determine the proximity of the two resonances in Action space and the amount of overlapping which may occur.

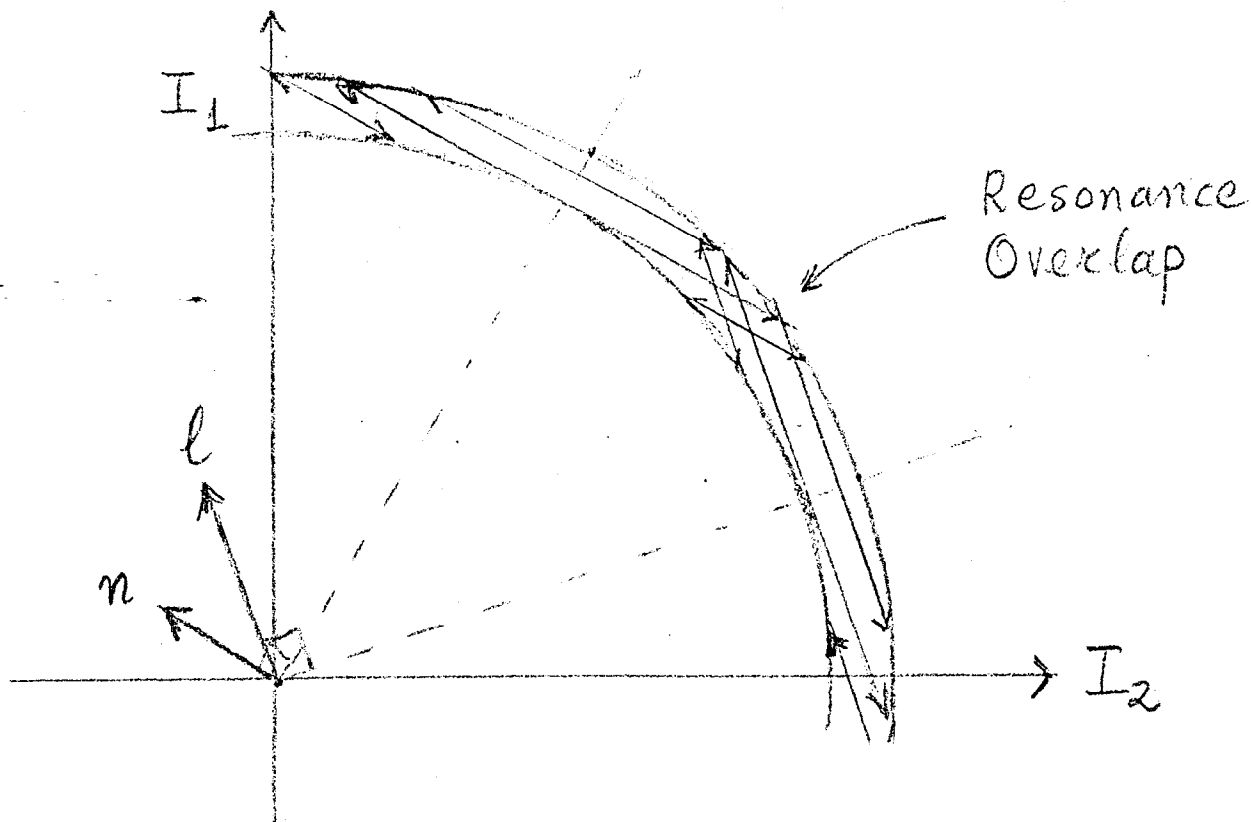


Fig. 2 Overlapping of resonances (2.9 and (2.11) in Action Space.

This simple picture clearly shows, therefore, that ϵ must increase beyond some threshold value ϵ_T for the separatrices of the two resonances to cross. It is precisely in that region of overlap that the motion is, so to speak, influenced by both resonances simultaneously and large scale "stochastic" regions appear. In the next section we derive, following Chirikov, a lowest order (over-) estimate for the threshold ϵ_T , based on the overlapping of the two main resonances.

An important point to keep in mind here is that the two resonances in (2.12) are nonlinearly coupled and give rise to higher order resonances:

$$(m_1 n_1 + m_2 l_1) \omega_1 + (m_1 n_2 + m_2 l_2) \omega_2 = 0.$$

These resonances appear in the Hamiltonian when we transform (I, θ) to new canonical variables (I', θ') , (I'', θ'') etc., using perturbation theory². They are multiplied by factors of ϵ^2, ϵ^3 , etc. and thus give rise to smaller scale "stochastic" regions. Higher order resonances, however, do overlap for $\epsilon < \epsilon_T$ and their combined effect often leads to large scale "stochasticity" at about a half or a third of the value ϵ_T at which the lowest order resonances begin to overlap (see next section).

* * * * *

3. Motion in "Stochastic" Regions

A. The Resonance Overlap Criterion

In order to derive the Resonance Overlap condition we need first an expression for the half width of a single resonance in the I, θ plane, c.f. fig. 1b. Following Chirikov², we introduce a new variable

$$p \equiv I - I_r; \quad |p| \ll 1 \quad (3.1)$$

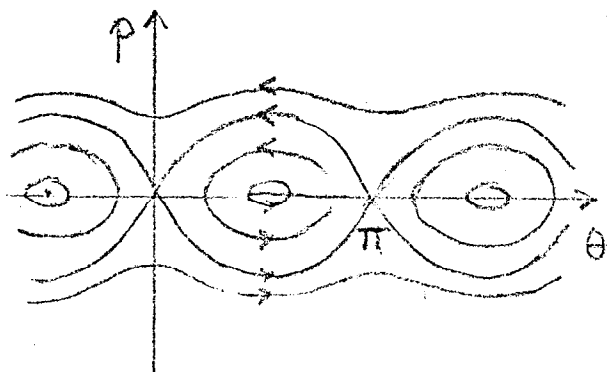
where I_r is the value of I at resonance and expand the terms of the Hamiltonian

$$H = H_0(I) + \epsilon V(I) \cos \theta \quad (3.2)$$

in powers of p . Keeping up to quadratic terms we find that (3.2) reduces to ²

$$\tilde{H} = \frac{1}{2} \omega'(I_r) p^2 + \epsilon V(I_r) \cos \theta \quad (3.3)$$

which, in this approximation, is the Hamiltonian of a simple pendulum, c.f. fig. 3, with



$$\omega'(I_r) \equiv \left. \frac{\partial^2 H_0}{\partial I^2} \right|_{I=I_r} \quad (3.4)$$

On the separatrix of fig. 3

$$\tilde{H} = \epsilon V; \quad p_s \equiv I_s - I_r$$

Fig. 3 Phase plane curves
for the Hamiltonian
(3.3).

whence (3.3) yields

$$\frac{1}{2}\omega' p_s^2 = \epsilon V(1-\cos\theta) = 2\epsilon V \sin^2\left(\frac{\theta}{2}\right)$$

Solving for p_s and using (3.1) we find

$$I_s = I_r \pm (\Delta I)_r \sin\frac{\theta}{2}$$

where

$$(\Delta I)_r \equiv 2\left[\frac{\epsilon V(I_r)}{\omega'(I_r)}\right]^{1/2} \quad (3.5)$$

is the half width (in Action space) of the resonance of fig. 3. If there is a second resonance I_r^* the Chirikov Overlap Criterion predicts large scale "stochasticity" when

$$2(\Delta I)_r \geq |I_r^* - I_r| \quad (3.6)$$

[In general, $\omega(I) \neq I$ and using the approximation $\omega'(I_r) = (\Delta\omega)_r / (\Delta I)_r$ (3.6) may be written in frequency space in terms of $(\Delta\omega)_r$, see ref. 2, section 4].

To apply the above criterion to the case of the Standard Mapping^{2,13-15} written in reduced form:

$$\begin{aligned} p_{t+1} &= p_t + \frac{K}{4\pi} \sin 2\pi x_t \\ x_{t+1} &= x_t + 2p_{t+1} \end{aligned} \quad t=0,1,2,\dots, \quad (3.7)$$

Chirikov first writes down a periodically "kicked" Hamiltonian corresponding to (3.7):

$$H = p^2 + \frac{K}{8\pi^2} \sum_{n=-\infty}^{\infty} \cos 2\pi(x-nt). \quad (3.8)$$

Note that the sum in (3.8) is the expansion of the δ -function representing the periodic "kicks", that H here is explicitly time dependent and that we have used K instead of ϵ to denote the perturbation parameter.

Since the mapping (3.7) remains invariant when x_t, p_t are translated by an integer the motion may be studied on the unit torus $[0,1] \times [0,1]$ in the x, p plane. There are two main resonances there centered at $(\frac{1}{2}, 0)$ and $(\frac{1}{2}, \frac{1}{2})$ and pictured schematically in fig. 4a below [the resonance at $(\frac{1}{2}, 1)$ is the same with the one at $(\frac{1}{2}, 0)$]. We consider the motion "stable" if there exist some invariant (KAM) curves, extending from $x=0$ to $x=1$, which prevent the orbits about, say, the $(\frac{1}{2}, 0)$ resonance from entering the domain of the other resonances and eventually reaching $p=1$.

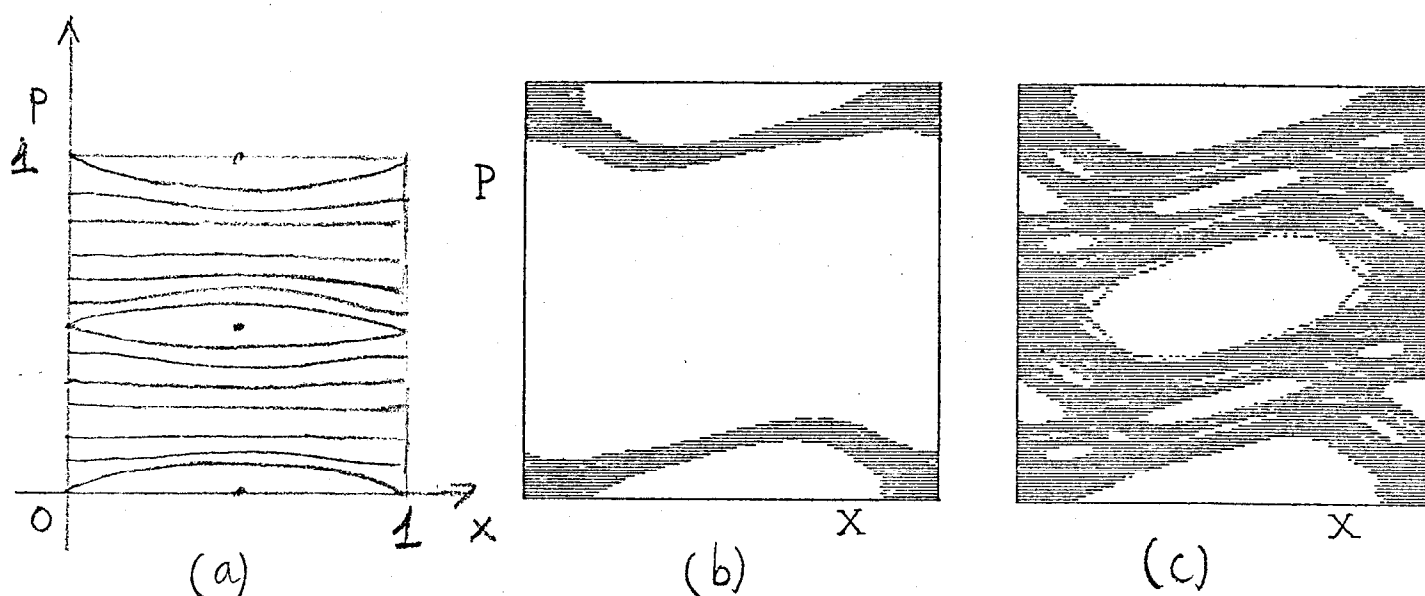


Fig. 4 Numerically observed transition to large scale "stochastic" or unstable behavior for the mapping (3.7), (see ref. 2 section 5): (a) $K \ll 1$; (b) $K = 0.96$; (c) $K = 1.13$.

It is numerically observed that the motion is indeed "stable" for $0 < K \leq 1$. Note in fig. 4b that orbits started near the $(\frac{1}{2}, 0)$ resonance even though they "stochastically" fill a thin layer about the separatrix are not allowed to "diffuse" into the central region. Apparently large scale "stochasticity" has not settled in at $K = 0.96$. Fig. 4b, however, suggests that there must exist some threshold value $K_T \approx 1$ at which the main resonances overlap and maximal excursions of orbits from $p=0$ to $p=1$ become possible.

The Chirikov Overlap Criterion (3.6) [with (3.5)] yields

$$2(\Delta I)_r = 4 \left[\frac{K}{16\pi^2} \right]^{1/2} \geq \frac{1}{2}$$

$$\therefore K_T^{(0)} = \frac{\pi^2}{4} \approx 2.5 \quad (3.9)$$

which considerably overestimates the experimental result $K_T \approx 1$. One of the reasons for this discrepancy is the fact that in deriving (3.6) [with (3.5)] we have entirely neglected the effect of higher order resonances which overlap and make the motion "unstable" at K values lower than (3.9). [Chirikov has extended his criterion to include next higher order resonances²; in the case of the Standard Mapping this leads to the improved estimate $K_T^{(1)} \approx 1.35$].

There have been several other attempts at evaluating K_T experimentally and theoretically^{2,13-15}. The best result so far seems to have been obtained by J.M. Greene¹⁴ who finds $K_T = 0.971635\dots$. His method is essentially a numerical prescription for finding the K ($\equiv K_T$) value at which, the "last" KAM invariant curve - extending from $x=0$ to $x=1$ in fig. 4, is destroyed!

In recent years a number of criteria determining the onset of large scale "stochastic" behavior has appeared in the literature, see e.g. ref. 16-20. To describe them and discuss their individual merits here would take us too far afield. We refer the interested reader to ref. 2, section 5, where the results of some of these criteria on the Standard Mapping are compared, and to M. Tabor's recent review paper.²⁰

B. Diffusion in Large Scale "Stochastic" Regions

We have seen how the overlapping of resonances can lead to large scale "stochastic" behavior in two degree of freedom (or periodically "kicked" one degree of freedom) Hamiltonian systems. What is of great interest now (especially for the stability studies of particle beams in accelerators!) is to compute the rate at which the orbits of such systems diffuse in the "stochastic" regions.

Consider (again!) the Standard Mapping (3.7) for $K \gg 1$, where the motion on the unit torus is predominantly "stochastic". In this

case, following Chirikov², we assume that x_t is a random variable taking equally weighted values over all of $[0,1]$. Thus, changing coordinates to $I_t \equiv 4\pi p_t$ and $\theta_t \equiv 2\pi x_t$ in (3.7) we find that the total change

$$\Delta I = K \sum_{t=1}^{t_{\max}} \sin \theta_t$$

averaged over $t_{\max} \approx 10^6$ for a single trajectory (time average $\overline{\Delta I}$) or over all possible initial θ values (ensemble average $\langle \Delta I \rangle$) gives

$$\overline{\Delta I} = \langle \Delta I \rangle = 0, \quad \overline{(\Delta I)^2} = \langle (\Delta I)^2 \rangle = \frac{1}{2} t_{\max} K^2. \quad (3.10)$$

Thus, the motion resembles a classical diffusion process whose rate is

$$D_T \equiv \langle (\Delta I)^2 \rangle / t_{\max} \equiv K^2 / 2. \quad (3.11)$$

Chirikov² has calculated experimentally the diffusion rate D_E by averaging $(\Delta I)^2$ over 100 orbits for various values of K . After a least squares fit of the data he obtains the approximate relation

$$D_E \approx K^{1.982} / 1.866; \quad K \gtrsim 10,$$

which is in good agreement with the theoretical estimate (3.11)! And there is still further evidence that certain properties of "stochastic" orbits can be well described by the laws of random process: Chirikov studied the distribution of $|\Delta I|$ changes over time intervals t_{\max} experimentally:

- a) by computing 10^5 orbits with evenly distributed initial conditions for $t_{\max} = 100$, and
- b) by computing one orbit over 10^7 iterations and averaging $|\Delta I|$ over $t_{\max} = 10^2, 10^3, 10^4$ intervals.

Plotting the natural log of the (normalized) distribution f_n of the above orbits as a function of the quantity

$$E \equiv (\Delta I)^2 / t_{\max} K^2, \quad (3.12)$$

Chirikov obtains results which are very well approximated by the

(normalized) Gaussian:

$$f_n = e^{-E},$$

c.f. (3.12) and fig. 5.7 in ref. 2.

Our discussion has so far been limited to Hamiltonian systems of at most 2 degrees of freedom in which truly unstable motion (i.e. extensive particle loss in a machine) requires the presence of large scale "stochastic" regions. We now turn to more appropriate models for colliding beams. They involve more than two degrees of freedom and may be represented by four dimensional mappings, in which practically anything is possible!

* * * * *

4. Arnol'd Diffusion in 4-Dimensional Mappings

The phenomenon of Arnol'd Diffusion has been recently studied numerically as well as theoretically by Tennyson et al⁴ (TLL model) and by Chirikov et al⁵ (CFV model). These two models are four dimensional mappings which have been judiciously chosen so that different types of motion can be isolated and systematically analyzed. In this section we summarize the results of TLL and CFV, draw attention to their common points and suggest how they may be used to study a similar system which accurately describes a Beam-Beam Interaction (see also next section).

A. The Tennyson Lieberman Lichtenberg Model (TLL)

The TLL model may be viewed as describing a free particle in 3 dimensions bouncing between a flat wall at $z=h$ and a "rippled" wall given by

$$z = -a_x \cos k_x x - a_y \cos k_y y - \epsilon \cos(k_x x + k_y y). \quad (4.1)$$

There are four variables here: the angles of incidence α_t, β_t (in the

x , z and y , z planes respectively) and the coordinates x_t , y_t which are "updated" after every collision with the "rippled" wall according to the 4-dimensional mapping

$$\begin{aligned}\alpha_{t+1} &= \alpha_t + 2[a_x k_x \sin k_x x + \epsilon k_x \sin(k_x x + k_y y)] \\ x_{t+1} &= x_t + 2h \tan \alpha_{t+1} \\ \beta_{t+1} &= \beta_t + 2[a_y k_y \sin k_y y + \epsilon k_y \sin(k_x x + k_y y)] \\ y_{t+1} &= y_t + 2h \tan \beta_{t+1}\end{aligned}\tag{4.2}$$

$t = 0, 1, 2, \dots$, see fig. 6 below.

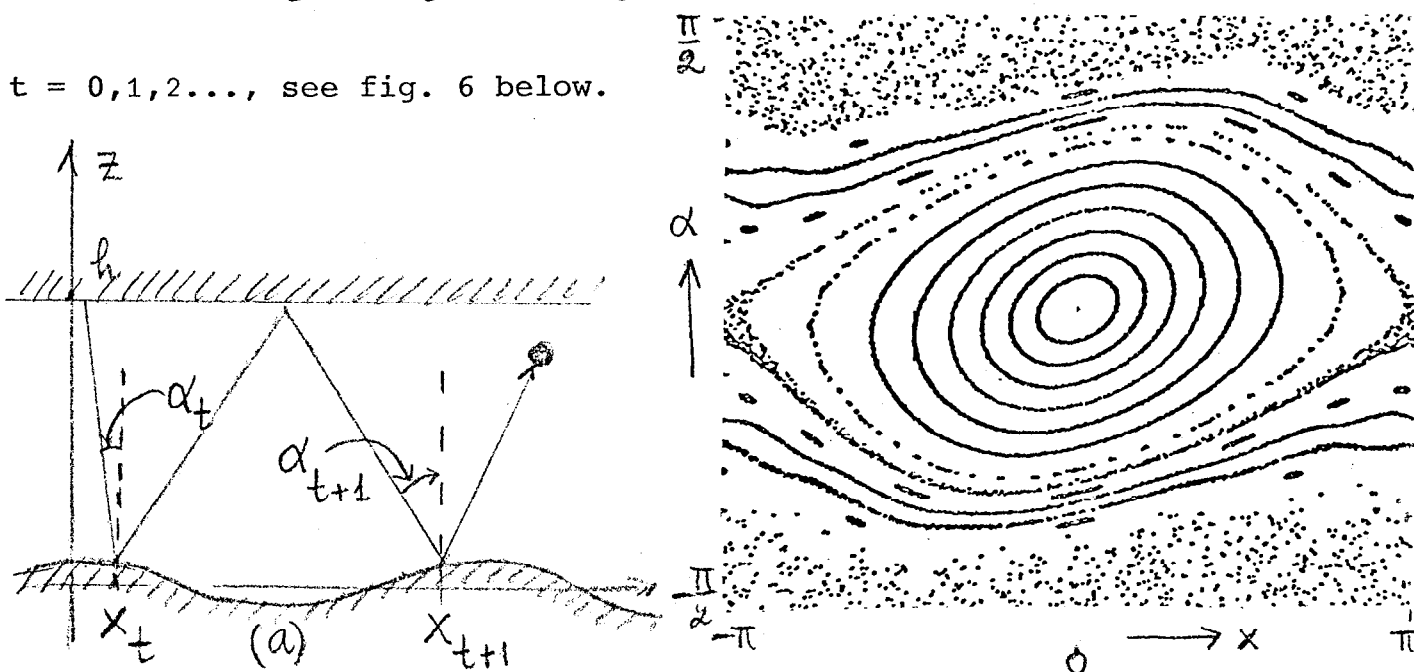


Fig. 6 (a) The (x, z) projection of the motion described by (4.2).
(b) The mapping (4.2) for $\epsilon=0$ in the x, α plane, see ref. 4.

The situation is quite similar to a three degree of freedom Hamiltonian system in the presence of three spatial resonances:

$$H = H_0(I) + \epsilon V_n e^{i(n, \theta)} + \epsilon V_\ell e^{i(\ell, \theta)} + \epsilon V_k e^{i(k, \theta)} + \text{c.c.}\tag{4.6}$$

where

$$H_0(I) = \frac{1}{2} (I_1^2 + I_2^2 + I_3^2),\tag{4.6a}$$

c.f. (2.7), (2.12) and the discussion in section 2. The presence of the third resonance in (4.6)- and for that matter in (4.1) as well!- is very crucial: Note that the equation

$$\dot{I} = \frac{\partial H}{\partial \theta} = i\epsilon [nV_n e^{i(n,\theta)} + \ell V_\ell e^{i(\ell,\theta)} + kV_k e^{i(k,\theta)}] + c.c. \quad (4.8)$$

implies that the Action can change in all possible directions in the energy "surface" (4.6) and motion along resonance lines is now allowed for arbitrarily small values of ϵ ! Thus orbits may wander over most of the available phase space for all values of ϵ and this is what one refers to as Arnol'd Diffusion.

In order to study the diffusive behavior of the orbits of (4.2) Tennyson et al.⁴ concentrated on the motion near the center of the x, α plane, see fig. 6b, and considered two types of processes:

- 1) "Thick layer" diffusion, in which the initial y_0, β_0 values lie in the large scale "stochastic" regions of the y, β plane [similar to the ones at the upper and lower part of fig. 6b],
- 2) "Thin layer" diffusion, in which y_0, β_0 are chosen in the "stochastic" layer about the central resonance in the y, β plane [similar to the one shown in fig. 6b].

To estimate theoretically the diffusion rates for the above two processes Tennyson et al. first approximate the Hamiltonian of their mapping near the center of the x, α plane⁴, by

$$H_x = h\alpha^2 - 2a_x \cos\theta - 2\epsilon \cos[\theta + \phi(t)]$$

where

$$\theta \equiv k_x x, \quad \phi(t) = k_y y. \quad (4.9)$$

Neglecting small oscillatory terms which produce no net effect after long times, we find that the variation of H_x in t is given by

$$\frac{dH_x}{dt} = 2\epsilon \frac{d\theta}{dt} \sin[\theta + \phi(t)]. \quad (4.10)$$

For small oscillations near the center of the x, α plane one takes

$$\theta \approx \theta_0 \cos\omega_0 t \quad (4.11)$$

where

$$\omega_0 \equiv 2k_x (a_x h)^{1/2}.$$

Substituting (4.11) in (4.10) and integrating over one iteration of the mapping gives

$$\Delta H_x \cong 2\epsilon\theta_0\omega_0 \sin\omega_0 t \sin[\theta + \phi(t)]. \quad (4.12)$$

At this stage the assumption is made that $\phi(t)$ behaves like a random variable all of whose values are equally weighted. This assumption rests on the fact that $\phi \equiv k_y y$ lies in the large scale "stochastic" regions of the y, β plane and was seen to yield good results in the case of the Standard Mapping (section 3B).

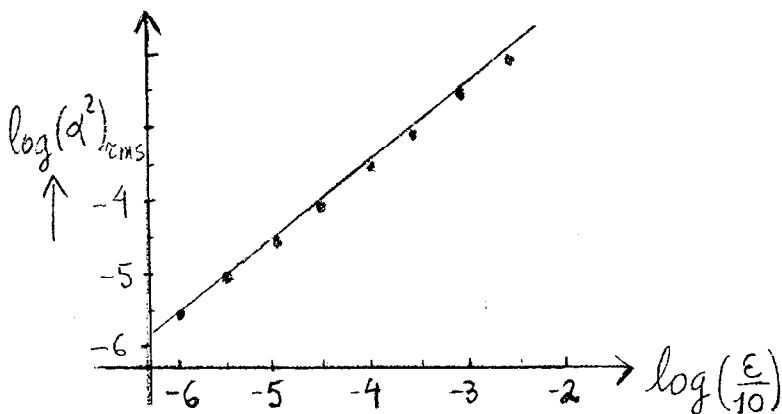
Squaring (4.12) and averaging over t and ϕ gives

$$\langle \Delta H_x^2 \rangle = \epsilon^2 \theta_0^2 \omega_0^2$$

from which the rate for "thick layer" diffusion is directly obtained

$$D_1 = \frac{1}{2} \langle \Delta H_x^2 \rangle = \frac{1}{2} \epsilon^2 \theta_0^2 \omega_0^2 \quad (4.13)$$

This expression was found to agree well with the results of computer experiments⁴, see fig. 7 below.



Thus the theoretical considerations which led us to equation (4.13) apparently are justified and our understanding of the statistics of large scale "stochastic" regions seems adequate.

Fig. 7 Dispersion in the x, α plane vs. ϵ for thick layer diffusion. Comparison between theory and experiment, c.f. ref. 4.

In deriving an expression for the rate D_2 of "thin layer" diffusion the calculations become considerably more involved. Again, we start with (4.10) but now we must keep in mind that $\phi(t)$ is not randomized; rather, it is the phase on the separatrix of a simple pendulum, since the y, β motion does take place near such a separatrix [similar to the one shown in fig. 6b]. In this case also, Tennyson et al obtain a diffusion rate D_2 which is in accordance with all their numerical evidence⁴.

This study of diffusion in the TLL model suggests that first one ought to identify the main resonances in the two planes (here x, α and y, β), as well as a third coupling resonance through which they influence each other. Thus, starting for example, with x_0, α_0 values near the center of a main x, α resonance we could compute how fast points in the x, α plane disperse outward depending on where the point y_0, β_0 lies.

It was found⁴ that the dispersion of points in the x, α plane due to (y_0, β_0) being in a "thick layer" is much faster than the one due to (y_0, β_0) being in a "thin layer". Following, thus, a systematic approach similar to the one of Tennyson et al one must look for initial conditions away from "thick layer" (i.e. large scale) "stochastic" region as a first step in minimizing the dispersive effects of the nonlinear coupling on the particle beam of an Accelerator. Some form of "thin layer" diffusion, however (essentially due to the overlap of higher order resonances), will be unavoidable. The best we can do there is try to calculate diffusion rates as Tennyson⁴ and Chirikov⁵ do in their work on the two models discussed in this section.

B. The Chirikov Ford Vivaldi Model (CFV)

The 4-dimensional mapping considered by these authors⁴ is

$$\begin{aligned}
 p_{t+1}^x &= p_t^x - x_t^3 + \mu y_t + \epsilon f(t) \\
 p_{t+1}^y &= p_t^y - y_t^3 + \mu x_t \\
 x_{t+1} &= x_t + p_{t+1}^x \\
 y_{t+1} &= y_t + p_{t+1}^y
 \end{aligned}
 \qquad t=0,1,2,\dots \quad (4.14)$$

($\mu \epsilon > 0$ and small)

which, for $|P_{t+1}^x - P_t^x| \ll 1$, $|x_{t+1} - x_t| \ll 1$, etc., may be represented by the Hamiltonian

$$H = \frac{1}{2}(P_x^2 + P_y^2) + \frac{1}{4}(x^4 + y^4) - \mu xy - \epsilon x f(t). \quad (4.15)$$

A mapping of the type (4.14) may describe colliding beams in the so-called weak-strong approximation in which the influence of the weaker beam on the strong one is ignored. In this context the variables x_t , y_t in (4.14) represent respectively the horizontal and vertical deviations of a single particle (of the weak beam) from its ideal (unperturbed) path, and $f(t)$ is an external driving force acting in the x direction.

Choosing an $f(t)$ of the form

$$f(t) = \frac{\cos \Omega t}{1 - A \cos \Omega t} \sim \sum_n f_n \cos(n \Omega t)$$

leads to an infinity of resonance lines in the ω_x , ω_y plane (see fig. 8 below) where ω_x and ω_y are the frequencies of the two anharmonic

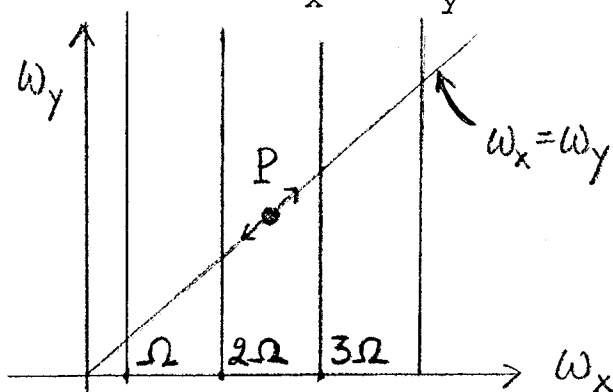


Fig. 8 Lines of lowest order resonances for CFV Model. P marks the choice of initial conditions.

oscillators at $\epsilon = \mu = 0$. In the uncoupled case they are proportional to the oscillation amplitudes A_x , A_y , i.e.

$$\omega_x \sim \beta A_x, \quad \omega_y \sim \beta A_y;$$

where

$$\beta = 0.8472$$

c.f. section 2.3 of ref. 2.

The main coupling resonance (or guiding resonance as Chirikov calls it) "connecting" the vertical driving resonances in fig. 8 and

leading to Arnol'd diffusion is

$$\omega_x - \omega_y = 0. \quad (4.16)$$

The diffusion studied here occurs in the "stochastic" layer about the separatrix of (4.16) which is analogous to "thin layer" diffusion in the TLL model (see section 4.A). To attain the slowest diffusion rate possible, initial conditions were chosen at the midpoint between two driving resonances (see fig. 8).

Chirikov's method for calculating diffusion rates for the CFV model consists of computing a group of orbits over $t_{\max} \sim 10^7$ iterations and performing a series of averaging procedures: First t_{\max} was divided in, say, $N=10$ intervals $\Delta t (= t_{\max}/10)$. The value of H , in (4.15), was averaged over each Δt and a diffusion rate was computed for each pair of Δt 's a distance $\Delta t|m-n|$ apart

$$\frac{(\bar{H}_m - \bar{H}_n)^2}{\Delta t|m-n|},$$

which was averaged over all possible pairs in N intervals to yield the rate⁵

$$D = \frac{2}{N(N-1)} \sum_{m>n} \frac{(\bar{H}_m - \bar{H}_n)^2}{\Delta t(m-n)}. \quad (4.17)$$

In (4.17) the averaging over Δt decreases the effect of bounded oscillations while the averaging over all pairs of Δt 's decreases the time scale over which diffusion is noticeable.

Performing the above calculation twice, i.e. dividing t_{\max} into $N_1 = 100$ and $N_2 = 10$ intervals of length $(\Delta t)_1 = t_{\max}/100$ and $(\Delta t)_2 = t_{\max}/10$, Chirikov et al⁵ obtain two diffusion rates (4.17) D_1 and D_2 . In regions of bounded oscillations one expects that

$$\frac{D_2}{D_1} \sim \frac{(\Delta t)_1^3}{(\Delta t)_2^3} = 10^{-3} \quad (4.18)$$

c.f. (4.17), while in Arnol'd diffusion regions

$$D_1 \sim D_2. \quad (4.19)$$

Indeed, starting with initial conditions near the center of the resonance (4.16), it was found that (4.18) was well approximated, while for initial conditions in the thin "stochastic" layer of (4.16) $-D_2/D_1 \approx 0.8$, i.e. (4.19) seemed to hold.

Arnol'd diffusion in the CFV model was observed for coupling strengths in the range 10^{-4} to 6×10^{-6} and should be distinguished from the motion in large scale "stochastic" regions which appear when low order resonances overlap at $\mu \geq 2.0 \times 10^{-4}$. This number differs by only one order of magnitude from the corresponding one for the TLL model⁴, where "thin layer" diffusion was observed for coupling strengths ranging from 10^{-5} to 10^{-3} .

* * * *

5. Future Plans, Work in Progress

We propose to investigate numerically and theoretically 4-dimensional mappings, describing as faithfully as possible the Beam-Beam Interaction. As a first step, we plan to study in detail the case of a "bunched", cylindrically symmetric beam for which the beam-beam force components in the x, y directions are given by^{6,21,22}

$$\begin{aligned} F_x(x, y) &= 2x(1 - e^{-\frac{1}{2}r^2})/r^2 \\ F_y(x, y) &= 2y(1 - e^{-\frac{1}{2}r^2})/r^2 \end{aligned}, \quad r^2 \equiv x^2 + y^2. \quad (5.1)$$

This system can be represented by a mapping in (x_t, y_t, p_t^x, p_t^y) space as in the case of the CFV model, c.f. (4.14). It is more convenient, however, to combine the corresponding 4 first order difference equations into two second order ones^{6,21,22}

$$x_{t+1} = -x_{t-1} + 2Cx_t + (BS/Q)F_x(x_t, y_t) \quad t=0, 1, 2, \dots \quad (5.2)$$

$$y_{t+1} = -y_{t-1} + 2Cy_t + (BS/Q)F_y(x_t, y_t)$$

where Q is the "tune" of the machine, B is the Beam-Beam strength, $S \equiv \sin 2\pi Q$, $C \equiv \cos 2\pi Q$. We then follow the orbits in $(x_t, x_{t+1}, y_t, y_{t+1})$ space.

One conclusion we may draw from our discussion of the TLL and CFV models in section 4, is that main (lowest order) resonances can play a central role in the study of diffusion properties of 4-dimensional mappings. In particular, we saw that it is possible to analyze various types of (Arnol'd) diffusion processes and calculate diffusion rates by making appropriate choices of initial conditions near the center of the lowest order resonances, in the "stochastic" layer of their separatrices, etc.

Such resonances (best pictured in two dimensional projections of the 4-dimensional space) are also present in the mapping (5.2), see fig. 9 below. For values of $Q = 3.76667$ and $B = 3.34666$ at which ISABELLE is expected to operate^{1,21,6} the motion in the x_t, x_{t+1} and y_t, y_{t+1} planes is clearly dominated by a 4th order resonance.^{6,21,22}

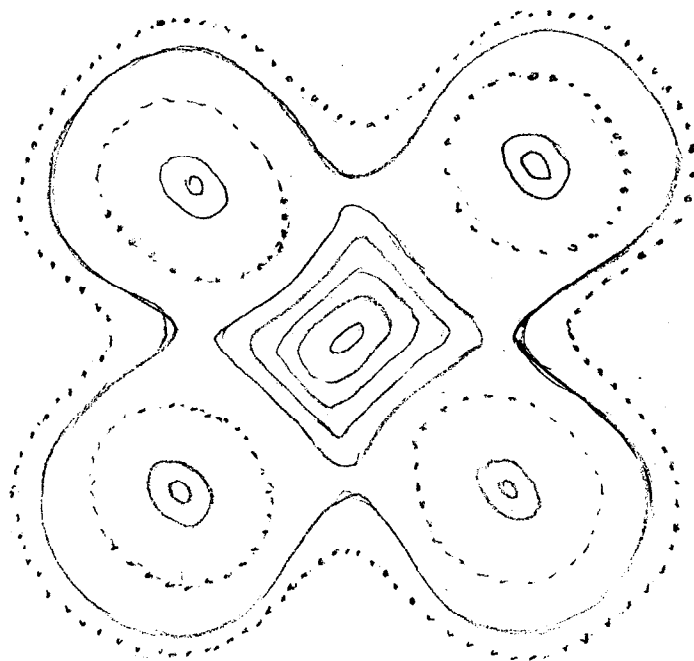


Fig. 9 Projection of the orbits of (5.2), (5.1) on the y_t, Y_{t+1} plane, see references 6,21.

In a preliminary numerical study of (5.2), it was observed that motion along the separatrix of the 4-resonance in the y_t, y_{t+1} plane

induces a rapid (after $t \sim 5,000$ iterations!) dispersion of points started near the center of the x_t, x_{t+1} plane. This may be due to the large amplitudes that the orbits attain in going around the four islands of fig. 9.

Work is currently in progress²², in which the ideas discussed in this paper shall be used to calculate numerically and theoretically diffusion rates for mappings of the type (5.2). Eventually, however, one is interested in studying mappings which model elliptically shaped beams. As we heard from several speakers at this Conference, the results of many experiments indicate that the Beam-Beam Interaction often has a significantly stronger effect in the vertical (y-) rather than the horizontal (x-) direction of the particle motion.

This asymmetry between the x- and y- motion cannot be observed by our cylindrically symmetric model (5.2), (5.1). We can, however, incorporate in our model the so-called "synchrotron oscillations", along the beam, by multiplying the Beam-Beam force by a periodic modulation factor^{6,21}. We plan to discuss the effects of these oscillations on the resonance structure of the mapping (5.2) in a later report.

6. Acknowledgements

My understanding of the material presented in this paper has benefited considerably from many useful discussions with Boris Chirikov, Jürgen Moser, John Greene, Mel Month, Jeff Tennyson, Robert Helleman and Charles Eminhizer. I would like especially to thank Dr. Mel Month for inviting me to participate in this Conference and for his continued encouragement as I begin to learn about the Beam-Beam Interaction.

7. References

1. "Nonlinear Dynamics and the Beam-Beam Interaction", A.I.P. Conf. Proc., ed. M. Month and J. Herrera, A.I.P., 57 (1980).
2. B.V. Chirikov, "A Universal Instability of Many-Dimensional Oscillator Systems", Phys. Reports, 52, (1979).
3. V.I. Arnol'd, Dokl. Akad. Nauk SSSR, 156 (1964) 9.
4. J. Tennyson, M. Lieberman and A. Lichtenberg, in ref. 1.
5. B.V. Chirikov, J. Ford and F. Vivaldi in ref. 1.
6. C.R. Eiminhizer, in this volume.
7. M.V. Berry in "Topics in Nonlinear Dynamics", A.I.P. Conf. Proc. ed. S. Jorna, A.I.P., 46 (1978); also see R. Helleman, p. 400, in same volume.
8. J. Moser, "Integrable and Near-Integrable Hamiltonian Systems", in same volume as ref. 7.
9. J. Moser, "Stable and Random Motions", Princeton Univ. Press (1973).
10. E. Fermi, J. Pasta, S. Ulam, reprinted in "Nonlinear Wave Motion", ed. A.C. Newell, Lectures in Appl. Math. A.M.S., Vol. 15 (1974) 143.
11. J. Moser, "Lectures on Hamiltonian Systems", Mem. Am. Math. Soc. 81 (1973) 1; see Theorem 4, p. 20.
12. See for example: M. Hénon, C. Heiles, Astron. J. 69 (1964) 73; J. Ford, G. Walker, Phys. Rev. 188 (1969) 416; J. Ford and G. Lunsford, J. Math. Phys. 13 (1972) 700.
13. M. Lieberman, A. Lichtenberg, Phys. Rev. A5 (1972) 1852.
14. J.M. Greene, J. Math. Phys., 20(1979) 1183.
15. L.J. Laslett, 9th Intern. Conf. on High En. Accel., SLAC Stanford (1974).
16. Ya. Sinai, Proc. Intern. Congress of Mathematicians, 1962 and Izv. Akad. Nauk SSSR, Mat. 30 (1966) 15.
17. C. Froeschlé, Astron. Astrophys. 9 (1970) 15.
18. B.V. Chirikov and F. Izraelev, Coll. Intern. du C.N.R.S. Transf. Ponctuelles et leur Applications (Toulouse 1973) 409.
19. G. Bennetin et al, Phys. Rev. A 14 (1976) 2338.
20. M. Tabor, "The Onset of Chaotic Motion in Dynamical Systems", Adv. in Chem. Phys. (1980) to appear.
21. R. Helleman, in ref. 1.
22. C.R. Eiminhizer, T. Bountis, R. Helleman (in preparation).

A PRELIMINARY NUMERICAL STUDY
OF THE
BEAM-BEAM INTERACTION IN TWO DIMENSIONS†

BY
C. R. EMINHIZER*

PHYSICAL DYNAMICS, INC.
P. O. Box 1883
LA JOLLA, CA 92038

† Lecture presented at the "Seminar on the Beam-Beam Interaction" on May 22 nd and 23 rd, 1980, at the Stanford Linear Accelerator Center, Stanford, CA 94305.

* Work supported in part by the U. S. Department of Energy under contract EG-77-C-03-1538.

TABLE OF CONTENTS

<u>Section</u>	<u>Page</u>
Abstract	ii
1. Introduction	1
2. Models of the Beam-Beam Effect	3
3. Numerical Study of Beam-Beam Effects in Two Dimensions	8
4. Future Studies	28
5. Conclusions	29
6. Acknowledgements	30
7. References	31
Appendix A - Additional Graphs	32

ABSTRACT

A preliminary numerical study of the beam-beam interaction in two dimensions was undertaken to determine the feasibility of an extensive numerical and analytic effort to locate regions of "stable" motion if they exist. In particular, to find the parameter ranges (Δv , Q , etc.) and the size of the regions in phase space over which the "weak" beam will be stable. Because of the difficult problem of displaying phase space trajectories in a space of more than two dimensions, it is helpful to select a two-dimensional beam shape and charge distribution which reduces these difficulties. The present study deals only with a two-dimensional "bunched" beam with symmetrical charge distribution. It is shown that a three-dimensional phase space is adequate for the display of its motion (which significantly reduces display problems and the number of parameter values to be tested). Preliminary numerical results indicate that a region of "stable" motion may exist and that a systematic effort to locate the "boundaries" and the "degree" of stability would be useful. It is shown that there are trajectories of the motion of the two-dimensional beam which remain bounded for 100,000 iterations of the mapping, $t_{\max} = 100,000$.

1. INTRODUCTION

The current numerical study is the continuation, into two dimensions, of the beam-beam interaction study presented in the article by Dr. R.H.G. Helleman, "Exact Results for Some Linear and Nonlinear Beam-Beam Effects".² It was shown that the beam-beam force is virtually linear over a considerable region about the origin and some analytical results for the linear case were derived. In addition, it was proven that there exists a region of nonlinear stability for all time (which is 50% wider than the width of the beam) for the beam-beam force of a "rectangular" beam [a (3-) piecewise-linear force]. This region was obtained only for one value of the b-b strength Δv at each value of the tune Q . He intends to extend these results to other beam shapes as well, i.e., the "error function" (1.4) and the "bunched" b-b force in one and two dimensions.

Before attempting analytic calculations in two dimensions, preliminary numerical calculations are being made; the purpose of this study. For the one-dimensional beam model discussed in Reference 2, the phase space is two dimensional and the K.A.M. Invariant Curves divide the phase space into regions. However, for the two-dimensional beam, the phase space is four dimensional, in general, (equivalent with $x_t, x_{t+1}, y_t, y_{t+1}$ space). The only known nonlinear stability argument² no longer applies. The "K.A.M. Invariant Tori" (the analog of the "K.A.M. Invariant Curves") no longer contain all the orbits for all time! An orbit starting "inside" such a torus can, and likely will, escape from it. In a $2N$ -dimensional phase space the invariant tori are N -dimensional surfaces. Therefore, for a 4-dimensional phase space the invariant tori are 2-dimensional surfaces. It is shown that for a beam with a

cylindrically symmetric gaussian charge distribution, the four dimensional phase space can be reduced to three (this reduction does not exist for the elliptic shaped beam). We take advantage of this simplification by transforming from x_t, y_t to $r_t, \Delta\theta_t$.

2. MODELS OF THE BEAM-BEAM EFFECT

In the usual accelerators and storage rings, without colliding beams, the deviation $y(\theta)$ of the particles motion from the ideal orbit is successfully described by a simple harmonic oscillator,

$$\frac{d^2 y}{d\theta^2} + Q^2 y = 0 \quad (1.1)$$

where θ is the azimuth angle ($\propto t$), about the center of the ring. The 'tune' Q is one of the important parameters in its design. When a second beam, crosses the first, its effect may be modelled by an additional periodic, non-linear, "kick" on a test particle whose motion is described by a modified version of (1.1)

$$\frac{d^2 y}{d\theta^2} + Q^2 y = P(\theta) F_y(y) \quad , \quad (1.2)$$

where $F(y)$ is proportional to y for $y \rightarrow 0$, i.e., we have absorbed the "beam-beam" strength in the periodic function $P(\theta)$. Since the beams collided over a very short θ interval only, we model $P(\theta)$ by a periodic δ -function,

$$\frac{d^2 y}{d\theta^2} + Q^2 y = B \sum_t \delta(\theta - t 2\pi) F_y(y) \quad , \quad (1.3)$$

where t is an integer counting the passages through a collision region. Equation (1.3) describes the deviation y , perpendicular to the plane of revolution. If we also consider the deviation in this plane, i.e., in the x -direction (along a radius of the ring), there is a second equation with some force $F_x(x,y)$, while the F_y depends on x as well in this case.

In Ref. 2, the beam-beam force in the one-dimensional 'un-bunched' case was modeled by the error function

$$F(y) = \int_0^y e^{-t^2} dt \quad (1.4)$$

of Ref. 2. In the case of a 'bunched' (cylindrical) beam in two dimensions, we use the as x- and y- forces, F_y, F_x

$$F_y(x,y) = 2y \left(1 - e^{-\frac{r^2}{2}}\right)/r^2 \quad (1.5a)$$

$$F_x(x,y) = 2x \left(1 - e^{-\frac{r^2}{2}}\right)/r^2 \quad (1.5b)$$

we have set the rms half width of the beam at 1, with

$$r^2 \equiv x^2 + y^2 \quad (1.5c)$$

of Ref. 3. This selection has two advantages over the more realistic elliptic shaped beam. First there is a simple closed form for the deflection where as the deflection for the Gaussian distribution with arbitrary aspect ratio involves the evaluation of an integral. Secondly, it will be shown that due to the cylindrical symmetry, the phase space can be reduced by one to three.

Instead of the B of (1.3) one often uses the so-called "tune-shift" $\Delta\nu$,

$$\Delta\nu \equiv B/4\pi Q \quad (1.6)$$

as an indicator of the Beam-Beam (force) strength. Since (1.3) is linear between the pulses, it can be solved analytically over (nearly) 2π . "During" the pulse the momentum is changed suddenly by the force F. Hence (1.3) is equivalent to a pair of first-order difference equations³ expressing the Y_{t+1} and (momentum) P_{t+1} [just after the (t + 1)st pulse] in terms of the Y_t and P_t . Combining these two first-order equations into one second-order equation we find in Ref. 2,

$$Y_{t+1} + Y_{t-1} = 2 \cos(2\pi Q) Y_t + 4\pi\Delta v \sin(2\pi Q) F_y(Y_t) \quad (1.7)$$

with $t = 0, 1, 2, \dots$

In the two-dimensional case (1.5), the equations analogous to (1.7) are

$$Y_{t+1} + Y_{t-1} = 2CY_t + (BS/Q) F_y(X_t, Y_t) \quad (1.8a)$$

$$X_{t+1} + X_{t-1} = 2CX_t + (BS/Q) F_x(X_t, Y_t) \quad (1.8b)$$

where $C \equiv \cos(2\pi Q)$, $S \equiv \sin(2\pi Q)$, and F_y and F_x are the non-linear force in the y and x directions respectively.

To take advantage of the cylindrical symmetry for the case where F_y and F_x are described by (1.5), we transform (1.8a-b)

$$r_{t+1} \cos \theta_{t+1} = -r_{t-1} \cos \theta_{t-1} + f(r_t) \cos \theta_t \quad (1.9a)$$

$$r_{t+1} \sin \theta_{t+1} = -r_{t-1} \sin \theta_{t-1} + f(r_t) \sin \theta_t \quad (1.9b)$$

where $f(r_t) \equiv 2 r_t [C + (BS/Q) (1 - e^{-\frac{r_t^2}{2}}) / r_t^2]$, $r_t \equiv (X_t^2 + Y_t^2)^{1/2}$, and $\theta_t = \tan^{-1}(X_t/Y_t)$.

After squaring (1.9) we have

$$r_{t+1}^2 = r_{t-1}^2 - 2r_{t-1} f(r_t) \cos \Delta\theta_t + f^2(r_t) \quad (1.10a)$$

and multiplying (1.9a) and (1.9b) by $\cos \theta_t$ and $\sin \theta_t$ respectively and adding we have

$$\Delta\theta_{t+1} = \cos^{-1} \left\{ \frac{[-r_{t-1} \cos(\Delta\theta)_t + f(r_t)]}{[r_{t-1}^2 - 2r_{t-1} f(r_t) \cos(\Delta\theta)_t + f(r_t)^2]^{1/2}} \right\} \quad (1.10b)$$

$$\text{with } \Delta\theta_t \equiv \theta_t - \theta_{t-1} \quad (1.10c)$$

The initial conditions r_0 , r_1 , $\Delta\theta$ and a phase δ can be expressed in terms of the initial values of X_0 , X_1 , Y_0 and Y_1 as follows:

$$r_i = (X_i^2 + Y_i^2)^{1/2}, \quad i = 0, 1 \quad (1.11a)$$

$$(\Delta\theta)_1 = \cos^{-1} (X_0 X_1 + Y_0 Y_1) / r_0 r_1 \quad (1.11b)$$

and

$$\delta = \theta_0. \quad (1.11c)$$

We can express X_0 , X_1 , Y_0 and Y_1 as a function of r_0 , r_1 , $\Delta\theta$, and δ as follows

$$Y_0 = r_0 \cos \delta \quad (1.12a)$$

$$Y_1 = r_1 \cos (\Delta\theta_1 + \delta) \quad (1.12b)$$

$$X_0 = r_0 \sin \delta \quad (1.12c)$$

$$X_1 = r_1 \sin (\Delta\theta_1 + \delta) \quad (1.12d)$$

Since (1.10) does not explicitly depend on δ , with δ being an arbitrary phase, it is most convenient to specify r_0 , r_1 , $\Delta\theta$, and solve in terms of r , and $\Delta\theta$. In this way we have reduced the problem from four to a three dimensional phase space. Obviously for the beam with aspect ratio other than 1, the elliptic beam, this simplification does not exist and one is forced to deal with the much more difficult four-dimensional phase space.

In addition to the above x , y motion there can be, so-called 'synchrotron' oscillations along the (z -) direction of the beam. In the case of bunched beams (only) this would lead to an apparent periodic modulation of the b - b strength, modelled by inserting a term,

$$[1 - \beta p(w_s t)] \quad , \quad (1.13)$$

behind the Δv in (1.7), where p is a "periodic" function with (synchrotron) frequency w_s (in units where the ring-revolutions have unit frequency) and β its strength, both depending on the shape of, and particle distribution inside, the bunches. This, in effect, changes the problem to one in three dimensions [since the $p(w_s t)$ itself may be thought of as the solution of some third equation, in $p(w_s t)$ only]. We shall refer to it as a 2 + 1 dimensional system [and a 1 + 1 dimensional system if we have $X_t \equiv 0$ in (1.3) and (1.13)].

3. NUMERICAL STUDY OF BEAM-BEAM EFFECTS IN TWO DIMENSIONS

Before discussing the motion of particles in the two-dimensional case, we first look at the one-dimensional case in the region of interest. We have selected the proposed Isabelle tune $Q = 3.76667$, as the most frequently used value; however some additional Q values between $Q = 3.70$ to $Q = 3.75$ have been studied. As we see from the one-dimensional case, the phase space has a prominent period four resonance, c.f., Reference 2, for more detail. The hyperbolic fixed point of Figure 1a and 1b, when magnified, Figure 1c, clearly shows the chaotic region. In the two-dimensional case, Figure 2a, when the trajectories are projected on the y_t, y_{t+1} and x_t , and x_{t+1} planes, (for small initial x_t values) Figure 2b,c, the points begin to fill the space shown. In Figure 3, this same region is plotted in the phase-space r_t, r_{t+1} and $\Delta\theta_t$, as described in Section 2. Here we see the projected motion in x_t, x_{t+1} is a result of a slow rotation in x_t, y_t and growth of x_t with time. In Figure 4, we show that the motion is independent of δ , the initial phase between x_0 and y_0 , the same r_t, r_{t+1} motion occurs but depending on the initial x_0, x_1, y_0, y_1 . The projections are different.

We are interested in understanding the variations in the motion of the particles as a function of r_0, r_1 and $\Delta\theta_1$. A sequence of runs were made, holding r_0 fixed and varying r_1 and $\Delta\theta_1$ the resulting r_{\max} and r_{\min} after 1000 iterations are displayed for a typical case for $Q = 3.76667, B = 1.67333$ in Figures 5 a and b. Additional graphs for other Q values can be found in Appendix A. Note that as the value of $\Delta\theta_1$ approaches $\pi/2$, the r_{\max} occurs at a larger value of r_1 , the value of r_1 decreasing for $\Delta\theta_1 > \pi/2$. Note also that the minimum value of r_t increases to a maximum at $\Delta\theta_1 = \pi/2$. A sequence of r_t, r_{t+1} plots, Figure 6, clearly displays this behavior. For the case shown of $\Delta\theta_1$ near 0 and π , the motion is "above" the resonance,

and for $\Delta\theta_1$ near $\pi/2$ the motion is "below" the resonance. Using this procedure it is possible to systematically probe the three-dimensional phase space and map the resonance regions.

Most of the preceding graphs were made for short time intervals $t \leq 5000$. The r_{\max} values for longer times (100,000 iterations), for a sequence of $\Delta\theta_1$ values (0.0, $\pi/100$, $\pi/10$, $\pi/2$, π) are shown, c.f., Figures 7 and 8. For a region below the hyperbolic fixed point, c.f., Figure 1, the r_{\max} remains constant. Note however the jump after 30,000 iterations for the case $\Delta\theta_1 = \pi/100$. The reason for this is not yet understood, and further study is planned.

Least we leave the reader with the impression that irregular motion in two-dimensions occurs only in the stochastic region, see Figure 9. For this set of initial conditions, the motion projected in all planes is quite complicated, and it seems quite unlikely that a simple transform or projection will make it otherwise.

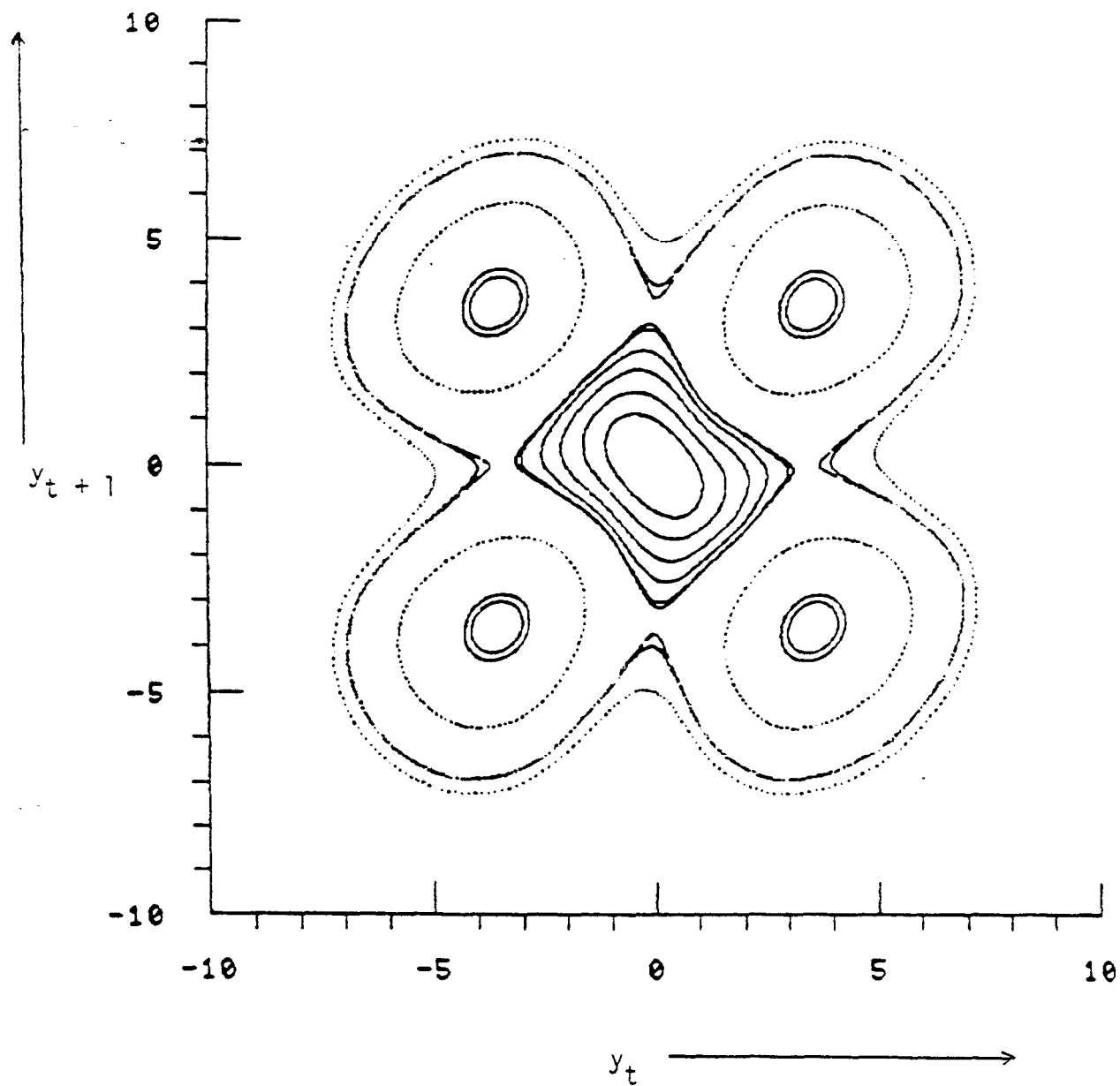


Figure 1a. Phase-plane plot as $B = 3.34666$ in (1.3), (1.5.a), (1.6) at $Q = 22.6/6 \approx 3.7666$. See text.

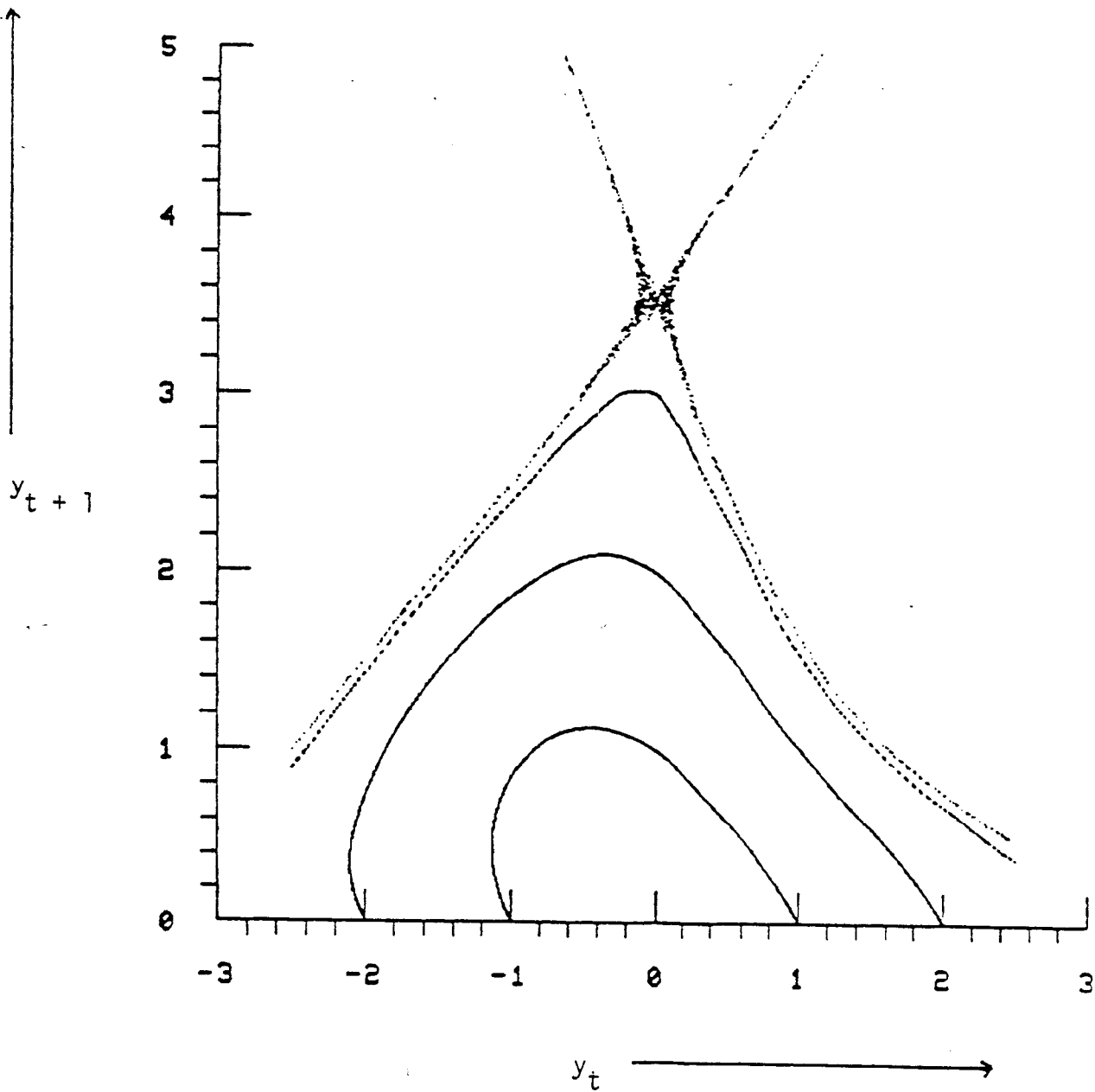


Figure 1b. A magnification of the region about one of the 4th order 'hyperbolic' points of Fig. 1a. Note the chaotic region created by just one orbit (whole chaotic region here from $y_0 = 0.0001$, $y_1 = 3.5$).

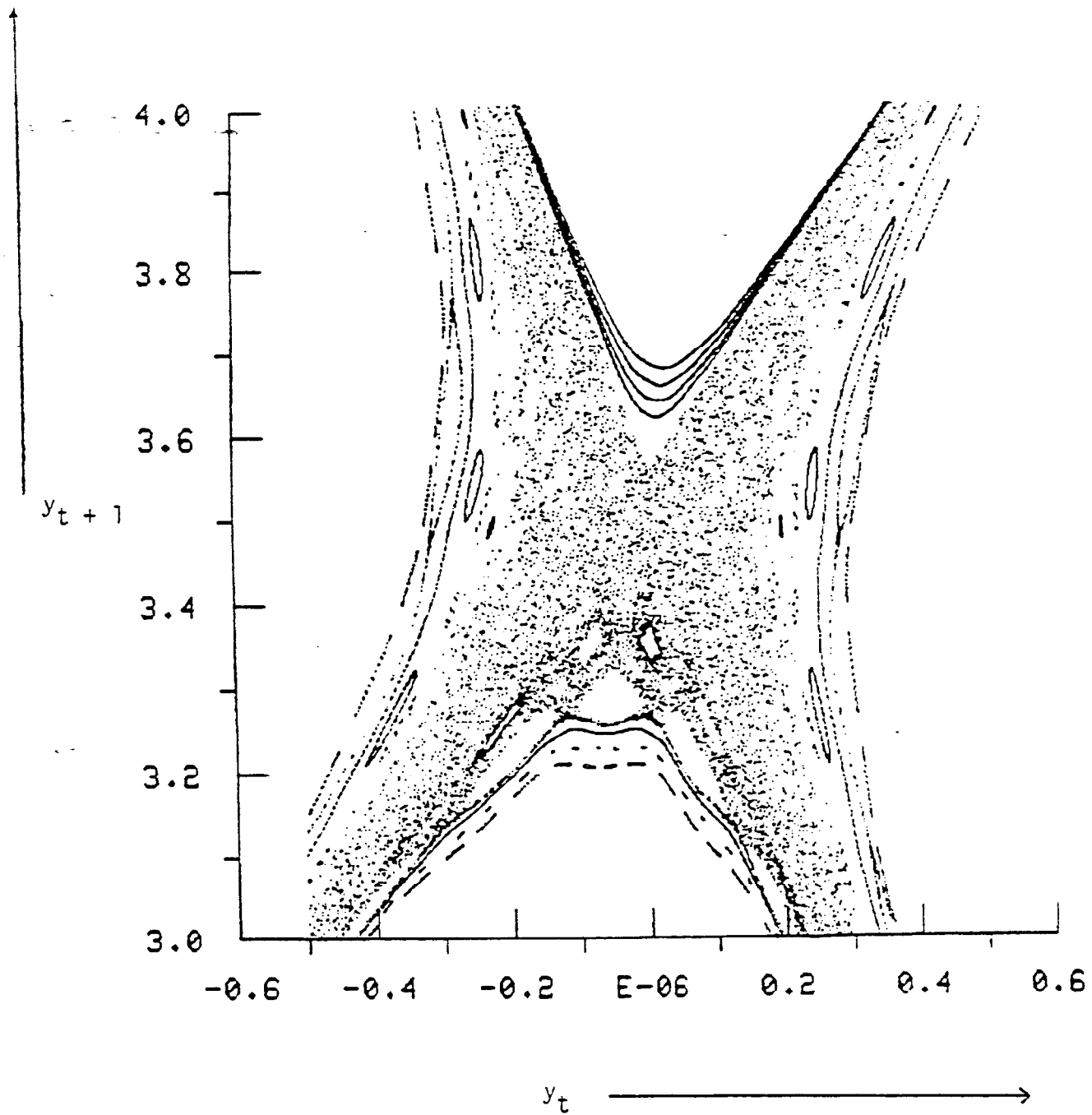


Figure 1c. A further magnification of the chaotic region visible in Fig. 1b. The chaotic collection of dots is again created by one orbit. There are 19 other, more regular, orbits plotted as well. See text.

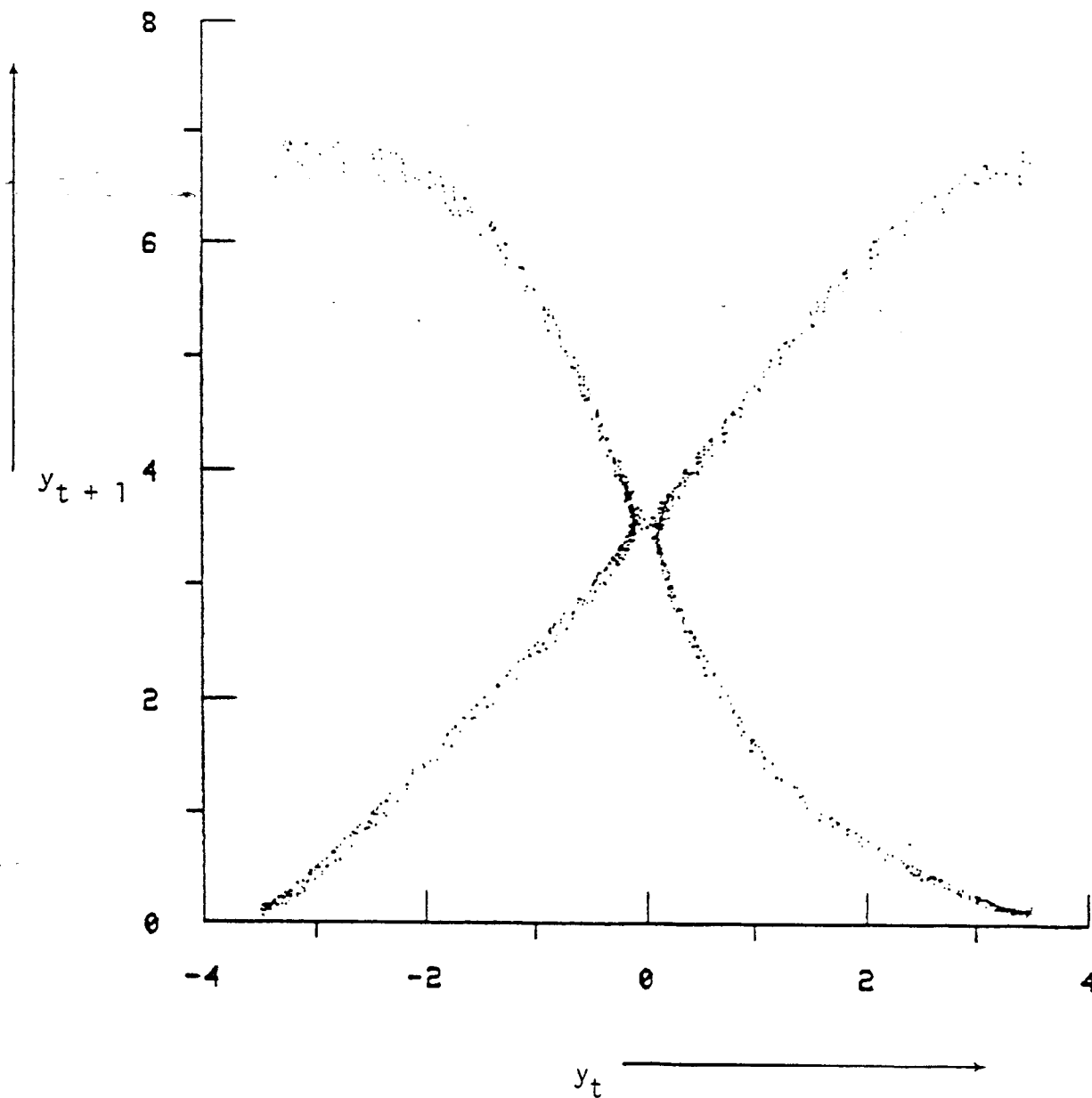


Figure 2a. A projection of one orbit in the 4 dimensional phase space on the y_t, y_{t+1} plane. Note how the chaotic region of Fig. 1b is "measured" out along the 'separatrix' of Fig. 1b.

Parameters: $B = 5.02$ }
 $y_0 = .0001$ } (same as in Fig. 1)
 $y_1 = 3.5$ }
 $x_0 = 0.01$ }
 $x_1 = 0.01$ }

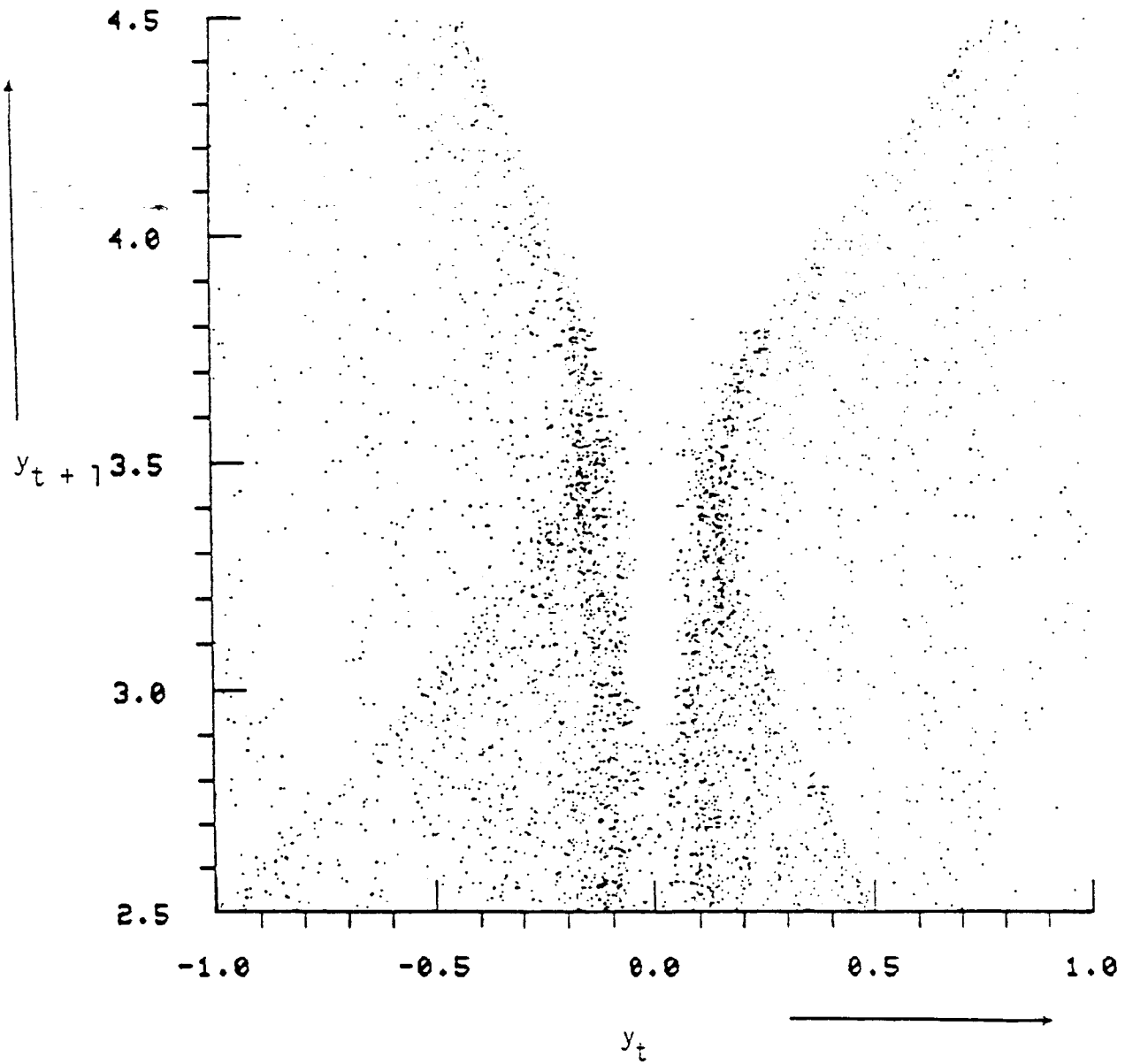


Figure 2b. A magnification of a portion of Fig. 3a followed over a much longer time than in Fig. 3a.

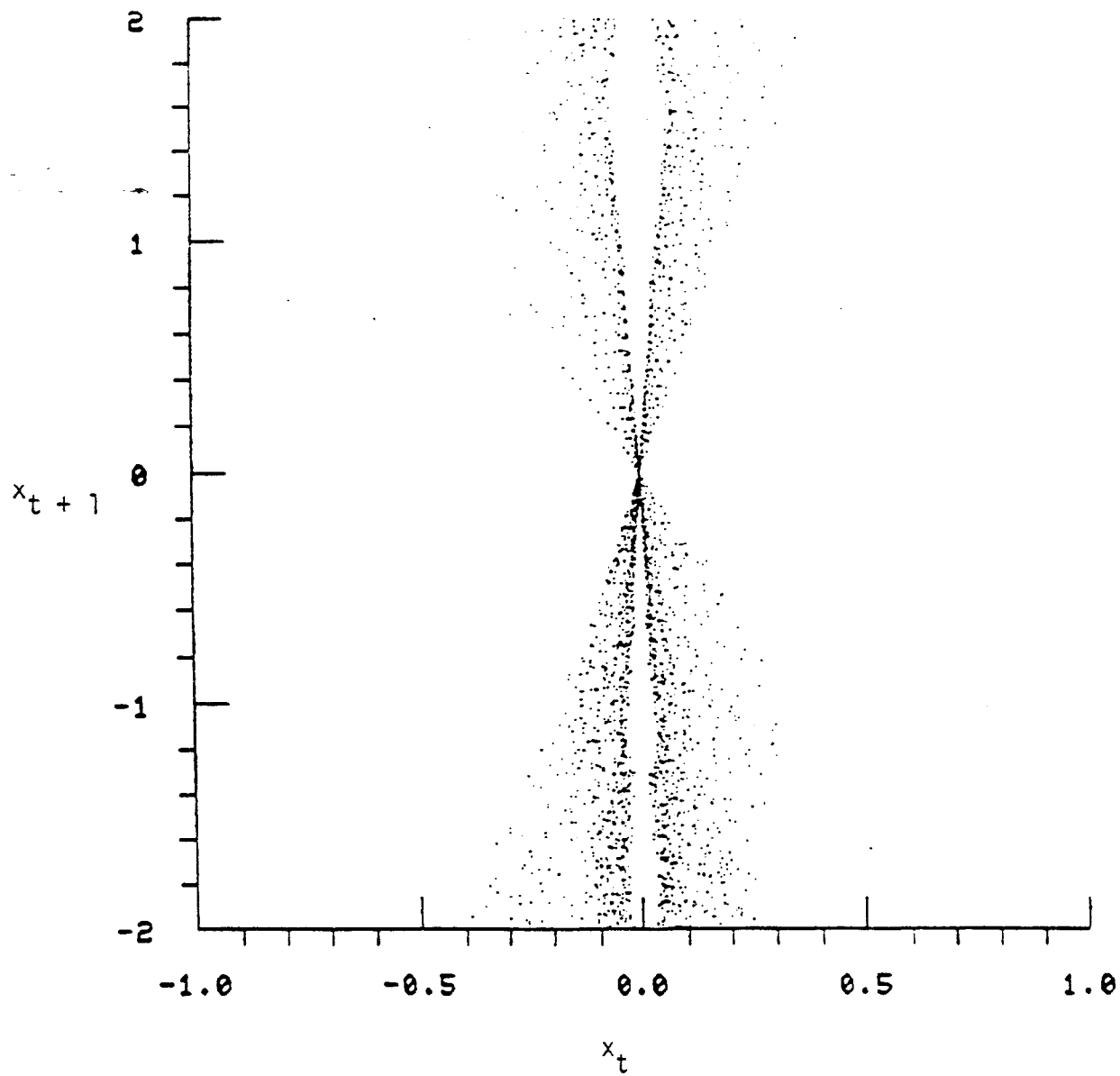


Figure 2c. A projection of the orbit of Fig. 3a, on the x_t, x_{t+1} plane. Note that while $x_0 = x_1 = 0.01$ the x amplitude ('chaotically') driven out beyond 2, and back.

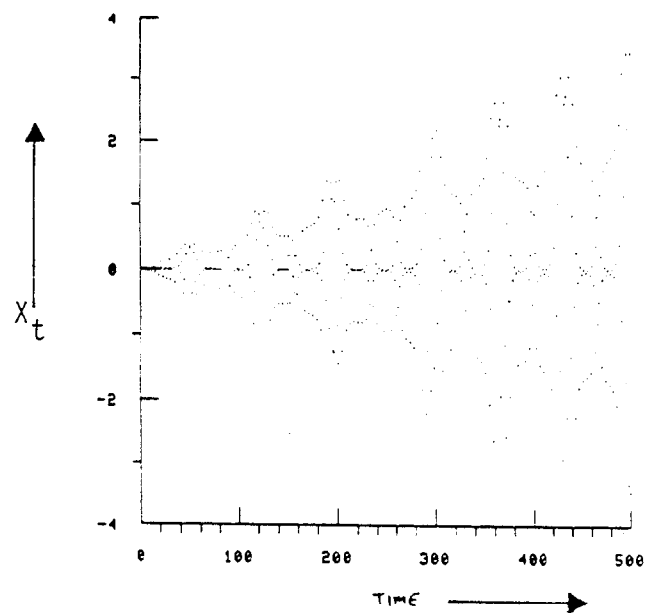
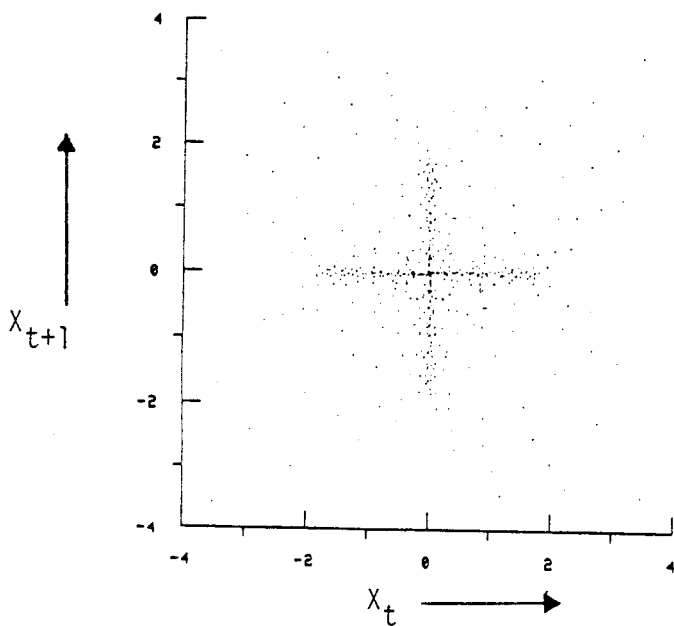
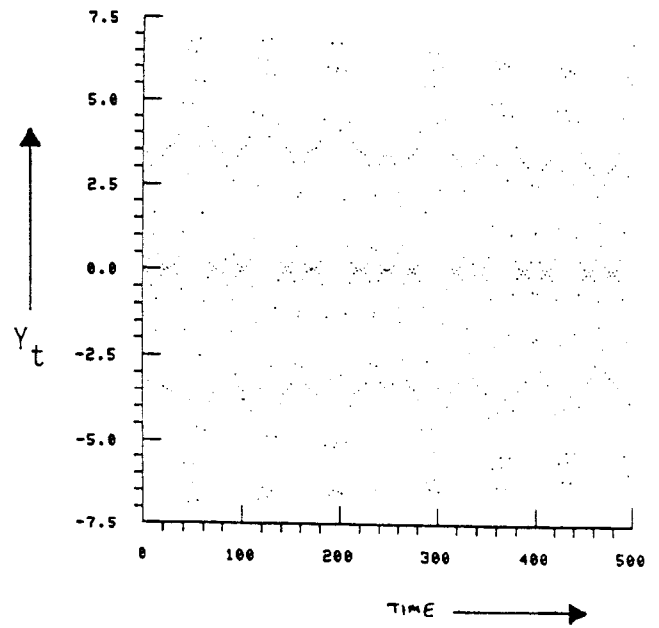
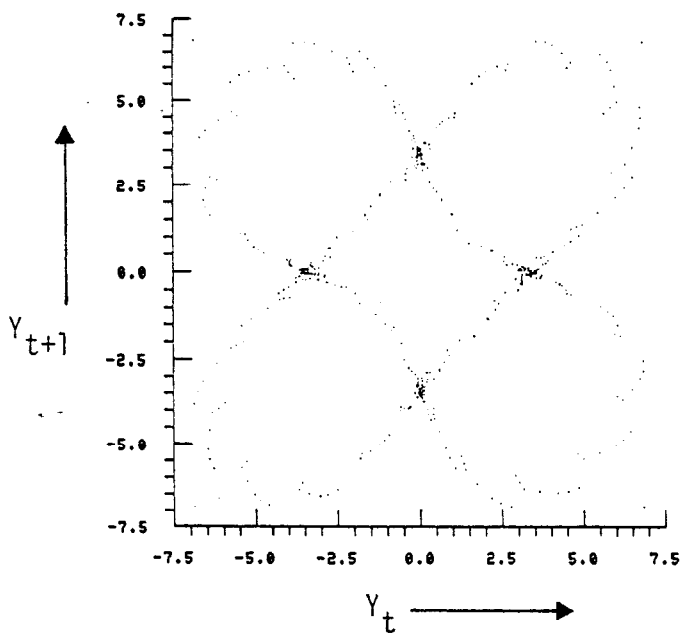
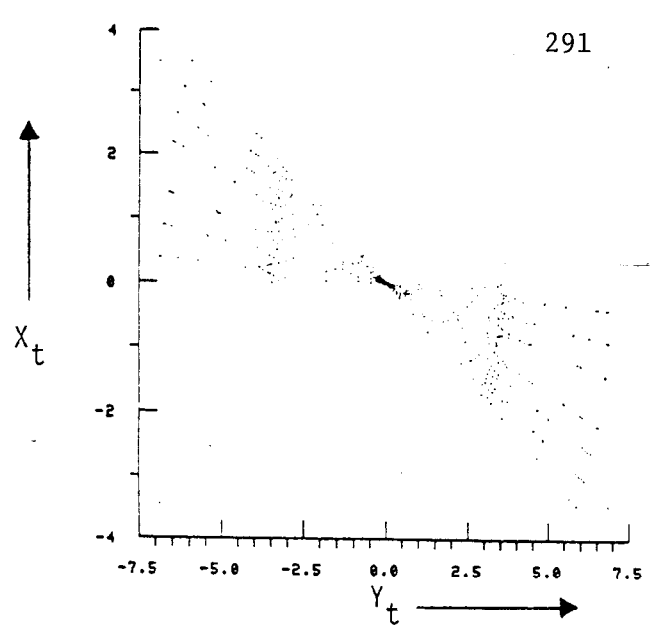
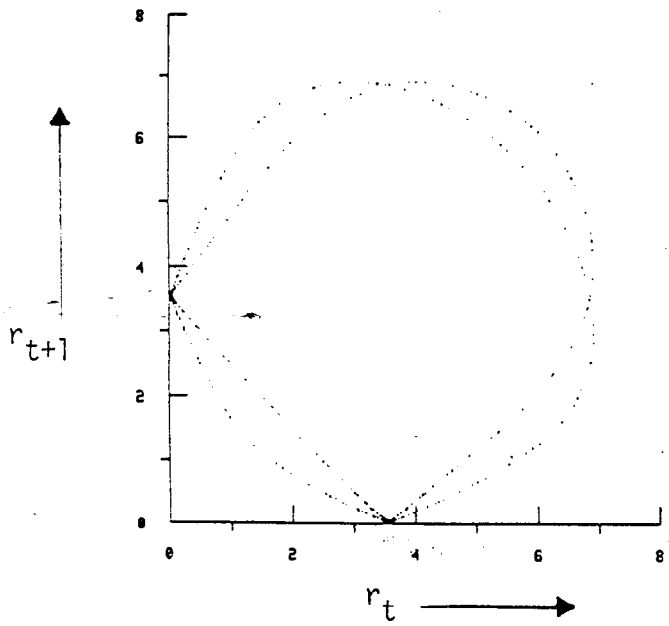
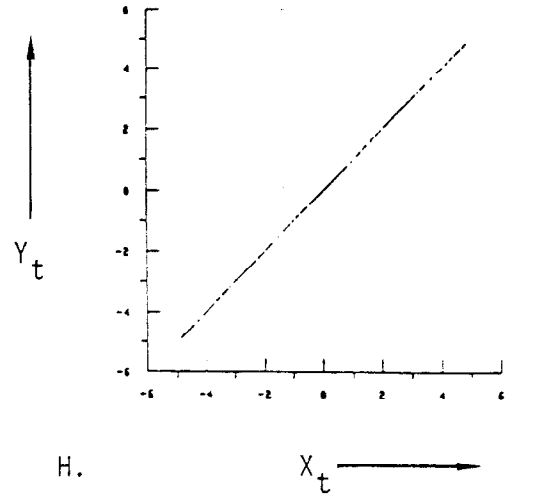
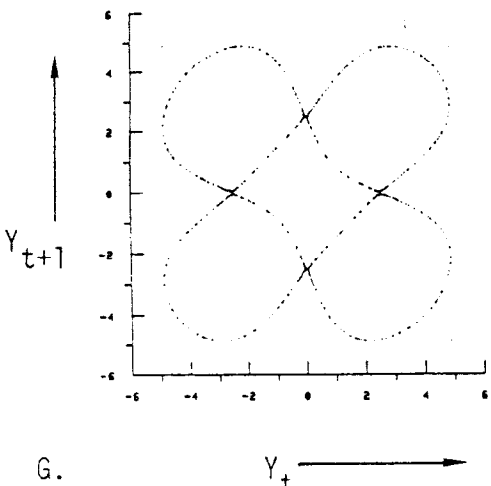
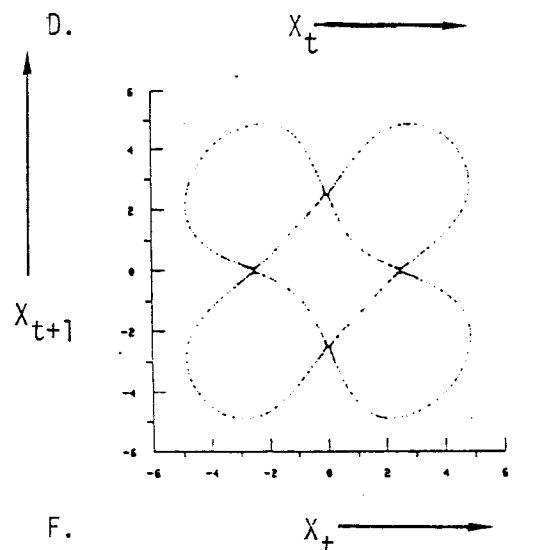
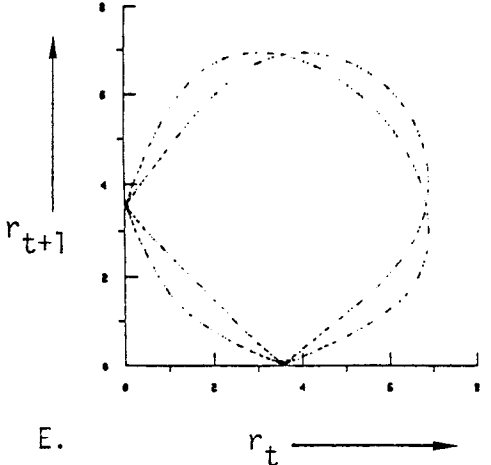
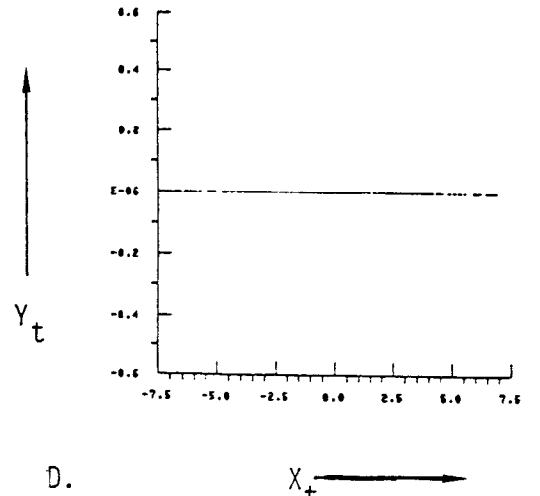
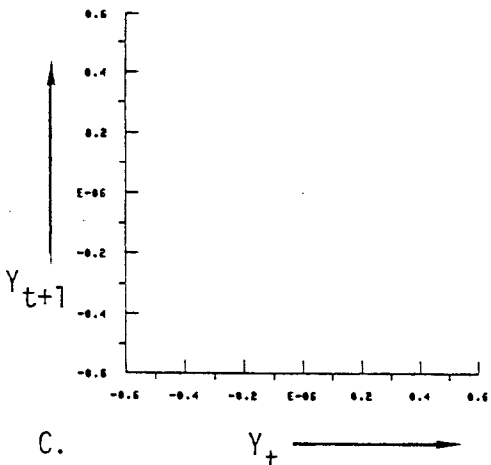
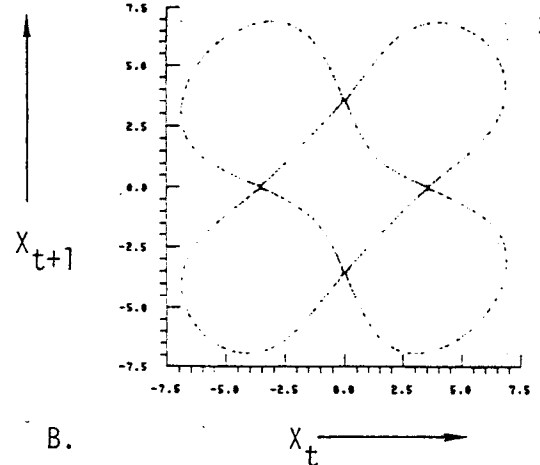
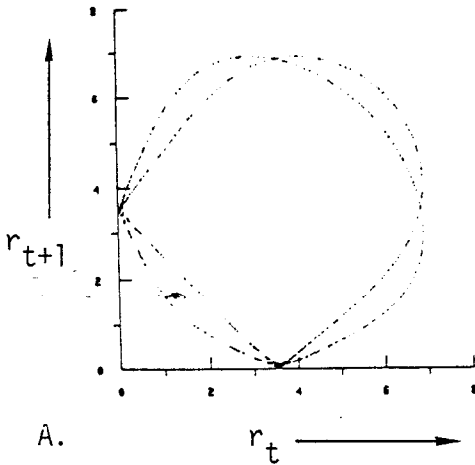


Fig. 3. Motion near hyperbolic fixed point with $Q = 3.76667$, $B = 3.34666$, $Y_0 = 0.0001$, $Y_1 = 3.5$, $X_0 = 0.01$ and $X_1 = 0.01$.



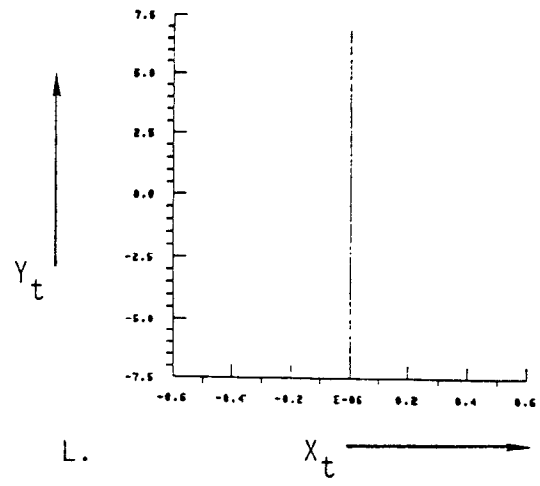
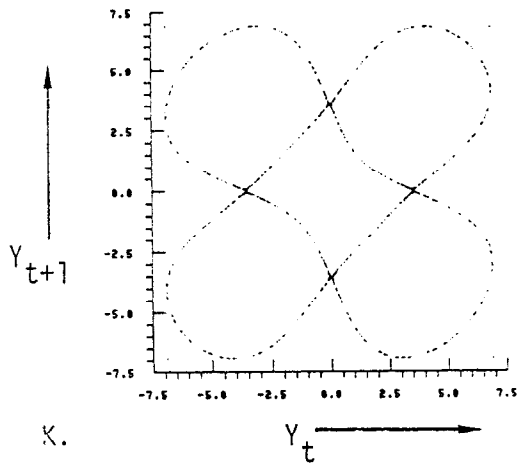
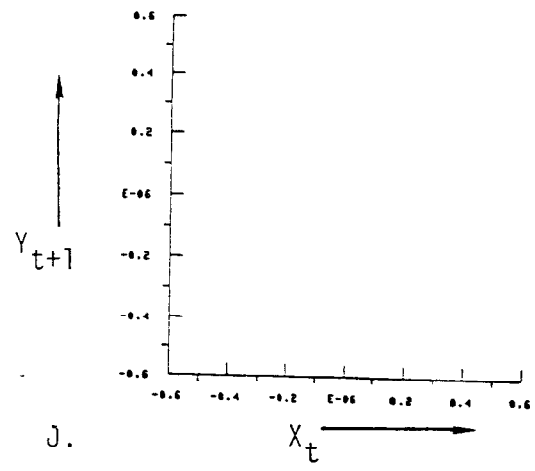
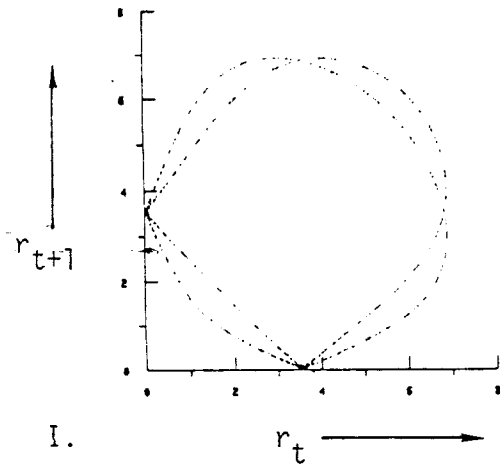
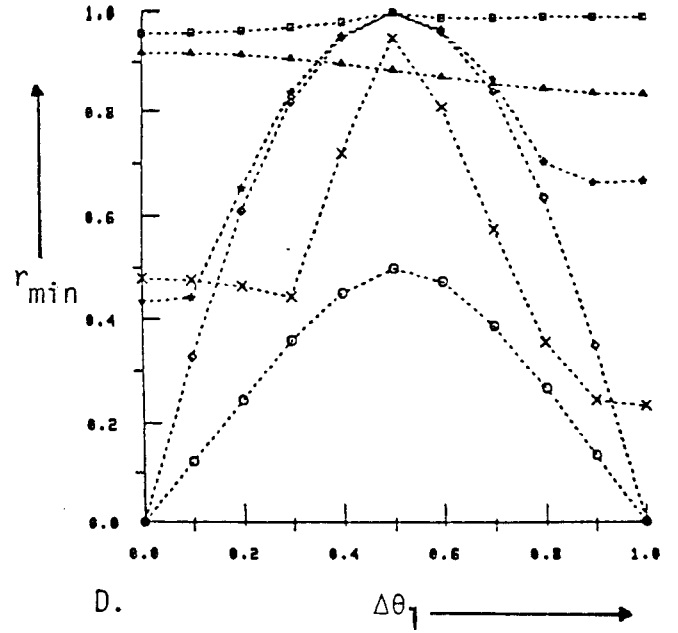
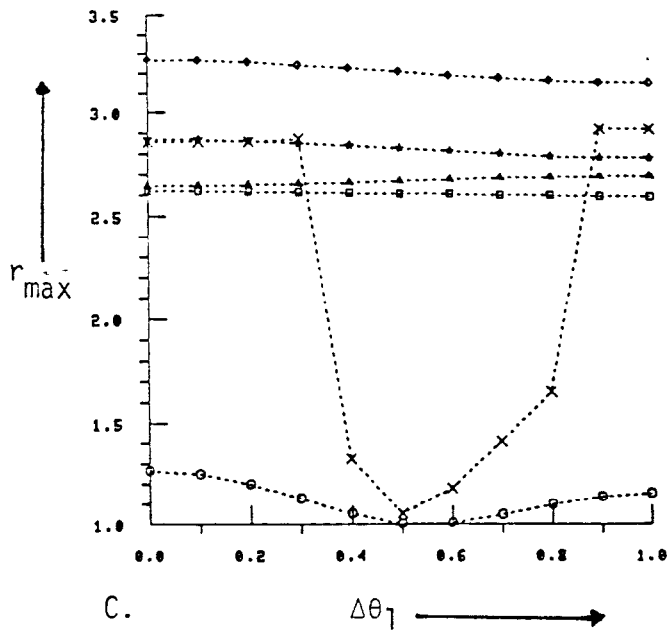
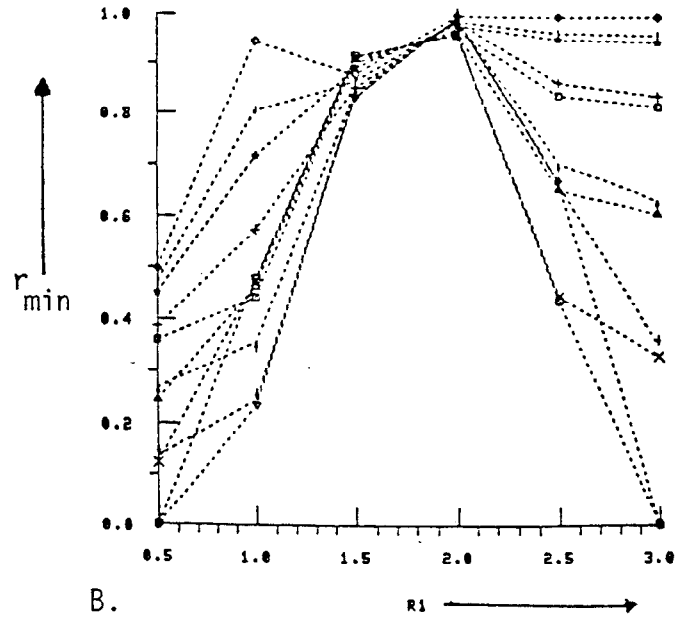
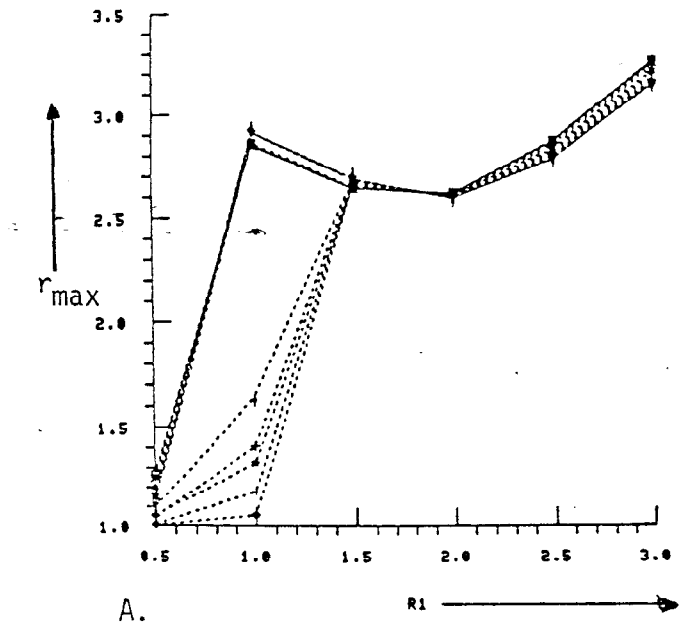


Fig. 4. Sequence A-D shows motion starting with $X_0 = 0.00001$, $X_1 = 3.5$, $Y_0 = 0.0$ and $Y_1 = 2.4749$, and I-L with $X_0 = 0.0$, $X_1 = 0.0$, $Y_0 = 0.00001$, and $Y_1 = 3.5$, with $Q = 3.76667$, and $B = 3.34666$.



	A&B	C&D	Symbol
1	0.0	0.5	o
2	$\pi/10$	1.0	x
3	$\pi/5$	1.5	Δ
4	$3\pi/10$	2.0	\square
5	$2\pi/5$	2.5	\star
6	$\pi/2$	3.0	\diamond
7	$3\pi/5$		
8	$7\pi/10$		+
9	$4\pi/5$		↑
10	$9\pi/10$		↓
11	π		▽

Figure 5a. Plot of maximum and minimum of r_t (after 1000 iterations), versus r_1 in A and B, respectively and $\Delta\theta$ in C and D, for $G = 3.7667$, $B = 1.67333$ and $r_0 = 0.50$.

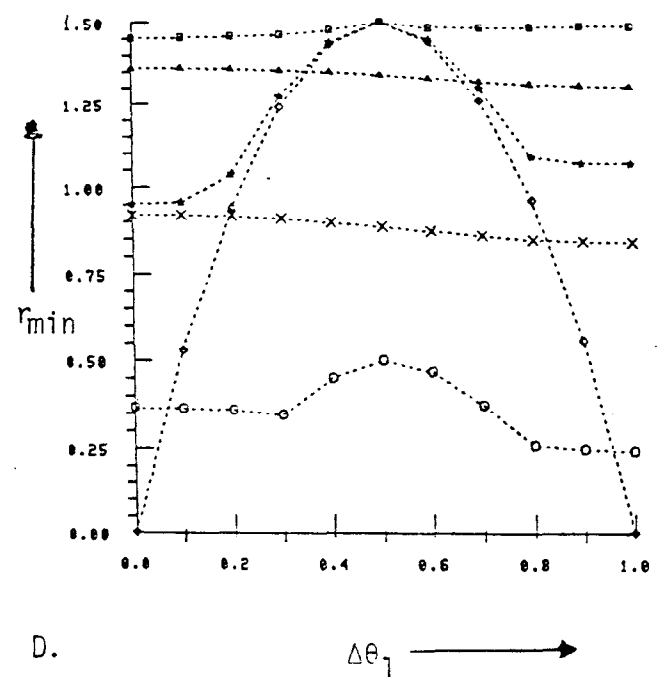
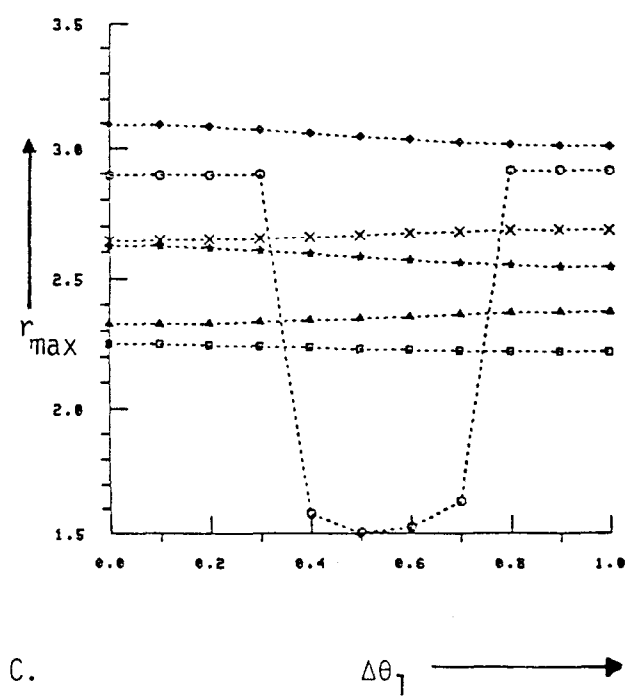
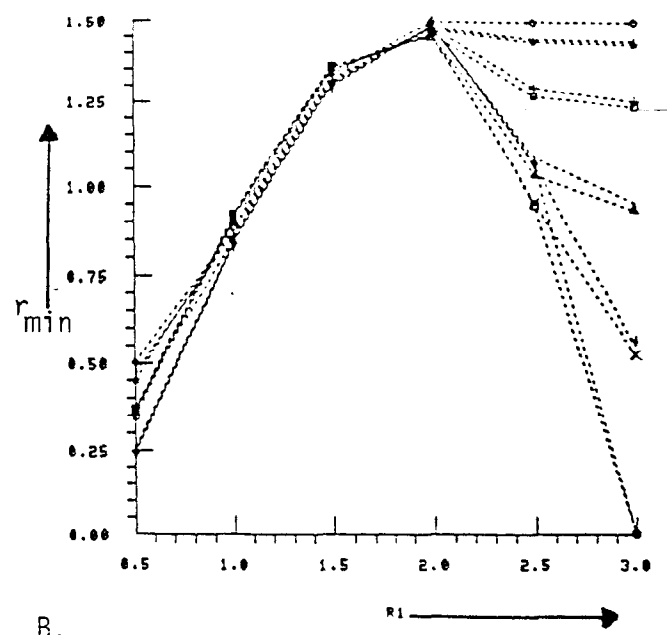
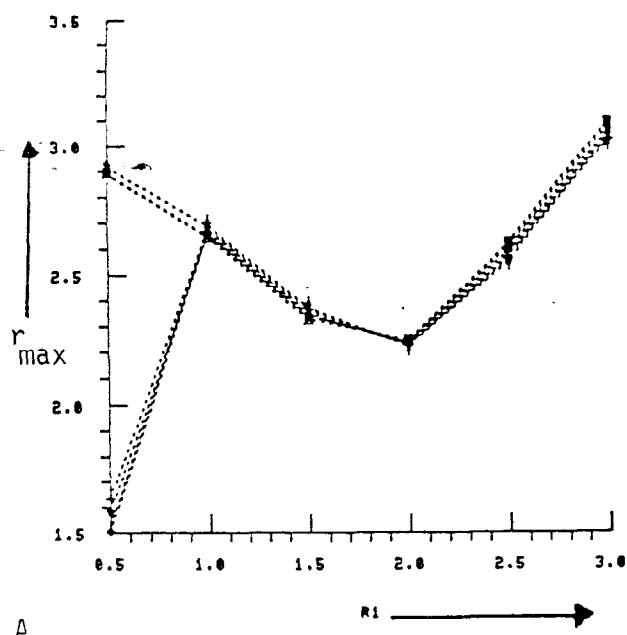


Figure 5b. Same as Figure 5a except $Q = 3.76667$, $B = 1.67333$ and $r_0 = 1.500$

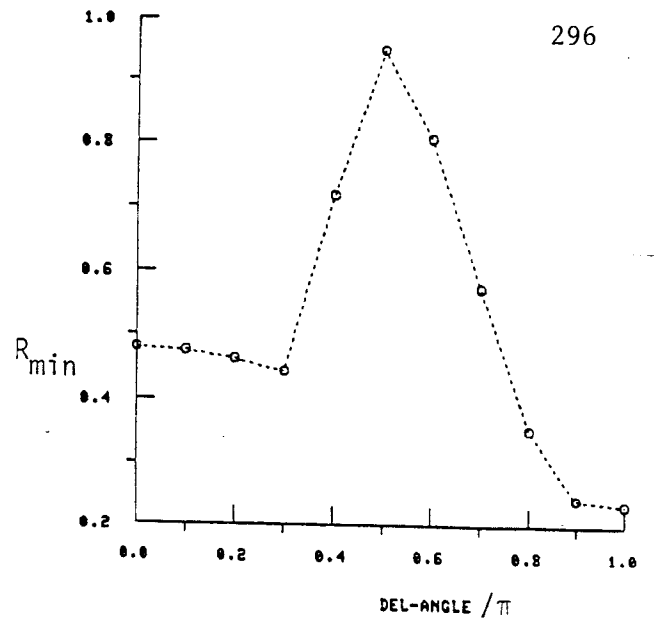
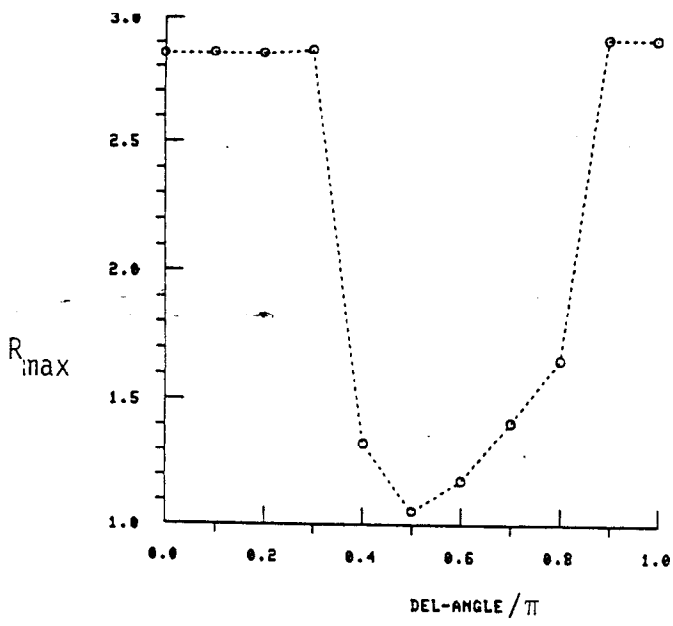
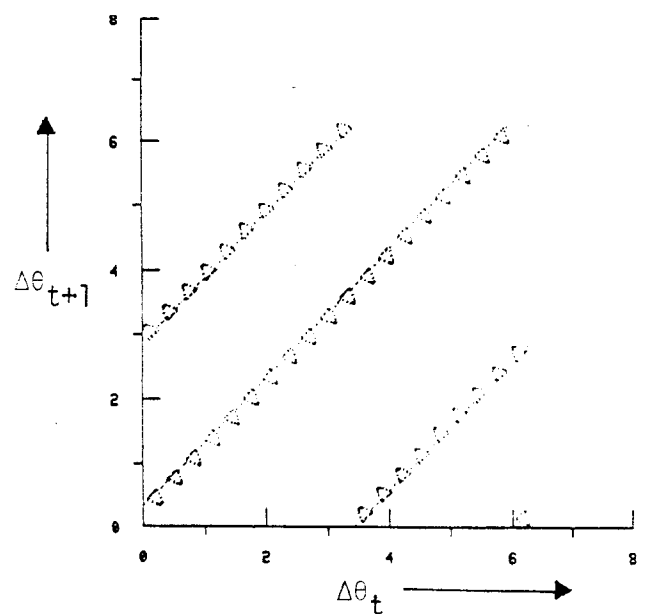
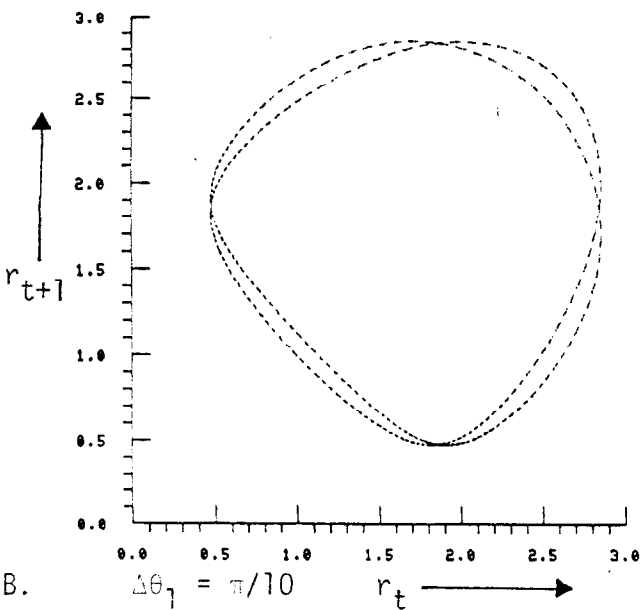
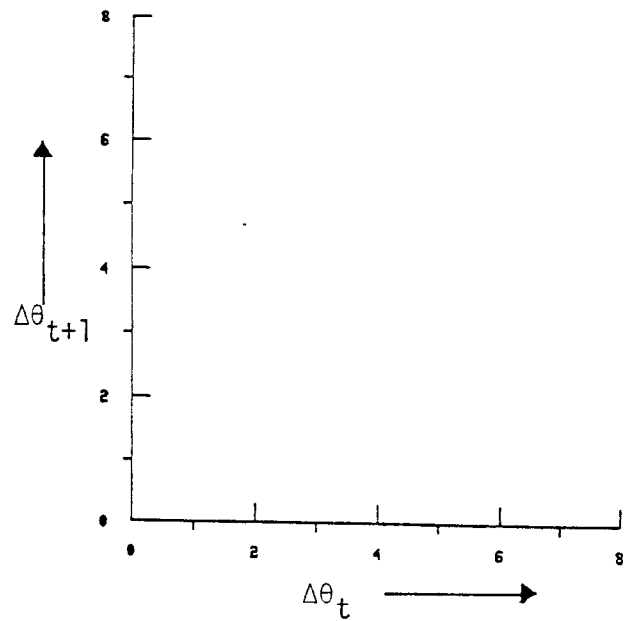
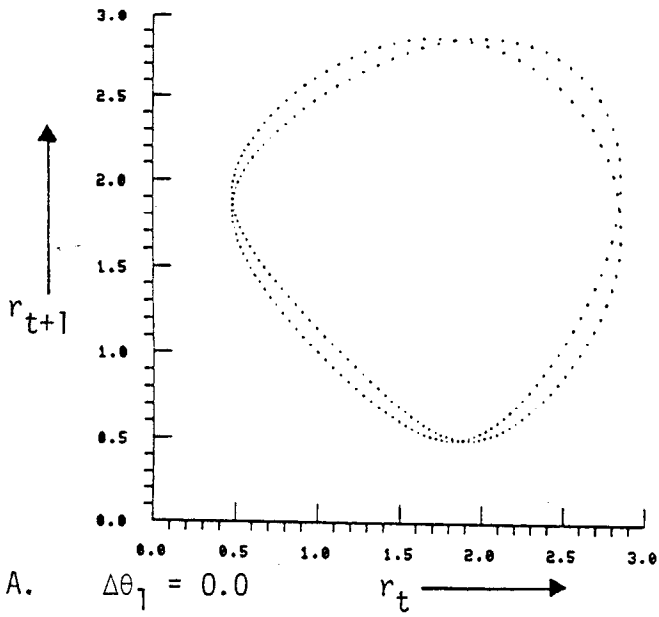
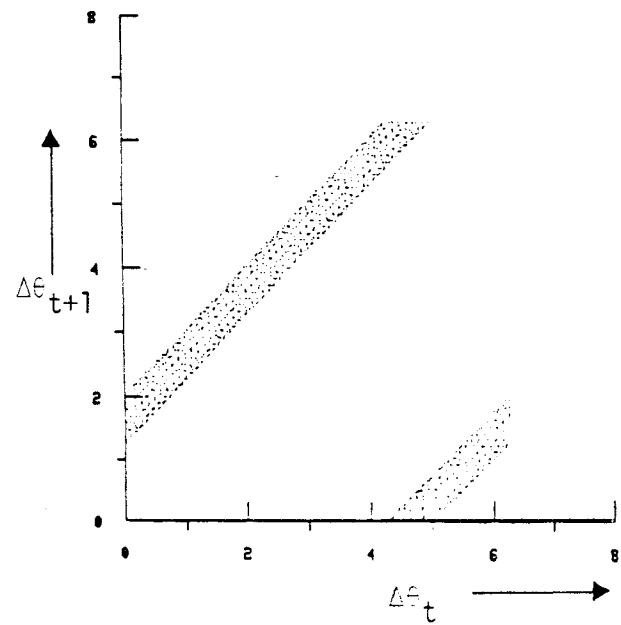
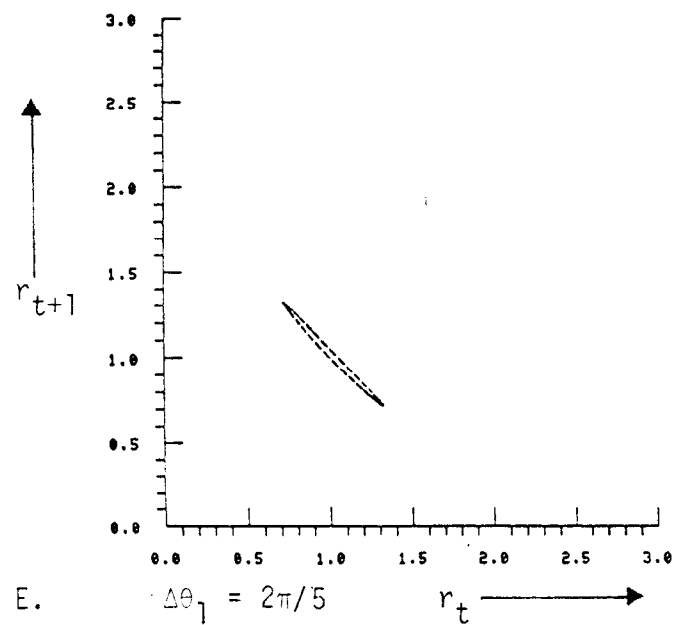
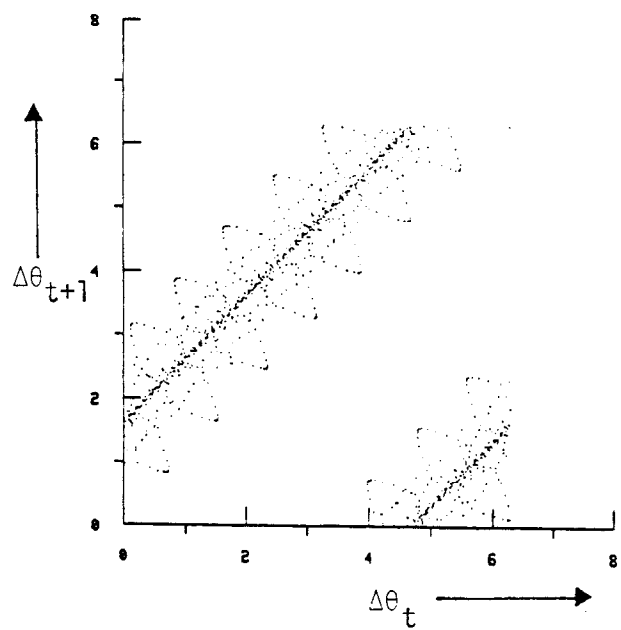
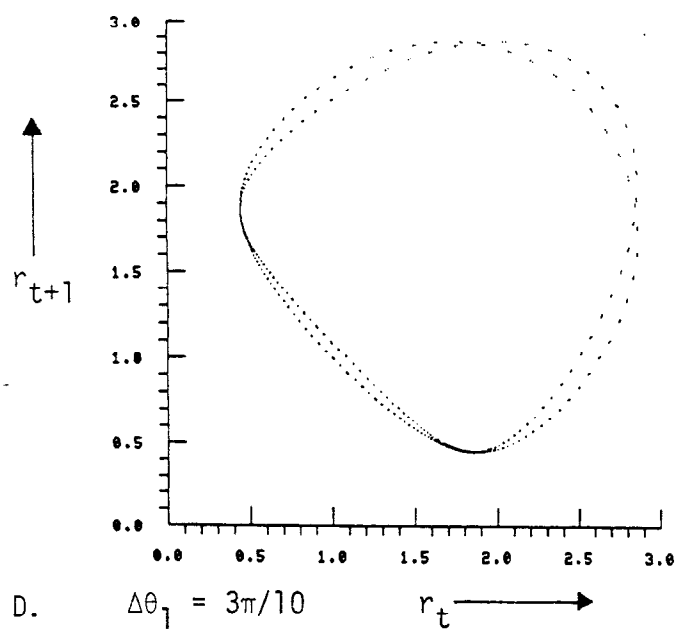
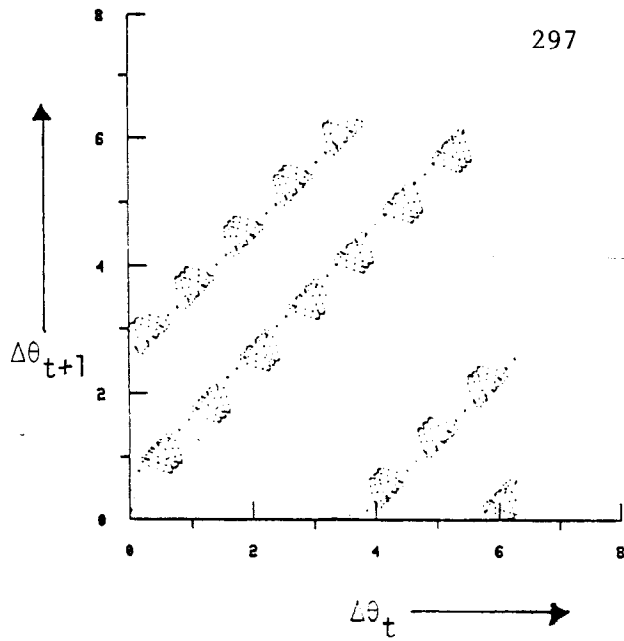
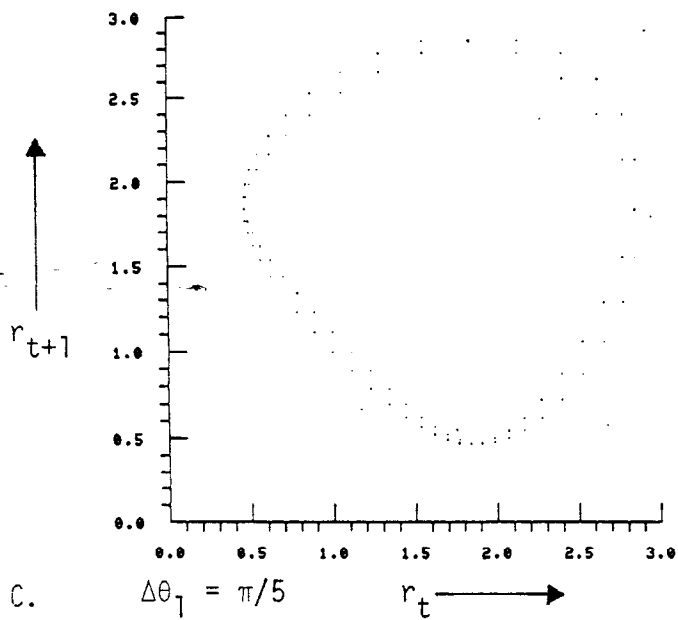
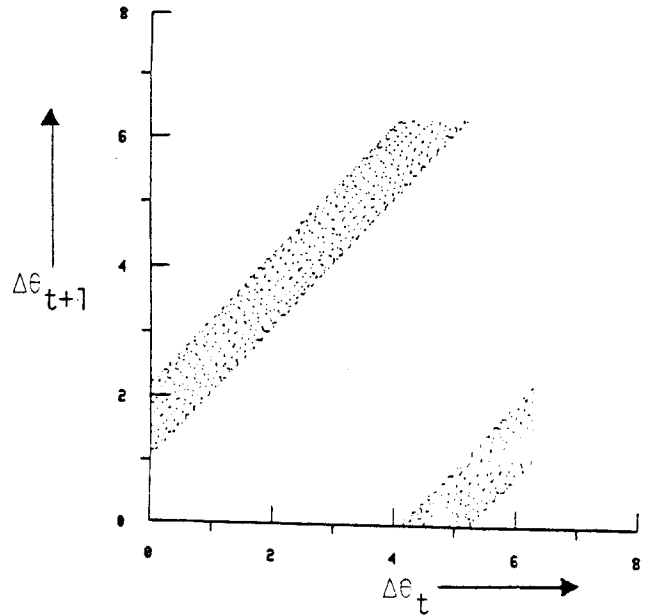
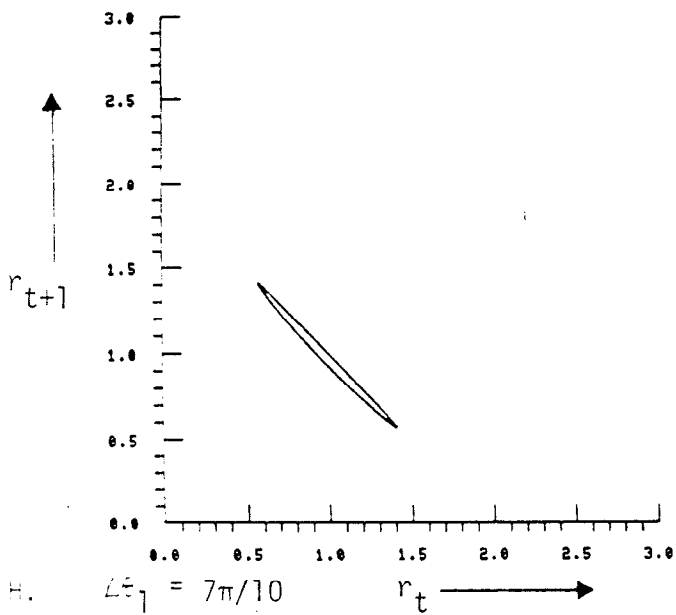
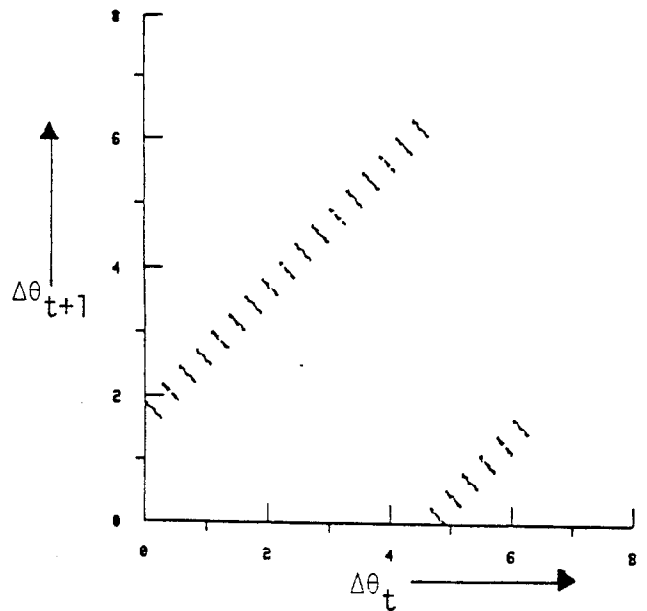
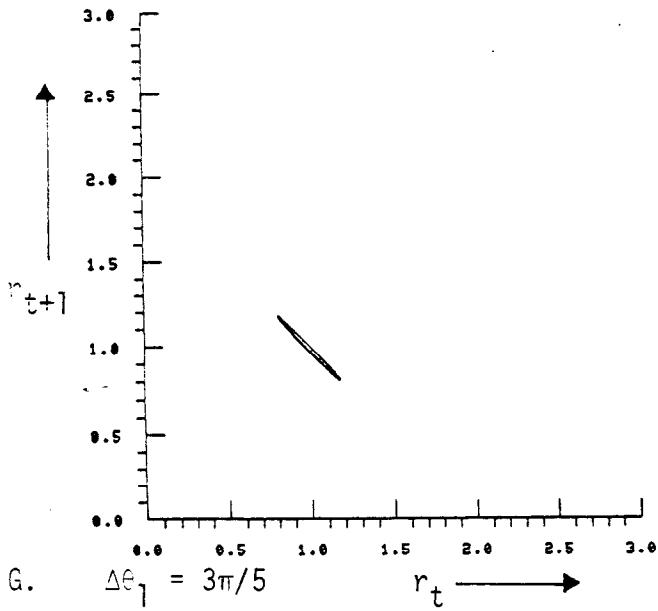
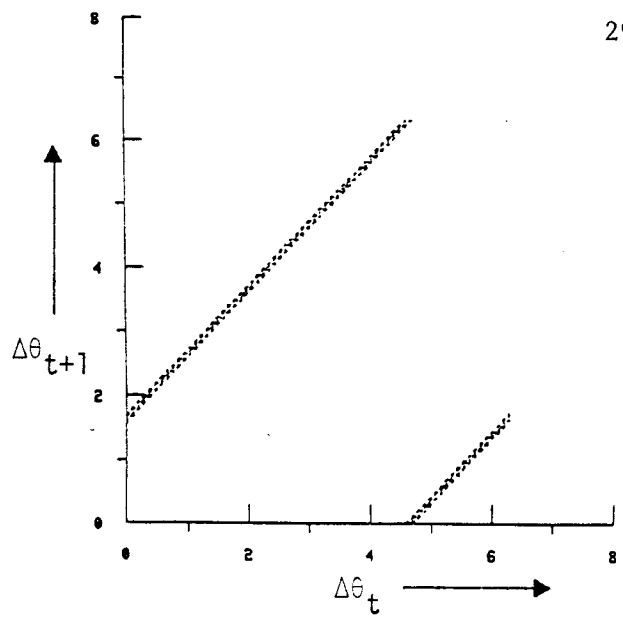
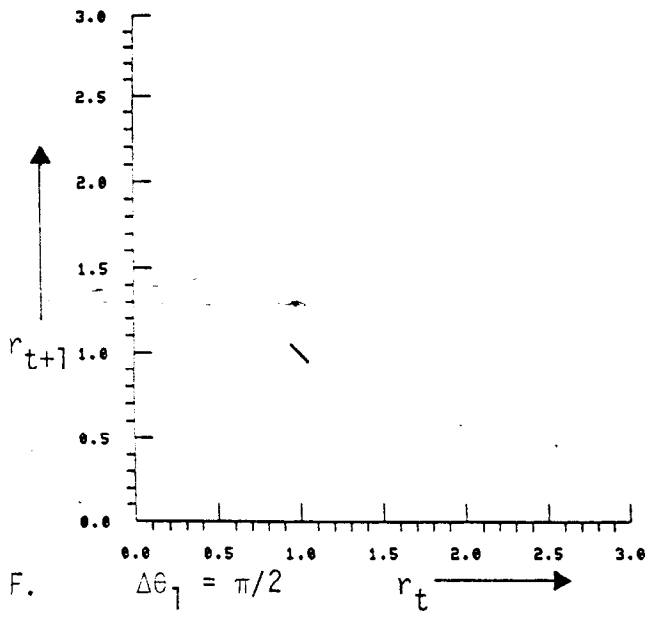
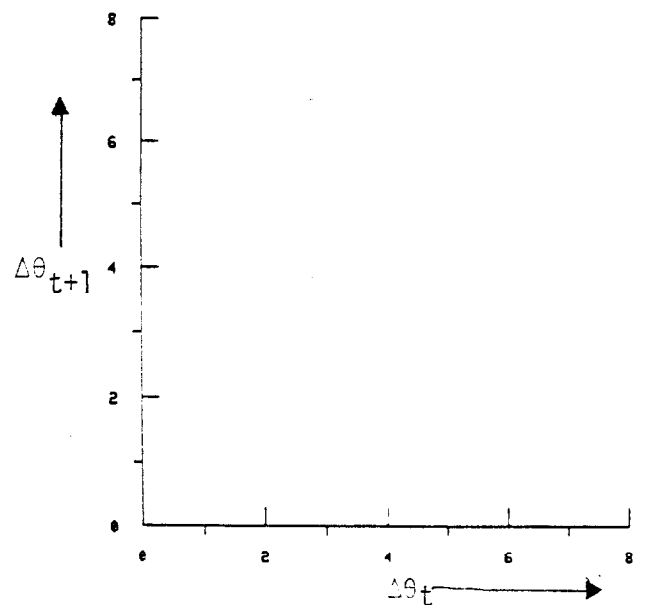
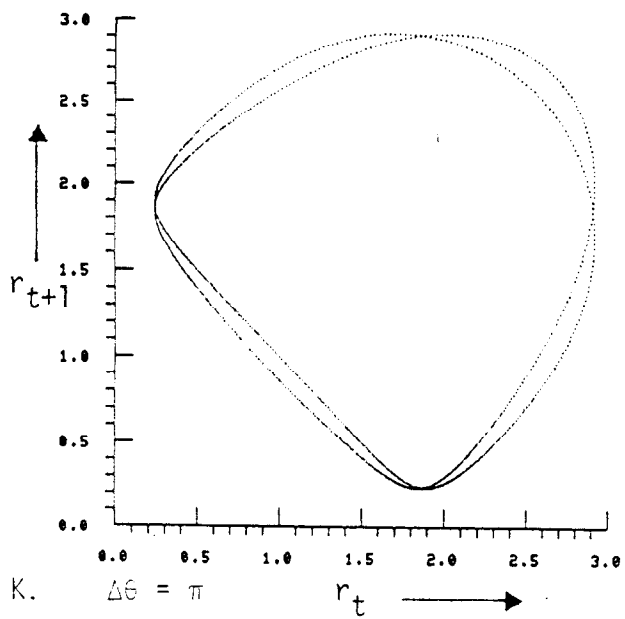
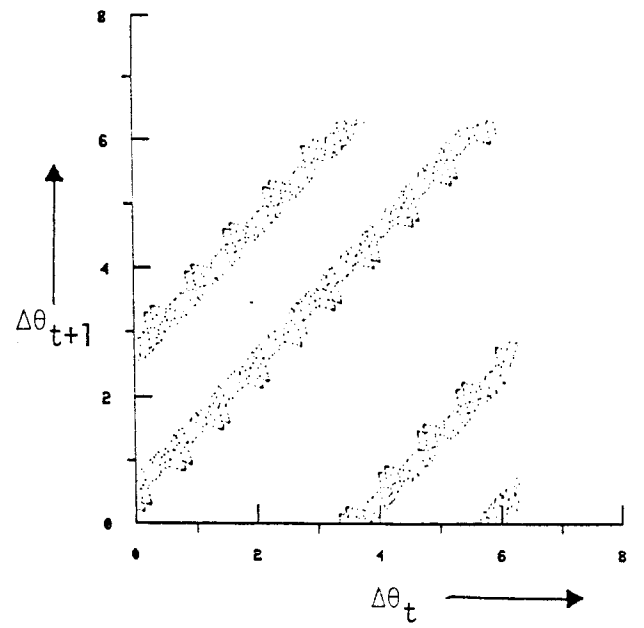
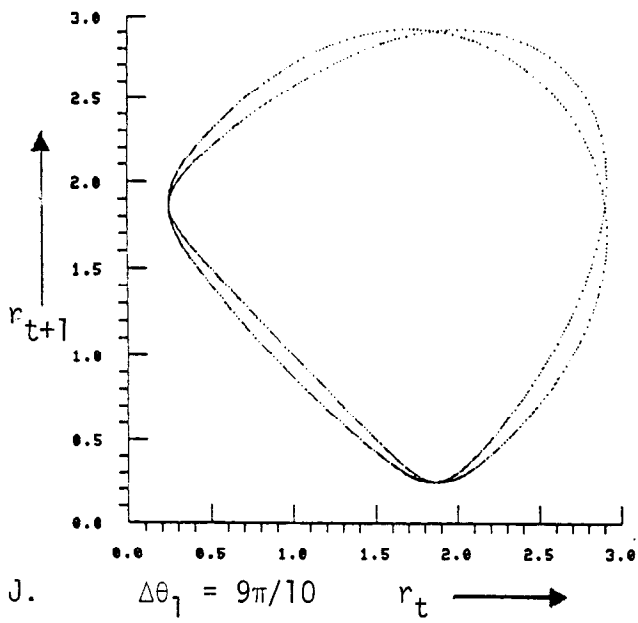
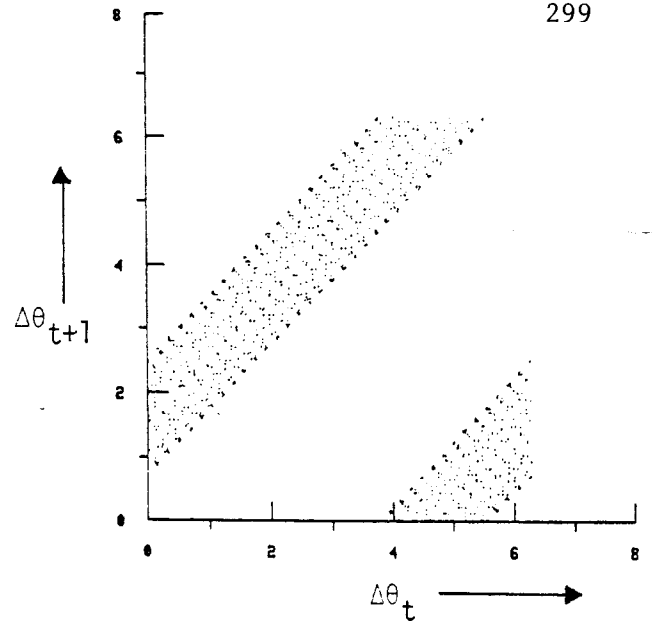
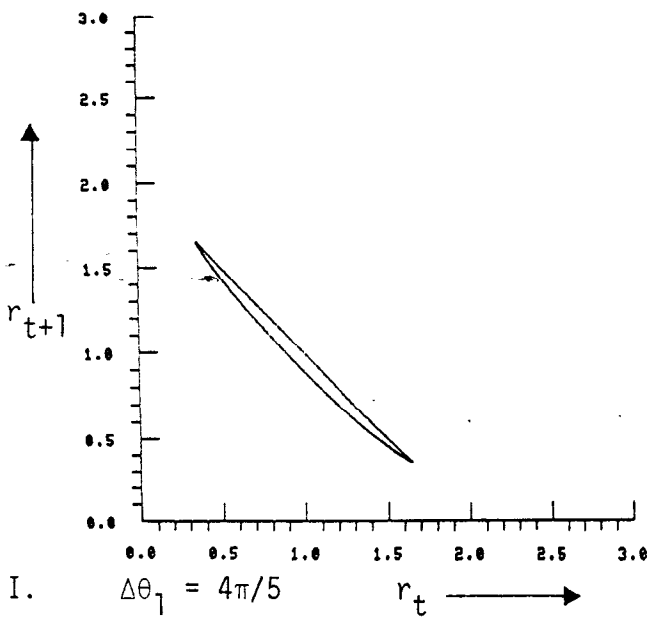


Fig.6. The max. and min. of r_t (after 1000 interactions) is plotted versus $\Delta\theta_1$ (the initial angle between the y and x direction), for $Q = 3.76667$, $r_0 = 1.0$, and $B = 1.67333$.









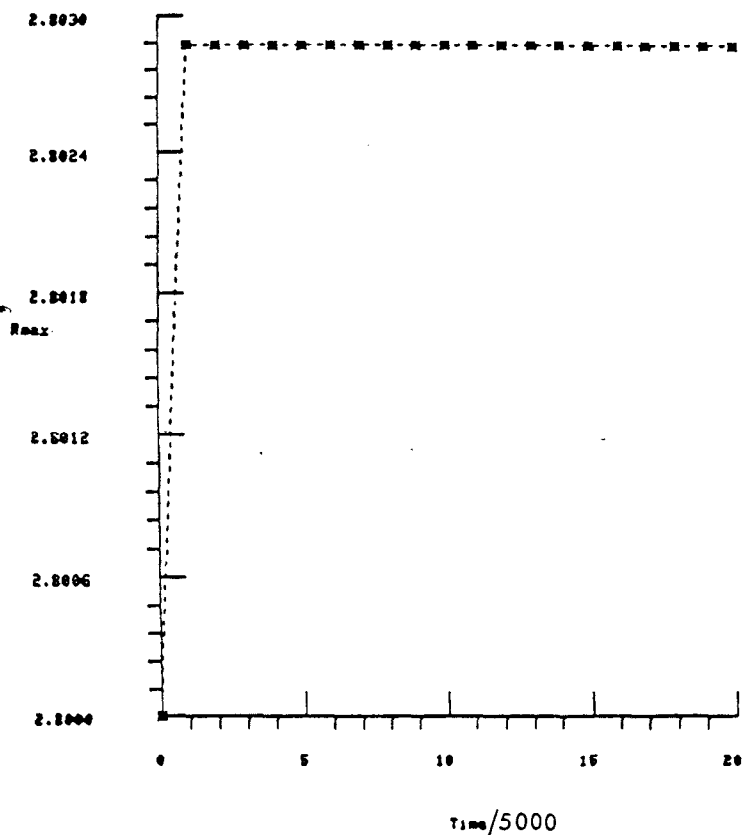


Fig. 7. Max. r_t plotted at 5000 iterations intervals $t_{\max} = 100,000$, for $Q = 3.76667$, $B = 3.34666$, $Y_0 = 1.0 \times 10^{-8}$, $r_1 = 2.80$, $\Delta\theta_1 = 0(o)$, $\pi/100(x)$, $\pi/10(\Delta)$, $\pi/2(\square)$, and $\pi(\star)$.

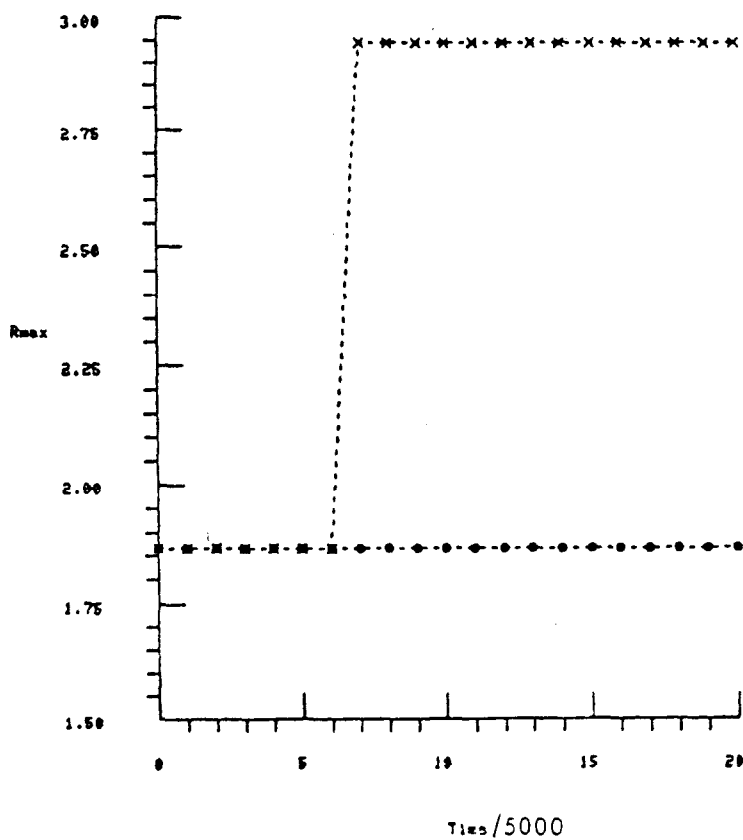
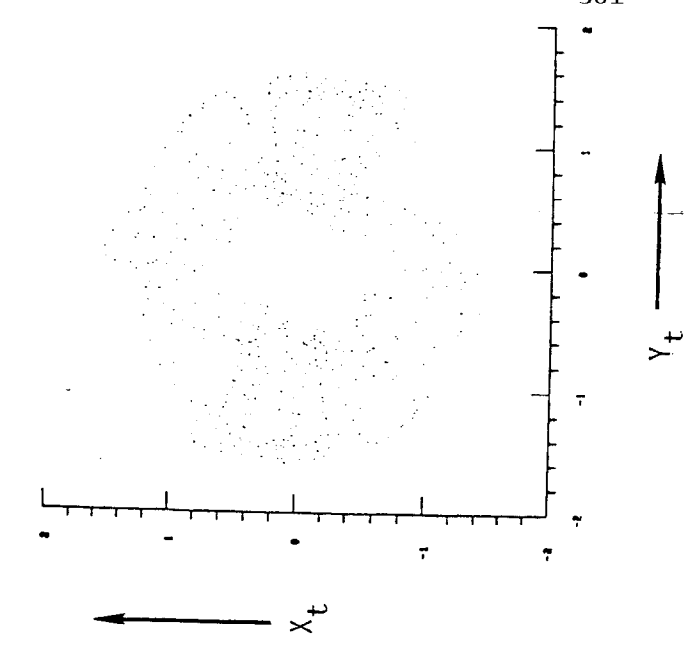
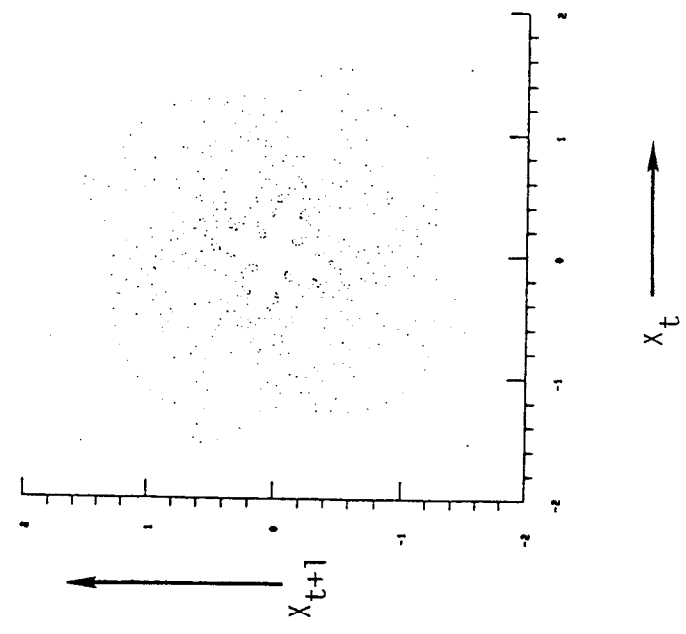
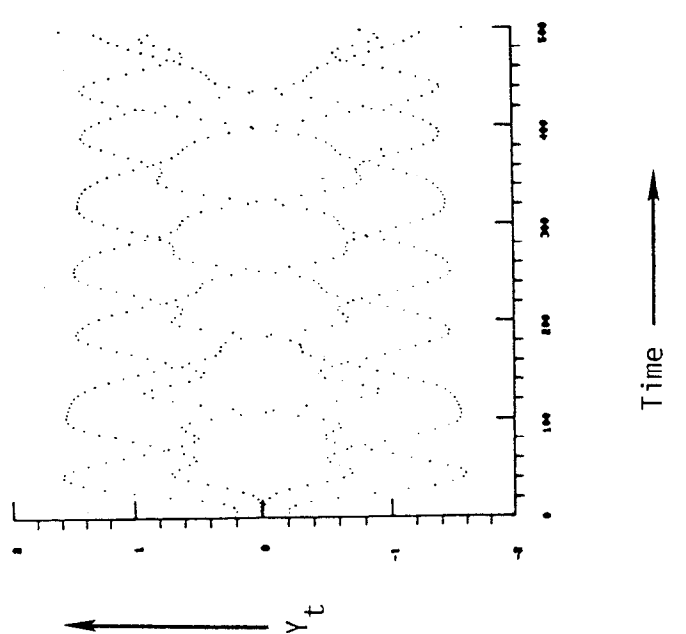
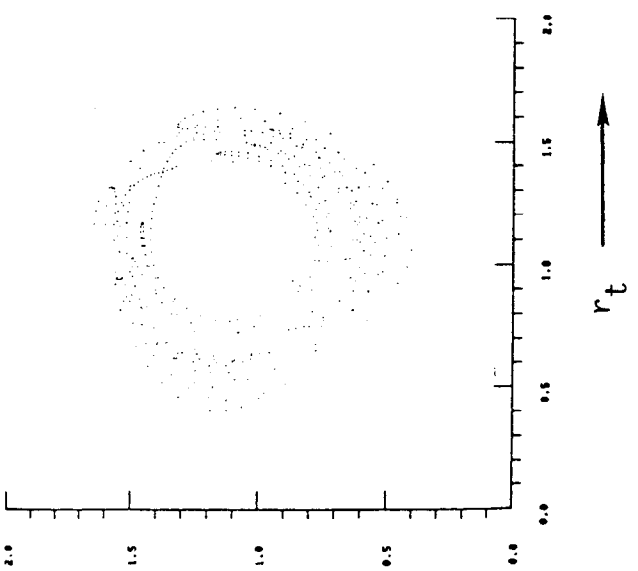
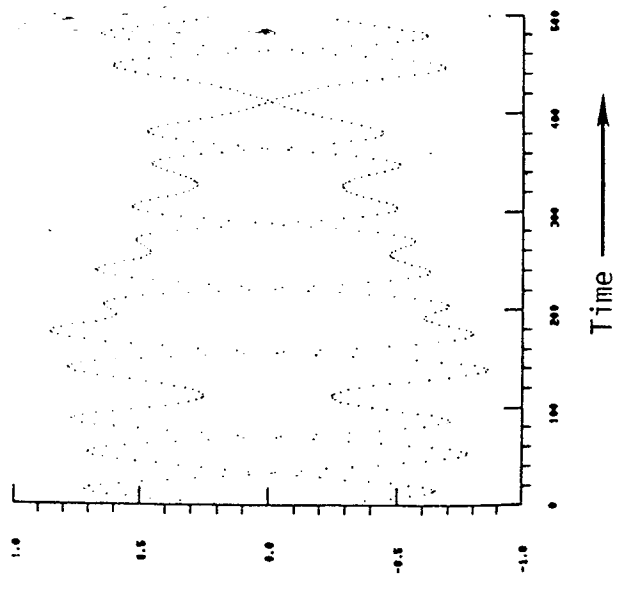


Fig. 8. Same as above but with $B = 1.67333$ and $r_1 = 1.8675$. Note jump after 30,000 interactions for $\Delta\theta_1 = \pi/100(x)$.



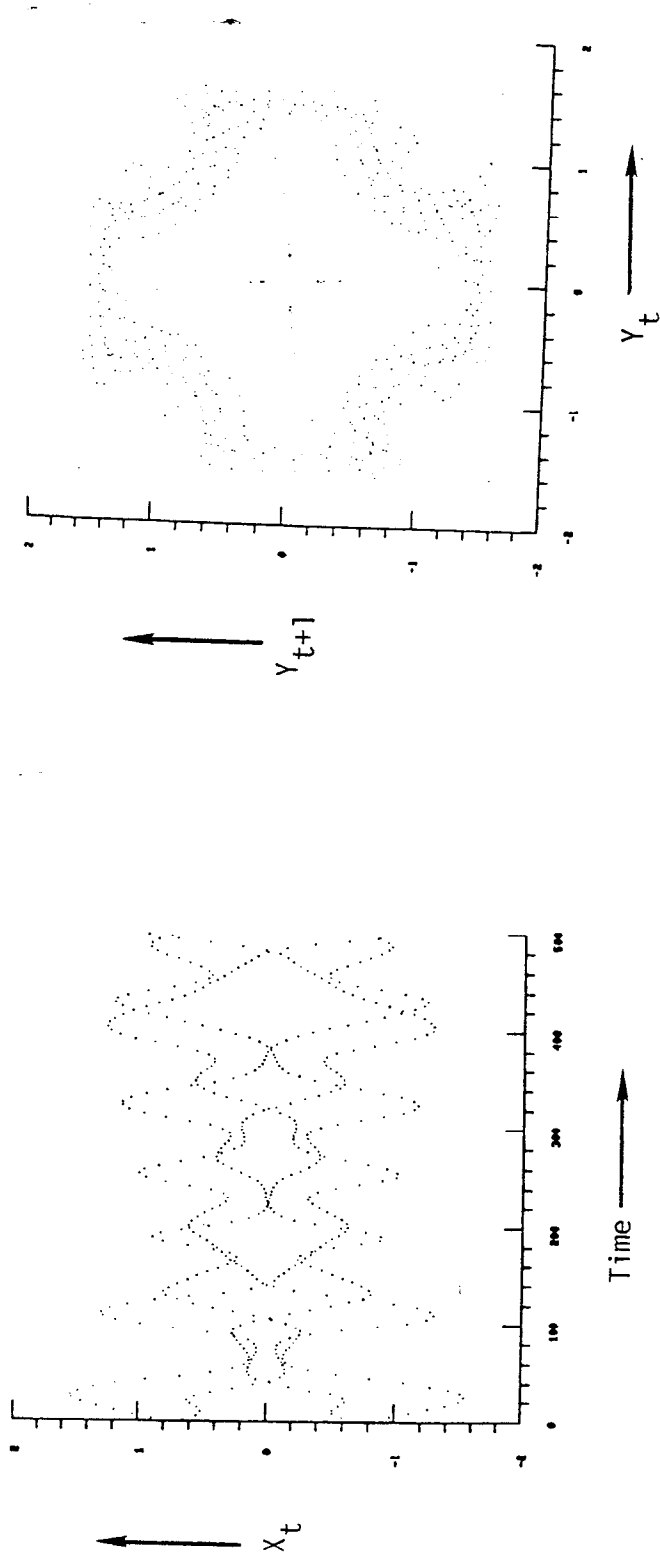


Fig. 9. Plots show complicated motion even in the r_t, r_{t+1} plane for $r_0 = 0.75, r_1 = 0.75, \theta_0 = \pi/2,$
 and $\theta_1 = 4.39823$, which corresponds to a $Y_0 = 0.0, Y_1 = -0.231763, X_0 = 0.75$ and $X_1 = -0.713292,$
 with $Q = 3.76667$ and $B = 3.34666$.

4. FUTURE STUDIES

Continuing effort is planned in the study of the beam-beam effects (and limits) for p-p and p- \bar{p} colliding beams in storage rings in two dimensions. We plan to find the parameter ranges (Δv , Q, etc.) and the size of the regions in phase space over which the ("weak") beam will be stable. If no regions of "stability" exist, which is Moser's belief..., expressed in Reference 1, we hope to obtain estimates of the time intervals needed for the amplitude of the motion to reach some specific value. As is apparent from the preceding discussion, a combination of numerical and analytic methods will be necessary as a result of the complexities arising from the higher dimensional phase space of two-dimensional beams.

A study of the stability regions for a one-dimensional beam-beam force in the presence of nonlinear synchrotron oscillations is also planned. The two-dimensional x-y beam problem and the one-dimensional beam with synchrotron oscillations may require similar numerical and analytical methods and the two efforts will complement each other.

After sufficient understanding is acquired for these two cases, we will attempt a study of the full two-dimensional beam with synchrotron oscillations.

5. CONCLUSION

This numerical study was undertaken as a first step into the area of interacting two dimensional beams. It was shown that although the motion of particles in a two-dimensional beam can be and usually are quite complicated, a systematic numerical study is possible. However, much additional numerical work is required before a clearer understanding of the complicated motion in two-dimensional beams can be attained.

6. ACKNOWLEDGMENT

The numerical calculations presented in this report were made in conjunction with the investigations of the beam-beam limit (numerically and analytically) of Dr. Robert H.G. Helleman. The author expresses his appreciation to Dr. Helleman for his assistance in this effort. The author acknowledges that some sections of this report were based closely on the articles of Dr. Helleman, References 2 and 9. This work was supported by D.O.E. under Contract EG-77-C-03-1538.

6. REFERENCES

1. Nonlinear Dynamics and Beam-Beam Interaction, Eds. M. Month and J. C. Herrera, Am. Inst. Phys. Conf. Proc., Vol. 57, (A.I.P., New York 1979).
2. R.H.G. Helleman, Ref. 1., pp. 236-256, cf., Appendix A, attached to this report.
3. J. C. Herrera, Ref. 1, pp. 29-41.
4. J. C. Herrera, M. Month, and R. F. Peierls, Ref. 1, pp. 202-209.
5. Topics in Nonlinear Dynamics, Ed. S. Jorna, Am. Inst. Phys. Conf. Proc., Vol. 46 (A.I.P., New York, 1978).
6. M. V. Berry, Ref. 5, pp. 16-120.
7. J. Tennyson, "The Instability Threshold for Bunched Beams in Isabelle," Ref. 1, pp. 158-193.
8. J. L. Tennyson, M. A. Lieberman, A. J. Lichtenberg, "Diffusion in Near Integrable Hamiltonian Systems with Three Degrees of Freedom," Ref. 1, pp. 272-301.
9. R.H.G. Helleman, "Nonlinear Beam Dynamics of Storage Rings and Accelerators," a Proposal submitted to U.S. Department of Energy, May 1980.

APPENDIX A

Additional Graphs

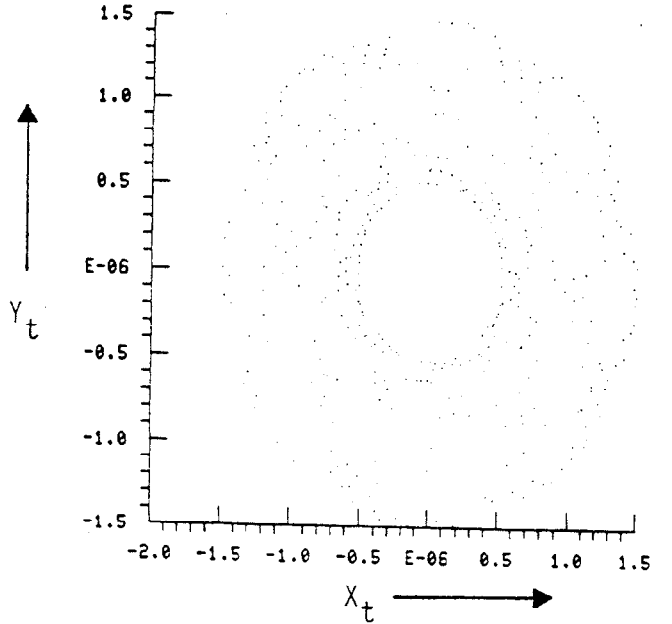
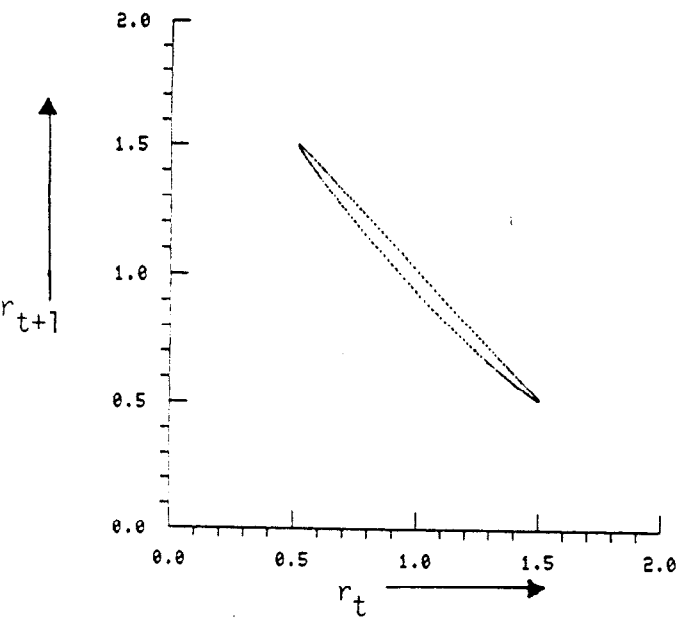
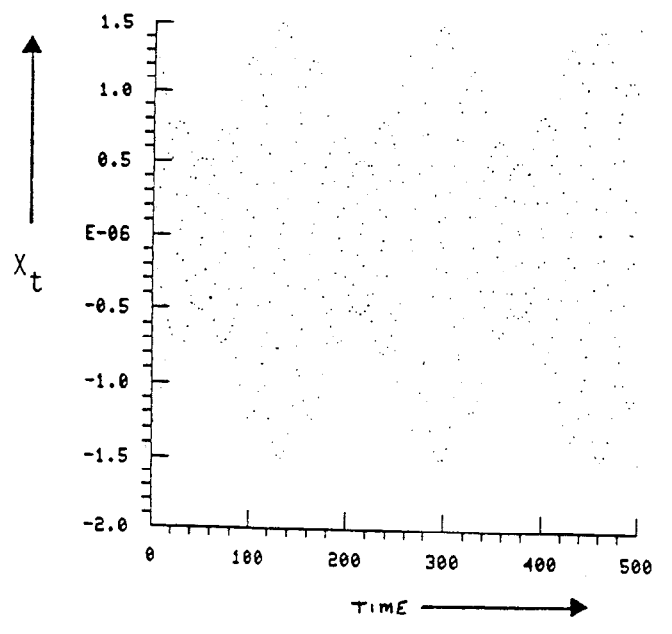
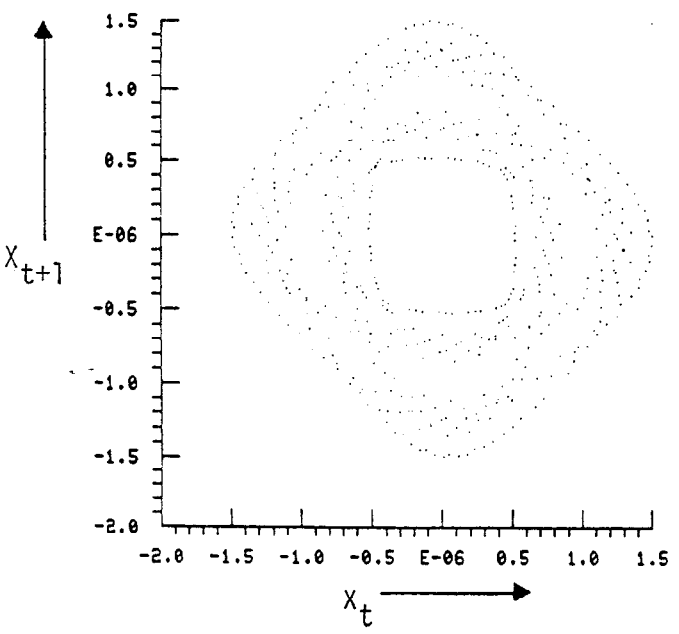
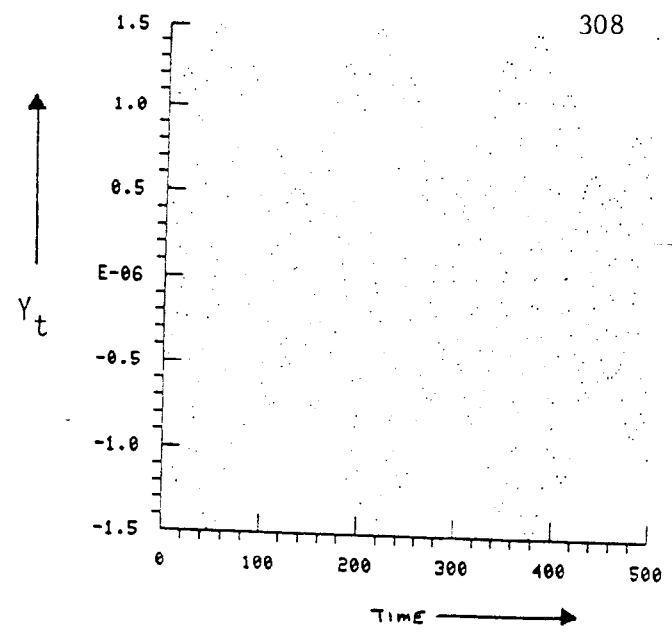
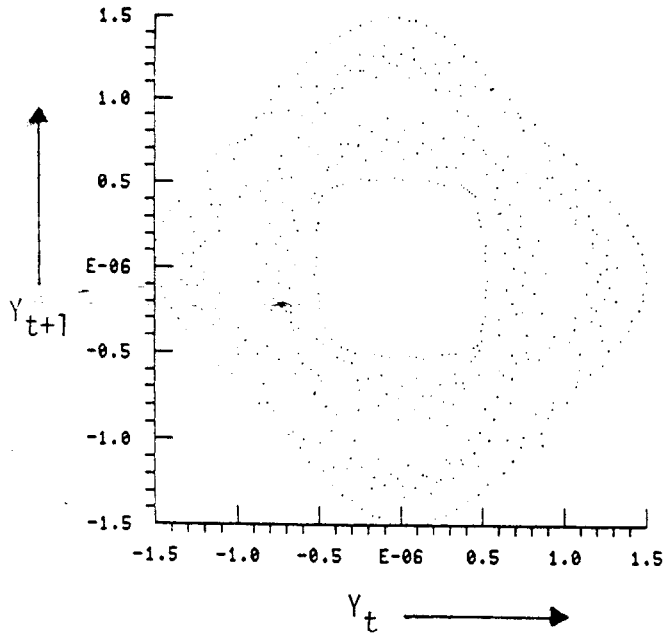


Fig.A1. Motion below hyperbolic fixed point with $Q = 3.76667$, $B = 3.34666$, $Y_0 = 0.00001$, $Y_1 = 1.29$, $X_0 = 0.6$ and $X_1 = -0.600$.

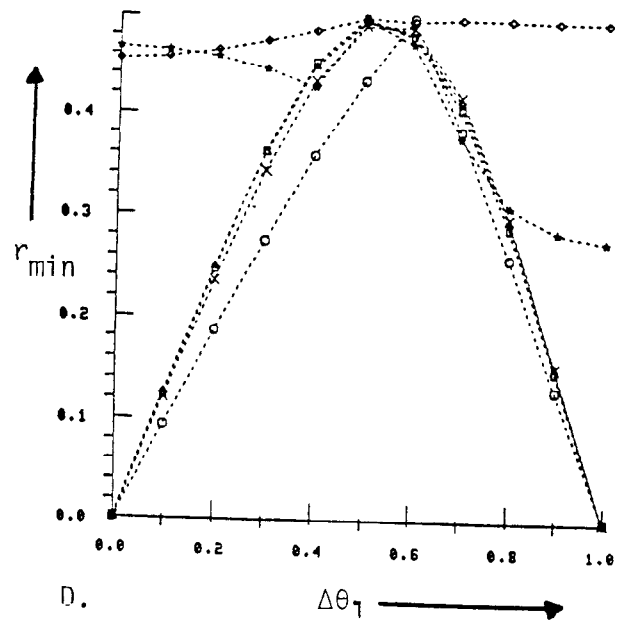
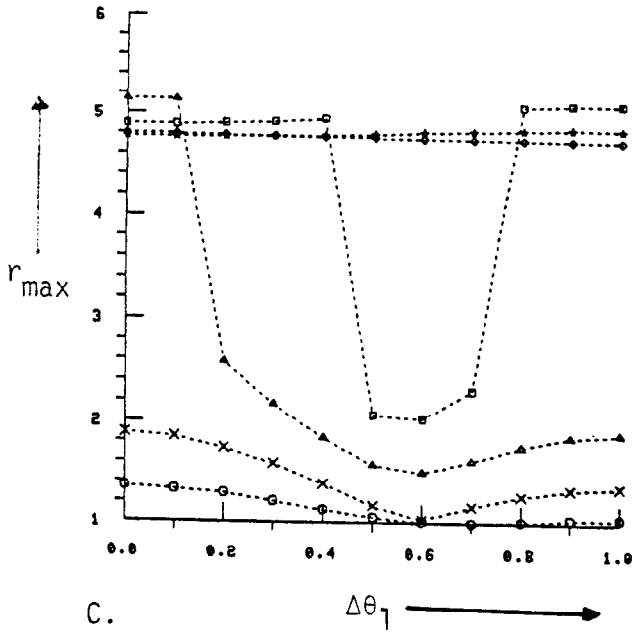
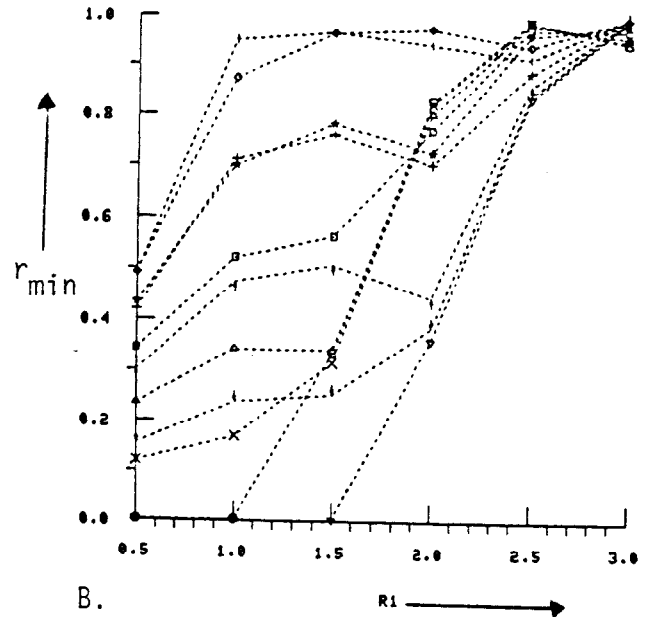
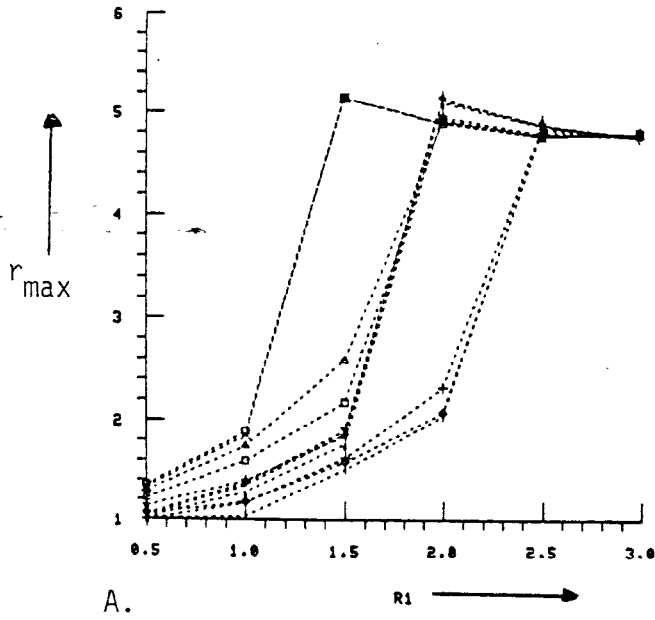


Figure A2. Same as Figure 4a, except $Q = 3.76667$, $B = 3.34666$, and $r_1 = 0.50$.

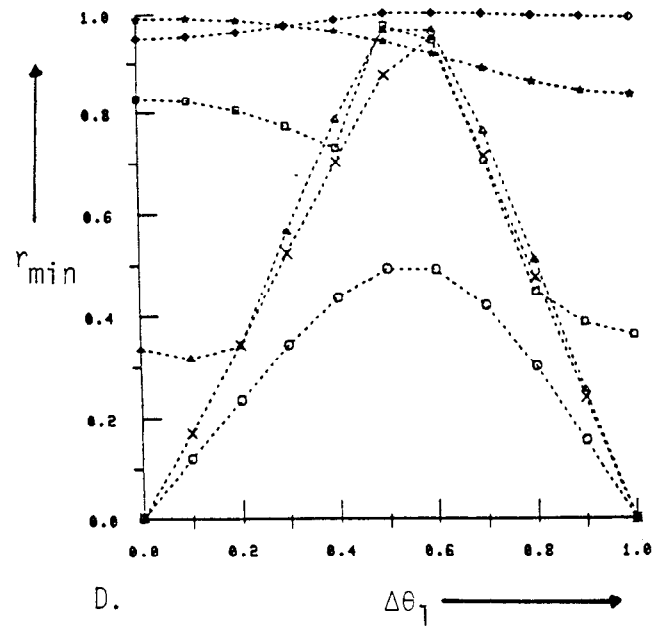
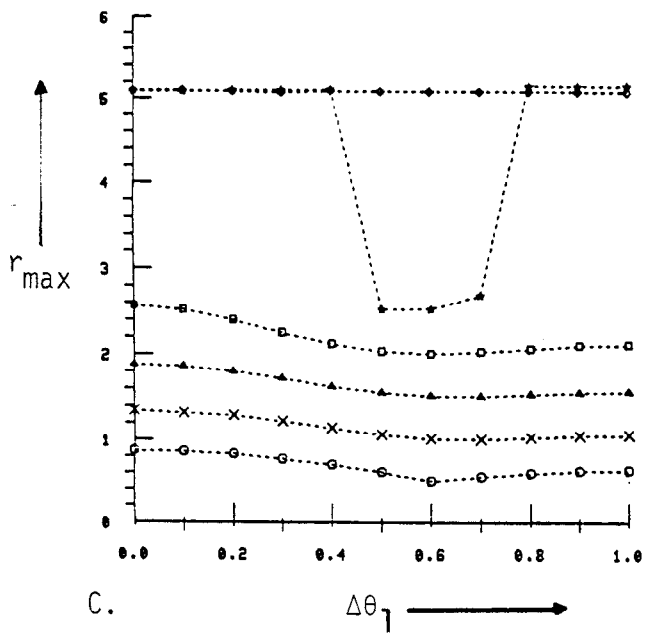
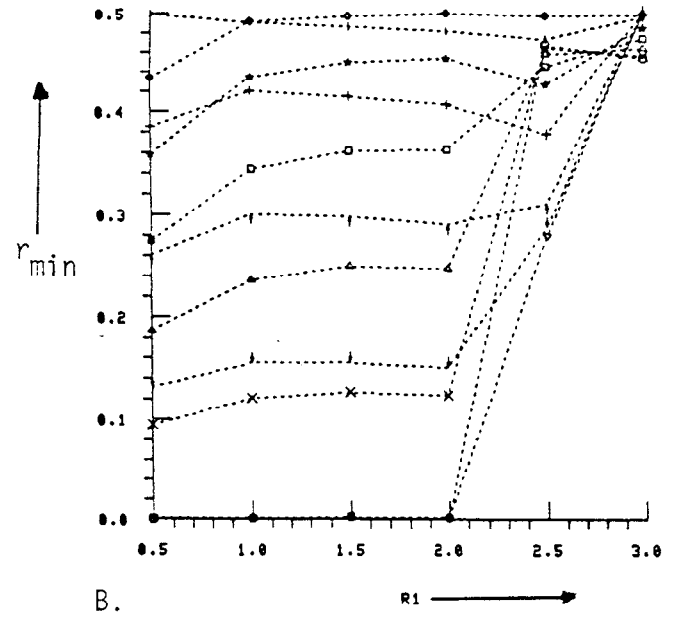
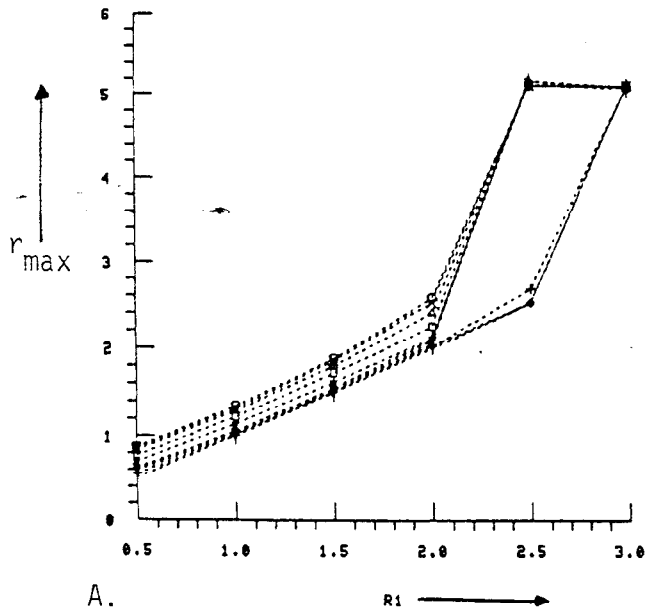


Figure A3. Same as Figure 4a, except $Q = 3.76667$, $B = 1.67333$ and $r_0 = 1.000$.

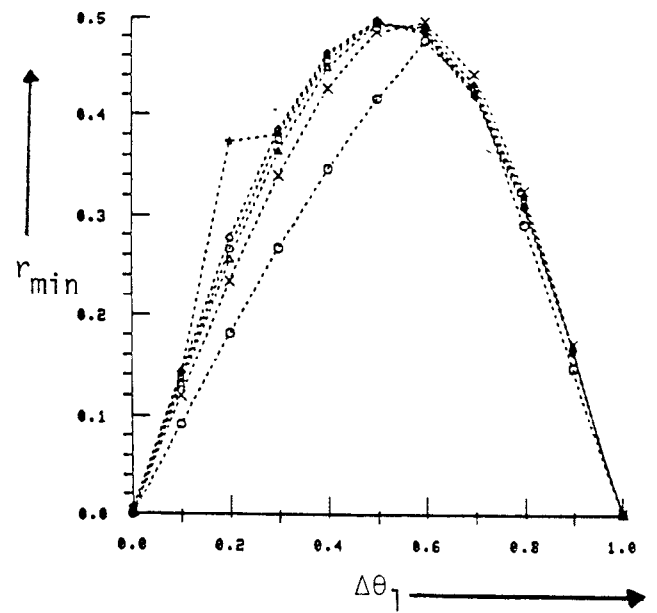
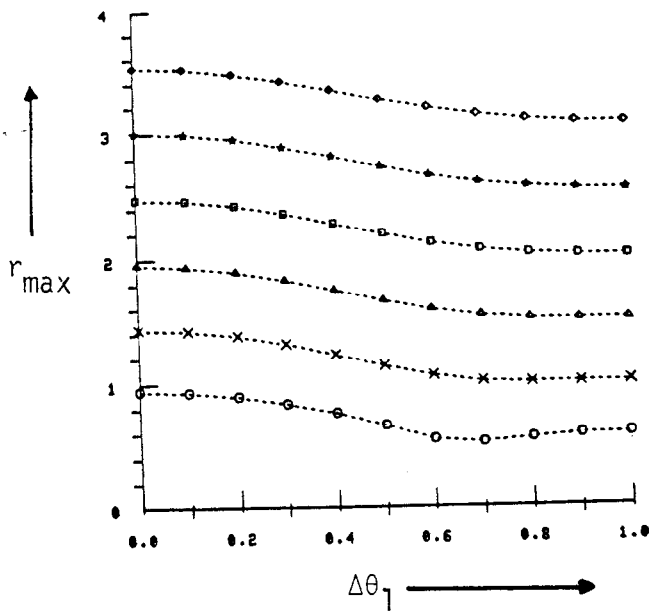
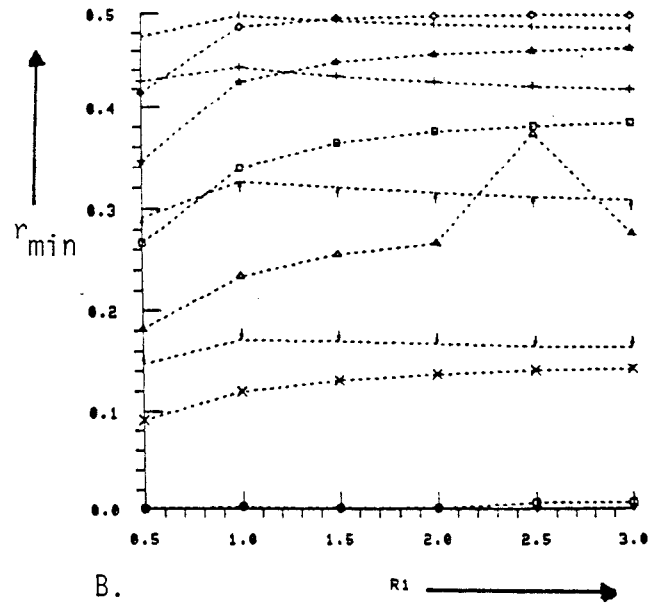
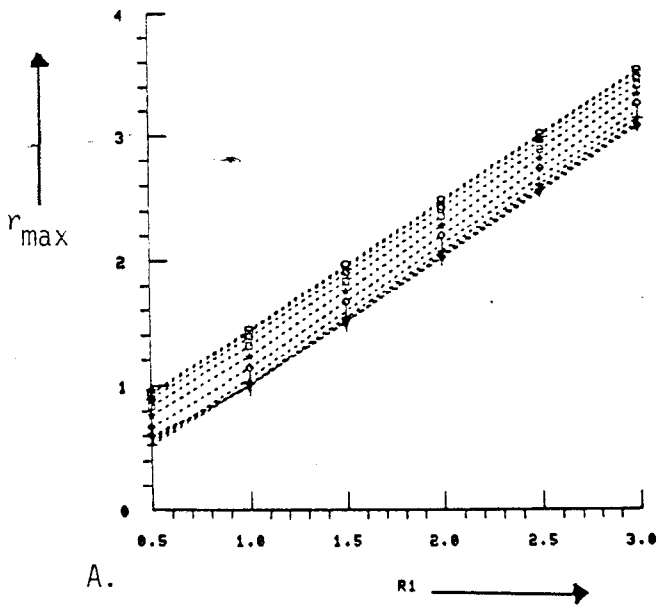


Figure A4. Same as Figure 4a, except $Q = 3.7000$, $B = 1.07528$ and $R_0 = 0.50$.

NONLINEAR HILL'S EQUATIONS AND THE
BEAM-BEAM INTERACTION[†]

PIERRE A. VUILLERMOT^{*}

School of Mathematics
Georgia Institute of Technology
Atlanta, Georgia 30332

[†]Lecture delivered at the "Seminar on the Beam-Beam Interaction" on May 22nd and 23rd, 1980, at the Stanford Linear Accelerator Center, Stanford, CA 94305.

^{*}Work supported in part by the U.S. Department of Energy under contract EG-77-C-03-1538.

I. INTRODUCTION.

Nonlinear Hill's equations of the form

$$z''(\theta) + n(\theta)z(\theta) = F(\theta; z) \quad (\text{I.1})$$

frequently occur in the description of betatron oscillations in cyclic accelerators and in intersecting storage rings ([1] - [3]). In equation (I.1), θ stands for the azimuth around the machine (of radius 1), n denotes a periodic function with (minimal) period $T \leq 2\pi$, while F generally depends nonlinearly on z and also periodically on θ with, however, a minimal period T' in general different from T . In this paper, we present without (detailed) proofs new results regarding the stability properties of a class of equations of the form (I.1), relevant to the problem of the beam-beam interaction in the "weak-strong" approximation. Specifically, we discuss new inequalities for the corresponding action functional, valid in particular whenever the strong beam has an anisotropic (ribbon-like) Gaussian current density. We then solve the variational problem by direct methods, establish its connection with the existence problem of periodic orbits, and finally briefly indicate how to construct the minimizing sequences involved. A general theory, along with complete proofs, will appear in [4].

2. A CLASS OF NONLINEAR HILL'S EQUATIONS AND THE "WEAK-STRONG"
BEAM-BEAM INTERACTION: A VARIATIONAL FORMULATION.

Consider a continuous periodic function Δ with minimal period 2π and let $W_{2,2\pi}^1$ be the space of all real square integrable functions z on $[0,2\pi]$ that have a square integrable (generalized) derivative z' ; equip $W_{2,2\pi}^1$ with the norm

$$|||z|||_{1,2}^2 = ||z||_2^2 + ||z'||_2^2 \quad (2.1)$$

where

$$||z||_2^2 = \int_0^{2\pi} z^2(\theta) d\theta \quad \text{and} \quad ||z'||_2^2 = \int_0^{2\pi} (z')^2(\theta) d\theta \quad (2.2)$$

Now consider a function G from $W_{2,2\pi}^1$ into itself which satisfies the following properties:

$$(1) \quad 0 \leq G(z) \leq \frac{z^2}{2} \quad \text{for all} \quad z \in W_{2,2\pi}^1.$$

(2) G is concave in z^2 ; in other words, there exists a function H such that

$$H(x) = G(z) \quad (2.3)$$

where $x = z^2$, which satisfies the inequality

$$H(\lambda x + (1-\lambda)y) \geq \lambda H(x) + (1-\lambda)H(y) \quad (2.4)$$

for all nonnegative x and y in $W_{2,2\pi}^1$ and for each $\lambda \in (0;1)$.

(3) G is (Fréchet)-differentiable on $W_{2,2\pi}^1$ with bounded derivative

$$G'(z) = F(z) \quad (2.5)$$

In other words one has the relation

$$G(z+v) - G(z) = F(z)v + R(z;v) \quad (2.6)$$

for all $v \in W_{2,2\pi}^1$, where $R(z;v)$ is the remainder satisfying the relation

$$\lim_{\|v\|_{1,2} \rightarrow 0} \frac{R(z;v)}{\|v\|_{1,2}} = 0 \quad (2.7)$$

For z twice continuously differentiable on $[0, 2\pi]$ we then consider the differential equation

$$z'' + nz = \beta \Delta F(z) \quad (2.8)$$

where n is a positive real number and β a real parameter. We are concerned with the stability properties of equation (2.8) in terms of n and β ; in other words we would like to know for what values of n and β all the solutions of (2.8) are bounded (stability), and for which ones at least one of the solutions is unbounded (instability). Likewise, we would like to know how the solutions of (2.8) bifurcate away from those of the linear equation corresponding to $F(z) = z$ in (2.8). In this paper, we shall restrict our attention to the existence problem

of periodic orbits and address ourselves to these more general questions in [4].

There are two elementary examples that have motivated this study in the first place, for which G satisfies the properties (1)-(3) above.

EXAMPLE 1: The linear case. We have $F(z) = z$ in (2.8); we may then choose $G(z) = \frac{z^2}{2}$ and thereby $H(x) = \frac{x}{2}$; properties (1)-(3) are here obvious.

EXAMPLE 2: The anisotropic (ribbon-like) Gaussian beam. In this case we have $F(z) = \text{erf}(z)$ (error function), namely

$$F(z) (\theta) = 2\pi^{-1/2} \int_0^{z(\theta)} \exp[-t^2] dt \quad (2.9)$$

for $z \geq 0$, and $F(-z) = -\text{erf}(z)$ otherwise (see [1]-[3]). We then may choose

$$G(z) = z \text{erf}(z) + \pi^{-1/2} (\exp[-z^2] - 1) \quad (2.10)$$

and consequently

$$H(x) = \sqrt{x} \text{erf}(\sqrt{x}) + \pi^{-1/2} (\exp[-x] - 1) \quad (2.11)$$

An elementary calculation shows that H is concave in x if, and only if,

$$\int_0^{\sqrt{x}} \exp[-t^2] dt \geq \sqrt{x} \exp[-x] \quad (2.12)$$

for all nonnegative x 's in $W_{2,2\pi}^1$. Relation (2.12) can then be proved using the power series expansions for $\exp[-x]$ and $\text{erf}[\sqrt{x}]$, namely

$$\text{erf}[\sqrt{x}] = 2\pi^{-1/2} \sum_{n=0}^{\infty} \frac{(-1)^n (\sqrt{x})^{2n+1}}{n! (2n+1)} \quad (2.13)$$

This shows that property (2) above is satisfied; property (1) can be proved by similar arguments. Property (3) is the result of a direct computation; in particular (2.7) follows from elementary estimates for $\|R(z;v)\|_{1,2}$. We refer the reader to [4] for details. Observe that, in this specific example, G itself is convex in z ; this is, however, irrelevant. The crucial property is the concavity in z^2 , as we shall see below.

Now consider the action functional

$$\begin{aligned} S[z] &= \frac{1}{2} \int_0^{2\pi} (z')^2(\theta) d\theta - \frac{n}{2} \int_0^{2\pi} z^2(\theta) d\theta + \beta \int_0^{2\pi} \Delta(\theta) G(z)(\theta) d\theta \\ &\equiv S_q[z] + \beta \int_0^{2\pi} \Delta(\theta) G(z)(\theta) d\theta \end{aligned} \quad (2.14)$$

where S_q stands for the quadratic, harmonic oscillator functional

$$S_q[z] = \frac{1}{2} \int_0^{2\pi} (z')^2(\theta) d\theta - \frac{n}{2} \int_0^{2\pi} z^2(\theta) d\theta \quad (2.15)$$

In terms of (2.2), one can then rewrite (2.14) as

$$2S[z] = \|z'\|_2^2 - n\|z\|_2^2 + 2\beta \int_0^{2\pi} \Delta(\theta)G(z)(\theta)d\theta \quad (2.16)$$

In the next section, we shall present a set of inequalities for S and indicate how to determine its critical points using direct variational methods. This, in turn, will allow us to discuss the existence problem of periodic orbits of equation (2.8). Observe that S is not convex in z in general, so that the traditional convex minimization techniques (see for instance [5]) may not be applied.

3. INEQUALITIES FOR THE FUNCTIONAL S AND SOLUTION OF THE VARIATIONAL PROBLEM FOR PERIODIC ORBITS.

We shall denote by $W_{2, [2\pi]}^1$ the subspace of $W_{2, 2\pi}^1$ containing all the real periodic functions of the form

$$z(\theta) = \sum_{k=-\infty}^{+\infty} a_k \exp[ik\theta] \quad (3.1)$$

which satisfy the conditions

$$z(0) = z(2\pi)$$

and

$$a_0 \equiv \int_0^{2\pi} z(\theta)d\theta = 0 \quad (3.2)$$

In order to detect the critical points of S on $W_{2, [2\pi]}^1$, we shall need an upper bound as well as a lower bound for $S[\frac{z-v}{2}]$, where both z and v belong to $W_{2, [2\pi]}^1$; we shall equip $W_{2, [2\pi]}^1$ with the kinetic energy norm

$$||z||_{1,2}^2 = \int_0^{2\pi} (z')^2(\theta) d\theta \quad (3.3)$$

which, under the conditions (3.2), is equivalent to (2.1) since we have

$$||z||_2 \leq ||z'||_2 \quad (3.4)$$

A typical situation is described in the following

PROPOSITION 3.1. Consider the functional (2.14) where G satisfies the properties (1)-(3) above. Assume moreover that $0 < n < 1$, $\beta\Delta \leq 0$, $|\Delta(\theta)| \leq K$ for some positive K independent of θ and that

$$0 \leq |\beta| \leq \frac{1-n}{K} \quad (3.5)$$

Then one has

$$0 \leq \frac{1}{8} (1-n-|\beta|K) ||z-v||_{1,2}^2 \leq S[\frac{z-v}{2}] \leq \frac{1}{2} (S[z]+S[v]) - S[\frac{z+v}{2}] \quad (3.6)$$

for all $z, v \in W_{2, [2\pi]}^1$.

SKETCH OF THE PROOF (see [4] for details). From (2.15) one has

$$S_q\left[\frac{z+v}{2}\right] + S_q\left[\frac{z-v}{2}\right] = \frac{1}{2} (S_q[z] + S_q[v]) \quad (3.7)$$

Moreover for G concave in z^2 and such that $G(0) \geq 0$, one has the estimate

$$G\left(\frac{z+v}{2}\right) + G\left(\frac{z-v}{2}\right) \geq \frac{1}{2} (G(z) + G(v)) \quad (3.8)$$

Combination of (3.8), (3.7) and (2.14) with the fact that $\beta\Delta \leq 0$ then leads to the upper bound in (3.6). On the other hand one has

$$2\beta \int_0^{2\pi} \Delta(\theta) G(z) (\theta) d\theta \geq -K|\beta| \|z\|_2^2 \quad (3.9)$$

which follows from property (1) above and our assumptions on β and Δ ; relation (3.9), along with (2.16), (3.4), (3.5) then implies the lower bounds in (3.6). This completes the proof.

REMARK. The concavity of G in z^2 is crucial to establish (3.8); concavity in z , along with the parity of G , would only lead to

$$G\left(\frac{z+v}{2}\right) + G\left(\frac{z-v}{2}\right) \geq G(z) + G(v) \quad (3.10)$$

which is not sufficient to establish (3.6).

Proposition (3.1) now allows us to construct a critical point of S on $W_{2, [2\pi]}^1$; indeed, since $S[z] \geq 0$ for all z in $W_{2, [2\pi]}^1$,

there exist a greatest lower bound

$$0 \leq \delta = \inf_{z \in W_{2, [2\pi]}^1} S[z] \quad (3.10)$$

and a minimizing sequence $z^{(N)}$ such that

$$\lim_{N \rightarrow \infty} S[z^{(N)}] = \delta \quad (3.11)$$

The fact that S actually takes on its minimal value δ in $W_{2, [2\pi]}^1$ is described in the following

PROPOSITION 3.2. Under the same conditions as in proposition (3.1), with the exception of (3.5) which is replaced by

$$0 \leq |\beta| < \frac{1-n}{K} \quad (3.12)$$

there exists a function z in $W_{2, [2\pi]}^1$ such that

$$S[z] = \delta \quad (3.13)$$

Moreover one has $\lim_{N \rightarrow \infty} z^{(N)} = z$ in the norm (3.3).

PROOF. Apply (3.6) to the minimizing sequence $z^{(N)}$; we get

$$0 \leq \frac{1}{8} (1-n-|\beta|K) \|z^{(M)} - z^{(N)}\|_{1,2}^2 \leq \frac{1}{2} (S[z^{(M)}] + S[z^{(N)}]) - \delta \quad (3.14)$$

since $S\left[\frac{z^{(M)} + z^{(N)}}{2}\right] \geq \delta$; from (3.11) and (3.14) we then get

$$\lim_{M, N \rightarrow \infty} \|z^{(M)} - z^{(N)}\|_{1,2} = 0 \quad (3.15)$$

which proves that $\lim_{N \rightarrow \infty} z^{(N)} = z$ since $W_{2, [2\pi]}^1$ is complete.

Relation (3.13) then follows from (3.11) and the continuity of S . This completes the proof.

EXAMPLE: Solution to the variational problem for the Gaussian, ribbon-like beam-beam interaction. We shall simply rephrase our results in physical terms, in the context of example 2. Consider the equation

$$z'' + nz = \beta\Delta \operatorname{erf}(z) \quad (3.16)$$

which describes the vertical betatron oscillations of one particle in the weak beam, going through the strong Gaussian, ribbon-like, counterrotating beam at one of the interaction regions of an intersecting storage ring; one then has the following

THEOREM 3.3. Under the same conditions as in proposition 3.2, in particular with a magnetic field index n satisfying $0 < n < 1$ (weak focusing regime), there exists a periodic orbit z in $W_{2, [2\pi]}^1$ with period 2π which minimizes the action functional

$$S[z] = \frac{1}{2} \int_0^{2\pi} (z')^2(\theta) d\theta - \frac{n}{2} \int_0^{2\pi} z^2(\theta) d\theta \\ + \beta \int_0^{2\pi} \Delta(\theta) (z \operatorname{erf}(z) + \pi^{-1/2} (\exp[-z^2] - 1))(\theta) d\theta$$

Moreover, the minimizing orbit z vanishes at least once in $[0, 2\pi]$ (relation 3.2).

Similar results can be obtained for the strong focusing regime and for minimizing orbits which may vanish more than once in $[0, 2\pi]$ (see [4]).

One important question now remains: is the minimizing orbit z in proposition (3.2) (respectively in theorem (3.3)) necessarily a (classical) solution of equation (2.8) (respectively of equation (3.16)) and is it possible to devise algorithms or iterative procedures to actually construct minimizing sequences $z^{(N)}$ converging to z ?

We shall address ourselves to this question in the next section.

4. CONNECTION BETWEEN THE VARIATIONAL PROBLEM AND THE EXISTENCE OF NON TRIVIAL PERIODIC ORBITS.

We first have to mention that the solution to the variational problem of the preceding section may be chosen twice continuously differentiable if $G(z)$ is regular enough in z ; this follows from very general circumstances (see for instance [6]). In this case, we have the following

THEOREM 4.1. Let z be a twice continuously differentiable function in $W_{2, [2\pi]}^1$ which minimizes S ; then z satisfies equation (2.8), namely

$$z'' + nz = \beta \Delta F(z) \quad (4.1)$$

In this case one has the representation

$$s = \beta \int_0^{2\pi} \Delta(\theta) \left\{ G(z) - \frac{1}{2} z F(z) \right\}(\theta) d\theta \quad (4.2)$$

for the minimal value of S .

PROOF. Since z minimizes S on $W_{2, [2\pi]}^1$ one has

$$S[z + \lambda v] \geq S[z] \quad (4.3)$$

for all v in $W_{2, [2\pi]}^1$ and for each real λ ; thus the function $\lambda \rightarrow S[z + \lambda v]$ has a minimum at $\lambda = 0$, which implies

$$\frac{d}{d\lambda} S[z + \lambda v](\lambda=0) = \int_0^{2\pi} \{-z'' - nz + \beta \Delta F(z)\} v(\theta) d\theta = 0 \quad (4.4)$$

for all v in $W_{2, [2\pi]}^1$. An elementary density argument then shows that (4.4) actually holds for each v in $L_{[2\pi]}^2$ which, in turn, implies

$$z'' + nz - \beta \Delta F(z) = 0 \quad (4.5)$$

which is (4.1). Now from (4.5) (or (4.1)) one gets

$$z''z + nz^2 = \beta \Delta zF(z) \quad (4.6)$$

and consequently the relation

$$-\int_0^{2\pi} (z')^2(\theta) d\theta + n \int_0^{2\pi} z^2(\theta) d\theta = \beta \int_0^{2\pi} \Delta(\theta) zF(z)(\theta) d\theta \quad (4.7)$$

after an integration by parts of $z''z$. One can then express (4.7) in terms of $S[z]$ using (2.14), which leads to

$$\Delta = S[z] = \beta \int_0^{2\pi} \Delta(\theta) \left\{ G(z) - \frac{1}{2} zF(z) \right\}(\theta) d\theta \quad (4.8)$$

This completes the proof.

A few remarks are necessary at this point; we first observe that the relation

$$S[z] = \beta \int_0^{2\pi} \Delta(\theta) \left\{ G(z) - \frac{1}{2} zF(z) \right\}(\theta) d\theta \quad (4.9)$$

is a necessary condition for any twice continuously differentiable function in $W_{2, [2\pi]}^1$ to be a periodic solution of equation (4.1) with period 2π . This fact, combined with the lower bound

in (3.6), then leads to statements regarding the existence of periodic orbits which allow us to distinguish between the trivial solution $z \equiv 0$ and the non trivial ones $z \neq 0$. A typical example is the following

THEOREM 4.2 (The linear case). Consider equation (2.8) with $F(z) = z$, namely

$$z'' + (n - \beta\Delta)z = 0 \quad (4.10)$$

Then, under the same conditions as in proposition (3.2), equation (4.10) has no non trivial periodic solution with period 2π .

PROOF. Choose any non zero z in $W_{2, [2\pi]}^1$. Since $1 - n - |\beta|K > 0$ from (3.12), the lower bound in (3.6) implies

$$S[z] > 0 \quad (4.11)$$

On the other hand one has

$$\beta \int_0^{2\pi} \Delta(\theta) \{G(z) - \frac{1}{2} zF(z)\} = 0$$

since $F(z) = z$ and $G(z) = \frac{z^2}{2}$; the necessary condition (4.9) can therefore not be satisfied. This proves the theorem.

REMARK. The preceding result has nothing surprising. Indeed, condition (3.12) can be rewritten as

$$0 \leq \frac{|\beta|}{n} < \frac{1-n}{Kn} \quad (4.12)$$

and consequently represents the two-dimensional region in the $\frac{\beta}{n} - n$ plane bounded by the positive coordinate axes and the hyperbola

$$C(n) = \frac{1-n}{Kn} \quad (4.13)$$

From Floquet's theory and the Liapounov-Haupt oscillation theorem however, it is known that the periodic orbits of equation (4.10) are not likely to exist in such two-dimensional domains, but only on well defined curves in the $\frac{\beta}{n} - n$ plane (see for instance [7] and [8]). In particular for $\beta = 0$, one has non trivial periodic orbits with period 2π only if $n = 1$, namely where the curve (4.13) intersects the horizontal axis; this is hardly a surprise since the fundamental period associated with the equation

$$z'' + nz = 0 \quad (4.14)$$

is $T = \frac{2\pi}{\sqrt{n}}$.

We now show that the above structure may persist in the nonlinear case: a typical example is the following

THEOREM 4.3 (The anisotropic (ribbon-like) Gaussian beam).

Consider the equation

$$z'' + nz = \beta\Delta \operatorname{erf}(z) \quad (4.15)$$

in the weak focusing regime $0 < n < 1$, and under the same conditions as in proposition (3.2). Then equation (4.15) has no non trivial periodic orbit with period 2π .

PROOF. The same argument as in theorem (4.2) is applicable if one observes that one has

$$G(z) - \frac{1}{2} zF(z) = \frac{1}{2} z \operatorname{erf}(z) + \pi^{-1/2} (\exp[-z^2] - 1) \geq 0 \quad (4.16)$$

along with $\beta\Delta \leq 0$. Inequality (4.16) follows from the convexity of $G(z) - \frac{1}{2} zF(z)$ and $G(0) = 0$. One then has

$$\beta \int_0^{2\pi} \Delta(\theta) \{G(z) - \frac{1}{2} zF(z)\}(\theta) d\theta \leq 0 \quad (4.17)$$

so that the necessary condition (4.9) cannot be satisfied since $S[z] > 0$ for any non zero z . This completes the proof.

Similar results hold for the general case as long as $G(z) - \frac{1}{2} zF(z) \geq 0$.

The actual construction of approximation sequences $z^{(N)}$ converging to non trivial periodic orbits is a much less simple matter; we shall only give the main ideas here, and refer the reader to [4] for details. We first observe that the method of the variation of parameters applied to equation (4.1) leads to the solution

$$z(\theta) = z_0(\theta) + \frac{\beta}{\sqrt{n}} \int_0^\theta \sin(\sqrt{n}(\theta-\tau)) \Delta(\tau) F(z(\tau)) d\tau \quad (4.18)$$

where z_0 satisfies (4.14). Define then the Volterra operator V by

$$V(f)(\theta) = \frac{\beta}{\sqrt{n}} \int_0^\theta \sin(\sqrt{n}(\theta-\tau)) \Delta(\tau) f(\tau) d\tau \quad (4.18)$$

on $W_{2,2\pi}^1$ and the function A from $W_{2,2\pi}^1$ into itself by

$$A(z) = z - z_0 - V(F(z)) \quad (4.19)$$

Provided a sufficiently smooth F in (4.1) (typically once continuously differentiable), one can then apply the contraction mapping argument to show that there exists a $z \in W_{2,2\pi}^1$ satisfying (4.18) along with $z(0) = z(2\pi)$, in other words such that

$$A(z) = 0 \quad (4.20)$$

One can then numerically implement the computation of the root in (4.20) using Newton's method. Indeed the derivative of $A(z)$ is

$$A'(z) = 1 + V(F'(z)) \quad (4.21)$$

where 1 denotes the identity function on $W_{2,2\pi}^1$; one can then show that $A'(z)$ is invertible, so that the sequence of approximations to the periodic orbit is recursively given by

$$z^{(N+1)} = z^{(N)} - (1 + V(F'(z^{(N)})))^{-1} A(z^{(N)}) \quad (4.22)$$

Quadratic convergence can be obtained. We hope to present our complete results at the next follow-up sessions.

ACKNOWLEDGMENTS. The author would like to thank Dr. Melvin Month and Dr. Helmut Wiedemann for their invitation to the meeting and their financial support, Professor Les Karlovitz and the School of Mathematics at Georgia Tech for financial assistance. He also thanks Mrs. Sharon Wilson for her very expert typing of the manuscript.

REFERENCES.

- [1] Eminhizer, C., Vuillermot, P., Bountis, T. and Helleman, R., "Variational Studies of the Beam-Beam Interaction", Brookhaven National Laboratory Report BNL-25703 (1979).
- [2] Month, M. and Herrera, J. C. (editors), "Nonlinear Dynamics and the Beam-Beam Interaction", AIP Conference Proceedings, American Institute of Physics, New York (1979).
- [3] Vuillermot, P., "A Review of Some Concepts in Accelerator Physics: A Mathematical Approach", to be submitted for publication (1980).
- [4] Vuillermot, P., "Convergence of Periodic Orbits for a Class of Nonlinear Hill's Equations", in preparation (1980).
- [5] Ekeland, I. and Temam, R., "Convex Analysis and Variational Problems", Studies in Mathematics and its Applications (Volume 1), North-Holland Publishing Company (1976).
- [6] Ladyzenskaja, O. A. and Ural'ceva N. N., "Equations Aux Dérivées Partielles De Type Elliptique", Monographies Universitaires De Mathematiques, Dunod, Paris (1968).
- [7] Magnus, M. and Winkler, S., "Hill's Equation", Interscience Publishers, John Wiley and Sons, New York (1966).
- [8] MacLachlan, N. W., "Theory and Applications of Mathieu Functions", Oxford at the Clarendon Press (1947).



Fermilab

ENHANCEMENT OF DIFFUSION BY A NON-LINEAR FORCE

David Neuffer and Alessandro Ruggiero

April 1980

Several observers^{1,2} have recently speculated that the simultaneous presence of diffusion processes and the beam-beam interaction may lead to enhanced diffusion or beam loss greater than that present with either diffusion or the beam-beam interaction alone. To test these ideas we have written a computer code to simulate the effects of random diffusion and the beam-beam interaction. In this paper some first results of these simulations are presented. It is found that when the strength parameter of the beam-beam force Δv includes a resonance within its tune width (see below) enhanced diffusion occurs.

In section 1 we outline the simulation of the beam-beam interaction and diffusion. In section 2 we describe some first simulation results, obtained with a 1-dimensional "weak-strong" non-linear (beam-beam) force. In section 3 we discuss features of these results and plans for future simulations.

1. Simulation procedure

In all of the simulations reported in this note, particle transport is calculated in three steps: a linear transport, a non-linear beam-beam kick, and a random diffusion kick. Particle motion through these steps is calculated for thousands of cycles to simulate beam storage for finite times.

Particle motion through the machine from interaction region to interaction region is simulated by a linear matrix calculation:

$$\begin{pmatrix} x \\ x' \\ y \\ y' \end{pmatrix} = \begin{pmatrix} M_x & 0 \\ 0 & M_y \end{pmatrix} \begin{pmatrix} x \\ x' \\ y \\ y' \end{pmatrix} \quad (1)$$

with the submatrices M_x and M_y given by:

$$M_x = \begin{pmatrix} \cos\mu_x + \alpha_x \sin\mu_x & \beta_x \sin\mu_x \\ -\frac{(1+\alpha_x^2)}{\beta_x} \sin\mu_x & \cos\mu_x - \alpha_x \sin\mu_x \end{pmatrix} \quad (2)$$

where α_x , β_x and μ_x are the usual Courant-Snyder functions. In this transport matrix x and y motion are completely decoupled, and the effects of any nonlinearities or dispersion in the lattice are not included.

The beam-beam interaction is simulated by adding a non-linear kick to the velocity:

$$\begin{pmatrix} x \\ x' \\ y \\ y' \end{pmatrix}_2 = \begin{pmatrix} x_1 \\ x_1' + F_x(x_1, y_1) \\ y_1 \\ y_1' + F_y(x_1, y_1) \end{pmatrix} \quad (3)$$

For the case of a beam-beam interaction caused by a cylindrically symmetric Gaussian beam we use

$$F_x(x, y) = -\frac{4\pi \Delta v}{\beta_0} \frac{\left(1 - e^{-\frac{(x^2+y^2)}{2\sigma^2}}\right)}{\left(\frac{x^2+y^2}{2\sigma^2}\right)} x \quad (4)$$

$$F_y(x,y) = -\frac{4\pi \Delta v}{\beta_0} \frac{\left(1 - e^{-\frac{(x^2+y^2)}{2\sigma^2}}\right)}{\left(\frac{x^2+y^2}{2\sigma^2}\right)} y \quad (4)$$

where Δv is the "linear tune shift." Other forms for F_x, F_y , can be chosen to simulate other geometries. In the form of the beam-beam interaction chosen so far we have assumed that the longitudinal length of the interaction is zero, and that the collisions of the bunches are centered and "head-on". We have also chosen the "weak-strong" approximation, that is, the beam-beam force function is the same on every turn, and is not affected by changes in the calculated beam.

Diffusion is simulated by adding a random kick to the velocities on each turn:

$$\begin{aligned} x' &\rightarrow x' + \theta_x \cdot R_x \\ y' &\rightarrow y' + \theta_y \cdot R_y \end{aligned} \quad (5)$$

where θ_x, θ_y are maximum kick amplitudes and R_x, R_y are independent random numbers between -1 and +1, which are changed at each crossing.

The simulation procedure outlined above will be changed in the future in order to obtain more realistic simulations as results and discussions develop.

2. First Results of the Beam-Beam Simulations

In the cases studied in this note the particle motions are reduced to one-dimensional (1-D) motions by setting $x \equiv x' \equiv 0$ in equations 1-5. The interactions are studied by generating a set of particles in an initial gaussian distribution and following their motion through a large number of turns. For most cases discussed

in this note the number of particles N_p is 100 and the number of turns N_T is 200,000. We calculate the emittance as a function of time, where the emittance is defined as

$$\epsilon = 6 \sqrt{\langle (y-y_0)^2 \rangle \cdot \langle (y'-y'_0)^2 \rangle} , \quad (6)$$

and the averages are over the total number of particles N_p . Phase space plots are also generated, and the distributions of the particles can be studied.

We present the results in 4 categories, depending on whether or not the beam-beam kick and/or the diffusion kick is non-zero.

(A) No beam-beam and no diffusion ("linear" and "quiet"): In this case the beam behavior is trivial with particle positions exactly repeating themselves whenever $n_T \mu_i = p 2\pi$ where n_T is the number of turns and p is any integer. It has been checked that the program does produce this result. There is no change in emittance and no change in the particle distribution.

(B) Beam-beam kick and no diffusion ("non-linear" and "quiet"): Particle motion is affected by the beam-beam interaction, but there is no significant increase in beam size. The major change in particle motion is in the phase of motion as the tune is shifted from μ to $\mu + 2\pi \Delta\nu \equiv 2\pi \nu_0$ as $y \rightarrow 0$ where the beam-beam tune shift is largest ($\mu \rightarrow \mu$ as $y \rightarrow \infty$). In figure 1 we show beam emittance as a function of time (number of turns) for $\nu_0 = 0.4$ and $\Delta\nu = 0, 0.005, 0.02, 0.5$ and 0.10 . From these cases and others we find that there is no increase in time ("diffusion") for any values of ν_0 and $\Delta\nu$.

The phase space distributions are distorted by the nonlinear force and this provides the increase in the scatter of

measured emittance with large tune shifts shown in figure 1.

(C) No beam-beam and a "diffusion" kick:

In this case the measured emittance increases linearly with time. The increase can be calculated, obtaining

$$\begin{aligned}\epsilon(n_T) &= \epsilon_0 + 6n_T\beta \frac{\langle(\Delta y')^2\rangle}{2} \\ &= \epsilon_0 + n_T\beta \theta_y^2\end{aligned}\tag{7}$$

where n_T is the number of turns and ϵ_0 the initial emittance and where ϵ is calculated using equation 6. Typical cases of such emittance increase are shown in figures 2 and 3 in the cases with $\Delta\nu = 0$. The increase in this and similar cases agrees with equation 7.

We can define a diffusion coefficient through equation

7

$$D_0 = \frac{\partial\epsilon}{\partial t} = \frac{\beta}{T}(\theta_y)^2\tag{8}$$

where T is the time associated with one turn.

(D) Beam-beam interaction and diffusion kick ("non-linear" and "noisy"):

Our first simulations have showed some interesting effects connecting diffusion and the non-linear interaction. Figure 3 shows a typical set of results in which the tune at vanishing amplitude ν_0 is kept constant at a value of 0.2 and the beam-beam parameter $\Delta\nu$ is varied. For $\Delta\nu = 0, 0.005, 0.02, 0.03$ and 0.033 the diffusion is constant and agrees with equation (8) within expected statistical accuracy. For $\Delta\nu = 0.04, 0.06$ and 0.10

the diffusion has doubled, approximately.

This increase is shown in figures 2 and 3 and also in Table 1A, where we have tabulated the diffusion coefficient D and the enhancement factor x_E ($D = x_E D_0$) as a function of Δv and D_0 . D is calculated using a least squares fit, solving the equation:

$$\epsilon(n) = \epsilon_0 + D \frac{n}{100,000}$$

where we have set 100,000 turns equal to one unit of time. Table 1A includes cases with Δv ranging from 0.0 to 0.10, for two different values of D_0 , all with $v_0 = 0.2$.

We note the following features of the simulations:

1. There is no measurable diffusion enhancement ($x_E \cong 1$) for $\Delta v \lesssim .033$. For $\Delta v \gtrsim .04$ the diffusion is roughly doubled ($x_E \cong 2$). The diffusion enhancement is roughly constant for all $\Delta v \gtrsim 0.4$. This seems to imply that measurable diffusion enhancement ($x_E \gtrsim 1.2$) occurs when the resonant tune $1/6 = .1666$ is within the beam-beam tune spread, and implies that the enhancement does not change greatly with tune spread providing only that the major resonance is within the tune spread.

2. We have calculated diffusion enhancement for two very different values of D_0 (.008 and .032). The diffusion enhancement factor x_E appears to be independent of D_0 .

3. In the cases tested to date the change in emittance seems to remain linearly increasing with time whether or not the diffusion is "resonance-enhanced". These cases have so far been limited to a few hundred thousand turns and to an increase in emittance by a factor of ~ 4 .

4. Although diffusion enhancement is relatively constant for $\Delta v \gtrsim .04$, the particle phase-space distributions change significantly. For $\Delta v = .04$, much of the enhancement is due to a few particles kicked to very large amplitudes, whereas for $\Delta v = 0.10$ the enhancement seems to be distributed throughout the particle distribution.

In Figure 4 we show the variation of x_E with D_0 and Δv .

In table IB we show results of other simulations for various values of D_0 , v_0 , Δv . Diffusion enhancement occurs when the major resonances $1/4$ (.25) and $1/8$ (.125) are within the tune spreads. Enhancement by the $v = 0.25$ resonance is much larger ($x_E \cong 6$), and enhancement by the $v = .125$ resonance is somewhat less ($x_E < 1.5$). In the cases considered to date only ~ 100 particle trajectories have been followed; statistical inaccuracy makes it difficult to notice enhancement with $x_E \lesssim 1.2$. We have not yet identified enhancement due to resonances of order higher than eight. We have not yet determined whether diffusion enhancement caused by a particular resonance is strongly dependent on v_0 . The cases with $v_0 = 0.175$ imply some dependence.

3. Discussion and Summary

In these first simulations we have limited ourselves to a one-dimensional, "weak-strong" simulation with only 100 particles tracked for a few hundred thousand turns. In two (or three) dimensions the situation becomes much more complex, and the simple identification of diffusion enhancement with resonant tunes in 1-D may be more difficult in higher dimensions. We plan to explore 2-D effects soon.

We do not yet completely understand the nature of the

diffusion enhancement in one dimension. We have not fully explored or explained the dependence of diffusion enhancement on v_0 , Δv , D_0 , the beam-beam force shape, and time. Future numerical and analytic studies will explore the details of this effect and may provide analytic methods of calculating the enhancement.

In the work to date, we have begun exploration of the relationship between a non-linear periodic force ("beam-beam") and the increase in the mean-square emittance with time ("diffusion") due to the beam-beam force and/or random processes. We have found that when the beam-beam tune shift includes a major low-order resonance significant enhancement of diffusion due to random processes can occur.

References

1. F. Mills, private communication
2. A. Ruggiero, "The Theory of a Non-Linear System in the Presence of Noise", February 1980

Table 1A

Diffusion as a function of tune shift with $\nu_0 = 0.20$. In each simulation we have chosen $\epsilon_0 = 0.02$, a total number of particles of 100, and 200,000 turns of calculation.

D_0 (calculated diffusion)	$\Delta\nu$ (tune shift)	D (measured diffusion)	x_E (enhancement factor)
.008	0.	.00765	0.96
.008	0.005	.00886	1.11
.008	0.02	.00902	1.1
.008	0.03	.00675	0.85
.008	0.033	.0111	1.39
.008	0.04	.0174	2.18
.008	0.05	.0199	2.49
.008	0.06	.0141	1.76
.008	0.10	.0178	2.23
.032	0.0	.0302	0.94
.032	0.03	.0383	1.20
.032	0.04	.0820	2.56
.032	0.05	.0612	1.91
.032	0.06	.0654	2.04
.032	0.10	.0770	2.41

Table 1B

Other cases of diffusion simulation with various values of D_o , v_o , Δv . A typical case has $\epsilon_o = 0.02$, $\beta_o = 2$, $N_p = 100$ and is tracked for 200,000 turns.

v_o	Δv	D_o	D	x_E
0.30	0.0	.008	.00691	0.86
0.30	0.04	.008	.0101	1.26
0.30	0.06	.008	.0595	7.44
0.30	0.08	.008	.0322	4.03
0.30	0.10	.008	.0254	3.18
0.15	0.02	.032	.0297	0.93
0.15	0.04	.032	.0394	1.23
0.175	0.005	.032	.0296	0.93
0.175	0.02	.032	.0394	1.23
0.175	0.04	.032	.0346	1.08
0.175	0.06	.032	.0670	2.09

Figure 1: Beam emittance E as a function of time for beam-beam interaction strengths $\Delta v = 0, 0.02, 0.05, 0.10$. There is no diffusion in these cases. In all these cases we have used $v_0 = 0.2, \beta_0 = 2. \text{ m}$.

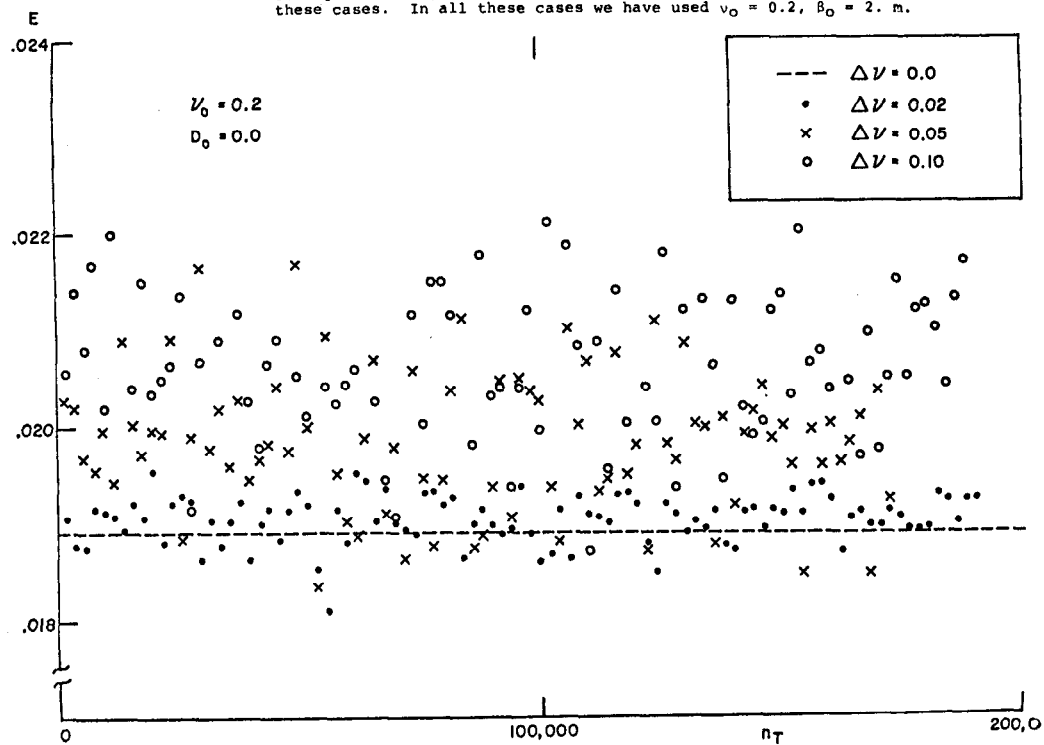


Figure 2: Beam emittance E as a function of time n_T with diffusion. We have set $v_0 = 0.2$ and included cases with $\Delta v = 0., 0.02, 0.05, 0.10$.

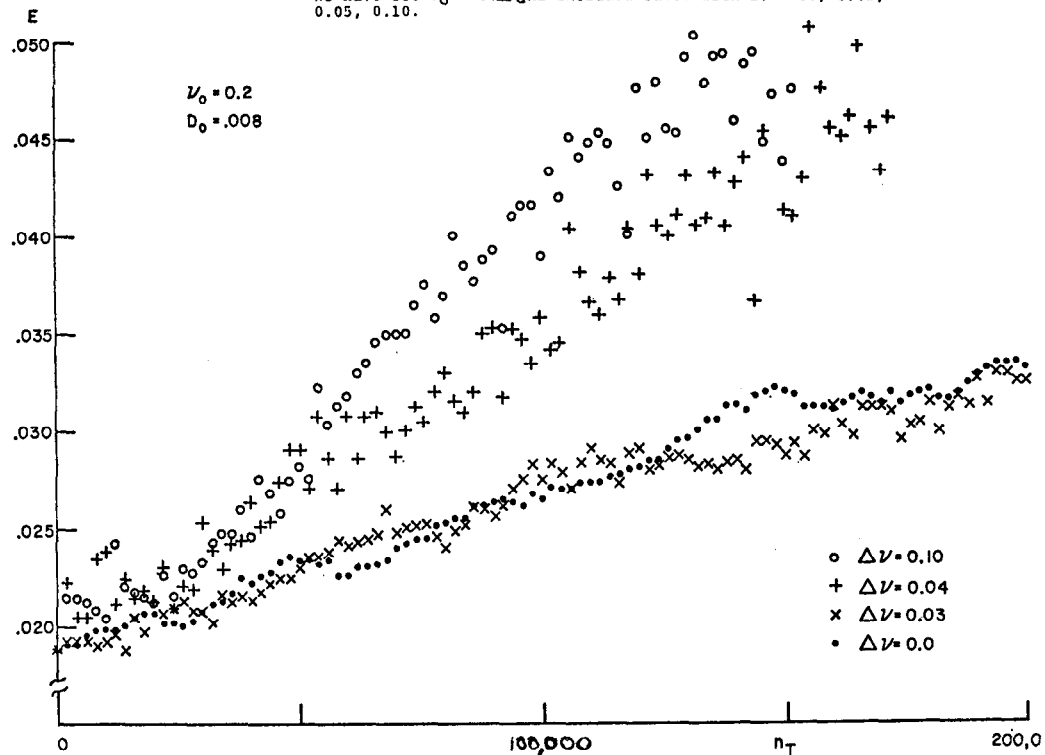


Figure 3: Beam emittance as a function of time n_T with the diffusion kick twice as large as in figure 2, which means an initial diffusion four times as large.

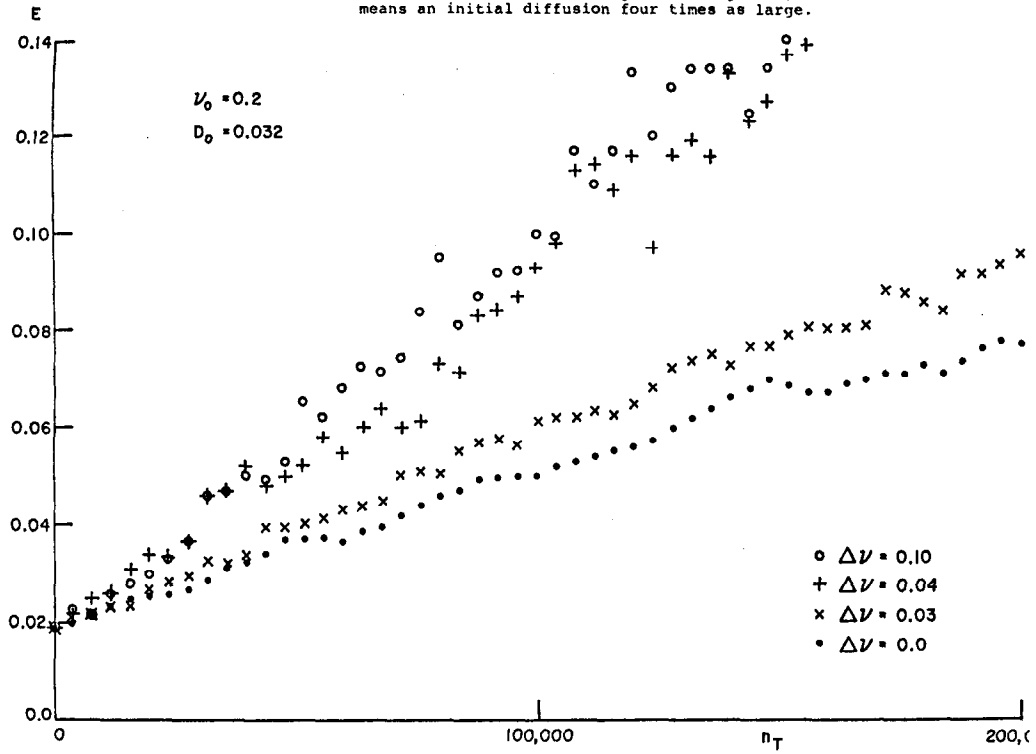
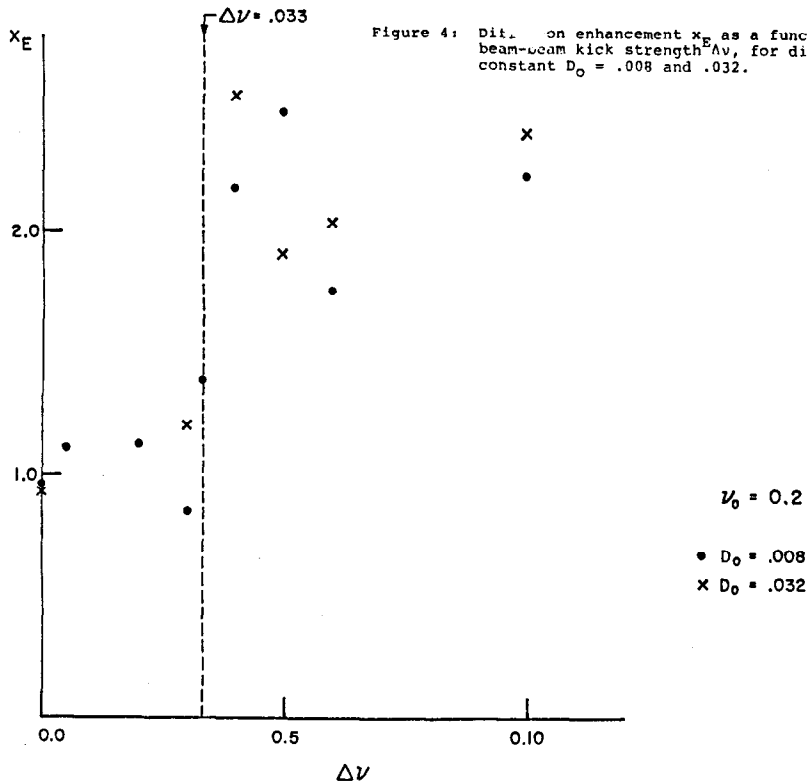


Figure 4: Diff. on enhancement x_E as a function of beam-beam kick strength ΔV , for diffusion constant $D_0 = .008$ and $.032$.



AN INVESTIGATION OF THE 'FLIP-FLOP' BEAM-BEAM EFFECT IN SPEAR*

M. H. R. Donald[†] and J. M. Paterson[‡]Abstract

When colliding electron and positron bunches in SPEAR at high values of the beam-beam tune shift parameter $\Delta\nu$, it had been observed that sometimes one of the equal intensity beams would blow up in the vertical plane more than the other beam. It was subsequently found that a small adjustment to the phase difference between the RF accelerating cavities would make the beam 'flip' the other way. The results of the investigation of this phenomenon are presented in this paper.

Introduction

The flip-flop has been known at SPEAR for some time but it is only recently that it has had an impact on routine operation. The operating luminosity of SPEAR has been gradually improved by control of the orbits, dispersion functions, betatron coupling and synchro-betatron resonances. This routine operation at high values of the beam-beam tune shift has led to the flip-flop effect becoming more noticeable and more troublesome. One can balance the beam sizes and thereby optimize the luminosity using RF phasing. However this phenomenon exhibits considerable hysteresis and close to the beam-beam limit it can limit the peak luminosity attainable. A further undesirable effect, which prompted this investigation, is that when the Bunch Lengthening Cavity (BLC) is powered the flip-flop condition is usually very much worse.

It is important to get some understanding of the phenomenon in order to: (a) use the proven good effects of the BLC, (b) be able to predict the effects in PEP and larger e^+e^- storage rings, and (c) perhaps gain some more understanding of the beam-beam effect in general. So far we have made some interesting measurements but have no theory to explain them. We hope that further measurements will give us some more clues to the nature of the effect.

We shall group the evidence under three headings:

- (1) 'hard' effects, which are very noticeable and reproducible,
- (2) 'soft' effects, which are less sharp or less reproducible, and
- (3) 'null' effects, in which parameter changes have no discernable effect on the flip-flop.

We mention first some of the easily calculated effects of changing the intercavity phase. The biggest of these effects is the separation of the electron and positron orbits which cause the bunches to collide not quite head-on. Orbit measurements are in fairly good agreement with calculations and for 30° of intercavity phase shift we find an orbit separation at one of the interaction points of $\Delta x \approx 2 \times 10^{-3} \text{ m} \approx 0.4\sigma_x$. Another easily calculated effect is the difference in synchronous energy of the beams at the interaction points. At the East interaction point the energy difference is $\Delta E \approx 0.3 \times 10^{-3} \approx 0.6\sigma_E/E$ for the same phase difference.

The Measurements

The position of the RF cavities in SPEAR are shown in Fig. 1.

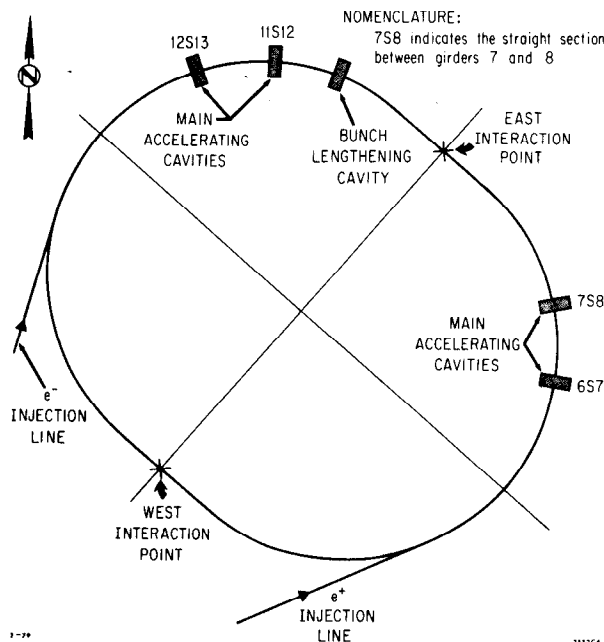


Fig. 1. Layout of RF cavities in SPEAR.

The experiments were usually done with cavities 7S8 and 11S12 powered but the cavity pair 6S7 and 12S13 has also been used. When the phase control to cavity 7S8 is varied we observe changes to the heights of the e^+ and e^- bunches. We observe the height of the bunches by means of a vertical profile scan of the synchrotron light emitted by the particles.¹ The light is scanned across a narrow slit in front of a phototube detector by means of a mirror vibrating about its suspension at 100 Hz. To produce profile scans the X plates of an oscilloscope are driven from a signal proportional to the mirror deflection.

To obtain plots of relative beam height as a function of intercavity phase the signal from the phototube is passed through a peak detector and fed to the Y terminals of a chart recorder, the X terminals being driven by a signal proportional to the intercavity phase.

Hard EffectsDependence on $\Delta\nu$

The effect is strongly dependent on the beam-beam tune shift parameter appearing when $\Delta\nu > .025$ per interaction region.

Horizontal Dispersion Function

SPEAR usually operates with the nominal value of the horizontal dispersion function η_x^* set equal to zero at the interaction points. With this condition the flip-flop is relatively easy to control and its polari-

* Work supported by the Department of Energy under contract number EY-76-C-03-0515.

[†] Lawrence Berkeley Laboratory, University of California, Berkeley, California 94720.

[‡] Stanford Linear Accelerator Center, Stanford University, Stanford, California 94305.

ty (direction of phase change needed to blow up a particular beam) depends on the configuration used and the closed orbit errors. If however the nominal value of η_x^* is set outside the range $-2\text{cm} < \eta_x^* < 2\text{cm}$, then a very strong hysteresis effect is evident and the flip-flop becomes uncontrollable. Typical hysteresis loops for a range of η_x^* are shown in Fig. 2.

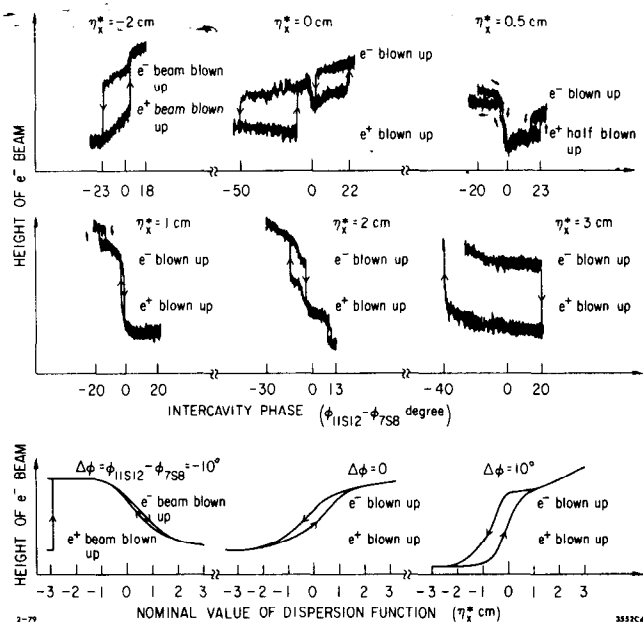


Fig. 2. Hysteresis Loops. Beam height vs intercavity phase and dispersion function.

It is unfortunately not possible to measure η_x^* to a precision better than 1cm but averaged data indicate that differences from the nominal value are approximately 0.5-1cm and that the dispersion function is different at the two interaction points.

Keeping the intercavity phase at a constant value we have scanned the value of η_x^* from -3cm to $+3\text{cm}$ obtaining the flip-flop condition. The hysteresis loops obtained by this method are much more smooth than those obtained by varying the intercavity phase at constant η_x^* . We also observed a reversal of the polarity close to the condition of zero misphasing.

Beam Separation

Recently we have used the stripline monitor plates to make a small horizontal separation of the two beams at the interaction points. We have found that when separating voltages are applied the hysteresis loops shift along the phase axis with very little change otherwise. The orbit separation due to such a shift in intercavity phase corresponds to the orbit separation due to the separation voltage. Measurements will be continued using combinations of separating voltage and cavity phasing to separate the beams at the two interaction points independently.

Energy Dependence

The experiments described here have been done at energies of 1.88 GeV and at 2.4 GeV, most of the quantitative work being done at the former energy. In the absence of detailed quantitative data for comparison we can only report our findings at these two energies and quote operational experience at other energies.

The flip-flop is only apparent close to the beam-beam limit at any energy. At low energies (1.5-1.9 GeV) the onset is sudden and the flip-flop is very hard to control and appears to be sensitive to very small changes in conditions. In the medium energy range (2.0-2.5 GeV) the onset is more gradual and the phenomenon is much more reproducible. At energies higher than 3 GeV the flip-flop disappears.

Bunch Lengthening Cavity

A bunch lengthening cavity (BLC) was installed in SPEAR in order to improve performance.² The BLC is a powered cavity operating at 860 MHz at the 672th harmonic of the revolution frequency. This cavity modifies the potential well of the synchrotron phase oscillations (this potential well is provided by the main RF cavities operating at the 280th harmonic). The flattened potential well thus produced can lengthen the bunches so as to avoid single bunch instabilities that cause energy broadening. The lengthened bunches also produce less higher mode RF heating and cure the problem of synchro-betatron resonances.

On one occasion only, powering the BLC made the flip-flop better, but on every other occasion it made the flip-flop uncontrollable.

Risetime Measurements

We have measured the risetime of the flip-flop beam growth by applying a square wave modulation to the intercavity phase. To obtain a measure of the height of the beams we took an output from the profile monitor and displayed this on an oscilloscope, the oscilloscope being triggered from the pulse generator used in the phase switch. The height of the pulses from the profile monitor system is inversely proportional to the beam height. Measurements suggest that the risetime is independent of energy and is about 80-100 msec which is long compared to the transverse damping time.

Soft Effects

Rotated Quadrupole

A detailed study of these effects has not yet been done but measurements and operational experience indicate that increasing the linear coupling by means of the rotated quadrupoles makes the flip-flop less sensitive. This is probably due to an increase in the non beam-beam contribution to the height of both beams resulting in a decrease in beam-beam tune shift. The increased strength of the rotated quadrupoles might also be expected to change the flip-flop by coupling residual horizontal dispersion to the vertical plane.

Chromaticity and Sextupoles

SPEAR normally operates with horizontal and vertical chromaticities $\xi_x = \xi_y = +3.2$. The natural chromaticities for normal operation with $\beta_y = 10\text{cm}$ are $\xi_x = -10$ and $\xi_y = -20$, the correction being accomplished by two families of sextupoles.

Increasing the chromaticity substantially (25% increase in sextupole strength) made the flip-flop worse but not disastrously so. Decreasing the horizontal chromaticity towards zero had an effect on the hysteresis print of the flip-flop. This effect was not however reproducible between experiments and no dramatic effect was observed close to the value $\xi_x = 0$. Decreasing the vertical chromaticity alone had no effect. The most probable explanation for this behaviour is the effect that the sextupoles have on orbits and dispersion functions at the interaction points.

Horizontal Beam Size

Measurements indicate that, when the beam heights are flipped and flopped, the widths also change. We might expect that if the effect were due to coupling, then an increase in beam height should be accompanied by a reduction in beam width. We in fact noticed an increase in width of the beam that was blown up vertically. For moderate values of beam-beam tune shift the change in beam width was about 5% but at the higher currents the change was about 10%. The effect is most easily seen by applying a square wave phase modulation at a frequency of about 1 Hz.

Null Effects

Vertical Orbit and Dispersion Function

No correlation could be found between the flip-flop and measured vertical orbits and dispersion functions.

Coherent Motion

We have not detected any coherent motion associated with the flip-flop. Since the beam cross section is small compared to the distance between the beam and the monitors, it is only possible to detect the barycentric (dipole) mode of oscillation by using these monitors. We have however also viewed samples of the beam profile by using the synchrotron light monitoring system. This technique should be sensitive to higher modes of oscillation.

Longitudinal Motion

We have looked for changes in bunch shape or bunch length associated with the flip-flop. Both by direct observation of the synchrotron light using a fast photodiode and by observing the spectrum of signals from the beam monitors, we have been unable to detect any such changes when the beams undergo a change in state.

Conclusions

For a small intercavity misphasing all calculated effects are extremely small except for the beam separation, beam crossing angle and energy separation. By keeping the cavities phased and varying the dispersion function η_x^* we can also make the beams flip and flop. This observation combined with the evidence from the horizontal separation experiment leads us to believe that the energy separation is not necessary to the phenomenon. We believe that a beam separation (or possibly crossing angle) at a finite value of η_x^* is the combination necessary to drive the flip-flop. We think that coherent motion is unlikely because (a) the rise-time is long compared to the transverse damping time, (b) we have not observed any coherent motion, and (c) the dependence on chromaticity is not very strong. Single resonance effects are also unlikely since the effect is independent of machine tune and because the bunch lengthening cavity cures the individual synchro-betatron resonances by creating a continuum of synchrotron tunes.

The calculated changes in amplitude function β and dispersion function η as a function of orbit difference and energy difference are very small and are unlikely to play a part in deciding which beam should blow up.

Because of the sensitivity to horizontal dispersion function it is possible that synchro-betatron resonances are excited by the beam-beam force as in Ref. 3 but that these resonances are of high order and

are associated with the nonlinearity of the beam-beam force.

Acknowledgements

We wish to acknowledge the help of all members of the SPEAR operations group and we particularly thank K. Underwood and T. Taylor for their help in devising and setting up test apparatus. R. Steining has recently joined us in this investigation and he initiated the experiment whereby horizontal beam separation was achieved using the stripline monitor plates.

References

1. A. P. Sabersky, "Monitoring the Beams in SPEAR with Synchrotron Light," IEEE Trans. on Nucl. Sci. (June 1973), vol. NS-20, no. 3, p. 638.
2. W. R. Fowkes and P. B. Wilson, "Predicted Bunch Shapes in SPEAR using Active Bunch Lengthener (ABLE)," SPEAR-209, (January 1977), unpublished.
3. A. Piwinski, "Satellite Resonances Due to Beam-Beam Interaction," IEEE Trans. on Nucl. Sci. (June 1977), vol. NS-24, no. 3, p. 1408.